UNIVERSIDADE FEDERAL DE SANTA CATARINA
CENTRO TECNOLÓGICO
PROGRAMA DE PÓS-GRADUAÇÃO EM ENGENHARIA QUÍMICA E DE ALIMENTOS

Maíra Debarba Mallmann

Polymer-derived mesoporous Si-M-N nanocomposites as co-catalysts for hydrogen evolution reactions

Florianópolis
2020

Maíra Debarba Mallmann

Polymer-derived mesoporous Si-M-N nanocomposites as co-catalysts for hydrogen evolution reactions

Tese submetida ao Programa de Pós-Graduação em Engenharia Química e de Alimentos da Universidade Federal de Santa Catarina para a obtenção do título de doutor em Engenharia Química.
Orientador Ricardo Antonio Francisco Machado, Dr.
Co-orientador Samuel Bernard, Dr.

Florianópolis
2020

Ficha de identificação da obra elaborada pelo autor,
através do Programa de Geração Automática da Biblioteca Universitária da UFSC.

Mallmann, Maíra
Polymer-derived mesoporous Si-M-N nanocomposites as co catalysts for hydrogen evolution reactions / Maíra Mallmann ; orientador, Ricardo Machado, coorientador, Samuel Bernard, 2020.
158 p.

Tese (doutorado) - Universidade Federal de Santa Catarina, Centro Tecnológico, Programa de Pós-Graduação em Engenharia Química, Florianópolis, 2020.

Inclui referências.

1. Engenharia Química. 2. hydrogen. 3. polymer-derived ceramics. 4. nanocasting. I. Machado, Ricardo. II. Bernard, Samuel. III. Universidade Federal de Santa Catarina. Programa de Pós-Graduação em Engenharia Química. IV. Título.

Maíra Debarba Mallmann

Polymer-derived mesoporous Si-M-N nanocomposites as co-catalysts for hydrogen evolution reactions

O presente trabalho em nível de doutorado foi avaliado e aprovado por banca examinadora composta pelos seguintes membros:

Prof.(a) Regina de Fatima Peralta Muniz Moreira, Dra.
Universidade Federal de Santa Catarina

Emanoelle Diz Acosta, Dra.
Universidade Federal de Santa Catarina

Estela de Oliveira Nunes, Dra.
Empresa Brasileira de Pesquisa Agropecuária

Certificamos que esta é a **versão original e final** do trabalho de conclusão que foi julgado adequado para obtenção do título de doutor em Engenharia Química.

ICP-Edu
Documento assinado digitalmente
Debora de Oliveira
Data: 01/02/2021 07:34:32-0300
CPF: 728.453.929-15

Debora de Oliveira, Dra.
Coordenadora do Programa

RICARDO ANTONIO FRANCISCO MACHADO:62237713987
Digitally signed by RICARDO ANTONIO FRANCISCO MACHADO:62237713987
Date: 2021.02.01 15:21:47 -03'00'

Ricardo Antonio Francisco Machado, Dr.
Orientador

Samuel Bernard, Dr.
Co-orientador

Florianópolis, 02 de Dezembro de 2020.

RESUMO

O hidrogênio é uma alternativa chave para o futuro da geração de energia e está atualmente passando por um momento sem precedentes, impulsionado pelas inúmeras novas políticas e projetos em todo o mundo que oferece a chance de tornar o hidrogênio um essencial vetor de energia. Dependendo de sua fonte, o hidrogênio pode desempenhar um papel estratégico no processo global de “descarbonização”. No entanto, como não está prontamente disponível, apresenta enormes desafios para armazenamento e transporte devido à sua densidade extremamente baixa. Para tanto, o desenvolvimento de novos materiais que possam ser incorporados na transição energética, envolvendo suas tecnologias de conversão, transmissão e armazenamento, é de grande importância para promover um desenvolvimento bem-sucedido da energia à base de hidrogênio. Espera-se que novos catalisadores avançados, especialmente em sistemas nanoestruturados, sejam robustos e duráveis sejam robustos e duráveis, capazes de resistir a severas condições de reação e gerar a quantidade máxima de hidrogênio com custos reduzidos. Esta tese teve como foco a síntese e caracterização de cerâmicas de Si-M-N (M = metal) preparadas por meio da rota das Cerâmicas Derivadas de Polímeros (PDC). Além disso, o desenvolvimento de monólitos micro-/mesoporosos foi realizado combinando a rota PDC com *nanocasting*, a fim de explorar o desempenho do material como suporte catalítico para a hidrólise de borohidreto de sódio. Este hidreto metálico foi selecionado para teste devido ao seu elevado teor de hidrogênio teórico (10,8 % em massa) e por fornecer as condições mais adversas durante o processo de hidrólise entre as fontes conhecidas de armazenamento químico de hidrogênio. Nesse trabalho, é relatada a modificação química de precursores do tipo organossilício com compostos de titânio, vanádio, molibdênio, cobalto e níquel e a produção de cerâmicas de área superficial elevada à base de nanocompósitos de TiN/Si_3N_4 e Si_3N_4 dopado com metal (metal = Ti/Co, Co, Ni). Mais do que isso, descreve-se a síntese e deposição in-situ de nanopartículas de platina, cobalto e níquel nos monólitos de TiN/Si_3N_4 obtidos. O desempenho dos monólitos como suporte catalítico foi avaliado medindo o volume de hidrogênio gerado durante a hidrólise. A temperatura de pirólise e a razão molecular silício/metal foram de fundamental importância para as características finais do material. A modificação do precursor cerâmico PHPS com cloreto de cobalto (II) promoveu a formação de micro e nanopartículas de cobalto nos monólitos Si_3N_4. Em conclusão, a rota PDC permitiu a produção de pós altamente puros, e quando associada à técnica de *nanocasting* proporcionou de forma eficiente a produção de materiais avançados para aplicações de catálise.

Palavras-chave: Hidrogênio. Cerâmica Derivada de Polímero. Nanocasting.

RESUMO EXPANDIDO

Introdução

A utilização do hidrogênio como fonte de energia é de alto interesse econômico devido a sua abundância e caráter não-poluente. No entanto, seu armazenamento é ainda um grande desafio, o qual tem sido um obstáculo em sua aplicação. Algumas fontes químicas de hidrogênio como hidrocarbonetos, boranos de amônia e borohidreto de sódio tornaram-se temas de intensa pesquisa por oferecerem maior segurança e efetividade do que o armazenamento físico geralmente é utilizado. Espera-se que a catálise heterogênea tenha papel central na inserção de materiais para armazenamento no ciclo de utilização do hidrogênio. Para isso, materiais com elevadas áreas superficiais, com destaque para os mesoporosos, com alta durabilidade e que propiciem a distribuição homogênea de sítos catalíticos ao longo de sua estrutura, são buscados para gerar hidrogênio em quantidades expressivas com baixos custos por meio de reações catalíticas, como a hidrólise do borohidreto de sódio. Tais fatores se fazem necessários para obter o maior desempenho em geração de hidrogênio com a menor quantidade em massa de metal. Metais nobres apresentam excelente atividade catalítica, porém sua escassez e elevados custos dificultam sua aplicação. Metais de transição, no entanto, quando trabalhados de forma a gerar materiais nanoestruturados, são vistos como excelentes candidatos para substituir metais nobres. Além disso, a necessidade de produzir materiais que atendam aos requisitos de alta atividade e durabilidade tem impulsionado estudos especialmente com cerâmicas avançadas. A rota de obtenção das cerâmicas derivadas de polímeros (Rota PDC) tem sido empregada para a produção de materiais avançados, que não são obtidos por outras rotas de síntese. É um meio efetivo para produzir cerâmicas avançadas com homogeneidade composicional e estrutural, e tem se mostrado promissor na produção de componentes cerâmicos avançados como materiais porosos, fibras, revestimentos ou peças com formatos complexos. Essa rota tem atraído significativa atenção, pois os polímeros inorgânicos fornecem cerâmicas com composição química controlada e organização nanoestrutural estreitamente definida. Dessa forma, esse trabalho envolveu o uso da rota das cerâmicas derivadas de polímeros, modificando quimicamente polissilazanos para a produção de materiais cerâmicos mesoporosos contendo (nano)partículas/(nano)cristais metálicos finamente distribuídos ao longo da superfície porosa para aplicação como co-catalisadores na hidrólise do borohidreto de sódio para reações de evolução de hidrogênio.

Objetivos

O principal objetivo da presente tese foi desenvolver cerâmicas de nitreto de silício suportadas com metal baseando-se na modificação de precursores de organossilício com metais de transição para reações de evolução de hidrogênio. Os objetivos específicos compreenderam produzir materiais mesoporosos com elevada área superficial específica; gerar nitretos de titânio, molibdênio e vanádio em uma matriz amorfa de nitreto de silício; substituir nanopartículas de platina por metais de transição (níquel e cobalto) em nanocompósitos de nitreto de titânio/nitreto de silício sintetizados pela rota das cerâmicas

derivadas de polímeros; promover o surgimento de nanopartículas de cobalto e níquel em uma matriz amorfa de nitreto de silício empregando uma nova metodologia; testar o desempenho dos materiais sintetizados em temos de geração de hidrogênio por meio da reação de hidrólise de borohidreto de sódio.

Metodologia

A parte experimental da tese se divide em duas partes principais: (1) síntese de nanocompósitos de nitreto de silício modificados com metais e (2) síntese de nitreto de silício dopado com metais. A primeira estratégia teve como etapa inicial a modificação química do perhidropolissilazano PHPS com precursores metálicos de titânio, molibdênio e vanádio. O procedimento foi realizado em solução e os polímeros obtidos caracterizados após evaporação do solvente sob pressão reduzida. A transformação cerâmica foi conduzida em atmosfera reagente de amônia, até 1000 °C. A elaboração de materiais mesoporosos foi realizada por meio da técnica de moldagem conhecida como *nanocasting*, utilizando-se monólitos de carvão ativado como suportes a serem impregnados. Após impregnação com o polímero obtido a partir de PHPS e TDMAT (precursor de titânio), os monólitos foram tratados termicamente em atmosfera de nitrogênio até 400 °C para reticulação do polímero e até 1000 °C em amônia para remoção do suporte de carbono. Os monólitos foram ainda submetidos a um segundo aquecimento até 1400 °C sob nitrogênio. Nanopartículas de platina, cobalto e níquel foram reduzidas diretamente sobre os monólitos obtidos a 1400 °C. A segunda estratégia teve abordagem diferente. PHPS e HTT1800 (polissilazano) foram utilizados em reações com cloretos de cobalto e níquel, além de complexos desses metais. Nessa abordagem, testaram-se diferentes temperaturas, tempos de reação e razões moleculares entre silício e metal (Si:M). A principal diferença com a primeira estratégia consistiu em promover o crescimento de partículas metálicas em meio a matriz amorfa de nitreto de silício durante a pirólise, eliminando a necessidade de realizar a redução de nanopartículas sobre os materiais mesoporosos ao fim do processo. Além de profunda caracterização dos materiais obtidos, seu desempenho como suportes catalíticos foi avaliado de acordo com o volume de hidrogênio medido durante hidrólise de borohidreto de sódio em condições controladas.

Resultados e Discussão

A reação entre o PHPS e o precursor de titânio TDMAT foi profundamente investigada e provou ter grande reprodutibilidade e pode ser estendida a outros precursores de metais de transição, formando nitretos metálicos (MN) em matriz cerâmica amorfa de nitreto de silício MN/Si_3N_4 (M = Ti, Mo, V). Valores expressivamente altos de área superficial específica (até 1165,7 $m^2.g^{-1}$) foram obtidos para monólitos do tipo TiN/Si_3N_4. Tal resultado foi possível devido a dificuldade de remover completamente o suporte de carvão ativado, pois nanocristais de nitreto de titânio agiram como barreira de difusão que impediu a reação da amônia com o carbono. Nanopartículas de platina, níquel e cobalto foram reduzidas em monólitos de TiN/Si_3N_4 e apresentaram robustez para suportar as condições de hidrólise e boa atividade catalítica na geração de hidrogênio. As taxas de geração

de hidrogênio, baseadas na inclinação das curvas a <50 % conversão e considerando 1 wt % de catalisador, alcançaram os valores: 12 $L.min^{-1}.g_{Pt}^{-1}$ (Pt), 6,4 $L.min^{-1}.g_{Co}^{-1}$ (Co) e 5,9 $L.min^{-1}.g_{Ni}^{-1}$ (Ni). Um efeito sinérgico entre nanoaglomerados de Pt-TiN e Si_3N_4 foi confirmado como essencial para a alta taxa de geração de hidrogênio. Além disso, um novo nanocompósito baseado em titânio e cobalto foi produzido e demonstrou ter alto potencial para aplicações catalíticas, devido à interessante distribuição de nanopartículas de cobalto no nanocompósito. Mais estudos são necessários para melhorar o acesso aos sítios ativos, uma vez que os monólitos obtidos pela impregnação do silazano modificado com titânio-cobalto não apresentaram resultados eficientes na hidrólise do $NaBH_4$. No que se refere aos materiais elaborados por meio da segunda estratégia, os polímeros obtidos à base de PHPS e Co ou Ni apresentaram altos níveis de reticulação e, portanto, excelentes rendimentos cerâmicos (91,2 e 89,5 % em massa). PHPS com $NiCl_2$ gerou cerâmica amorfa Si_3N_4 até 1000 ℃, com nanocristais de níquel na estrutura, diferentemente de $CoCl_2$, que apresentou a formação de, junto com Co, $CoSi_2$, que provou acelerar a cristalização de α- e β-Si_3N_4. As reações podem ser estendidas aos complexos de Co e Ni também sintetizados. Modificações na pirólise e no tempo de reação alteraram os processos de cristalização e mais uma vez comprovaram as excelentes características proporcionadas pela rota PDC na produção de materiais cerâmicos. Foi possível observar o crescimento de partículas de cobalto e níquel em matriz amorfa de nitreto de silício, de modo a simplificar a estratégia (1) e promover a distribuição das (nano)partículas por toda a estrutura mesoporosa do material final. Os testes de hidrólise mostraram que o monólito mesoporoso obtido a partir de polímero de PHPS e cloreto de cobalto (II) após pirólise até 1000 ℃, foi capaz de produzir o maior volume de hidrogênio após 180 minutos de reação (221,65 mL). As amostras obtidas a 800 ℃ apresentaram menor produção de hidrogênio porque as nanopartículas de cobalto provavelmente foram circundadas pela matriz amorfa de nitreto de silício, reduzindo o acesso do borohidreto de sódio aos sítios ativos durante a hidrólise. No entanto, a redução do tempo de reação de 72 para 15 horas e a temperatura de pirólise de 1000 a 800 ° C, rendeu monólitos capazes de gerar 165,3 mL de hidrogênio em uma razão molar de Si:Co = 10. Isso demonstra que tais monólitos ainda podem ser adaptados e capazes de apresentar atividade catalítica ainda mais elevada.

Considerações Finais

Observa-se o potencial da produção destes materiais aqui descritos no processo de transição energética, com resultados animadores, tornando viável a estratégia de um futuro com energia limpa de possível acesso a todos. A rota PDC é uma metodologia que pode servir como ferramenta para progredir rapidamente no desenvolvimento de materiais avançados para aplicações em tecnologias limpas. Como conclusão deste trabalho, espera-se que o mesmo contribua com os esforços de pesquisa e desenvolvimento que vêm crescendo para alcançar avanços nos campos relacionados à energia.

Palavras-chave: Hidrogênio. Cerâmica Derivada de Polímero. Nanocasting.

ABSTRACT

Hydrogen is a key alternative for the future of energy production and is currently going through what is considered an unprecedented momentum, propelled by the numerous new policies and projects worldwide that offer the chance to make hydrogen an essential energy carrier. Depending on its source, hydrogen can play a strategic role in the global decarbonisation process. However, since it is not readily available, it presents enormous challenges for storage and transportation due to its extremely low density. For that, the development of new materials that can be incorporated in the energy transition, involving its conversion, transmission and storage technologies is of major importance to promote the successful growth of hydrogen-based energy. Novel advanced catalysts, especially in nanostructured systems, are expected to be robust and durable, able to withstand severe reaction conditions and generate the maximum amount of hydrogen with reduced costs. This thesis was focused on the synthesis and characterization of Si-M-N (M = metal) ceramics prepared via Polymer-Derived Ceramics (PDC) route. Moreover, the design of micro-/mesoporous monoliths was performed combining the PDC route with nanocasting, to explore the material performance as catalytic support for the hydrolysis of sodium borohydride. This metal hydride was selected for testing due to its elevated theoretical hydrogen content (10.8 wt%) and because it provides the harshest conditions during the hydrolysis process among the known feasible sources of chemical hydrogen storage. Herein, it is reported the chemical modification of organosilicon precursors with titanium, vanadium, molybdenum, cobalt and nickel compounds and the production of elevated surface area ceramics based on TiN/Si_3N_4 nanocomposite and M-doped/Si_3N_4 (M = Ti/Co, Co, Ni). More than that, the in-situ synthesis and deposition of platinum, cobalt and nickel nanoparticles on the obtained TiN/Si_3N_4 monoliths is described. The monoliths performances as catalyst supports were assessed measuring the volume of hydrogen generated during hydrolysis. The pyrolysis temperature and silicon/metal ratio were of fundamental importance for the final material characteristics. The modification of the organosilicon precursor PHPS with cobalt chloride (II) promoted the formation of cobalt micro and nanoparticles on the Si_3N_4 monoliths. In conclusion, the PDC route allowed for the production of highly pure powders, and when associated with nanocasting technique efficiently provided the production of advanced materials for catalysis applications.

Keywords: Hydrogen. Polymer-Derived Ceramics. Nanocasting.

LIST OF FIGURES

LIST OF TABLES

LIST OF ABBREVIATIONS AND ACRONYMS

BET - Brunauer-Emmett-Teller
DOE - The United States Department of Energy
EDS - Energy Dispersive X-Ray Spectroscopy
FCEV - Fuel Cell Electric Vehicle
FTIR - Fourier-transform infrared spectroscopy
IEA - International Energy Agency
IPCC - Intergovernmental Panel on Climate Change
PEMFC - Polymer Electrolyte/Proton-Exchange Membrane Fuel Cell
PDC - Polymer-Derived Ceramics
PSD - Pore Size Distribution
SDA - Structural Directing Agent
SEM - Scanning Electron Microscopy
SSA - Specific Surface Area
TGA - Thermogravimetric Analysis
XRD - X-Ray Diffraction

CONTENTS

1 INTRODUCTION

The clean energy field has had a great progress in the last two decades and is expected to keep a fast growing in the coming years. This industry sector generates hundreds of billions in economic activity, and it is seen as an extraordinary business opportunity for the countries that develop, manufacture and export clean energy technologies. To embrace this opportunity, more work has to be made to enhance the renewable energy share worldwide. The increasing energy demands, that have been doubled in the past ten years, act as a driving force for the advances in this field (DOE, 2020). Nonetheless, despite the representative growth of clean energy-related technologies that has been observed in recent years, the current state is still distant from the full potentiality that is accomplishable and necessary for an expressive worldwide energy transition.

Future advances in clean energy applications demand the development of a new generation of materials. High costs, material scarcity, difficulties for upscaling, poor yields and lack of robustness are some of the main obstacles to develop high-profile materials. Many of these obstacles, however, are being succesfully overcome thanks to the persistent effort of scientists from different work areas, that have been creating and tailoring materials for the rise of more efficient ways to generate and store energy (LINARES et al., 2014).

Due to its abundancy and non-polluting nature, there is a remarkable growing interest in hydrogen generation. Although being an excellent energy carrier, its challenging storage remains a huge complication to bring this technology to our everyday lives. Storage materials such as hydrocarbons, ammonia borane and sodium borohydride have become the center of intensive research. Sodium borohydride fulfills technical requirements that involve its high capacity to store hydrogen, safety and cost-effectiveness (SANKIR; SANKIR, 2018). Heterogeneous catalysis is expected to play a key for the insertion of storage materials in the hydrogen energy cycle. Within this area, ordered mesoporous materials have become more and more relevant in the production of new types of catalytic systems, with robust and durable catalysts that can withstand medium conditions and generate great levels of hydrogen at low costs (LALE; MALLMANN, et al., 2020)

This thesis is the result of an extensive work on Polymer-Derived Ceramics (PDCs) to generate nanocomposite mesoporous materials with high catalytic activity to be applied in catalyst-assisted reactions such as hydrogen evolution reactions. The materials performance was assessed in the hydrolysis of sodium borohydride, because this reaction offers the harshest conditions of pH and temperature among the materials that can chemically release the stored hydrogen.

PDCs are generated by the heat treatment of preceramic polymers, that possess great processability and can be chemically modified and shaped to produce advanced

materials that cannot be obtained by traditional ceramic processing techniques (RIEDEL; MERA, et al., 2006). This brings advantages for the creation of new materials with customized structure, size, morphology, surface chemistry and porosity. For this reason, the so-called PDC route was selected as the tool to chemically modify silazanes - PHPS (based on silicon, hydrogen and nitrogen) and HTT1800 (Si, H, N and C) - with transition metals (titanium, molybenum, vanadium, cobalt and nickel) under toluene reflux and promote the *in-situ* growth of metallic nanoparticles and/or metal nitrides in an amorphous silicon nitride matrix during heat treatment under ammonia.

The utilisation of transition metals was investigated due to the elevated price and low availability of nobel metals. The possibility to achieve high levels of catalytic performance without the use of nobel metals could accelerate a remarkable breakthrough of advanced materials towards catalysis applications.

The polymer-to-ceramic conversion was observed by FTIR at intermediate temperatures and a comprehensive XRD study from 700 to 1000 °C was developed to evaluate the crystallization process of the materials as powders.

Nanocasting technique was selected for the production of catalyst supports, using the chemically modified-silazanes to impregnate activated carbon monoliths to generate micro-/mesoporous structures after a two-steps pyrolysis: until 400 °C under nitrogen for crosslinking and then until 800 or 1000 °C under ammonia for the polymer-to-ceramic conversion and template removal. Monoliths produced with titanium precursor (TDMAT) and PHPS yielded micro-/mesoporous titanium nitride in a silicon nitride matrix (TiN/Si_3N_4) and the crystallization behavior was evaluated until 1400 °C.

Herein, the organosilicon chemistry role behind the generation of these novel materials is thoroughly discussed. More than that, it is demonstrated that micro-/mesoporous supports with elevated specific surface area are significant for the acessibility of active sites and work not only in the nanoparticles stability but also act in synergy with nanoparticle surfaces to activate substrates.

1.1 OBJECTIVES

1.1.1 General Objective

Develop metal-supported silicon nitride ceramics based on the modification of organosilicon precursors with transition metals for hydrogen evolution reactions.

1.1.2 Specific Objectives

1. Produce mesoporous materials with high specific surface area;

2. Generate titanium, molybdenum and vanadium nitrides in an amorphous silicon nitride matrix;

3. Replace platinum nanoparticles by non-noble metals (nickel and cobalt) on titanium nitride/silicon nitride (TiN/Si_3N_4) nanocomposites;

4. Promote the growth of cobalt and nickel nanoparticles in an amorphous silicon nitride matrix applying an one-step process;

5. Test the mesoporous materials performance in terms of hydrogen generation yield for the hydrolysis of sodium borohydride.

2 LITERATURE REVIEW

2.1 HYDROGEN AND THE CLEAN ENERGY PERSPECTIVE

Fossil fuels are still the most used resources to supply energy since the industrial revolution. This dependence has caused an elevated increase of greenhouse gases emissions, that is strongly related to climate change and global warming. Moreover, the continuous growth of the world population and the economic/industrial development have a direct effect on the energy demand, which increases year after year (HAMILTON et al., 2009). Projections over global energy demand, taking into account the current policies, demonstrate a growth trend of 1.3 %, with annual consumption predicted to reach approximately 778 Etta Joule by 2035.

In the year of 2018, for example, the energy demand increased 2.3 %, the fastest boost of the decade, and global energy-related CO_2 emissions rose by 1.7 %. It is estimated that almost one-fifth of the consumption growth in that year was caused by warmer temperatures around the world, enhancing the need of cooling systems. It is important to state that fossil fuels use was responsible for almost 70 % of total energy demand growth in 2018, and energy-related CO_2 emissions account for two-thirds of global greenhouse gas emissions.

That being said, it is possible to observe the relation between climate changes and anthropogenic acts is a major challenge for the current and future generations. An energy transition is necessary to break the link between economic growth and increased CO_2 emissions. Thus, climate is a decisive reason for the need of an energy transition. According to the IPCC report Rogelj et al. (2018), limiting global warming to 1.5 ℃ requires that global net anthropogenic CO_2 emissions decline by around 45% until the year of 2030, from 2010 levels, reaching net zero by around 2050. For that, an inexpensive, abundant and clean energy source is essential to reduce the greenhouse effect emissions, ensure security of energy supply and, at the same time, assure the economic prosperity with the energy base modification (MOLLER et al., 2017; EDWARDS et al., 2008; DINCER; ACAR, 2015).

For these reasons, renewable energies have been extensively studied during the past decades. By definition, they are originated from sources that do not deplete or can be replenished within a human's life time. The most common renewable energy sources examples include wind, solar, geothermal, biomass and hydropower. Applying available technologies, the natural energy can be converted in electricity, water and air cooling or heating, and fuels.

Since it is a storable, transportable and utilisable energy carrier, hydrogen is consid-

ered a key alternative to carbon-based fuels and a good solution for the future of energy. However, the used resource to obtain hydrogen is an essential aspect in the discussion about the future of clean energy. Hydrogen can be obtained from renewable (hydro, wind, solar, biomass, geothermal) and non-renewable sources (coal, natural gas, nuclear) (DAWOOD; ANDA; SHAFIULLAH, 2020).

Currently, hydrogen production is mostly carried out through steam-methane reforming, a process that demands the application of high temperatures and generates significant carbon emissions. In this process, methane reacts with 700-1000 ℃ heated steam in the presence of a catalyst, under 3-25 bar pressure, to generate hydrogen with CO and CO_2. This originates what is known as “grey” hydrogen. Pollutant gases can be captured and stored, or reused, and for that it can be called “blue” hydrogen. There is also what is called “green” hydrogen, which is generated by renewable energy sources without producing carbon emissions. After its generation, it can then be applied in high-efficiency power generation systems, such as fuel cells, for vehicular transportation and distributed electricity generation (EDWARDS et al., 2008).

According to IEA (2019), green hydrogen can help to achieve a clean, secure and affordable energy future. This is directly related to its properties, since it presents the highest gravimetric energy density of all known substances with the highest known energy content of any fuel, i.e. a lower heating value (LHV) of 120 $kJ.g^{-1}$ (three times higher than petroleum). Table 1 reports volumetric and gravimetric energy densities of some fuels.

Moreover, hydrogen is non-toxic and, unlike petroleum, natural gas or coal, has water as the only exhaust product during energy conversion, becoming an environmentally pleasant and beneficial energy carrier (MOLLER et al., 2017; ACAR; DINCER, 2018). Furthermore, hydrogen possesses a natural compatibility with fuel cells, presenting higher efficiency (60 %) when compared to gasoline (22 %) or diesel (45 %) (NIAZ; MANZOOR; PANDITH, 2015).

The most common type of fuel cell is the Polymer Electrolyte Membrane or Proton-Exchange Membrane Fuel Cell (PEMFC). These cells run on hydrogen at fairly low temperatures around 80 ℃. There are also other types of cells, such as the alkaline fuel cells, that can work with non-noble metals. PEMFC systems are specially attractive in comparison to current energy conversion technologies due to their potential to directly convert chemical energy into electrical energy. This conversion is illustrated in Figure 1. Its electrocatalyst technology is mostly based on platinum blacks or nanoparticles (2-5 nm) dispersed onto larger carbon black particles (FARCAS; DOBRA, 2014; DEBE, 2012).

The process that occurs in a fuel cell is known as reverse electrolysis, in which hydrogen reacts with oxygen. The hydrogen comes from one or two storage tanks that are installed inside the fuel cell electric vehicle (FCEV), whilst oxygen comes from the

Table 1 – Gravimetric and volumetric energy densities of common fuels compared to hydrogen

Material	Energy per kilogram $MJ.kg^{-1}$	Energy per liter $MJ.L^{-1}$
Hydrogen (liquid)	143	10.10
Hydrogen (compressed, 700 bar)	143	5.60
Hydrogen (ambient pressure)	143	0.01
Methane (ambient pressure)	55.6	0.04
Natural gas (liquid)	53.6	22.20
Natural gas (compressed, 250 bar)	53.6	9.00
Natural gas	53.6	0.04
LPG propane	49.6	25.30
LPG butane	49.1	27.70
Gasoline (petrol)	46.4	34.20
Biodiesel oil	42.2	33.00
Diesel	45.4	34.60

Source: Mazloomi and Gomes (2012)

atmosphere. The only emissions that are the results of such reaction are heat and water, which is exhausted as water vapor. The electricity that is generated in the cell can follow two routes, depending on the demands of the specific driving situation. It flows to the electric engine that directly feeds the FCEV or charges a battery, which stores the energy until it is demanded by the engine. This light battery is called traction battery and it is constantly charged by the fuel cell (BMW, 2000). According to Debe (2012), fuel cells powered by hydrogen produced from renewable and secure sources are excellent alternatives for non-polluting vehicles.

Figure 2 represents a fuel cell electric vehicle scheme, which is composed by the following items:

- Power control unit: a mechanism to optimally control both fuel cell stack output under various operational conditions and drive battery charging and discharging;
- Fuel cell boost converter: is used to obtain an output with higher voltage than the input;
- Battery: stores energy recovered from deceleration and assists fuel cell stack output during acceleration;
- Motor: motor driven by electricity generated by fuel cell stack and supplied by battery;

Figure 1 – Proton-Exchange Membrane Fuel Cell

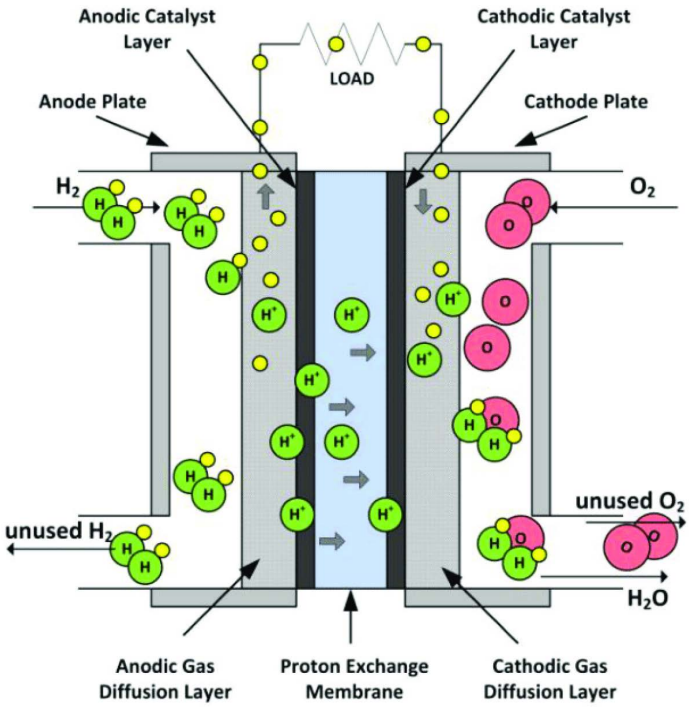

Source: Farcas and Dobra (2014)

- Fuel cell stack: the hydrogen fuel cell stack takes the place of a petrol engine. The fuel cell produces electricity that powers the motor that drives the car, all with no emissions other than water. Figure 1 shows in detail this component;

- High-pressure hydrogen tanks: tank storing hydrogen as fuel.

The idea concerning the employment of hydrogen as an energy carrier rose more than 200 years ago, but it has received more attention during the past 50 years, mainly after the global energy crisis of 1970s. However, there are still major scientific, technical, and socio economic challenges to overcome before a hydrogen economy can be implemented. Hydrogen economy infrastructure is based especially in five topics: production, delivery, storage, conversion and applications, which are in different stages of technological advancement. One of the most challenging topics is related to its storage, because hydrogen presents extremely low density that makes it a technical issue. Novel, safer and more efficient hydrogen storage systems for portable and stationary applications need to be developed in order to enable widespread use of this energy technology. Hence, the research over storage materials is one of the biggest technical challenges for the future

Figure 2 – Representative scheme of a fuel cell electric vehicle (FCEV)

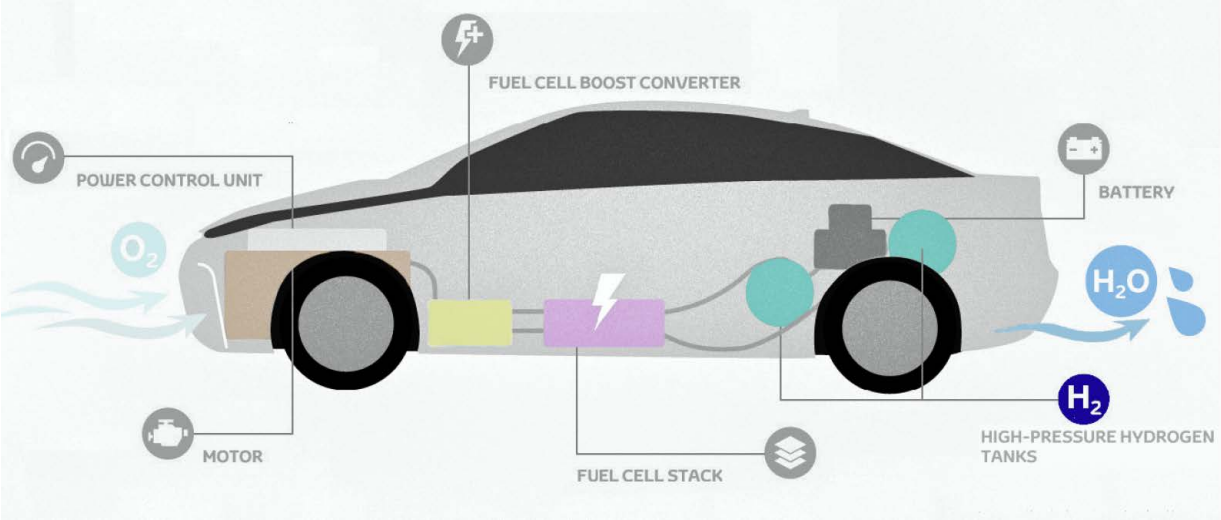

Source: Adapted from Toyota (2019)

of hydrogen economy (ABE; AJENIFUJA; POPOOLA, 2019; NIAZ; MANZOOR; PANDITH, 2015; NAVLANI-GARCIA et al., 2018).

2.1.1 Hydrogen storage materials

Hydrogen is the first element in the periodic table and the lightest known element, with an atomic weight of 1.008 $g.mol^{-1}$. It is a diatomic gas with molecular formula H_2, colourless, odourless, non-metallic, tasteless and highly flammable. There are three isotopes: protium (^1H), found in more than 99.985 % of the natural elements; deuterium (^2H), stable and present in 0.015 % of the nature; and tritium (^3H), which is the unstable and radioactive isotope that can be artificially produced by means of nuclear reactions.

However, under standard temperature and pressure (STP) conditions, hydrogen density is 0.000082 $g.cm^{-3}$, has a boiling point of -252.88 ℃ and melting point of -259.16 ℃. Considering these properties, it becomes clear that the search for safe, cost-effective hydrogen storage materials is an indomitable challenge. Furthermore, it is important to state that it is necessary to increase the material H_2 storage capacity. This feature is defined as the amount of H_2 stored per unit weight (gravimetric capacity) or volume (volumetric capacity) (MCWHORTER et al., 2011). High values of gravimetric and volumetric capacity are desired for suitable hydrogen storage (ABE; AJENIFUJA; POPOOLA, 2019). In recent studies, the Department of Energy (DOE) of the USA has suggested that values of 9 wt% and 81 g of $H_2.L^{-1}$, respectively, would be adequate to fulfill such requirements.

There are basically two main methods of storing hydrogen: physical and material.

In the physical approach, hydrogen can be stored as a gas or a liquid. The first strategy requires high pressure tanks (350-700 bar) and the last is only possible at cryogenic temperatures, due to the extremely low boiling point. The compressed hydrogen method is considered both volumetrically and gravimetrically inefficient, while the liquid hydrogen seems more promising. However, these methods cause high energy loss, are costly, mainly because they require resistant and well insulated tanks, and offer safety risks for operation due to the high flammability of hydrogen (NIAZ; MANZOOR; PANDITH, 2015; MCWHORTER et al., 2011).

The second approach can be divided in two categories: physisorption materials and chemical release systems. In the physisorption technique, hydrogen is adsorbed into porous networks, such as metal–organic framework (MOFs), carbon-based materials (e.g. graphene, fullerenes and nanotubes), zeolites, clathrate hydrates and conventional organic polymers. For chemical storage, hydrogen-rich materials pass through a decomposition process to release the gas, and this process can or cannot be reversible. Some materials that have been studied for this process are metal and non-metal hydrides, carbohydrates, synthetic hydrocarbons, ammonia (NH_3) and liquid organic hydrogen carriers (LOHC), such as N-ethylperhydrocarbazole, alcohols and formic acid. The capture and release of hydrogen on materials involves molecular adsorption, diffusion, chemical bonding and Van der Waals attraction and dissociation (MAZLOOMI; GOMES, 2012; ABE; AJENIFUJA; POPOOLA, 2019; DALEBROOK et al., 2013).

Metal hydrides have been extensively studied as hydrogen storage materials. They comprise conventional hydrides such as Mg_2NiH_4 and $LaNi_5H_6$ or complex hydrides e.g. borohydrides, alanates and amides. Because of its elevated theoretical hydrogen capacity of 10.8 wt%, sodium borohydride, $NaBH_4$, is the most-studied of the complex chemical hydrides (MARRERO-ALFONSO et al., 2009; REN et al., 2017). More detailed features are reported in the following subsection.

2.1.1.1 Sodium borohydride as chemical hydrogen storage

$NaBH_4$ is a very well known compound, widely used as a reducing agent in several industry sectors. The work of Schlesinger et al. (1953) was the first to report that alkaline $NaBH_4$ solutions when in contact with selected catalysts undergo hydrolysis to generate gaseous H_2 and the by-product $NaBO_2$. Nevertheless, the research on $NaBH_4$ as hydrogen carrier has gained significant attention since the 1990s. Its hydrogen content can be released by hydrolysis or thermolysis, but the first process is preferable, since the compound is stable only up to 400 ℃ and thermolysis is inconvenient for on-board application. The equation stoichiometry indicates that half of the hydrogen produced in the hydrolysis

reaction is derived from the water solution, which makes this reaction a more practical approach than thermolysis. Ideally, one mole of $NaBH_4$ reacts with 4 moles of water to generate 4 moles of pure H_2, which can be directly used in a fuel cell. This reaction is irreversible, however the by-product tetrahydroxyborate ($NaB(OH)_4$) can be recycled into $NaBH_4$. The reaction is exothermic, releasing 300 kJ (80 ℃), so no energy input is necessary to generate H_2. In order to control or inhibit the reaction, sodium hydroxide (NaOH) is typically added to the solution. Some researchers suggests the NaOH concentration should be between 3 and 5 %, and the $NaBH_4$ as high as possible, in order to improve the energy density (WEE; LEE; KIM, 2006; DEMIRCI, U. B.; MIELE, Philippe, 2009; SCHUTH; BOGDANOVIC; FELDERHOFF, 2004; JAIN; JAIN; JAIN, 2010). The hydrolysis reaction of $NaBH_4$ is represented in Equation 1.

$$NaBH_4(aq) + (2+x)H_2O(l) \xrightarrow{\text{catalyst}} NaBO_2.xH_2O(aq) + 4H_2(g) \quad (1)$$

If the reaction medium has a pH value lower than 9, hydrolysis occurs in a low level even without a catalyst, and this is a challenge in storing these solutions. NaOH acts by preventing $NaBH_4$ self-hydrolysis, which becomes inconsiderable when the pH is greater than 13. Moreover, without the presence of catalysts, H_2 production is not appreciable in such alkaline solutions. In order to increase the hydrolysis rate, heterogeneous or homogeneous catalysis can be applied. The present work is focused on the application of heterogeneous catalysis, using metals to reduce the activation energy and accelerate the reaction. The use of catalysts ensures the control on the hydrogen generation rate and the process is directly proportional to the catalyst amount and the specific surface area. This reaction is considered a more efficient, safer and simply controllable method to produce H_2 than other chemical approaches. Moreover, the solutions can be easily handled and could be directly fueled in vehicles, for example (AMENDOLA; SHARP-GOLDMAN, et al., 2000; SANTOS; SEQUEIRA, 2011). Table 2 depicts some important advantages of $NaBH_4$ hydrolysis for hydrogen storage and production.

Several works in the literature report heterogeneous catalysts to enhance hydrogen production from $NaBH_4$. The most researched catalysts are metal chlorides ($NiCl_2$, $CoCl_2$, $RuCl_3$), metal salts, fluorides, and borides (e.g. Ni/Co) activated carbon and Mg-based materials. Among cobalt salts, $CoCl_2$ shows the highest hydrogen production rate, which is influenced by its strong cationic charge, the electrophilic nature of Co^{2+} and higher solubility of Cl^- in aqueous solution than other salts. Well known catalysts such as Pt, Ru and Pd usually have the best performances for hydrolysis, being Ru-based catalysts considered the most effective for promoting H_2 generation. However, in order to make the process economically suitable, they are placed on appropriate supports (DALEBROOK et al., 2013; KAUR; GANGACHARYULU; BAJPAI, 2019).

Table 2 – Advantages of $NaBH_4$ hydrolysis reaction as H_2 storage and supplier

As the source of H_2	Advantageous features
Generation	- On-site generation of H_2 - Only occurs in the presence of selected catalysts and reaction rates are easily controlled by the catalysts - Carried out even at 0 ℃ - Sufficiently high purity of H_2
Storage and safety	- Theoretical hydrogen content of $NaBH_4$ is 10.8 wt% - Volumetric and gravimetric H_2 storage efficiencies are high - $NaBH_4$–NaOH aqueous solutions are stable in air for months and nonflammable
Reaction products	-The reaction products including $NaBO_2$ are environmentally safe and can be recycled back to $NaBH_4$

Source: Adapted from Wee, Lee, and Kim (2006) and Amendola, Sharp-Goldman, et al. (2000).

Some aspects are specially important for the catalyst performance. They are mainly related to the number of active sites, that can be significantly enhanced through the tailoring of catalyst features, such as composition, morphology and architecture. Thus, the development of robust supports with elevated surface area and pore size and distribution control directly influences the catalysts activity, durability and price (LALE; MALLMANN, et al., 2020).

Bai et al. (2006) synthesized platinum catalysts over carbon supports (Vulcan XC-72R) with a BET surface area of 235 $m^2.g^{-1}$. The supports were impregnated with different chloroplatinic acid solution concentrations for 24 h and then calcined in reductive gas atmosphere at 300 ℃ for 2 h. The Pt-loadings were 1.84, 6.88 and 13.1 %, which generated particle sizes of about 300, 500 nm and aggregate morphology, respectively. The catalyst was able to give satisfactory hydrogen generation rates when the Pt-loading was higher than 6.88 %. When hydrolysis tests were performed using 10% $NaBH_4$ and 5% NaOH solution, 13.1 % Pt/C catalyst could achieve a maximum hydrogen generation rate of 29.6 $L.min^{-1}.g^{-1}_{catalyst}$ and average rate of 23.0 $L.min^{-1}.g^{-1}_{catalyst}$, giving sustainable supply to a 3.7 W proton-exchange membrane fuel cell.

Xu, Zhang, and Ye (2007) also tested Pt catalysts supported on Vulcan XC-72 (BET surface area 250 $m^2.g^{-1}$) and, in addition, they tested active carbon (BET surface area 1055 $m^2.g^{-1}$) and alumina supports (BET surface area $m^2.g^{-1}$). The highest hydrogen generation was obtained with Pt catalysts support on active carbon, with a maximum rate

of 8.5 $L.min^{-1}.g_{Pt}^{-1}$ in solutions with 5 wt% $NaBH_4$ and NaOH. The better performance using active carbon support in comparison to the other materials was explained by the much larger BET surface area.

Innumerous authors consider transition metals and their chlorides as the best catalysts for hydrolysis reactions because of the elevated hydrogen generation rates and their low cost compared to noble metal catalysts (XU; DAI, et al., 2008). Cobalt and nickel have been the most commonly employed transition metals to date (BRACK; DANN; WIJAYANTHA, 2015). Cobalt, specially, soon stimulated several works due to its reactivity and cost. $CoCl_2$ is reported as the most reactive among the chlorides and four times more reactive when compared to other Co(II) salts, such as acetate, $[Co(CH_3COO)_2]$, sulfate $[CoSO_4]$, fluoride $[CoF_2]$ and nitrate $[Co(NO_3)_2]$ (DEMIRCI, U.; MIELE, 2010). In addition, Patel and Miotello (2015) affirm that it is possible to enhance the catalytic activity of a catalyst system using a transition metal alloyed with another element.

Walter et al. (2008) produced catalysts with the reductions of $NiCl_2$, $CoCl_2$ and $RuCl_3$ to react in $NaBH_4$ and NaOH solutions to observe the hydrolysis rates. The resulting reduced compounds were Ni_3B, Co_3B and Ru, which presented similar morphologies. For the hydrolysis tests, they were applied without a support. The maximum rates obtained were 1.29 $L.min^{-1}.g^{-1}$ (10 wt% $NaBH_4$ and 5 wt% NaOH), 6 $L.min^{-1}.g^{-1}$ (5 wt% $NaBH_4$ and 5 wt% NaOH) and 18.60 $L.min^{-1}.g^{-1}$ (5 wt% $NaBH_4$ and 5 wt% NaOH) for Ni_3B, Co_3B and Ru, respectively. Under other solution conditions, 20 wt% $NaBH_4$ and 30 wt% NaOH for Ni_3B and Co_3B, 20 wt% $NaBH_4$ and 5 wt% NaOH for Ru, the maximum rates were 1.28, 4.88 and 8.56 $L.min^{-1}.g^{-1}$, in the same order. The authors could observe that when the $NaBH_4$ concentration was variated, the highest hydrolysis rates occurred between 5 and 10 wt% for all the catalysts, while the rates decreased when the concentration was increased to more than 10 wt%. However, when the NaOH concentration was higher, the hydrolysis rate increased for non-noble metals while it decreased for the nobel metal ruthenium catalyst. The authors affirmed that catalysts that are able to bind hydrogen strongly can show lower hydrolysis rates due to the increasing concentration of OH^-, while the ones that allow a fast hydrogen release have better hydrolysis rates at higher OH^- concentrations.

In another work, transition metal chlorides $CoCl_2$, $NiCl_2$, $CuCl_2$, $ZnCl_2$ and succinic acid were evaluated as catalysts. The H_2 generation results were more elevated than the theoretical calculated amount (1.005 $L.g_{NaBH_4}^{-1}$) for the $NaBH_4$ applied in the test, showing that part of the released hydrogen came from the water in the reaction medium. Obtained results reported that for 1 g of $NaBH_4$ and 0.37 g of $CoCl_2$, 2.387 L of hydrogen were released (Figure 3) (CAKANYILDIRIM; GURU, 2009). Further tests were carried out using diatomite and γ-Al_2O_3 as supports for $CoCl_2$ compound. The catalyst amounts adhered on

the supports were 10, 25 and 55 wt%. Higher catalyst amounts resulted in faster hydrogen release times. Both supports demonstrated good resistance in the alkaline solution and, more than that, $CoCl_2$ did not dissolve and was able to hold the support surface even after 250 h of experiment. Thus, the authors stated that support and active materials must form a composite that keeps physical form against the reaction environment (CAKANYILDIRIM; GURU, 2010).

Figure 3 – Hydrogen yield applying different catalysts

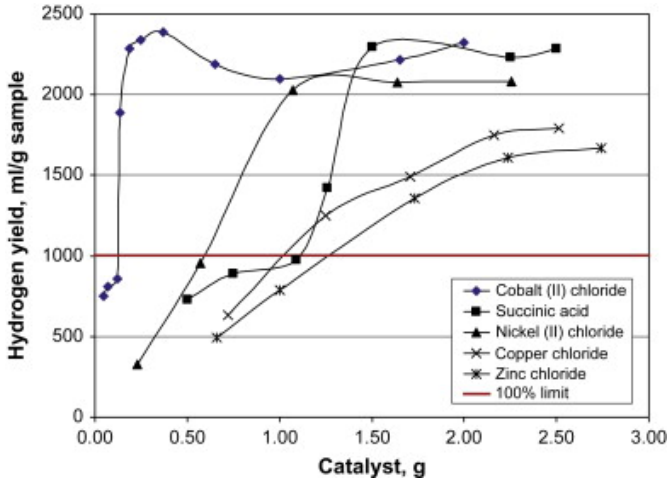

Source: Cakanyildirim and Guru (2009).

Graphene was also applied as support for hydrolysis, specially with Co-B catalysts modification. Shi et al. (2019) reported interesting results with this approach, with a hydrogen generation rate of 14.34 $L.min^{-1}.g^{-1}_{catalyst}$ and low activation energy of 26.2 kJ mol^{-1} for hydrolysis reaction of $NaBH_4$. The authors expressed that the amorphous structure, large specific surface area, uniform surface morphology and high electron density at active Co sites were the main reason for the outstanding hydrogen production. Saha et al. (2014) tested Co/Pt modified graphene and had the best results when Co and Pt were applied as co-catalysts. The presence of both metals on graphene support reduced their grain size when compared to the use of the Pt or Co alone. With the surface to volume ratio enhancement and consequently the number of catalyst sites per volume, the catalyst activity also increases.

The American company Millennium Cell developed systems for hydrogen generation using a solid-phase Ru-catalyst supported bed in a reactor. The main idea was to build a system in which a $NaBH_4$ solution simply contacts the catalyst bed and releases hydrogen. For the tests, the researches variated the solutions concentrations from 1 to 25 wt% of $NaBH_4$, and 1-10 wt% of NaOH. Moreover, the solutions temperatures were also studied, from 0 to 40 ℃. It was possible to observe that initial H_2 generation rates increased

and reached a maximum in the range from 7.5 to 12.5 wt% of $NaBH_4$. Applying 1 wt% of NaOH and 7.5 wt% of $NaBH_4$, the generation rates were 0.0456, 0.378, 0.606 and 1.098 $L.min^{-1}.g^{-1}_{catalyst}$ at 0, 25, 32.5 and 40 ℃, respectively. The authors estimated that, considering a 100 % stoichiometric H_2 production in the reaction, the volume required to store $NaBH_4$ solutions can be compared to pressurized or cryogenically stored H_2. In a cryogenic tank, 71 L of H_2 are necessary to store 5 kg, whilst a 34 MPa pressurized container requires 180 L. At the same time, to store 5 kg of H_2 in a 35 wt% $NaBH_4$ solution requires a volume of 65 L. Thus, the authors affirm that $NaBH_4$ solutions are a convenient, nonpressurized way to store H_2 (AMENDOLA; SHARP-GOLDMAN, et al., 2000). The reactor technology and the catalyst synthesis were later patented by the researchers (AMENDOLA; BINDER, et al., 2003). According to the mentioned patent, the catalysts that are useful for the hydrogen generation system, beyond noble metals, include transition metals, such as Cu, Zn, Sc, Ti, V, Cr, Mn, Fe, Co and Ni groups, transition metal borides, alloys of these materials, and mixtures thereof. Furthermore, Millennium Cell has tested its system with an integrated reactor and obtained good results. In the study, the catalyst bed was integrated with a heat exchanger for autothermal operation, which gave a 200 % enhancement in the reactor hydrogen throughput (ZHANG; SMITH; WU, 2007).

Herein, the hydrolysis of $NaBH_4$ was the chosen system because it offers the harshest conditions reactions in terms of temperature and pH among the potential sources of chemical hydrogen storage. The main aspects that can be observed in the literature survey that involve the development of materials for hydrolysis reactions of $NaBH_4$ are:

- Requirement of a support, usually highly porous, that can bear the harsh conditions of this process, so the material does not break or dissolve in the solution;
- The support choice strongly depends on the surface area, pore volume, arrangement and type of porosity;
- The chosen catalyst needs to have high surface area and to be homogeneously distributed over the support.

Most of the published works use oxide or carbon based materials as supports, however, although these materials display excellent properties, they present limitations in harsh conditions such as high temperatures, highly alkaline media and/or fast reaction rates. Oxide materials can collapse with the pH increase and carbon supports suffer from swelling, due to water adsorption. In order to overcome these problems, the investigation on catalytic supports for $NaBH_4$ hydrolysis that can withstand the harsh reaction conditions and provide high H_2 generation rates is essential for the faster development of hydrogen technology.

In this work, metal-doped silicon nitride mesoporous materials obtained through the Polymer-Derived Ceramics (PDCs) route are proposed as catalytic supports for $NaBH_4$ hydrolysis. Hence, a brief review on PDCs is given in the following chapter.

2.2 POLYMER-DERIVED CERAMICS

Ceramics are inorganic materials that are typically crystalline and contain metallic and non-metallic compounds such as aluminium oxide (Al_2O_3), calcium oxide (CaO), zirconium dioxide (ZrO_2), silicon carbide (SiC) and silicon nitride (Si_3N_4). There are several types of ceramics, which can be classified according to the application category: clays, white ceramics, refractory materials, glass, cements, abrasives and advanced ceramics (INGOLE et al., 2013). Advanced ceramics are materials that have excellent properties, including resistance to corrosion/oxidation and superior thermal, electrical, mechanical and magnetic properties, that can be modified by controlling their composition and internal structure. These ceramics can be divided in accordance to their application: structural ceramics (bioceramics, engine components, wear parts and cutting tools); electrical ceramics (capacitors, superconductors, insulators, integrated circuit packages, substrates, piezoelectrics and magnets); ceramic coatings (wear parts, engine components and cutting tools); chemical processing and environmental ceramics (filters, membranes, catalysts and catalyst supports) (RIEDEL; CHEN, 2015).

It is important to highlight that traditional processes for obtaining ceramic materials are industrially widespread due to the low cost of raw materials. However, the processes demands high temperatures as they are highly endothermic reactions and require the presence of sintering additives. Obtaining advanced ceramics via Polymer-Derived Ceramics route has proven to be a great alternative to obtain materials that are not easily produced using technologies normally applied in the ceramics industry (BORCHARDT et al., 2012; COLOMBO; MERA, et al., 2010).

The PDC route is based on the use of an inorganic precursor, known as preceramic polymer, which contains silicon in the backbone and, after a heat treatment process, is transformed into a ceramic material, the so-called PDC. Inorganic precursors can provide ceramics with controlled chemical composition and narrowly defined nanostructural organization, and for this reason, they have been considered as promising precursors in the production of advanced ceramics. In addition, it is important to note that PDCs are produced without the use of additives and their processing temperature is usually between 800 and 1100 °C, lower than those required by conventional ceramic processing. Moreover, it is possible to obtain ceramics with compositions in the ternary systems, such as SiCO and SiCN systems, not obtainable from non molecular processing routes (RIEDEL;

MERA, et al., 2006; IONESCU, 2013; GREIL, 2000).

Preceramic polymers can present different structures in inorganic or organometallic systems. The general structure of these polymers, as shown in Figure 4, is based on the presence of Si in the main chain, linked to X, which defines the class of the precursor. The group X can represent Si (polysilanes), CH_2 (polycarbosilanes), O (polysiloxanes), NH (polysilazanes), N=C=N (polysilylcarbodiimides), among others. The side groups attached to the Si atom (R^1 and R^2) are the functional groups responsible for the solubility, thermal stability, electronic, optical and rheological properties of the polymer.

Figure 4 – General structure of preceramic polymers

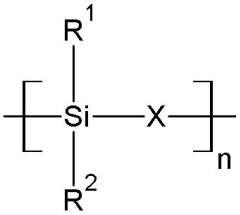

Source: Adapted from Colombo, Mera, et al. (2010).

Such preceramic polymers are specially interesting because they are polymeric at room temperature, so that they can be shaped into different components. That said, they are suitable to undergo a great variety of forming methods, such as casting, injection, moulding, tape casting, fiber drawing, coating and impregnation (COLOMBO; MERA, et al., 2010; RIEDEL; MERA, et al., 2006).

The molecular structure and type of preceramic polymer have an influence on the composition, phasesand distribution, and on the microstructure of the final ceramic material. This fact makes this process even more attractive, since the properties of preceramic polymers can be largely modified and adapted by manipulating their molecular structure (IONESCU; KLEEBE; RIEDEL, 2012).

The main process to produce ceramic materials from inorganic precursors involves three main steps: (1) the synthesis of the polymeric precursor from the appropriate monomer, (2) crosslinking and shaping of the polymer and then (3) pyrolysis of the crosslinked polymer (CHAVEZ et al., 2011). Depending on the molecular structure and compostion of the preceramic polymers, it is possible to obtain amorphous ceramics up to 1000-1800 ℃. The ceramics microstructure can undergo crystallization during pyrolysis and annealing, the last being characterized by a phase separation process and formation of nanocrystals. The general temperatures at which all these steps occur is illustrated in Figure 5. Several examples of polysilanes, polycarbosilanes, polysiloxanes and polysilazanes have been reported as excellent ceramic precursors (RIEDEL; MERA, et al., 2006).

Figure 5 – Polymer-Derived Ceramic route according to the temperature increase

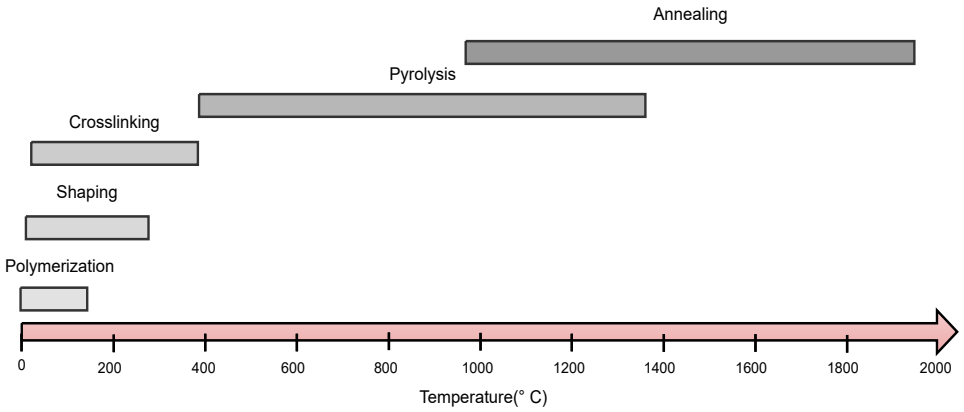

Source: Adapted from Colombo, Mera, et al. (2010) and Mera et al. (2015).

The most known PDC classes obtained through this strategy are in the binary systems Si_3N_4, SiC, BN and AlN, ternary systems SiCN, SiCO and BCN, as well as quaternary systems SiCNO, SiCN, SiBCO, SiAlCN and SiAlCO. Other than boron compounds, the preceramic polymers can be modified with metals, forming metal-containing polysiloxanes, polycarbosilanes or polysilazanes, for example. The typical classes of silicon-based preceramic polymers are exhibited in Figure 6.

The first reported works using the PDC route are from Ainger and Herbert (1960) and Chantrell and Popper (1965), in which the authors described the production of non-oxide ceramics from molecular precursors. In the following years other works were published, such those from Verbeek, Winter and Mansmann (1974), that presented the polymer-to-ceramic conversion of polysilazanes, polysilanes and polycarbosilanes, and from Yajima, Hayashi and Imori (1975), that worked on the synthesis of SiC-based ceramics employing the polycarbosilanes thermolysis process (COLOMBO; MERA, et al., 2010).

Another important pioneer work was published by Bahloul et al. (1993), where the authors studied the conversion of a polysilazane into ceramic. It is mentioned in the paper that this conversion depends on different parameters, such as the molecular structure of the preceramic polymer and the pyrolysis conditions (temperature, heating rate, dwell time and atmosphere). The authors tested several pyrolysis settings, and they could conclude that the heating rate during the pyrolysis has a strong influence in the final ceramic yield. The fastest heating rate generated the lowest ceramic yield. They also reported that the atmosphere nature, inert or reactive, affects the ceramic yield and the formation of different networks.

The research over PDCs has greatly increased over the past 50 years, enabling sig-

Figure 6 – Typical classes of Si-based preceramic polymers

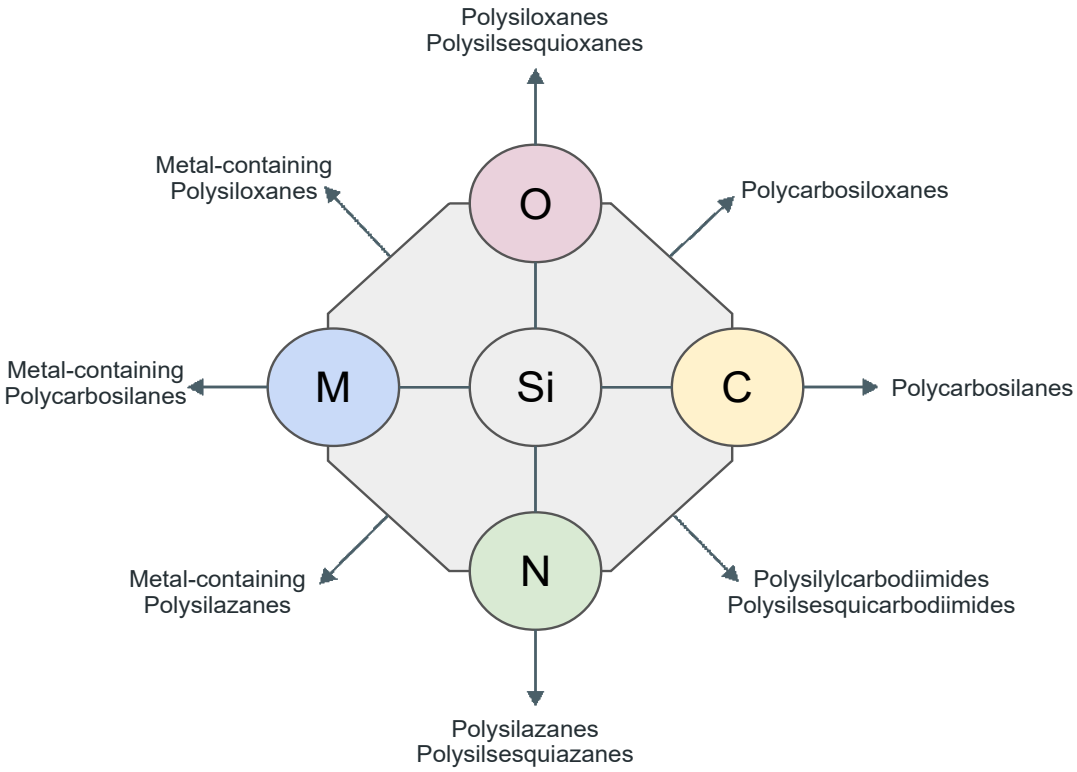

Source: Adapted from Colombo, Mera, et al. (2010) and Mera et al. (2015).

nificant technological breakthroughs in materials science. It can be considered an emerging chemical process, as proved by the continuous growth of commercial development of preceramic polymers. The PDC route is considered an effective method to produce advanced ceramics with compositional and structural homogeneity, specially in non-oxide systems (BERNARD; MIELE, 2014; BERNARD; FIATY, et al., 2006).

However, in favor of keeping the PDCs at high performance level materials, it is necessary to perform with great precision all the steps since the synthesis until the ceramic conversion. It means that detailed investigations of the preceramic polymer structures and the final ceramics is essential to achieve and maintain advanced properties and performances. Controlling the polymer-to-ceramic conversion and the amorphous/crystalline phases is essential to understand and improve the final materials (BERNARD; FIATY, et al., 2006).

In relation to the preceramic polymer, several authors affirm that it should present a sufficiently high molecular weight to avoid the volatilization of low-molecular weight components during pyrolysis to be fully effective for the heat treatment process. Additionally, it should have appropriate rheological properties and solubility to be shaped. The presence

of functional groups has a great importance due to the molecule reactivity that allows the curing and crosslinking steps (COLOMBO; MERA, et al., 2010; BERNARD, 2012). Since the present work is focused on polysilazanes, the next section approaches the features that concern this class of preceramic polymers.

2.2.1 Polysilazanes

Polysilazanes are the ideal precursors to obtain Si_3N_4 and ternary Si-C-N ceramics. Besides that, their mechanical, thermal and chemical properties are excellent for high temperature applications. Moreover, they offer great resistance and durabilty as barriers to prevent oxidation and corrosion (LI, Y.-L. et al., 2001; BIROT; PILLOT; DUNOGUES, 1995; TOREKI et al., 1990; GARDELLE et al., 2011).

They are usually prepared by means of ammonolysis of mono/di/tri/tetrachlorosilanes, or still chlorosilane mixtures (generating copolysilazanes).

$$R_2SiCl_2 + 4NH_3 \longrightarrow R_2Si(NH_2)_2 + 2NH_4Cl \quad (2)$$

R = e.g. mesityl, benzyl, *t*-butyl, i-propyl, H, methyl, ethyl, phenyl

According to the applied chlorosilane, this process can generate different kinds of polysilazanes. Hence, the physical and chemical properties of polysilazanes can be tailored already in this step. The several possible substituents for R play a crucial role on the polymer properties, its thermal beaviour and the polymer-to-ceramic conversion mechanisms.

Upon heating, condensation reactions occur forming ammonia (NH_3) and oligomeric silazanes. These processes are more commonly carried out in industries than university laboratories due to the elevated reactivity and hazardous characteristics of chlorosilanes on air and moisture. Still, this strategy is interesting because chlorosilanes are inexpensive, commonly obtained as byproducts in the silicone industry, so the reactants are readily available and easily purified (GREIL, 2000). In order to better illustrate the reaction, Figure 7 represents the synthesis of perhydropolysilazane (PHPS) from a dichlorosilane.

Stock and Somieski were the first authors to report the ammonolysis of dichlorosilane, in 1921, testing the reaction in benzene solution that generated a soluble viscous oil, not stable at room temperature. In the 60s, Kruger and Rochow (1964) performed the conversion of silazane oligomers in polysilazanes by ammonolysis reactions, using amonia halides as polymerization catalysts. Ammonia volatilized during the reaction. The Si-halide bonds were converted into Si-N bonds to finally obtain polysilazanes after solvent evaporation. Further works were published by Seyferth and coworkers in the 80s, that tested

Figure 7 – Synthesis of perhydropolysilazane by ammonolysis of dichlorosilane

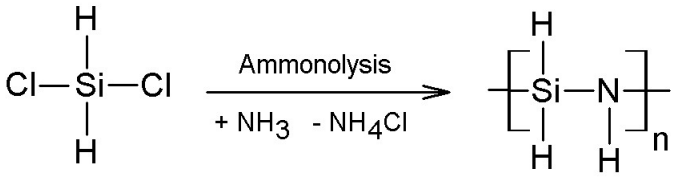

Source: Adapted from Birot, Pillot, and Dunogues (1995) and Riedel, Mera, et al. (2006).

the ammonolysis of dichlorosilane using diethylether and dichloromethane as solvents (KROKE et al., 2000).

Studies concerning the application of polysilazanes as precursors to silicon nitride ceramics have been providing a lot of progress until the present. Wide applications as coatings, adhesives and objects boosted the studies, broadening the application to areas such as fibers, nanostructures and mesoporous materials.

Several authors point out that higher ceramic yields can be obtained with well crosslinked polymers containing elevated molecular weight. Crosslinking reactions before pyrolysis provide higher ceramic yield to the final material. These reactions can be controlled to obtain polysilazanes with more or less solubility, meltable or unmeltable, according to the shaping process and desired application (CHOONG KWET YIVE et al., 1992; LI, Y.-L. et al., 2001; LAVEDRINE et al., 1991).

Polysilazanes crosslinking can be conducted either thermally or with the use of chemical agents, such as catalysts and peroxides. Four main crosslinking reactions are known to possibly happen: hydrosilylation, vinyl polymerization, transamination and dehydrocoupling, as shown in Figure 8 (KROKE et al., 2000; LI, Y.-L. et al., 2001; CHOONG KWET YIVE et al., 1992)

When thermally favored, the crosslinking reactions can happen at different temperature ranges. Hydrosilylation occurs between 100 and 120 °C, transamination between 250 and 500 °C, whilst vinyl polymerization and dehydrocoupling between 300 and 400 °C (KROKE et al., 2000).

The pyrolysis of organosilicon precursors such as polysilazanes consists in three main steps. Since the precursors are a mixture of oligomers and polymers, the initial weight loss during pyrolysis is associated to the volatilization of low molecular weight oligomers. Such decomposition of organic groups causes the release of gaseous products, such as H_2, NH_3 and CH_4, as well as molecular rearrangements.This first step finishes at about 400 °C and is also characterized as the transformation of the polymer from thermoplastic

Figure 8 – Polysilazane crosslinking reactions: (a) hydrosilylation by α and β-addition; (b) transamination; (c) vinyl polymerization; (d) dehydrocoupling

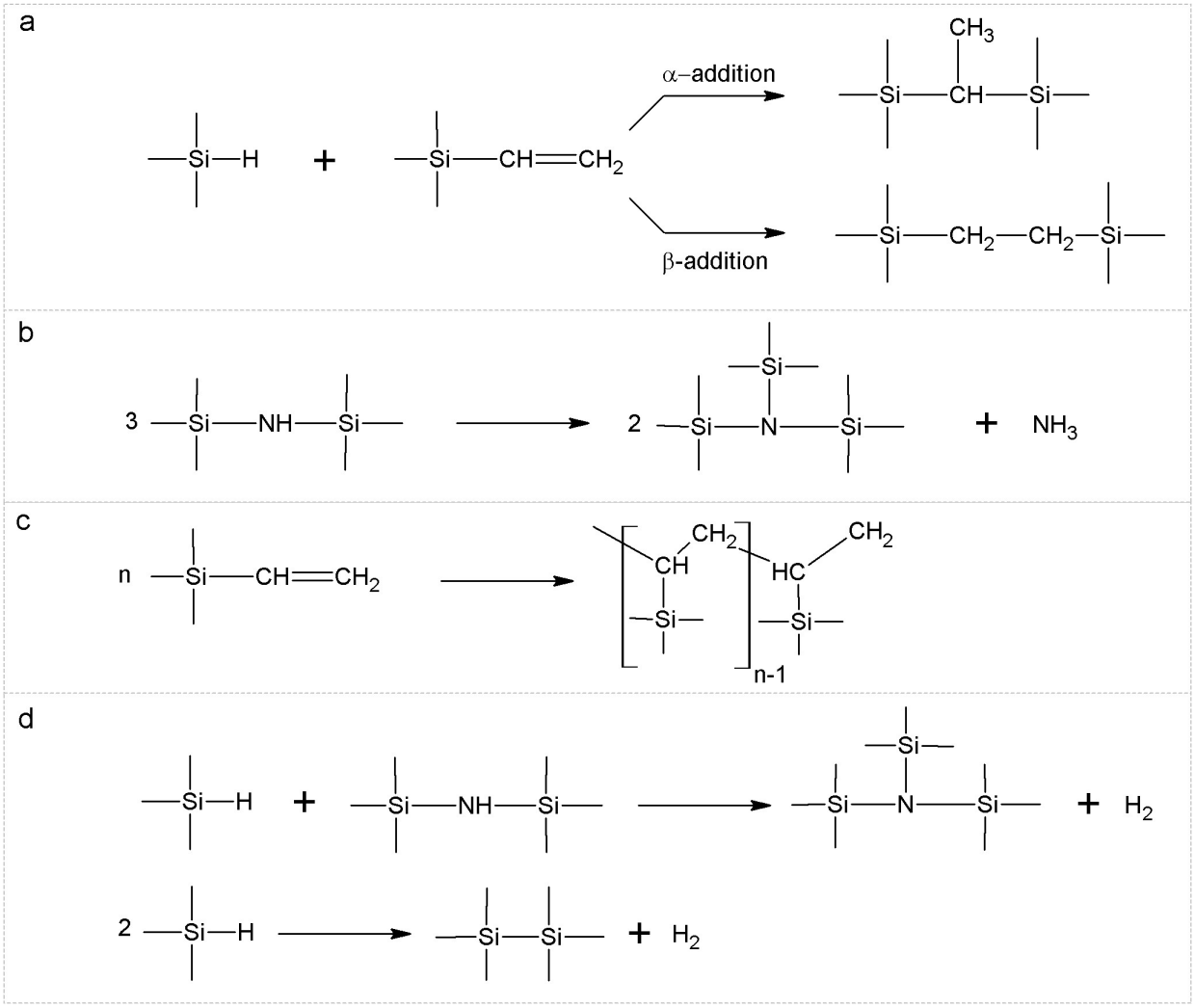

Source: Adapted from Kroke et al. (2000) and Choong Kwet Yive et al. (1992)

to thermoset. To the second step, 400 - 700 ℃, is attributed the highest weight loss, with the evolution of organic substituents and other volatile products. The last step is above 700 ℃, when almost no weight loss is detected. The polymer-to-ceramic transition is usually associated with a weight loss of typically 10 to 30 wt%. The reactions result in the formation of amorphous ceramics, normally at 800-1000 ℃, with large shrinkage due to the variation in the polymer density, normally from about 0.8-1.2 g.cm^{-3} to 2.2 g.cm^{-3} (CHOONG KWET YIVE et al., 1992; LI, Y.-L. et al., 2001; GUNTHNER et al., 2011; FLORES et al., 2013; COLOMBO; MERA, et al., 2010; KONEGGER et al., 2016; CHAVEZ et al., 2011; IONESCU; KLEEBE; RIEDEL, 2012; COLOMBO; BERNARDO; PARCIANELLO, 2013; BERNARDO et al., 2014).

The pyrolysis atmosphere is determinant for the definition of the final ceramic material. Selecting a reactive gas interferes in the nature of the precursor and thus the ceramic. Pyrolysis of polysilazanes under ammonia is greatly used because it leads to essentially pure Si_3N_4, independent of the type of polysilazane. Furthermore, ammonia can be applied to remove carbon from ceramic powders. Choong Kwet Yive et al. (1992) studied the pyrolysis of different polysilazanes under argon and ammonia by means of thermogravimetric analyses coupled with mass spectroscopy of the evolved gases. Under argon atmosphere the main reactions that could be observed were transamination and dehydrocoupling between N-H and Si-H bonds followed by homolytic cleavages of Si-H and Si-C bonds. When ammonia was applied the polymer decomposition happened through different processes, that depended on the nature of the organic groups. In the case of Si-H bonds, which are sensitive to nucleophilic substitution, the predominant amination reaction occurs by means of nucleophilic substitution by ammonia. For methyl and phenyl bonds however, free-radical substitution was the most likely reaction, because of the homolytic cleavages of Si-C bonds. The poly(methyl)silazanes and poly(phenylsilsesquiazane) presented amination of silicon between 300 and 750 °C, before ammonia thermal decomposition. For poly(vinyl)silazanes, the vinyl groups were not completely displaced by ammonia, which favored the formation of unsaturated excess carbon, which was eliminated above 750 °C, when reacted with ammonia decomposition products.

In summary, perhydropolysilazanes do not present carbon in their structure, as shown in Figure 7, so they are seen as ideal sources of carbon-free silicon nitride ceramics, however it has been demonstrated that ammonia is a reactive gas that can efficiently remove the carbon during pyrolysis if carbon-containing polysilazanes are applied.

2.2.2 Polymer-Derived Silicon Nitride

Silicon nitride ceramics are heterogeneous, multicomponent materials, composed by three silicon atoms and four nitrogen atoms, as Si_3N_4. It is extremely rarely found in natural sources and present no significance as a raw material. Thus, all Si_3N_4 ceramics are derived from synthetic materials. As mentioned in the previous section, following the PDC route it is possible to produce crystalline Si_3N_4 or amorphous SiN_x ceramics from polysilazanes composed by Si, N and H or by Si, N, C and H pyrolyzed under ammonia atmosphere.

Silicon nitride ceramics are characterized by their two main crystalline modifications: α, adopting a simple hexagonal close packing arrangement and β, a more complex stacking sequence of the close packed layers (Figure 9). These groups consist in different engineered materials with interesting applications. The main properties that make silicon

nitride ceramics be investigated are their lightness, mechanical and thermomechanical behavior, resistance to wear and corrosion and compatibility with metals (PETZOW; HERRMANN, 2002; PATEL; MIOTELLO, 2015).

Figure 9 – Crystal structures of α and β-Si_3N_4

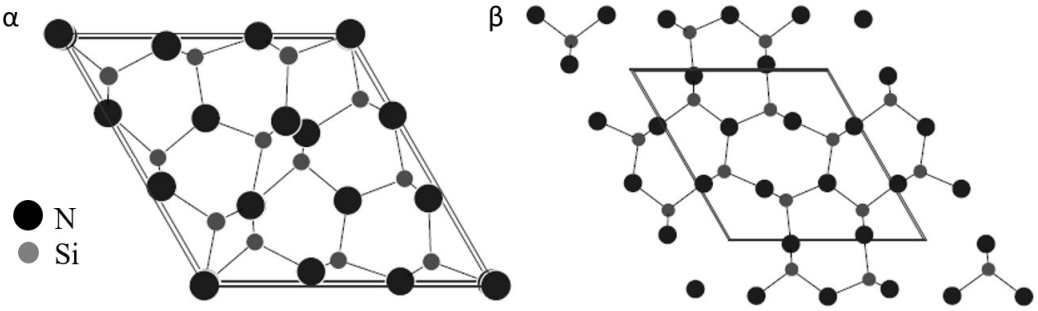

Source: Adapted from Petzow and Herrmann (2002)

Along with the crystal structure, the microstructure has a strong influence on the characteristic properties of such ceramics, so that higher requirements for the ceramics mean rigorous demands on the microstructure. Factors as type, amount, arrangement, size, shape and orientation of the phases have significant contribution to the material microstructure. These factors also result in the defects the material might contain: vacancies, dislocations, grain boundaries, pores and cracks. In addition, the microstructure is an important domain within the science of materials. Therefore, the amount, distribution, size and morphology of the α and β-particles, secondary and amorphous phases are crucial aspects for the quality and reliability of silicon nitride ceramics (PETZOW; HERRMANN, 2002).

PDCs are complex systems that go through deep microstructural changes upon heating to high temperatures. Studies demonstrated that high temperature properties of ceramics such as resistance to crystallization and to thermal degradation rely on the microstructure of the amorphous phase. The presence of nanodomains even at very high temperatures is one of the most interesting and curious characteristics of PDCs, and it might be a reason for the notable resistance of such ceramics to crystallization (COLOMBO; MERA, et al., 2010). In addition, the molecular structure of the starting polymer precursor has a strong contribution to the solid state structure and microstructure of the final ceramic (RIEDEL; MERA, et al., 2006). Pure Si_3N_4, for example, usually crystallizes above 1200-1300 ℃, but this process can be delayed with the presence of a suitable second phase in the material, that can be inserted at molecular scale (BIROT; PILLOT; DUNOGUES, 1995).

Glatz et al. (2010) synthesized copper aminopyridinato complexes and used them to metal-modify the commercially available polysilazane HTT 1800. The authors obtained copper-modified silicon carbonitride ceramics (Cu@SiCN) with crystallites and particles of different sizes. This molecular approach enables to tailor the copper amount and, to some extent, the particle size.

Schwab and Page (1995) investigated the microstructure of PHPS-derived Si_3N_4 by Scanning Electron Microscopy (SEM) and Transmission Electron Microscopy (TEM). The ceramic preparation consisted in the pyrolysis of PHPS to 1000 ℃ under nitrogen, followed by grounding the product and then classifying it through a 140 inch mesh. The product was then mixed with additional PHPS, pressed and pyrolysed until 1500 ℃. The product microstructure consisted of micrometer size grains, that were composed by sub-micron crystallites as well as fibrils with diameter of 40-50 nm. The authors affirm the crystallites are probably generated from the condensed phase during pyrolysis, while the fibrils are probably produced from the vapor phase.

PHPS has also been used with nanoparticle catalysts in order to control the single crystal Si_3N_4 nanowires and branched structures, and there is a high number of studies that use PHPS as the matrix phase in composite materials (HECTOR, 2016). Several strategies are reported on the production of ceramic–ceramic or metal–ceramic (nano)composites, that can be developed to enhance an specific property or to provide new functionalities. They can be called multifunctional materials, and are more weight and volume efficient, possess high flexibility without losing performance and function, besides presenting less maintenance needs (CHRISTODOULOU; VENABLES, 2003).

In this multifunctional materials branch, the PDC route offers the ability to synthesize silicon-based multicomponent ceramics through chemical modification of the precursors. During crystallization of the obtained amorphous ceramics the material is divided into thermodynamically stable phases, with its ratio controlled at molecular or atomic level. Thus, the PDC-route is expected to generate high-performance silicon-based multifunctional ceramics (IWAMOTO; KIKUTA; HIRANO, 2000a).

2.2.3 Transition Metal-Modified Silicon Nitride

Si_3N_4 reacts with Ni and Co at temperatures above 700 ℃ and might form silicides at greater temperatures. When in contact with titanium, zirconium and hafnium, silicide or nitride formation is possible, depending on the processing (PETZOW; HERRMANN, 2002). Several studies report the chemical modification of polysilazanes with transition metal alkoxides and non-oxidic organometallics. Additionally, transition metal nitrides have specially attracted the scientific environment attention due to their efficiency as electroca-

lysts for energy-related reactions, including hydrogen and oxygen evolution reactions as well as oxygen reduction reactions and methanol oxidation reactions. The catalytic activity of transition metal nitrides is associated to their unique electronic structure that results in high performance behaviour during the catalytic processes. However, locating the active sites for reactions is a great challenge in the development of such materials. Thus, elaborating new methods as well as improving the already known techniques to produce nitride structures with uniform and specific facet exposure is essential for optimization of energy-converting efficiency (XIE; XIE, 2016).

Iwamoto, Kikuta, and Hirano (2000a) synthesized multicomponent amorphous powders modifying PHPS with yttrium triisopropoxide and tetrakisdimethylaminotitanium. The authors obtained amorphous Si_3N_4 below 1400 ℃ under N_2. Above 1600 ℃, α and β-Si_3N_4 phases were obtained, and at 1800 ℃ it was possible to generate β-Si_3N_4-Ti(C, N)-Y_2O_3 ceramics. The ceramic refinement and microstructure uniformity were attributed to the titanium action as a catalyst on the formation of nano/micro Ti(C, N) and the acceleration of β-Si_3N_4 formation.

In further work, Iwamoto, Kikuta, and Hirano (2000b) focused on the synthesis of polytitanosilazanes by modifying PHPS with tetrakisdimethylaminotitanium and titanium tetra-isopropoxide - TiX_4 [X=$N(CH_3)_2$, $OCH(CH_3)_2$)] - in order to study the crystallization and microstructure development of Si_3N_4-TiN powders. The main objective of this study was to introduce titanium nitride (TiN) as a particle-reinforcement for Si_3N_4 by improving the fracture toughness and strength. Through FTIR and ^{1}H NMR analyses it was possible to verify that PHPS reacted with TiX_4 [X=$N(CH_3)_2$] to form N-Ti bonds, whilst for TiX_4 [X=$OCH(CH_3)_2$)], the produced $HOCH(CH_3)_2$ reacted with N_2SiH_2 from PHPS to form N_2SiH-$OCH(CH_3)_2$ groups and Si-N bond cleavage to some extent. The polymers were treated at 1000 ℃ under NH_3 and at 1800 ℃ under N_2. For pure PHPS, the first α- and β-Si_3N_4 started to appear at 1200 ℃, but for the titanium-modified polymers, the products still presented amorphous structure at 1400 ℃, exhibiting growing crystallization above 1600 ℃. This result shows that titanium was effective to suppress crystallization of Si_3N_4. Additionally, the poly-titanosilazane derived from PHPS and $Ti(N(CH_3)_2)_4$ resulted in Si_3N_4-TiN ceramics after heat treatment at 1800 ℃, and TiN particles smaller than 100 nm were observed by TEM analysis, proving that this approach is suitable to yield TiN nanoparticle-dispersed Si_3N_4 ceramics.

Yuan et al. (2014) prepared SiHfBCN ceramics using the polysilazane HTT 1800 containing Si-H and Si-vinyl groups chemically modified firstly with tetrakis(diethylamido) hafnium complex and then with borane dimethyl sulfide complex. The polymers were synthesized with different ratios between the polysilazane and the complexes, and were heat treated under N_2 or Ar until 1700 ℃. The materials annealing lead to ceramic nanocompos-

ites with interesting phase compositions: SiC/HfC(N)/HfB_2 in argon and Si_3N_4/HfNC/SiBCN in nitrogen. The produced ceramics are candidates for ultrahigh temperature ceramics and under extreme conditions, and the applied process could be extended to other materials compositions, such as MN/Si_3N_4, MN/SiCN or MCN/SiCN (M = Ti, Zr, Hf), depending on the pyrolysis/annealing conditions.

Studies published by the research group from Dr. Samuel Bernard, co-supervisor of this thesis, report the development of titanium nitride-silicon nitride nanocomposites. Bechelany, Proust, Gervais, et al. (2014) investigated the in situ controlled growth of TiN in amorphous Si_3N_4 without impurities. The synthesis consisted in a three-days reaction between $Ti(N(CH_3)_2)_4$ and PHPS, with a Si:Ti ratio of 2.5 that generated a perhydropolytitanosilazane relatively highly crosslinked. The objective was to shape this material as dense pellets, however it is essential to have a low weight loss during pyrolysis, to avoid large shrinkage and cracks. So, after synthesis, this inorganometallic precursor was ammonolyzed at –40 °C according to a procedure established for metal dialkylamides. This material was then warm-pressed, generating green bodies that were treated under NH_3 at 1000 °C and subsequently under N_2 at 1300 °C. The weight loss of the compound at 1000 °C decreased from 37.5 % to 30.4 % after ammonolysis, which shows the efficiency of this method. The final material consisted of 2-5 nm TiN particles embedded in an amorphous Si_3N_4 matrix, and displayed compositional and nanostructural homogeneity, attributed to the chemical composition of the precursors. In addition, the nanocomposite exhibited very high hardness values of 25.1 GPa. Veprek et al. (2000) have extensively studied films composed by nanocrystalline-TiN on amorphous Si_3N_4 matrix with ultrahardness, high fracture toughness and elastic recovery. The authors explained that these properties are a simple consequence of such nanostructure. The same authors also observed that Si_3N_4 prevents the oxidation of MN on applications at high temperatures.

Bechelany, Proust, Lale, et al. (2017) investigated the chemistry behind the design of TiN/Si_3N_4 nanocomposite and pointed out that this approach can be extended to other metals as the source of metal nitride nanocrystals and also to other single-source percursors as the matrix. Furthermore, a polymethylsilazane (PMSZ) and a polyvinylsilazane (HTT 1800) were also tested, and the Si:Ti ratios variated from 1 to 10. Lale, Proust, et al. (2017) observed that the crystallization behaviour of the polytitanosilazane-derived SiTiN ceramics is lead by the chemistry of the polyorganosilazanes and the Si:Ti ratio applied for the polytitanosilazane synthesis. The use of PHPS with a Si:Ti ratio below 2.5 yielded TiN/Si_3N_4 nanocomposites highly stable against Si_3N_4 crystallization. Regarding the application range, the group addressed such materials for functional applications in energy and environmental science.

An example of another transition metal used to chemically modify a polymeric pre-

cursor is in the work carried out by Zhang, Smith, and Wu (2007). Firstly a cobalt complex named tris(ethylenediamine-k^{2}N)cobalt(III) chloride ($[Co(en)_3]\cdot Cl_3$) was synthesized by $CoCl_2$ and used in a reaction with a poly[(methylvinylsilazane) -*co*- (methylhydrosilazane)] to yield a polycobaltsilazane that was then shaped as nanofibers by electrostatic spinning. The authors believe that during the reaction, the complex was first reduced to Co metal clusters, that promoted hydrosilylation reaction. The obtained fibers presented fluorescence that could be tuned by controlling excitation wavelengths in the visible range at low temperatures.

Based on the exceptional properties of Si_3N_4 and the wide range of possibilities given by the multicomponent ceramics science, it is possible to consider these materials as ideal candidates for catalytic supports. As mentioned in section 2.1.1.1, such supports should ideally present high surface area and the catalyst should be homogeneously distributed over the support, so that the active sites are readily available. The PDC route has been greatly investigated in order to elaborate ceramics with tailored porosity, however their application as metal-supports porous PDCs is still limited. In the following section, the science involved in the obtention of mesoporous ceramics via PDC route is comprised.

2.2.4 Mesoporous materials obtained through the PDC-route

Regarding the use of the PDC route to obtain porous materials, the literature reports two main methodologies: hard-template and soft-template. The use of templates is one of the main strategies for the manufacture of advanced materials with new structures in nano and micro scales, such as micro and mesoporous materials, and has attracted considerable efforts for its research in the last few decades. Hard-templates usually consist of solid-state materials with characteristic structure and morphology, and soft-templates are usually composed of materials in the fluid state (RODRIGUEZ-ABREU et al., 2011).

The concept of these templates started (on a macroscopic scale) as the moulding process when a hard wax, metal or plaster template is used. The interior of the mould is filled with the material to be processed and then the model is removed (LU; SCHUTH, 2006).

The soft-template approach can also be efficiently used for the introduction of porosity in ceramics. However, adjustment of the molecular and chemical structure of the precursor is necessary. The conformation of the pores is defined by a soluble structural directing agent (SDA), usually a block copolymer (BORCHARDT et al., 2012).

Strategies for incorporating metals into porous structures applying the soft-template approach have been reported with successful results. Ortel et al. (2012) studied the development of catalytic coatings where the active phase, composed of Pd nanoparticles,

is homogeneously distributed in mesoporous and meso-macro-porous TiO_2 films, in the elaboration of membranes. The objective was to observe if the synthesis strategy had the potential to control the size of nanoparticles, mesopores and macropores independently. The authors stated that the balance between large surface area and rapid diffusion of pores can be achieved in hierarchical porosity systems, where larger pores facilitate rapid transport while smaller ones provide large surface areas, supporting active metal sites. The optimization of membrane performance requires control over the pore morphology, as well as the number and size of the metallic nanoparticles.

Thus, the authors prepared mesoporous and meso-macro-porous TiO_2 films from a titanium precursor. For mesoporous films, they used two block copolymers using a co-assembly technique to provide the desired porosity, Pluronic F127 and 10k-PB, which generated mesoporous films with a pore size distribution of 7 and 21 nm, respectively. For the production of meso-macro-porous films, poly(methyl) methacrylate (PMMA) spheres were synthesized and used as sacrificial agents. They were mixed with the commercial copolymer Pluronic F127. The prepared films were then dipped in a solution containing Pd nanoparticles dispersed in H_2O (dip-coating technique). The combination of the block copolymer with the PMMA spheres produced TiO_2 films with hierarchical porosity, i.e. with mesopores located inside macroporous walls. The final materials had a nanocrystalline structure and exhibited large surface areas (160-200 $m^2.cm^{-1}$). Both structures (meso and meso-macro-porous) proved to be highly active and selective in the hydrogenation in gas phase from 1,3-butadiene to butenes.

The hard-template methodology is considered highly effective for the preparation of hollow structures that simulate (imitate) and complement the original conformation of the template. It is a well established technique known as nanocasting, which is adapted from the macro- to the nanoscale, and basically consists on the steps enumerated below. This approach can be associated to the PDC-route, whereas a preceramic polymer is infiltrated in the porous structure of the template, and then is thermally treated for the ceramic formation and template removal (Figure 10).

1. Formation of the template;
2. Casting step with the desired precursor (the impregnation of a preceramic polymer);
3. Removing the template during the polymer-to-ceramic conversion, to obtain a hollow structure that is a negative image (an inverse replica) of the initial template.

Nanocasting offers great versatility in relation to pore morphology, size, arrangement and distribution, consequently increasing the control over the nanostructure of catalyst supports (BERNARD; MIELE, 2014).

Figure 10 – The PDC route associated to the hard-template approach towards mesoporous ceramics

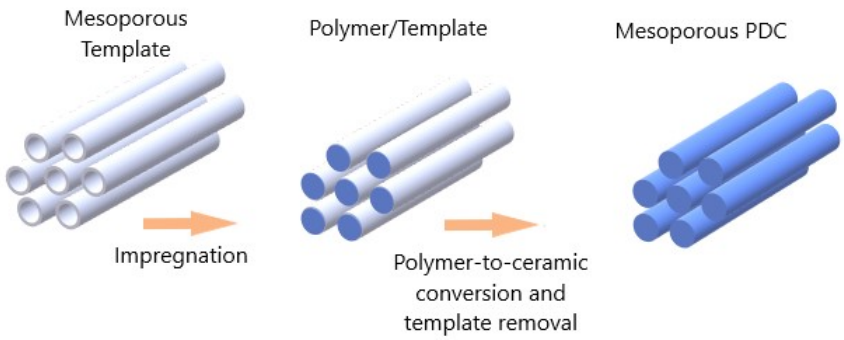

Source: Adapted from Lu and Schuth (2006)

The material porosity can be determined by three main parameters: specific surface area (SSA), total pore volume and pore size distribution (PSD). According to the IUPAC classification, porous solids can be classified according to the pore size (w) as: micro- (w < 2 nm), meso- (2 nm < w < 50 nm) and macroporous (w > 50 nm). Such classification is better applied when the geometrical shape of the pores is known and well defined. Some examples of pore geometry are: cylindrical, ink-bottled, slit-shaped and cone-shaped (ROUQUEROL et al., 1994; KANEKO, 1994).

Macropores lower flow resistance and facilitate physical transport, i.e. improve the mass transfer through the pore network, whilst the micro- and mesopores provide selectivity and active sites to be effectively acessed for catalysis and separations. Mesoporous structures offer great surface areas with relatively small volumes. The presence of mesopores enhances the diffusion properties of the material and increases the amount of accessible active sites (GROEN et al., 2007).

The pore structure of a material affects its performance in their applications, impacting dissolution rates, electron/ion current density at electrode interface with electrolyte, adsorption capacity and represents surface free energy available for bonding in tabletting and sintering (ERTL et al., 2008).

Zeolites, alumina membranes, ordered mesoporous silica or carbon have been employed as template to replicate other materials. 2D-hexagonal (e.g. SBA-15, CMK-3) and 3D-cubic (e.g. KIT-6, CMK-8) comprise the most common silica and carbon mesoporous materials. Activated carbon is a great template example for the creation of high-surface-area materials. They are cheap, readily available in different pore sizes and volumes and their surface polarity can be adjusted (SCHUTH, 2003).

In general, the template performance is driven by its composition, shape and poros-

ity characteristics. Nonetheless, it does not participate in the reactions that involve the polymer-to-ceramic conversion. Still, the replication of the templates display some difficulties, mainly due to three reasons. According to Borchardt et al. (2012) they are:

- Volume shrinkage of the preceramic precursors;
- Volatility of such precursors or synthesis intermediates;
- Difficulty to preserve the shape and ordering of the templates during thermal treatments in the nanocasting process.

Nanocasting process has been largely applied mainly for oxide ceramics, whereas the elaboration of porous silicon nitride, carbide and carbonitride ceramics are still limited because of the air and moisture sensitivity of the preceramic precursors (BERNARD; MAJOULET, et al., 2013). Our research group has recently published a review on PDCs with engineered mesoporosity for catalysis applications [Lale, Schmidt, et al. (2018)], more focused on non-oxide ceramics, reporting the different approaches to obtain such materials and their use as supports for metallic nanoparticles. This review has a significant impact because it is part of an ongoing development of polymer-derived porous materials for environmental and energy applications. Some works that were reported in the past years and that were the main drivers of ther current thesis are reported below.

Salameh et al. (2015) proposed in their study the synthesis of ordered mesoporous Si_3N_4 nanoblocks with hexagonal symmetry by nanocasting. Mesoporous carbon CMK-3 was chosen as hard template and PHPS was used as ceramic precursor. PHPS in xylene solution (20 wt%) was infiltrated in the template. The polymer-to-ceramic conversion was performed under N_2 to 1000 °C followed by a second cycle to the same temperature but under NH_3 for template removal. It resulted in the formation of mesoporous Si_3N_4 nanoblocks with SSA of 772.4 $m^2.cm^{-1}$, PSD of 4.83 nm and pore volume of 1.19 $cm^3.g^{-1}$. The materials were then used as supports to nucleate platinum nanoparticles (obtained through the reduction of $H_2PtCl_6{\cdot}6H_2O$), resulting in particles of 6.77 nm. The samples were subjected to hydrolysis of $NaBH_4$ at 80 °C and generated 13.54 $L.min^{-1}.g_{Pt}^{-1}$. This value was superior to mesoporous Si/Al/C/N impregnated with Pt nanoparticles, produced using the same pathway (5.67 $L.min^{-1}.g_{Pt}^{-1}$). It was also superior to Pt-supported CMK-3, demonstrating the attractivity of Si_3N_4 compared to carbon as Pt-support. Besides the excellent results, this work was particularly important to testify the starting development of non-oxide ceramics, mainly nitride- and carbonitride-based, for heterogeneous catalysis. Taking into account the recyclability of borates and the stability of the obtained Si_3N_4 nanoblocks, the material provides interesting performance for the implementation of $NaBH_4$ as a hydrogen source for fuel cell applications.

Sachau et al. (2016) worked with the soft-template approach, using the self-assembly of block copolymers to generate micro-/mesoporosity in the material. For that, polyethylene hydroxide was mixed with a polysilazane and then an aminopyridinato ligand-stabilized Pt complex was used to chemically modify the precursor. The Pt:Si ratios were 1:10, 1:20, 1:40 and 1:60. The template was removed during the heat treatment under nitrogen to 1000 °C and Pt^{II} was reduced to Pt^0 due to the in situ generation of methane, ammonia, and hydrogen, generating Pt@SiCN with Pt nanoparticles of 0.9-1.9 nm and maximum SSA of 259 $m^2.cm^{-1}$. When tested as heterogeneous catalysts in the hydrolysis of $NaBH_4$, the maximum rate was measured for Pt:Si ratio 1:60, that was 38.1 $L.min^{-1}.g_{Pt}^{-1}$.

Lale, Wasan, et al. (2016) used three preceramic polymers, namely allylhydridopolycarbosilane (AHPCS), HTT1800 and PHPS, to form mesoporous 3D structures of SiC, SiCN and Si_3N_4. As hard-template, mesoporous activated carbon of monolith/rod type was selected, presenting a SSA of 953 $m^2.cm^{-1}$ and pore size of 2.1 nm. The impregnated monoliths were subjected to pyrolysis for ceramic conversion and template removal at 1000 °C and further heat treatment to observe the porosity evolution with the temperature until 1600 °C. Moreover, Pt nanoparticles were directly reduced on the monoliths that presented the best SSA results by a procedure consisting on wet impregnation of $H_2PtCl_6{\cdot}6H_2O$, targetting 1 wt% of Pt, followed by heat treatment under H_2/Ar flow at 450 °C. The best SSA results for each sample before impregnation were: 581.4, 623.7 and 653.8 $m^2.cm^{-1}$ for SiC-monolith at 1200 °C, SiCN-monolith at 1200 °C and Si_3N_4-monolith at 1000 °C, respectively. After impregnation, the SSA reduced around 40 %, which suggests the encapsulation of Pt nanoparticles inside the pore channels. A hydrolysis rate of 24.2 $L.min^{-1}.g_{Pt}^{-1}$ was measured for Pt/Si_3N_4-monolith.

Lale, Proust, et al. (2017) used nanocasting to produce mesoporous SiTiN monoliths from polytitanosilazanes (as mentioned in section 2.2.3). Very high SSA values were obtained, varying between 1352 and 1797 $m^2.cm^{-1}$ for monoliths treated at 1400 and 1700 °C, respectively, proving the great stability of SiTiN ceramics at high temperatures and the ability of the transition metal-modified polymer to be used in the preparation of ceramics with tailored mesoporosity.

Therefore, it is possible to affirm that mesoporous 3D structures can be successfully prepared by nanocasting coupled with the PDC route. The possibility of using transition metals to chemically modify the precursor and/or impregnate the mesoporous ceramics with metal nanoparticles turn the association of these strategies a breakthrough achievement for the synthesis of new advanced materials for energy applications.

2.3 FINAL REMARKS ON THE LITERATURE REVIEW

This chapter comprised the research on the literature that guided this thesis work. The survey over technologies to generate energy from clean resources has been increasing year after year. Hydrogen is largely mentioned and seen with great perspective as the main character of the energy future. Sodium borohydride is a safe hydrogen storage material, however a lot of research over materials that can withstand the harsh conditions imposed by its hydrolysis must be done. In addition, heterogeneous catalysis is largely impacted by the specific surface area and requires pore morphologies that allow molecular transport to promote accessibility of active sites (ERTL et al., 2008).

The robust nature of ceramic materials makes them excellent candidates for the application as catalytic supports for hydrogen carriers, here $NaBH_4$. Non-oxide ceramics such as SiC, SiCN and Si_3N_4 differs from oxide supports showing higher resistance under extreme pH values and high temperatures. Considering mainly Si_3N_4, it was possible to observe that the interactions with the adsorbed reacting species and the catalytic properties of nitrides make such ceramics as the most appropriate candidates to be used as Pt supports for the hydrolysis of $NaBH_4$ in alkaline solution (pH > 13). However, the literature reports only a few papers concerning the application of Si_3N_4 as catalytic support materials.

The well documented ability of some transition metal nitrides to exhibit catalytic properties which are similar to platinum group metals as well as the acid-base properties of nitrides demonstrate interesting possibilities for the elaboration of nitride ceramics for catalysis applications.

Chemical modification of preceramic polymers by metals is a convenient approach taking into consideration that organosilicon precursors are in most cases soluble in polar and non-polar solvents and contain reactive groups that can easily react with metallorganic compounds.

The polymer-derived ceramics route offers an extremely large potentiality to produce advanced ceramics with tailored properties. It was demonstrated that organosilicon precursors can be chemically modified still at the first steps of the process. The design of nanocomposites exhibiting combining action with the metal is seen as a great strategy to optimize the catalytic properties of polymer-derived nitrides. Furthermore, when the PDC-route is associated to a templating process such as nanocasting, ceramics with highly controlled porosity and great specific surface area can be achieved.

Accordingly, this thesis reports the chemical modification of PHPS with titanium and vanadium, and, for the first time, with molybdenum, cobalt and nickel, besides the synthesis and deposition of platinum, cobalt and nickel nanoparticles on SiTiN mesoporous

monoliths, focusing on the production of micro-/mesoporous ceramics with high SSA and PSD for the hydrolysis reaction of $NaBH_4$.

3 MATERIALS AND METHODS

This chapter contains the experimental part of the thesis and it is divided in four main sections: materials, synthesis of metal-modified/doped preceramic polymers, preparation of mesoporous materials and characterization techniques. The first section presents the materials applied for all the syntheses reported in this thesis. The second section is subdivided in two subsections: synthesis of metal-modified silicon nitride nanocomposites (MN/Si_3N_4, M= Ti, Mo, V) and synthesis of metal-doped silicon nitride ($M@Si_3N_4$, M= Co, Ni). These syntheses were split because different metal precursors and/or pyrolyses methods were used.

The third section is related to the elaboration of mesoporous materials using the nanocasting approach, which was employed for the metal-modified/doped polysilazanes obtained in the second section. The generation of monoliths based on metal-doped silicon oxynitride ($M@Si_3N_4$, M= Co) is also described. The fourth section includes the characterization equipments and analyses specifications applied to and evaluate the produced materials.

The syntheses and characterizations of MN/Si_3N_4 (M= Ti, Mo, V) and $M@Si_3N_4$ (M= Co, Ni) were perfomed at IRCER, *Institut de Recherche sur les Céramiques*, in France, whilst the synthesis of M@Si-O-N (M= Co) was carried out at UFSC, *Universidade Federal de Santa Catarina*, in Brazil.

The accomplishment of such activities in France was possible due to a project from Coordination for the Improvement of Higher Education Personnel (CAPES) that financially supported the doctorate sandwich program for the author of this thesis.

3.1 MATERIALS

The chemical products that were used in the experimental procedure are listed in Table 3. All the products were handled in an argon-filled glove box (Jacomex JP(Campus); O_2 and H_2O concentrations kept at < 0.1 ppm).

Based on previous works from the group, presented in the literature review, the main organosilicon polymer that was selected as preceramic precursor was PHPS (MW: 45.117 $g.mol^{-1}$). Since it is highly reactive, PHPS is commercially available in 20 vol% solutions in di-n-buthylether to prevent it from RT crosslinking. Its density and viscosity are between 1 and 1.1 $g.cm^3$ and between 30 and 50 mPa.s at 25 °C, respectively. Hence, before all the reactions, the solvent was removed from PHPS at room temperature under reduced pressure (as described in the next section). HTT 1800 (MW: 65.365$g.mol^{-1}$) was also tested in some reactions, and presents viscosity of 20-50 mPa.s and density of 1 $g.cm^3$.

Table 3 – Chemical products applied in the syntheses

	Chemical	Manufacturer
1.	PHPS, perhydropolysilazane, 20 vol % in di-n-buthylether	Merck Performance Materials GmbH
2.	HTT 1800, vinyl polysilazane	AZ Electronic Materials
3.	Toluene 99.85 % Extra Dry over Molecular Sieve	AcroSeal™ ACROS Organics™
4.	TDMAT, Tetrakis(dimethylamido) titanium(IV) 99.999 % trace metal basis	Sigma-Aldrich
5.	Bis(t-butylimido)bis(dimethylamino) molybdenum(VI) 98%	ABCR
6.	TEMAV, Tetrakis(ethylmethylamino) vanadium(IV) 98%	ABCR
7.	Nickel(II) chloride 98 %	Sigma-Aldrich
8.	Cobalt(II) chloride, anhydrous for synthesis	Merck KGaA
9.	Chloroplatinic acid hexahydrate %	Sigma-Aldrich
10.	Sodium borohydride ≥ 98 %	Sigma-Aldrich
11.	Hexaamminecobalt(II) chloride 99 %	Sigma-Aldrich
12.	Tris(ethylenediamine)cobalt(III) chloride dihydrate	Sigma-Aldrich
13.	Nickel(II) chloride hexahydrate 99.9 % trace metals basis	Sigma-Aldrich
14.	Ethylenediamine ≥ 99 %	ReagentPlus®, Sigma-Aldrich
15.	Ethanol 96 %	Sigma-Aldrich
16.	Acetone ≥ 99.5 %	Sigma-Aldrich
17.	Ammonia solution 28-30 %	EMSURE®, Sigma-Aldrich
18.	Activated Carbon Monolith	Norit RX3®Extra, Cabot Corporation
19.	Sodium Hydroxide 98 %	Sigma-Aldrich

3.1.1 Perhydropolysilazane, PHPS

Since PHPS was applied all over this work, this subsection is dedicated to present the main charateristics of this material and its derived ceramic, that are well reported in the literature. Figure 11 presents the Fourier-Transformed Infrared Spectroscopy (FTIR) spectrum of PHPS. It is possible to observe the N-H, Si-N-Si and Si-H bonds that are present in its structure, according to the following bands: 3200-3400 cm^{-1} and 1180 cm^{-1} correspond to stretching (ν) and bending (δ) vibrational modes of N-H; 2150 cm^{-1} represents νSi-H and 800-1000 cm^{-1} correspond to Si-NH-Si. Weak signals at 2900-3000 cm^{-1} can be attributed to C-H bonds of protective groups added to the polymer solution (20 vol% in di-n-buthylether) or to residual solvent. The main bonds in PHPS are also confirmed by

^{1}H liquid NMR, which spectrum presents signals at 0.5 to 2.0 ppm ($Si_2N\mathbf{H}$), at 4.8 ppm ($Ni_3Si\mathbf{H}/Ni_2Si\mathbf{H}_2$), at 4.34 ppm ($NSi\mathbf{H}_3$) and at 0.1 ppm ($NSi(C\mathbf{H}_2)_3$).

Figure 11 – FTIR spectrum of PHPS

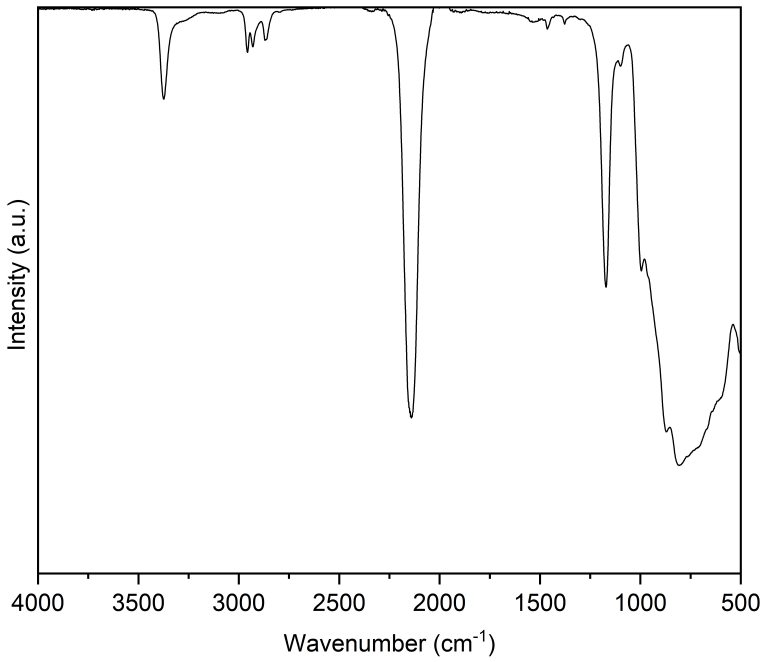

The syntheses of metal-modified/doped polymers and subsequent heat treatments to obtain ceramic materials were conducted taking into account the PHPS features presented in this subsection.

3.2 SYNTHESIS OF METAL-MODIFIED/DOPED PRECERAMIC POLYMERS

All the syntheses were performed under argon atmosphere due to the reagents sensitivity to air and moisture. The manipulations were conducted using a schlenk-line supplied with argon (> 99.995 %), which is purified by passing through successive columns of phosphorus pentoxide (Sicapent®, Sigma-Aldrich) and BTS catalyst (Sigma-Aldrich).

The reactions were performed in a system as the one illustrated in Figure 12. All the glassware was previously dried overnight at 100 ℃ before used. A 3-neck round-bottom flask was placed in an oil bath on a magnetic stirrer with temperature control. The flask was equipped with one inlet for the reagents, one inlet with a valve for argon/vacuum connected to the schlenk-line, and a reflux condenser. After the whole system was placed and connected, it was vacuum pumped for 30 minutes and then filled with argon to guarantee an inert atmosphere for the reaction.

The reactions conditions, type of metal precursor and Silicon:Metal (Si:M) ratio are specified in the following subsections. For all of them, the reaction media was cooled down

Figure 12 – Synthesis reactions setup

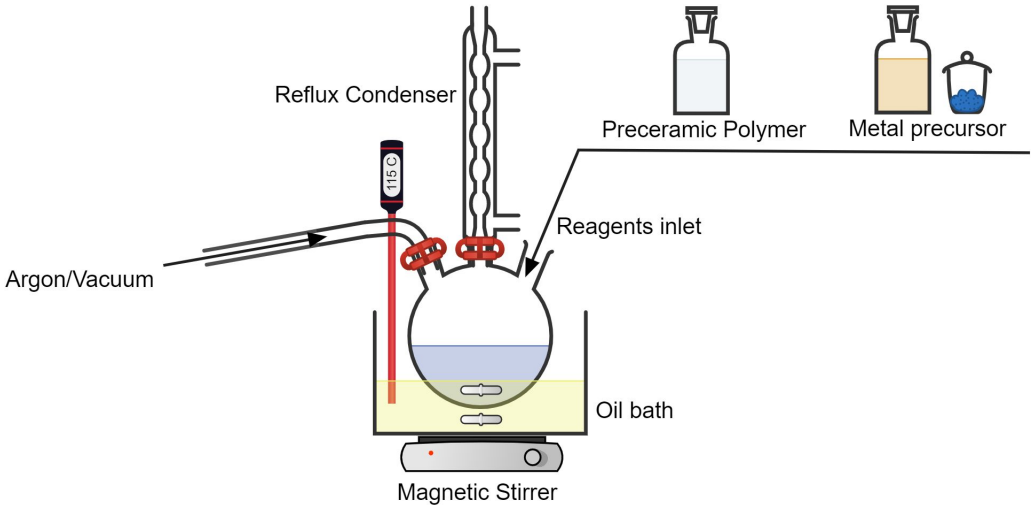

Source: The Author

to room temperature after the appropriate time and the solvent removed under reduced pressure. The system for solvent extraction can be observed in Figure 13. The reaction flask was kept at 30 ℃, connected to a distillation bridge and a schlenk, which was placed in liquid nitrogen. After the full solvent removal, the flask was put inside the glove box, where the polymetallosilazane was transferred to laboratory bottles, PYREX®, with screw cap. All subsequent polymer manipulations were conducted inside the glove box.

Figure 13 – Solvent extraction setup

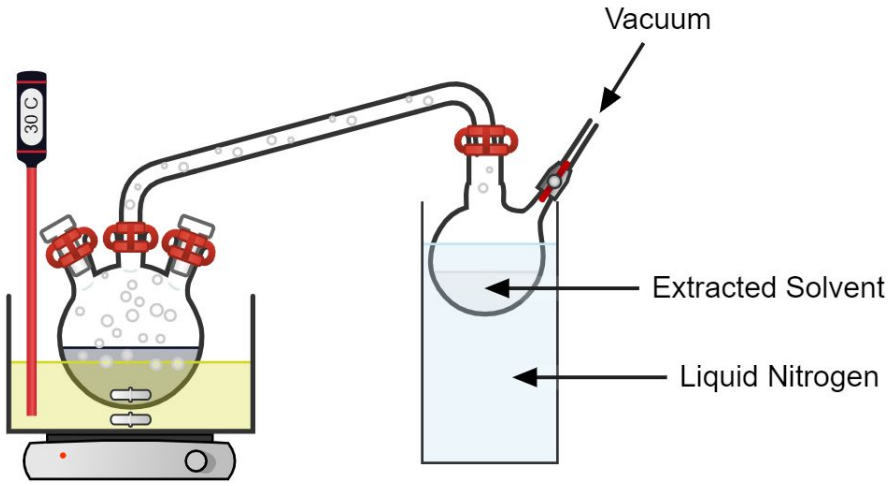

Source: The Author

The polymers were subjected to heat treatments to study their polymer-to-ceramic transformation and the ceramic features. For the pyrolyses done under ammonia, aiming

the formation of Si_3N_4, the treatments were performed in an horizontal tube furnace (Thermoconcept® OS50/450/12), with the samples deposited in alumina crucibles and inserted in the silica tube placed inside the furnace under argon flow. The tube was always pumped under vacuum for 30 minutes before starting the treatment, then filled with ammonia. The maximum temperature was 1000 °C, with a heating rate of 5 °C.min^{-1} and dwelling time of 2 h. Treatments at higher temperatures were conducted in a graphite vertical furnace. The specific pyrolysis conditions for each approach is detailed in the following subsections.

3.2.1 Synthesis of metal-modified silicon nitride nanocomposites (MN/Si_3N_4, M=Ti, Mo, V)

The synthesis of metal-modified polysilazanes, here called polymetallosilazanes was done through a reaction between PHPS and a metallic precursor. The molecular structures of Ti, Mo and V precursors (items 4, 5 and 6 of Table 3), are represented below.

Figure 14 – Titanium, Vanadium and Molybdenum precursors and their respective molecular weight

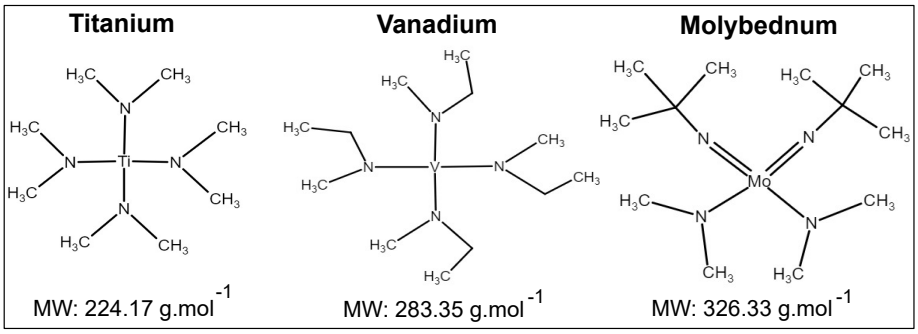

In a system as the one illustrated in Figure 12, 80 mL of toluene were added to the flask under argon flow at room temperature, followed by the addition of PHPS. Finally, the metal precursor was inserted dropwise to the solution. The Si:M (M=Ti, Mo, V) molecular ratio was fixed at 2.5, e.g. m(PHPS):m(TDMAT)= 2.5. This ratio was chosen based on the extensive works published by Bechelany, Proust, Lale, et al. (2017) and Lale, Proust, et al. (2017), that obtained highly crosslinked polytitanosilazanes using PHPS and TDMAT.

After the chemicals addition, the mixture was stirred for 3 hours before heating to 120 °C for three days. All the polymers were black-colored in the end of the reaction and were powders after solvent extraction.

The obtained polymetallosilazanes were named as **PHTiPS2.5**, **PHMoPS2.5** and **PHVPS2.5**. They were subjected to pyrolysis at 1000 °C under NH_3. The polytitanosilazane was also treated at 1400 °C under N_2 with a heating rate of 5 °C.min^{-1} and dwelling of 2 h.

Moreover, since it was found in the literature that the combination of two or more metals may lead to materials with enhanced catalytic properties, a last polymetallosilazane synthesis was tested in this step. For that, a reaction using TDMAT and $CoCl_2$ was carried out. The molecular ratios were calculated for each metal in relation to silicon, therefore: Si/Ti=5 and Si/Co=5. This ratio was chosen based on the studies involving $CoCl_2$ (Section 3.2.2) and on previous studies from the group, which reported that Si/Ti at ratio 5 the crosslinking was lower than at ratio 2.5, hence PHPS would still have available groups to react with $CoCl_2$.

Since there were no methodologies reported on this reaction prior to this thesis, two paths were considered, (a) and (b). Strategy (a) consisted on first mixing TDMAT with PHPS in toluene for 3 hours at room temperature, then adding $CoCl_2$ dissolved in toluene and mixing for more 3 hours and finally heating to 120 °C for 24 h. Strategy (b) consisted on first mixing $CoCl_2$ with PHPS in toluene for 3 hours at room temperature, then adding TDMAT dissolved in toluene and mixing for more 3 hours and finally heating to 120 °C for 24 h. Both reactions lead to black powders, named as (a) **PHTiCo5** and (b) **PHCoTi5**. Adding both metal precursors at the same time could be a dangerous approach, since TDMAT is a very reactive compound. The obtained polymetallosilazanes were treated at 700, 800, 900 and 1000 °C under NH_3 and at 1000 °C under N_2 for comparison.

3.2.2 Synthesis of metal-doped silicon nitride (M@Si_3N_4, M=Co, Ni)

In this approach, $CoCl_2$ and $NiCl_2$ were tested as Co and Ni precursors in reactions with PHPS and HTT 1800. Both chlorides are powders and were manipulated inside the glove box. Taking that into account, a 3-neck round bottom flask was placed inside the glove box and the selected amount of Co/$NiCl_2$ inserted in the flask, which was then taken to the schlenk line. Toluene (50 mL) was added under argon flow, followed by PHPS or HTT 1800 addition. The molecular ratio between Si:M (M= Co, Ni) was fixed at 5.0. The mixture was stirred for 3 hours and then heated to 115 °C, reacting for 3 days. The obtained polymers received the following names to make their identification easier: **PHCoPS5**, **PHNiPS5**, **HTTCo5** and **HTTNi5**.

The polymers were treated at 200, 450, 700, 8000, 900 and 1000 °C to observe the crosslinking reactions and polymer-to-ceramic conversion. Such heat treatments were perfomed under NH_3, 5 °C.min^{-1} rate and 2 h of dwelling.

Reactions with shorter durations (overnight ~15 h) were also tested for PHPS with $NiCl_2$ (**PHNiPS5-15h**) and a more extensive study was performed for PHPS with $CoCl_2$, testing ratios 2.5, 5, 10 and 25. Such reactions originated the polymers named **PHCoPS2.5-15h**, **PHCoPS5-15h**, **PHCoPS10-15h** and **PHCoPS25-15h**.

The final pyrolysis temperature for these polymers was 800 °C, which was defined according to the results obtained in the 3-days reactions. Rate and dwelling specifications were kept the same.

Moreover, two other Co and Ni precursors were also tested. Hexaamminecobalt(II) chloride was used as-received in reaction with PHPS perfomed using the same steps as with $CoCl_2$ on a Si:Co molecular ratio of 5. The system was kept at 115 °C overnight and the final polymer named as **PHCoHex5**. Tris(ethylenediamine)cobalt(III) chloride dihydrate was dried overnight at 100 °C and kept for 1 h under vacuum before transferring to the glove box. After reaction with PHPS (ratio 5), was called **PHCoTris5**. Both polymers were treated at 700 and 800 °C under NH_3.

Two nickel complexes were synthesized to be tested as Ni precursors as well. The procedures were conducted according to the work published by Crouse et al. (2012), using nickel(II) chloride hexahydrate. For the synthesis of tris(ethylenediamine) nickel(II) chloride hydrate ($Ni(en)_3Cl_2{\cdot}2H_2O$), 11.8 g of nickel(II) chloride hexahydrate were dissolved in 20 mL of warm deionized water in an Erlenmeyer flask. This mixture was placed in an ice bath and 10 mL of ethylenediamine were added to it, followed by the slowly addition of 15 mL of ethanol, which formed a purple coloured precipitate. The precipitate was filtered being washed by ethanol and acetone, and then dried at room temperature. The reaction can be observed in Equation 3.

$$[Ni(H_2O)_6]Cl_2 + 3en \rightarrow [Ni(en)_3Cl_2.2H_2O + 4H_2O \tag{3}$$

For the synthesis of hexaammine nickel(II) chloride (4), 6 g of nickel(II) chloride hexahydrate were placed inside an Erlenmeyer flask and dissolved in 10 mL of warm deionized water. After that, 20 mL of NH_3 concentrated solution were slowly added to the system. The flask was placed in an ice bath and 15 mL of cold ethanol were dropped inside, forming a precipitate of lavender colour. The precipitate was washed with ethanol and acetone and dried at room temperature.

$$[Ni(H_2O)_6]Cl_2(aq) + 6NH_3(aq) \rightarrow [Ni(NH_3)_6Cl_2(aq) + 6H_2O(l) \tag{4}$$

Before using the synthesized complexes, they were dried at 100 °C overnight and let under vacuum for one hour before being stored inside the glove box. The reactions with PHPS followed the same procedure as described for Co-complexes, and led to two polymers: **PHNiTris5** and **PHNiHex5**.

3.3 PREPARATION OF MESOPOROUS MATERIALS

Nanocasting was the selected process to produce mesoporous ceramics in this work. Activated carbon monolith/rod type, known as ACM, was used as template. It possess a specific surface area of 953 $m^2.g^{-1}$ and pore size of 5.2 nm. Prior to the nanocasting process, the monoliths were treated at 600 °C for 10 h in a tubular furnace under vacuum (5.10^{-1}). This heat treatment is a passivation process to remove any moisture, residual oxygen or -OH and -COOH groups. After passivation the ACMs were transferred to the glove box.

For the impregnation, the polymers synthesized according to the previous section were kept in toluene solution. The ratio between polymer and ACM was optimized in the thesis of Lale (2017). According to several tests, a polymer/ACM weight ratio of 1.4 was selected, because it was the minimal ratio to avoid the monolith structure to collapse during pyrolysis. Moreover, it was the ratio that could generate great porosity without bringing drawbacks to the mechanical robustness of the material. The monoliths were also impregnated with pure PHPS for comparison.

Figure 15 illustrates the nanocasting process from the ACM impregnation to the obtention of mesoporous metal-modified PDCs. The nanocasting process was performed in a 50 mL schlenk flask. The first step was to weigh the ACMs inside the glove box and put them inside the Schlenk flask with a silicon septum. The flask was then connected to the schlenk-line, where it was put under dynamic vacuum for 1 hour to remove the argon (from the glove box) out of the pores. Keeping the flask under static vacuum, a fraction of the polymetallosilazane in solution was inserted with a syringe. The impregnation is done under reduced pressure to provide a better impregnation of the polymer into the pores. After that, the Schlenk containing the monoliths + the polymer solution, still under static vacuum, was sonicated in an ultrasonic bath for 24 h (Figure 15a). After this, the excedent polymer solution was removed and the monoliths fastly washed with toluene under argon flow. The Schlenk was then put under dynamic vacuum once more to completely remove the solvent (Figure15b). After being taken to the glove box, the monoliths were deposited on alumina crucibles and inserted in the furnace for pyrolysis and template removal (Figure15c).

The polymer-to-ceramic conversion and template removal were conducted according to Lale (2017) optimisations. Hence, this process was done as described: the impregnated monoliths were first treated under N_2 in a 1 °C.min^{-1} ramp to 400 °C, to favor crosslinking reactions, and dwelling for 1 h. Then, the gas was switched to NH_3 and the temperature increased at 1 °C.min^{-1} to a maximum of 1000 °C, dwelling for 5 h. The maximum temperature was chosen according to the ceramic features observed, so it variated for different polymetallosilazanes. The monoliths impregnated with TDMAT were also eval-

Figure 15 – Nanocasting process towards mesoporous materials

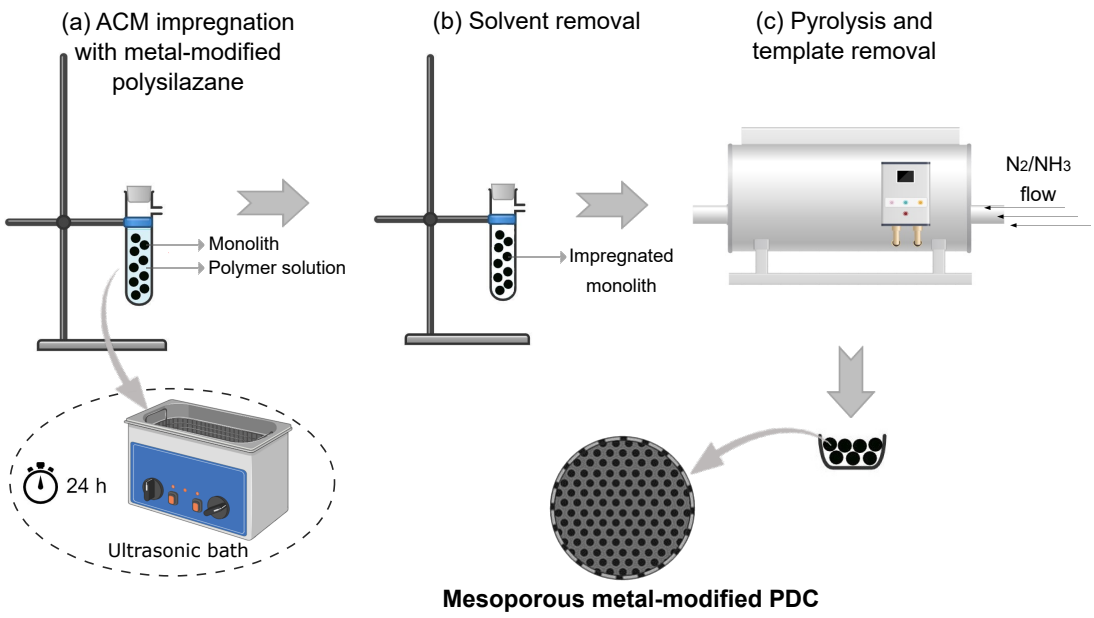

Source: The Author

uated with a second treatment, until 1400 ℃ under N_2 (since the template was removed at 1000 ℃ under NH_3).

Cobalt oxides have also been studied in this work, since they can be effective for $NaBH_4$ hydrolysis (SIMAGINA et al., 2011; KRISHNAN; HSUEH; YIM, 2007). Thus, Co-doped silicon nitride monoliths with the best performance in the catalysis tests were further studied in oxide systems. For that, the selected **PHCoPSX-15h** (X=Si:M Ratio), were used for impregnation applying the same methodology. However, after the crosslinking step under nitrogen until 400 ℃, the gas was switched to air instead of ammonia, aiming at the production of metal-doped silicon oxynitride (M@Si-O-N, M=Co) monoliths. For the pyrolyses done under air, the monoliths were deposited on alumina crucibles and transferred to a tubular alumina furnace (VHTEX). The maximum applied temperature was 800 ℃. The monoliths performances as catalyst supports for hydrolysis of $NaBH_4$ were compared with the ones in the nitride system.

3.3.1 Synthesis of Pt, Co and Ni nanoparticles on mesoporous monoliths

In our recent paper, we have described a method for the synthesis of platinum nanoparticles and their deposition on TiN/Si_3N_4 monoliths that involved the use of a Pt salt (Chloroplatinic acid hexahydrate ($H_2PtCl_6 \cdot 6H_2O$) and reduction under hydrogen (5 %). A second approach was used in this thesis to test if nanoparticles could be successfully

produced and attached to the monoliths mesopores without the use of hydrogen gas in the furnace. For that, a methodology described by Qi-Long Zhu et al. (2014) was selected and applied as follows: 100 mg of TiN/Si_3N_4 monoliths already treated at 1400 ℃ were placed in a round-bottomed flask and ultrassonically dispersed in 2.5 mL of deionised water. Then, 0.1 mmol of $H_2PtCl_6 \cdot 6H_2O$ were added to the flask and sonicated for 30 minutes. The flask was placed on a magnetic stirrer for agitation, followed by the addition of 12 mg of $NaBH_4$ dissolved in 1 mL of NaOH, that resulted in the generation of a dark suspension. After that, the monoliths were washed with deionised water, dried at 80 ℃ and then treated under argon at 450 ℃ in a tubular furnace for 4 h.

The same method was applied for the synthesis fo cobalt and nickel nanoparticles, using $CoCl_2$ and $NiCl_2$, aiming at equivalent performance with less expensive materials. The amount of metal was fixed at 1 wt % for the three metals.

3.3.2 Hydrolysis Tests

Hydrolysis were perfomed at *Institut Européen des Membranes - Université de Montpellier*. The experiments were based on the following methodology: 16 mg of the generated monoliths were added to an 1 mL of $NaBH_4$ solution (120 mg in 2% NaOH). The solution with the monoliths was transferred to a glass tube, here working as a reactor, completely closed and sealed. The tube was connected by a cold trap (0 ℃) for steam to a water-filled inverted burette. The reactor was then put into an oil bath at 80 ℃, while a camera recorded the water displacement in the inverted burette, that occurred while hydrogen was being generated. Each reaction took 180 minutes and the hydrogen volume was measured in mL.

3.4 CHARACTERIZATION TECHNIQUES

This section is dedicated to describe the equipments and techniques that were applied to characterize the obtained materials.

3.4.1 Fourier-Transformed Infrared Spectroscopy (FTIR)

In this method, the radiation absorbed by a molecule is converted into molecular vibration energy, so the spectrum reveals the atoms vibrations in the molecules. Every bond type has its own natural vibration frequency and, for an identical bond, but in different compounds, the environment where the bond is detected can be slighty different. For this reason, the FTIR of two different structures are never exactly identical. This technique is applied to identify structural information of a compound (PAVIA et al., 2010). Herein, FTIR

was used to observe how the reactive groups in the organosilicon compounds react in the presence of metal precursors and also their polymer-to-ceramic transformation.

For the analyses, KBr pellets were prepared inside the glove box with the polymers and pyrolysis intermediates. After pressing, the pellets were analysed in a Nicolet 6700 Thermofisher equipment, reading from 4000 to 400 cm^{-1}. The data was collected by Omnic™Software.

3.4.2 Thermogravimetric Analysis (TGA)

There are some essential observations provided by the use of thermogravimetric analysis for polymer-derived ceramics. The analysis consists in a continuous process that measures the variation of the sample weight by the increase of the temperature. For that, a high precision scale is coupled to a furnace that is able to be programmed to different heating rates and can work in distinct gas environments. The thermal conversion of preceramic polymers into ceramics occurs through the evolution of gases, causing the weight loss of the sample. Thus, it is possible to observe by the gravimetric curves, at which temperatures the weight losses happen, given an idea of the possible reactions that involve the polymer-to-ceramic conversion. The remaining sample is the so-called ceramic yield, since it is the sample after the loss of organic groups and chemical rearrengements (RIEDEL; MERA, et al., 2006).

In this thesis, the pyrolyses were performed under ammonia, however technical and safety circunstances prevented the TGA to run under this gas. Thus, TGA analyses were carried out under N_2. The final temperature was 1000 ℃ and the heating rate fixed at 5 ℃.min^{-1}, with a N_2 flow of 50 mL.min^{-1}.

3.4.3 X-Ray Diffraction Analysis (XRD)

X-Ray Diffraction is a non-destructive analysis applied to analyse the structure of crystalline materials, studying the crystalline phases in the material and revealing important information over the chemical composition. XRD is one of the most important techniques for the characterization of the microstructure in polymer-derived ceramics. PDCs have been described as intrinsically complex systems, that suffer deep microstructural modifications when subjected to heat treatments. Depending on the composition and molecular structure of the organosilicon percursor, these materials can remain amorphous up to 1000° - 1800℃ (COLOMBO; MERA, et al., 2010).

The obtained PDCs at different pyrolses temperatures were crushed into fine powders and evenly spread on Si low background sample holders (Bruker®). Then, they were transferred to the XRD equipment Bruker D8 Advance Serie II, measuring in 2θ=10 to

90°. The diffraction files were studied using the database from International Center for Diffraction Data (ICDD) Powder Diffraction File (PDF-4+).

3.4.4 Raman Spectroscopy

A technique that consists on the interaction of light with the chemical bonds within a material, Raman spectroscopy is a non-destructive method in which monochromatic visible laser with a phototube as detector, can analyse the scattered radiation of a sample. It is based on the absorption of photons of a specific frequency and subsequently scattering at higher or lower frequency.

This technique an important tool in the characterization of PDCs to evaluate the structural evolution of the free carbon phase in such materials. The PDCs ability to incorporate free carbon into the microstructure has been object of study, and Raman spectroscopy allows for the assessment to the existence of graphene sheets of carbon with some degree of long-range order. Thereby, Raman was used in this work to verify the disorder-induced bands to observe the existence of remaining carbon in the mesoporous samples. For that, the samples were analysed using an equipment InVia Reflex Renishaw (COLOMBO; MERA, et al., 2010).

3.4.5 Brunauer-Emmett-Teller (BET)

Since the current work reports the development of porous structures, Brunauer-Emmett-Teller (BET) was an essential technique to assess the monoliths porosity. Data on specific surface area and pore size distribution were collected using a 3Flex Physisorption equipment, from Micrometrics Instrument Corporation. The method consists in a mathematical theory that describes the physical adsorption of a gas (nitrogen) on the surface of the sample. Adsorption and desorption values generate isotherms that permits to verify the type of porosity present in the material.

3.4.6 Scanning Electron Microscopy (SEM)

The microscope for SEM is capable of generating images of a sample by scanning its surface with a focused bem of electrons. A machine Jeol IT 300 LV InTouchScope™, working in a magnification from x5 to x300,000 was used to acquire images from the monoliths and powders, and was coupled with and EDS (Energy-dispersive X-ray spectroscopy) for elemental characterization.

The samples were positioned on metallic stubs with the aid of a water-based conductive graphene carbon paint. A drop of liquid, colloidal silver was placed in the side of the sample to increase conductivity.

4 RESULTS AND DISCUSSION

The objective of this thesis was to develop metal-supported silicon nitride ceramics for applications in heterogeneous catalysis, here evaluated in the hydrolysis of sodium borohydride (Figure 16). This goal was based on the extensive study done along with the research group during the past years, that originated important papers, with special attention to the work related to Pt-supported TiN/Si_3N_4 nanocomposite catalysts for clean energy applications, published this year (LALE; MALLMANN, et al., 2020). The produced systems display excellent catalytic performance (even at a fixed concentration of 1 wt%), however the preparation of Pt-TiN/Si_3N_4 porous systems is complex and platinum is expensive in comparison to non-noble metals. Thus, one goal of this thesis was to simplify the preparation method and replace platinum for non-noble metals.

Figure 16 – Hydrolysis of sodium borohydride

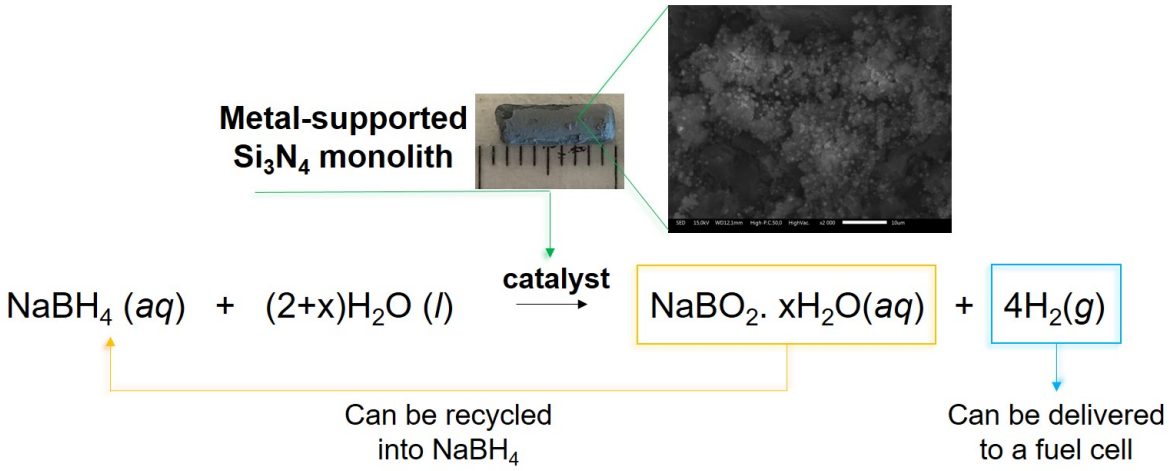

This chapter is divided in two main sections, that were split because of the different strategies applied. The first section is mostly related to the paper mentioned above, extending the synthesis method to produce nanocomposites consisting in other metals besides titanium, such as molybdenum and vanadium. Micro-/mesoporous monoliths composed by TiN/Si_3N_4 nanocomposite were used as supports for *in-situ* reduction of nanoparticles.

The second section of this chapter reports the results on the completely new materials that were developed with the objective to simplify the route used in the first section. For that, PHPS/HTT 1800 were reacted with metal-chlorides (metal = Ni, Co) to generate Co-/Ni-supported Si_3N_4 at relatively low temperatures.

Micro-/mesoporous monoliths had their catalytic activity tested in the hydrolysis of sodium borohydride. The hydrogen volume generated by the respective monoliths was measured and the generation rate calculated, that are presented in both sections.

4.1 SYNTHESIS OF METAL-MODIFIED SILICON NITRIDE NANOCOMPOSITES

The concept of nanocomposites comprises a wide range of systems based on polymers, metals and ceramics. The remarkable feature of such materials is that they are composed by different components mixed at nanometric scale. Our research group has already extensively worked on ceramic nanocomposites derived from the Si-M-N system. The main idea that has structured this research was to improve and extend some of the properties of Si_3N_4. For that, transition-metal nitrides as TiN were selected due to their high hardness, high melting points, and wear resistance. The ability to generate materials composed by TiN nanocrystals dispersed in an amorphous Si_3N_4 matrix has boosted the progress in exploring the design on 3D structures with exceptional potential for energy and environmental science and technology.

This section approaches the development of ceramic nanocomposites applying a straightforward method based on the Polymer-Derived Ceramics route, using Ti, Mo and V as metal precursors. Characterisation of a synthesized bimetallic compound based on Ti and Co is also reported. Finally, the design and catalytic performance of micro-/mesoporous TiN/Si_3N_4 monoliths, including in-situ formation of Pt, Co and Ni nanoparticles is presented.

4.1.1 Synthesis of polymetallosilazanes and ceramic conversion

The reaction between PHPS and TDMAT [tetrakis(dimethylamido)titanium] with Si/Ti ratio 2.5 generated a solid black powder after a three-days synthesis at 120 ℃. The resulting polymer, **PHTiPS2.5**, was analysed by FTIR and compared to pure PHPS, as shown in Figure 17.

The first fact that should be pointed out about the FTIR spectra is related to N-H bonds. The sign corresponding to the stretching vibration band (νN-H) at 3380 cm^{-1}, characteristic of PHPS, disappeared in the polymer. More than that, bending vibrations (δN-H) at 1180 cm^{-1} strongly reduced and the intense sign of νSi-H visibly decreased after the synthesis with TDMAT. These facts confirm that N-H and Si-H groups from PHPS were involved in the construction of the polytitanosilazane network, as proposed by Bechelany, Proust, Lale, et al. (2017) in Equations 5 and 6. According to the equations, N-H and Si-H react with $N(CH)_3$ groups from TDMAT.

$$\equiv Si-NH + Ti(N(CH_3)_2)_4 \longrightarrow \equiv Si-N-Ti(N(CH_3)_2)_3 + H-N(CH_3)_2 \quad (5)$$

$$\equiv Si-H + Ti(N(CH_3)_2)_4 \longrightarrow \equiv Si-N(CH_3)-Ti(N(CH_3)_2)_3 + CH_4 \quad (6)$$

Figure 17 – FTIR spectra of PHPS and the polymetallosilazane PHTiPS2.5

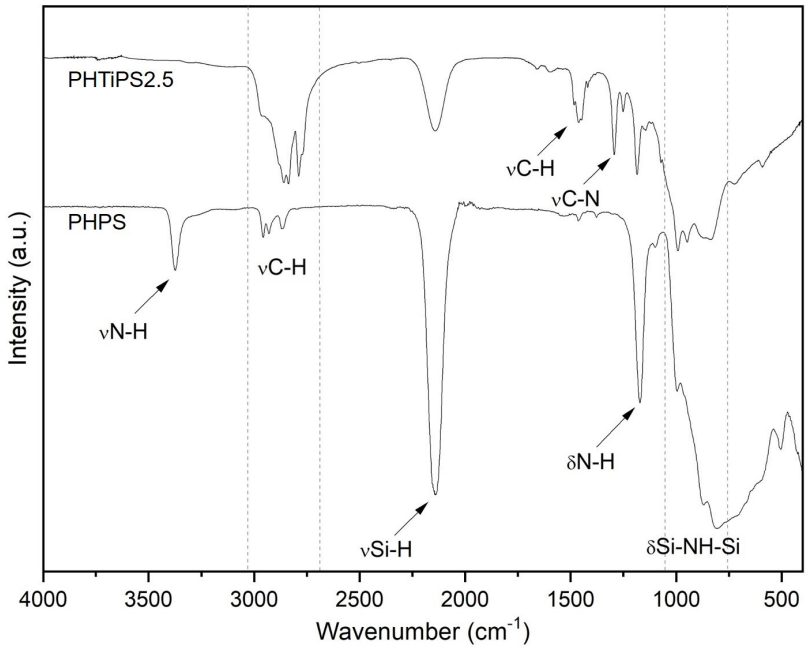

The $N(CH)_3$ groups could be detected by the νC-N sign at 1280 cm $^{-1}$. A new peak at 1360 $^{-1}$ was found in the synthesized polymer, attributed to C-H vibrations from the dimethyl group present in the titanium precursor.

The reaction between TDMAT precursor and polysilazanes has already been object of study. In a recently work published by Bechelany, Proust, Lale, et al. (2017), the chemistry role behind the synthesis was thoroughly investigated. Thus, a molecular structure was proposed for a polytitanosilazane synthesized by a polymethylsilazane (PMSZ) and TDMAT, using Si/Ti ratio 2.5 (Figure 18).

The molecular structure has been proposed based on FTIR, solid-state NMR coupled with mass spectroscopy and elemental analyses. The difference between PHPS and PMSZ structures is the presence of a CH_3 side chain attached to Si, nevertheless the reaction mechanism is the same. The authors could confirm that titanium atoms potentialize the crosslinking degree of the polymeric backbone. Such atoms are evenly distributed within the polysilazane network, acting as connection bridges between silazane units as well as terminal units. Accordingly, two types of bridges can be highlighted: those involving $(SiN)_nTiN_3$ (Equation 5) units and those involving $SiN(CH_3)TiN_3$ (Equation 6). Figure 19 clearly depicts the reactions and the obtained product. Dimethylamine and methane were the released gases during synthesis.

As a proof of concept, molybdenum and vanadium precursors, bis(t-butylimido) bis(dimethylamino) molybdenum(VI) and tetrakis(ethylmethylamino) vanadium(IV), were tested in the same reaction conditions with PHPS. The syntheses generated the poly-

Figure 18 – Molecular structure proposed for a polytitanosilazane synthesized from PMSZ and TDMAT

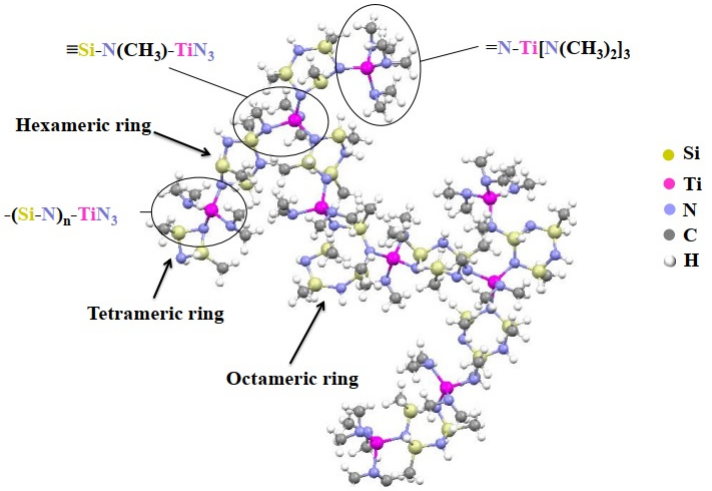

Source: Bechelany, Proust, Lale, et al. (2017)

mers **PHMoPS2.5** and **PHVPS2.5**. Both reactions resulted in black powders, similarly to **PHTiPS2.5**. The polymers FTIR spectra are presented in Figure 20.

Precursor moieties C-H (3000-2800, 1450 cm^{-1}) and C-N (1250 cm^{-1}) were detected, as expected. Following the same path as **PHTiPS2.5**, N-H bending vibrations at 1180 cm^{-1} visibly reduced in comparison to pure PHPS. At higher wavenumbers as 3400 cm^{-1}, N-H band decreased for **PHVPS2.5**. For **PHMoPS2.5** it went from a sharp peak to a broad shoulder. Interestingly, Si-H band strongly reduced its intensity in the molybednum polymer. It can indicate that Equation 6 occurred in larger proportion than Equation 5, i.e., Si-H groups reacted more than N-H groups in this system.

The polymetallosilazane-to-amorphous ceramic conversion was investigated by the monitoring of their thermal conversion by TGA. Figure 21 compiles **PHTiPS2.5**, **PHMoPS2.5** and **PHVPS2.5** conversions under nitrogen until 1000 ℃, with a heating rate of 5 ℃.min^{-1}.

Titanium and vanadium-modified PHPS had smaller weight losses than pure PHPS. **PHTiPS2.5** had a mass difference of -24.7 wt%, which means a ceramic yield of 75.3 wt%. **PHVPS2.5** weight loss was 29.2 wt% (ceramic yield = 70.8 wt%). Higher weight loss was recorded for the molybdenum-modified PHPS, 54 wt%. Above 800 ℃, all the polymers analysed under N_2 flow had their network decomposition stable and resulted in the formation of amorphous ceramics.

Observing the graph, it is possible to imply that **PHTiPS2.5** and **PHVPS2.5** were more crosslinked polymers than **PHMoPS2.5**. The latter had a 40 % weight loss between

Figure 19 – Reaction between NH (Scheme 1) or SiH (Scheme 2) units from PHPS and NCH_3 groups from TDMAT

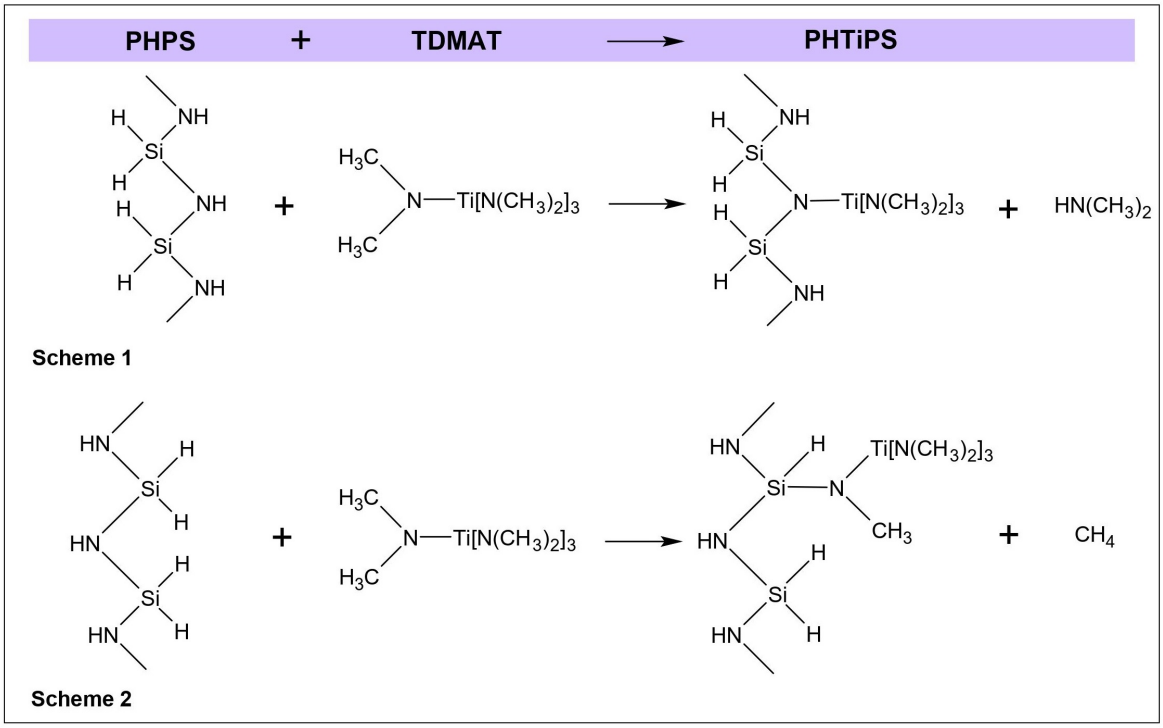

50 and 400 °C, meaning that the synthesized polymer still had a large amount of unreacted groups. Hence, such groups reacted during pyrolysis, causing gas evolution and consequently greater weight loss. The mass change below 200 °C is normally associated to the evolution of low molecular weight compounds, and in the range 250-400 °C to crosslinking reactions (FLORES et al., 2013). Transamination and dehydrocoupling reactions, with NH_3 and H_2 release, respectively, were the main reactions happening at this temperature.

For **PHTiPS2.5** TGA under nitrogen, represented by the blue dashes in the graph, the first derivative curve revealed two weight losses, centered at 108 and 350 °C and represented the loss of 22 wt%. Polytitanosilazanes have been pyrolysed under NH_3 in different studies and the mass loss was normally higher, between 25 and 40 wt% (IWAMOTO; KIKUTA; HIRANO, 2000b; BECHELANY; PROUST; LALE, et al., 2017; LALE, 2017). This is connected to the fact that dimethylamino groups in the sample react with NH_3 by transamination reactions, forming NH_2, that condense and release dimethylamine. Under NH_3, the most expressive weight loss of PHPS occurs between 100 and 350 °C, and is related to the dehydrogenation of Si-H/N-H and Si-H/Si-H bonds, yielding Si-N and Si-Si bonds that form the backbone structure of the ceramic material.

To better understand the mechanisms involved in the polymer-to-ceramic transformation during pyrolyses under NH_3, it is important to mention the mechanisms proposed by

Figure 20 – FTIR spectra of PHMoPS2.5 and PHVPS2.5

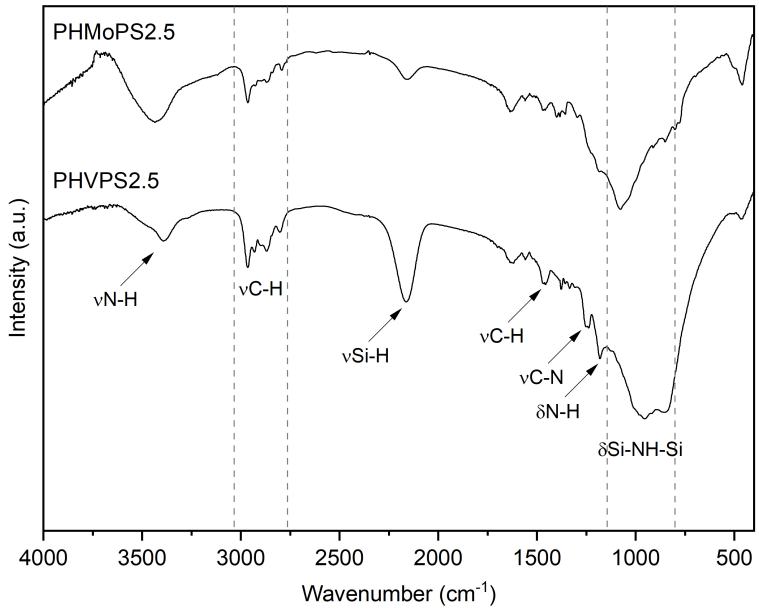

Figure 21 – TGA of PHMPS2.5 (M= Ti, Mo, V) under N_2

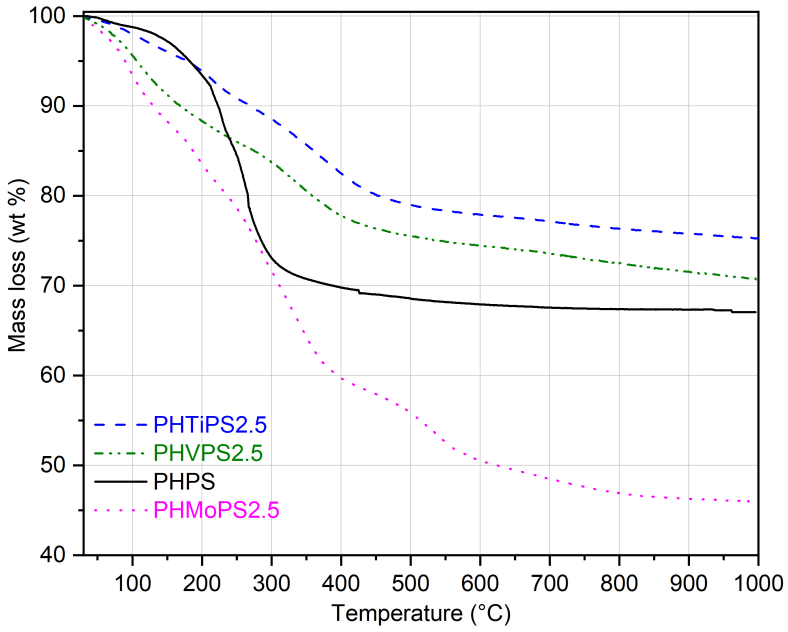

Yive et al. (1992). This pioneer work treated a investigation on the thermal degradation of different polysilazanes, polymethylsilazane, phenylsilsesquiazane and a polyvinylsilazane, under argon and NH_3. The authors used TGA coupled with a continuous mass spectrometry to analyse the gases involved during pyrolysis. According to this study, the mechanism showed in Equation 7 is favored, where R = H, CH_3, CH_2-Si≡. This occurs because Si-CH_3, Si-CH_2-Si and specially Si-H, can be easily modified by NH_3. Polymers containing Si-H units, as PHPS, are sensitive to nucleophilic substitution, hence this mechanism is pro-

moted, mainly at temperatures below 500 °C. Another mechanism that is certainly present concerns free-radical substitution, initiated by homolytic cleavages (Equations 8, 9 and 10).

$$\equiv Si-R+NH_3 \longrightarrow \equiv Si-NH_2+RH \tag{7}$$

$$\equiv Si-R \longrightarrow \equiv Si+R \tag{8}$$

$$R+NH_3 \longrightarrow RH+NH_2 \tag{9}$$

$$\equiv Si+NH_2 \longrightarrow \equiv Si-NH_2 \tag{10}$$

Si-NH_2 groups formed in Equation 10 probably suffer self-condensation, as already mentioned, releasing dimethylamine and generating the amorphous ceramic network at 1000 °C. The powders obtained herein were characterized and their features discussed in section 4.1.2.1.

4.1.1.1 Synthesis of polymetallosilazanes based on titanium and cobalt

Titanium and cobalt have been combined in numerous studies for catalysis applications. The studies mostly focus on the development of titanium cobalt nitrides/oxides or in the synthesis of bimetallic particles (FENG, G. et al., 2018; XIAO et al., 2015; SATO et al., 2005). Herein, the synthesis of polymetallosilazanes was based on TDMAT and cobalt chloride ($CoCl_2$) using PHPS as the silicon nitride precursor. The goal was to observe if a network such as $Ti_xCo_yN_z/Si_3N_4$ would be formed or even if cobalt particles would be able to grow along with the TiN/Si_3N_4 phases.

In the polymerization processes, Si/Co and Si/Ti ratios were fixed at 5, because the reaction between TDMAT and PHPS at ratio 2.5 leads to a highly crosslinked polymer, without any steric hindrance effect that could affect the reaction. Thus, at Si/Ti ratio 5, it was expected that there would be more available groups from PHPS to react with $CoCl_2$, increasing the possibility of inserting Co in the polymer network. After a process that lasted for 24 h at 120 °C, two polymers were generated: **PHTiCo5** and **PHCoTi5**. Both had the same physical aspect and could be characterized as black powders, as shown in Figure 22.

The polymers were analysed by FTIR and the spectra compared to **PHTiPS2.5** (Figure 23). There was no visible difference between the polymers **PHTiCo5** and **PHCoTi5** infrared. The main consideration that can be pointed out concerns the disappearance of

Figure 22 – Synthesized polymer after solvent extraction

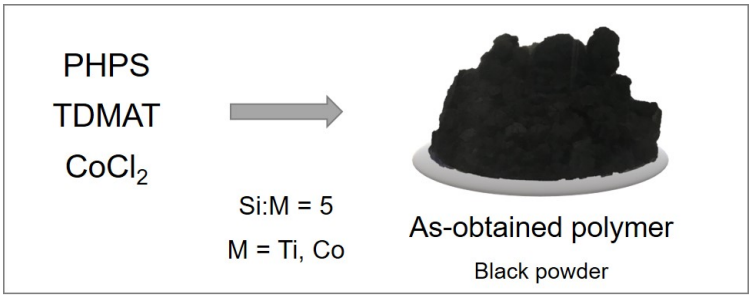

νN-H groups around 3380 cm^{-1}. At 1180 cm^{-1}, the peak suffered a considerable reduction in relation to pure PHPS, however such reduction was less intense than for **PHTiPS2.5**. Regarding νSi-H, it is possible to affirm that these groups were also part of the reaction mechanism. Hence, the results were in accordance with the findings discussed in the last section.

Figure 23 – FTIR of PHCoTi5 and PHTiCo5 compared to PHTiPS5

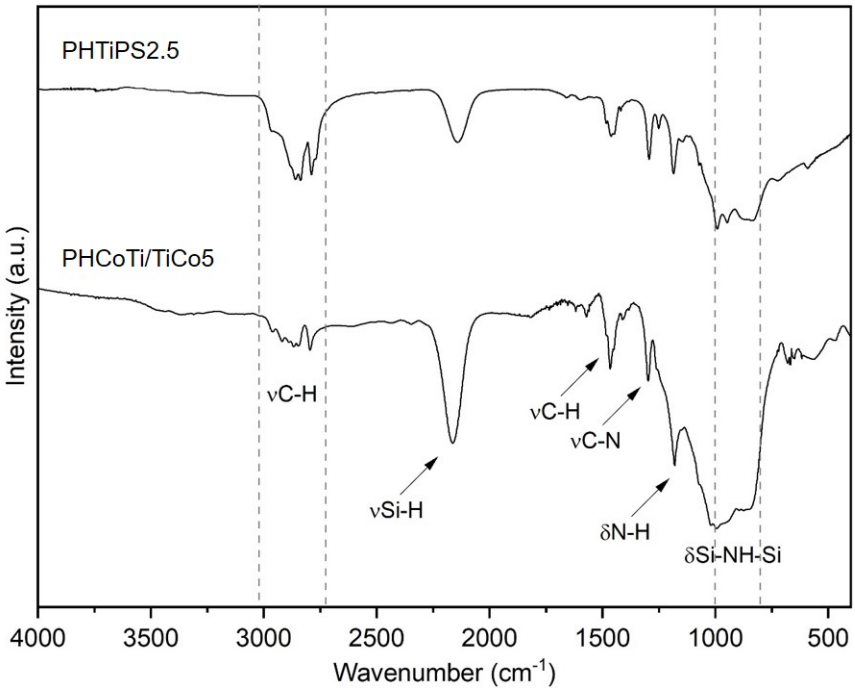

The weight change during polymer-to-ceramic conversion was investigated by TGA analyses. The atmosphere in the equipment was nitrogen. However, the process to obtain ceramic powders consisted on the pyrolyses in NH_3 environment, therefore the samples weight were measured before and after the heat treatment to have a better idea of these new compounds weight loss under NH_3 in comparison to the TGA in N_2. In the furnace, the polymer **PHTiCo5** lost circa 22 wt% of its initial mass at 1000 ℃, whilst **PHCoTi5** lost around 45 wt%, which results in ceramic yields of 78 and 55 wt% after pyrolysis in NH_3.

The same trend was noted for the TGA in N_2, as shown in Figure 24. The weight losses were 32 wt% for **PHTiCo5** and 45 wt% for **PHCoTi5**, meaning 68 and 55 wt% of ceramic yield, respectively. **PHTiCo5** ceramic yield was relatively close to **PHTiPS2.5** (75.3 wt %).

The polymer-to-ceramic conversion monitored by TGA had a major loss below 200 ℃, related to unreacted low molecular weight groups. **PHCoTi5** lost 10 wt % between 300 and 600 ℃, whilst **PHTiCo5** lost less than 2 wt %. The main aspect that can be pointed out for both polymers degradation behavior is related to the high level of unreacted groups that evoluted during the first 200 ℃. The silicon to titanium ratio (Si:Ti) influence in the crosslinking degree has already been investigated. Ratio 5 exhibitted lower crosslkinking levels than ratio 2.5, that were confirmed herein. Also, the order in which the metal precursors were added interfered in the weight loss. Adding $CoCl_2$ before TDMAT led to a higher weight loss between 300 and 600 ℃, when dehydrocoupling and transamination reactions occur (CHOONG KWET YIVE et al., 1992). The addition of TDMAT before $CoCl_2$ could be responsible for a higher ceramic conversion, promoted by the larger number of N-H and Si-H groups reacting with $N(CH)_3$ in the beginning of the synthesis.

Figure 24 – TGA under N_2 of PHCoTi5 and PHTiCo5 compared to PHPS

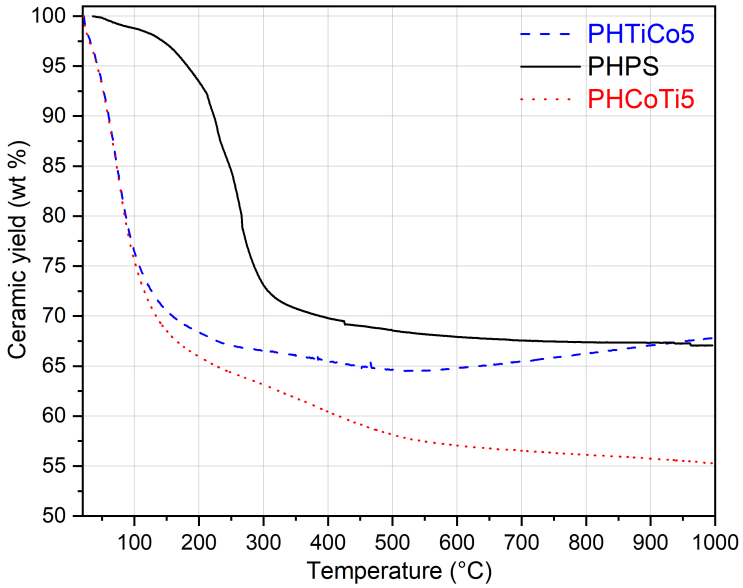

For the design of micro-/mesoporous monoliths with the polymers, solutions obtained after reaction were directly used to impregnate the activated carbon. This process was performed using **PHTiCo5**, because its weight change was smaller than **PHCoTi5**. In addition, as-obtained polymers **PHTiCo5** and **PHCoTi5** were treated in a furnace to produce ceramic powders. Their characterization is presented in Subsection 4.1.2.

4.1.2 Characterization of ceramics as powders

This subsection is dedicated to the study of ceramics yielded by pyrolysis of the synthesized polymers that were described in the previous sections. The objective is to verify the amorphous and/or crystalline phases in the material and if the desired structure was achieved.

PHTiPS2.5, **PHVPS2.5** and **PHMoPS2.5** were subjected to pyrolysis under NH_3 until 1000 ℃ to observe their XRD patterns and assess the formation of the ceramic structure. The prepared materials could be classified as predominantly amorphous at this temperature, in which the Si_3N_4 matrix was not crystallizing yet. The first graph regarding the XRD investigation on the as-obtained ceramics is represented in Figure 25. The graph shows the X-ray diffraction patterns generated upon analyses of vanadium and molybdenum-modified PHPS.

For the sample **PHVPS2.5**, despite the amorphous structure, it was possible to notice weak and broad diffraction peaks centered at 2θ values circa 37, 43 and 63°, corresponding to the typical stoichiometric face-centered cubic (fcc) vanadium nitride (VN) structure (JCPDS No. 35-0768) (HUANG et al., 2015).

Figure 25 – XRD patterns of PHVPS2.5 and PHMoPS2.5 pyrolysed at 1000 ℃ under NH_3

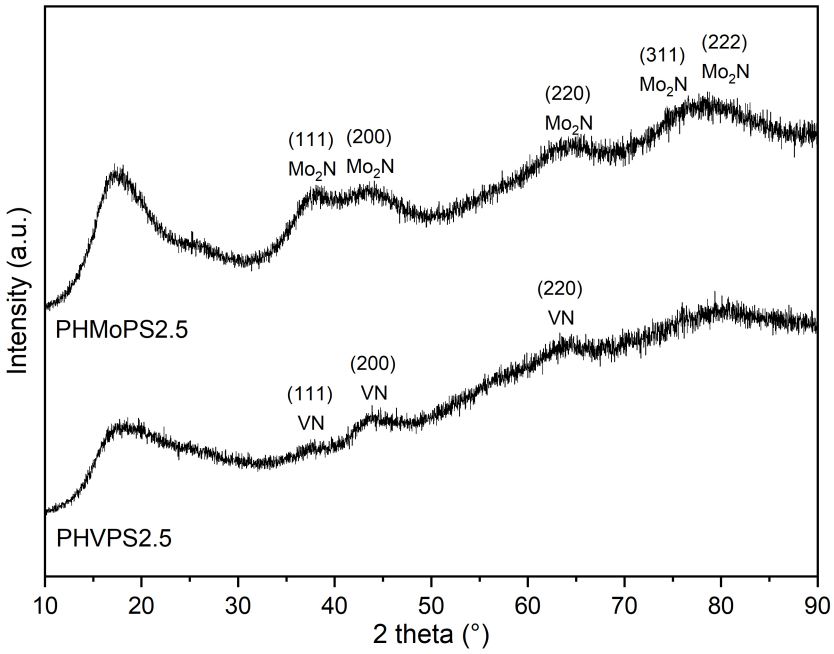

Regarding the powder obtained through the pyrolysis of **PHMoPS2.5**, XRD also displayed an overall amorphous structure. In the same way as **PHVPS2.5**, weak and broad signs of (111), (200), (220), (311) and (222) planes of Mo_2N indicate that cubic crystals were already being detected, in agreement with the database JCPDS card No. 00-025-

1366 (TAGLIAZUCCA; LEONI; WEIDENTHALER, 2014; KUZNETSOVA et al., 2016; XIE; TIAN, 2017). According to Jehn (1989), molybdenum nitrides are formed only at elevated N_2 pressures or in NH_3 environment at temperatures above 800 °C.

At 1000 °C, **PHTiPS2.5** exhibitted broad peaks matching the JCPDS file No. 00-038-1420, the XRD pattern for TiN cubic structure. These peaks correspond to the nucleation of face-centered cubic (fcc) TiN phase, at 2θ values of 36.5°, 42.63° and 62.11°. The powder was further annealed until 1400 °C under nitrogen, and the XRD revealed the (311) and (222) reflections, at 74° and 78.3°, respectively. The ceramic matrix, however, was still amorphous at 1400 °C, without peaks that characterize α- or β-Si_3N_4. The results are in agreement with the findings from the group, as reported by Lale, Proust, et al. (2017). For the same Si/Ti ratio, the authors observed that increasing the temperature of pyrolysis to 1500 °C and 1600 °C resulted in a increase from 2.6 to 27.6 nm in the crystallite size of the dominant TiN peak (111) and concluded that the amorphous matrix in TiN/Si_3N_4 presents higher stability in comparison to other polysilazanes, such as HTT1800.

Figure 26 – XRD patterns of PHTiPS2.5 pyrolysed at 1000 °C under NH_3 and annealed at 1400 °C under N_2

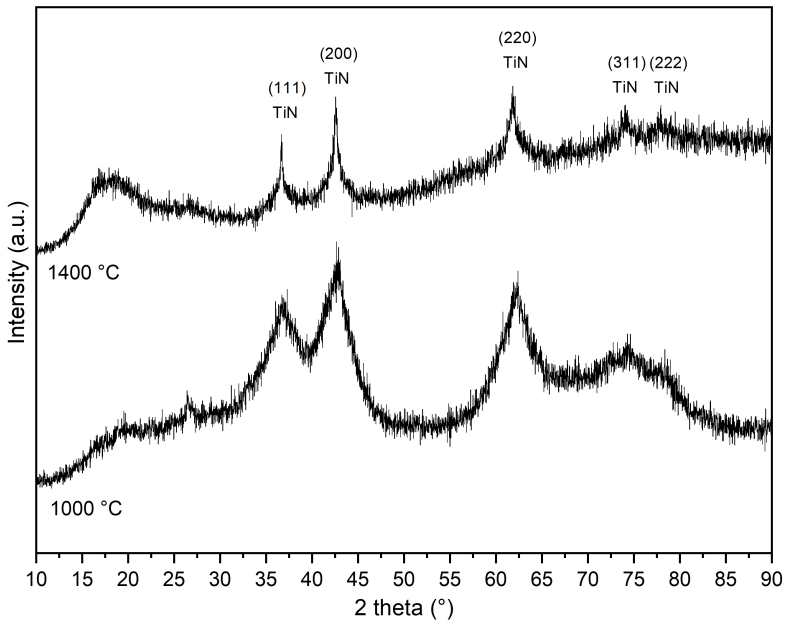

In conclusion to the XRD study, it was possible to produce nanocomposites composed by a TiN nanophase and an amorphous Si_3N_4 matrix. In contrast, pure PHPS pyrolysed in the same atmosphere conditions as the applied for **PHTiPS2.5** was fully crystallized at 1400 °C Figure 27. PHPS-derived ceramic microstructure is still amorphous at 1000 °C (label PHPS-1000 in Figure 27), when treated under NH_3. Annealing this ceramic at higher temperatures under N_2 leads to crystallization of α- and β-Si_3N_4.

Figure 27 – XRD patterns of Si_3N_4 crystallization on PHPS-derived ceramic treated under NH_3 at 1000 ℃ and until 1700 ℃ under N_2

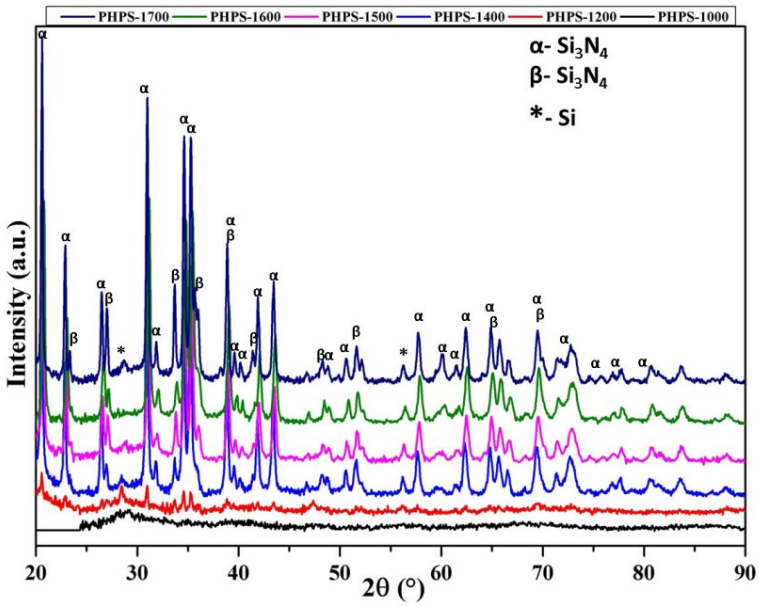

Source: Lale (2017)

PHTiPS2.5 powders obtained at 1000 and 1400 ℃ were subjected to Raman spectroscopy as a confirmation for the TiN nanophase growth. The graphs are presented in Figure 28. Acoustical phonons are characterized as the peaks below 400 cm^{-1} whilst the optical phonons are those above 500 cm^{-1}. Peaks corresponding to free-carbon could be observed as the D and G signs, namely disordered and graphitic carbon, respectively. The carbon increase comparing 1000 to 1400 ℃ samples could be attributed to impurities derived from the graphite furnace used for annealing above 1000 ℃, since the carbon amount in the powders should be neglegible after pyrolysis in NH_3. Two shoulders centered at 817 and 1075 cm^{-1} for the sample at 1400 ℃ correspond to A+O and 2O modes. At 210 cm^{-1}, the peak is assigned to the transverse acoustic mode (TA), followed by the longitudinal mode (LA) at 296.6 cm^{-1}, the latter only present at 1400 ℃. Transverse optic/longitudinal optical mode (TO/LO) is characterized by the peak around 540 cm^{-1}. After assigning the peaks, it was possible to conclude that they correspond to TiN, being the phonon bands in the lower acoustic range representative of Ti^{4+} ions, which are heavier than N^{3-} ions, detectable at higher optical range. Si_3N_4 signs were not identified at these temperatures.

Figure 28 – Raman spectra of PHTiPS2.5 powders obtained at 1000 °C after treatment under NH_3 and at 1400 °C after annealing under N_2

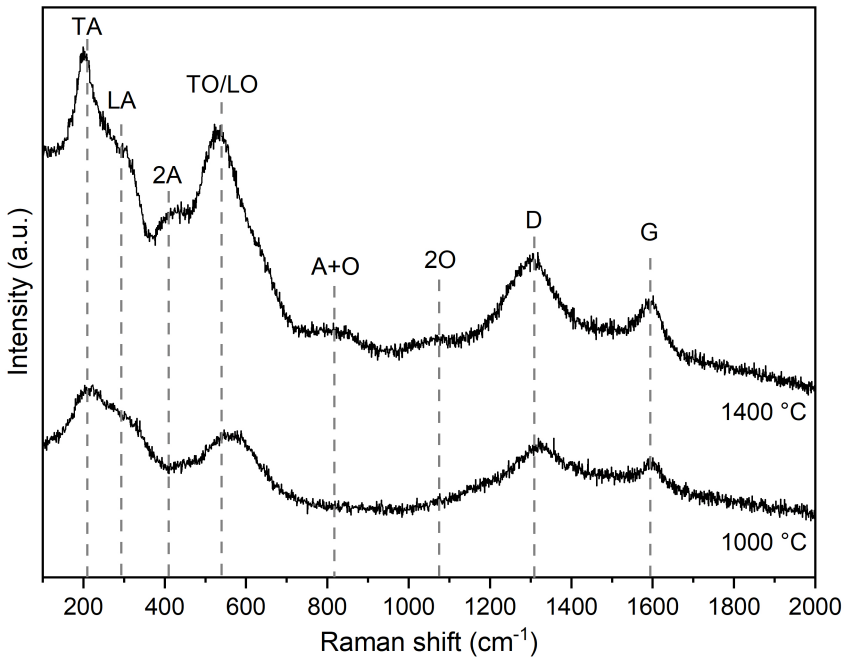

4.1.2.1 Characterization of ceramics based on titanium and cobalt as powders

Polymers **PHCoTi5** and **PHTiCo5** were pyrolysed at 700, 800, 900 and 1000 ℃ under NH_3. The powders were investigated by XRD technique and the patterns highlighted in the graphs represented in Figures 29 and 30. Differently from **PHTiPS2.5**, the ceramics produced by heat treatment of the polymers synthesized with $CoCl_2$ and TDMAT presented peaks in the XRD that correspond to α- and β-Si_3N_4.

For the ceramic **PHCoTi5**, it was possible to notice the formation of Co (cubic) already at 700 ℃, characterized by the peaks at 2θ = 44.2158°, 51.5225° and 75.8531°, corresponding to (111), (200) and (220) reflections. These patterns are in accordance with the ICDD file No. 00-015-0806. More than that, a peak at 42.6044° is most probably related to TiN. Two peaks were recognized as $CoSi_2$. The crystallization of α- and β-Si_3N_4 was more intense for the powders obtained through pyrolysis of **PHTiCo5**. Four peaks that are in accordance with TiN patterns are also highlighted in Figure 30. Cobalt (cubic) was preferentially crystallized than $CoSi_2$, as it can be seen comparing the graphs of both powders. As $CoCl_2$ was added in the beginning of the reaction in the **PHCoTi5** system, more Si groups were available to react with this compound, which might explain the formation of $CoSi_2$. Based on the analysis of the graphs, the presence of metallic cobalt improved the crystallinity of TiN, as recently observed by Qing Zhu et al. (2019).

Figure 29 – PHCoTi5 XRD patterns from 700 to 1000 ℃ of powders obtained through pyrolysis under NH_3

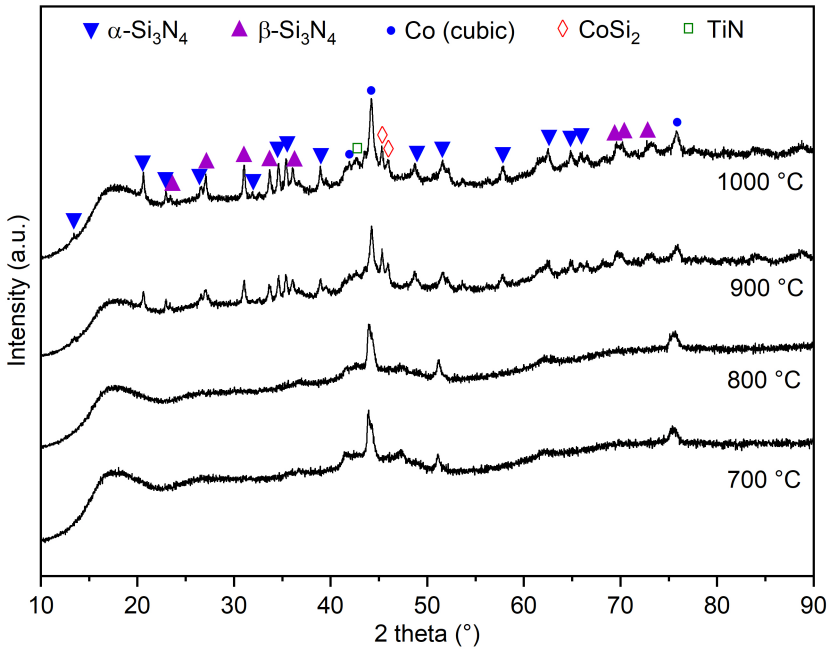

The powders diffractograms were also investigated after pyrolysis under nitrogen until 1000 ℃ to evaluate and compare their behavior in a non-reactive atmosphere. The

Figure 30 – PHTiCo5 XRD patterns from 700 to 1000 ℃ of powders obtained through pyrolysis under NH_3

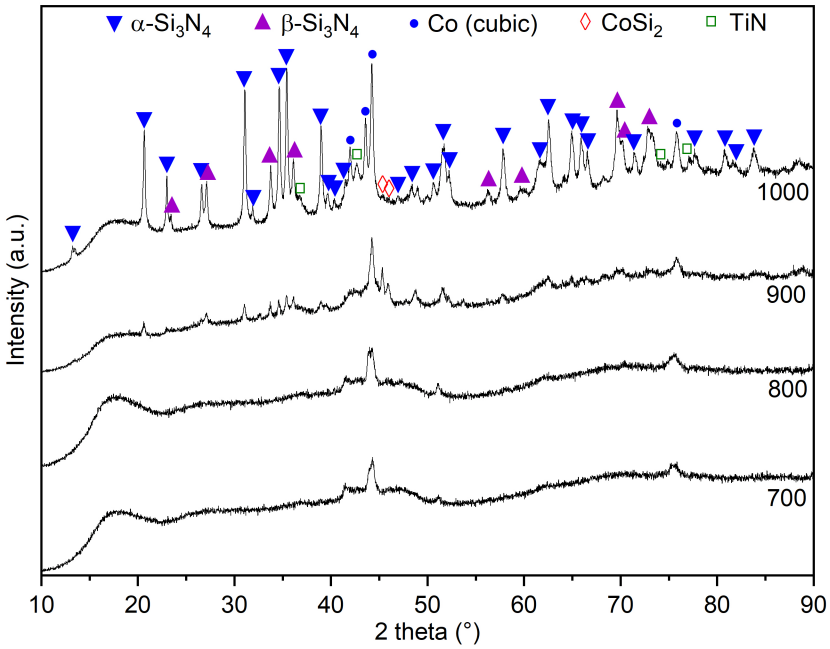

generated graphs are exposed in Figure 31. **PHTiCo5** and **PHCoTi5** yielded similar ceramics after heat treatment.

Figure 31 – PHTiCo5 and PHCoTi5 XRD patterns at 1000 ℃ after pyrolysis under N_2

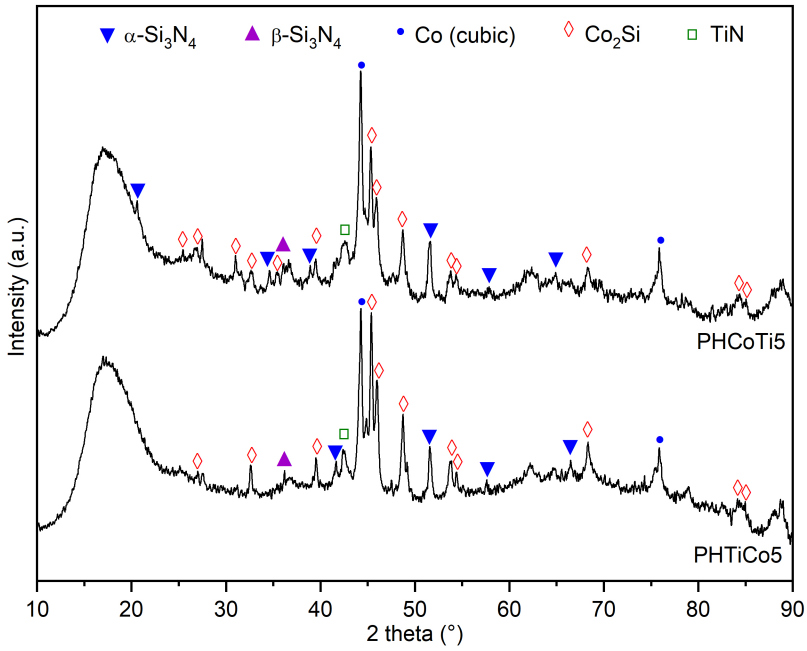

The main difference that was observed between the distinct pyrolysis atmosphere was that under N_2 flow Co_2Si were preferrably formed whilst almost no signs of Si_3N_4

crystallization were detected. For both samples three peaks were identified at 2θ = 53.82°, 54.14° and 68.46° corresponding to (203), (121) and (222) reflections of Co_2Si orthorhombic crystal system (ICDD File No. 04-010-3523). The other Co_2Si signs are in accordance with ICDD File No. 04-007-1523. Cobalt in cubic crystal system was marked by two peaks at 2θ = 44.21° and 75.85° and correspond to (111) and (220) reflections, in consonance with ICDD File No. 00-015-0806. Titanium nitride was identified by the peak at 2θ = 42.60°.

During pyrolysis under nitrogen, the reactions represented in Equations to 7 to 10 that have NH_3 participation did not occur. As a consequence, α- and β-Si_3N_4 did not largely crystallize at temperatures below 1000 ℃. Instead, the formation of cobalt silicides was favorable, and this phase could be observed by XRD. This proves that the use of NH_3 for pyrolysis has a strong impact in the microstructure of the final material.

The ceramics produced after pyrolysis under ammonia until 1000 ℃ were crushed into fine powders and analysed by SEM coupled with EDS. Such powders can be observed in Figure 32. The materials were constituted by grains apparently covered with smaller particles, evidenced by the white spots over the surface, as seen in Figures 32 b and d.

Figure 32 – SEM images of PHCoTi5 (a-b) and PHTiCo5 (c-d) powders after treatment under NH_3 until 1000 ℃

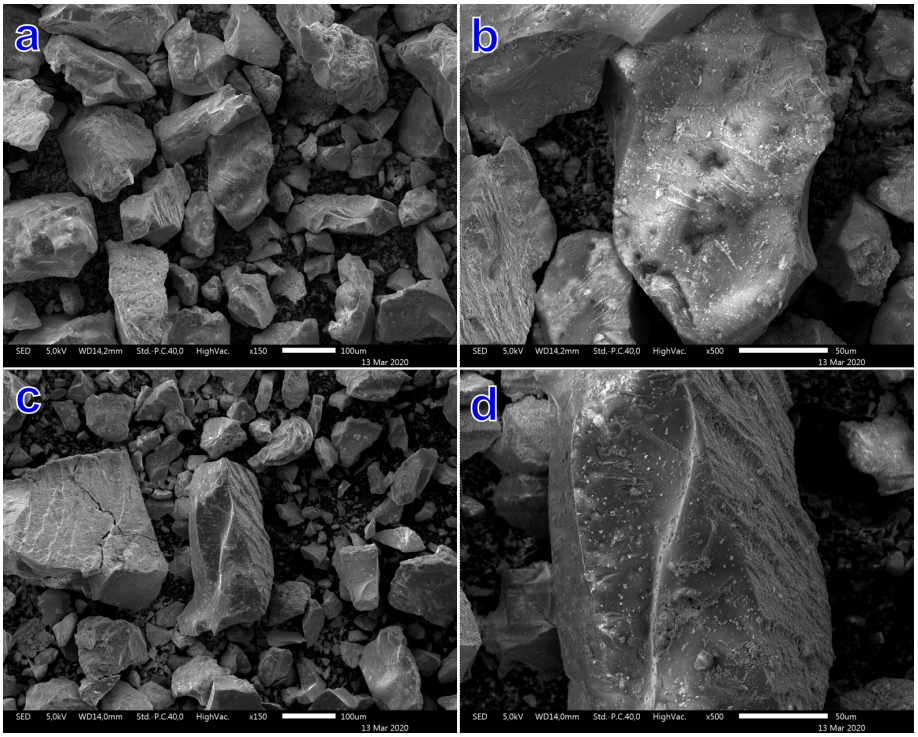

EDS technique was used to verify and confirm the elements presence and distribution over the samples. Silicon, nitrogen, titanium, cobalt, carbon, oxygen and chlorine were detected in both samples. The analysis was helpful to observe the elements along

the surface, as shown in Figure 33. The green spots in Figure 33 b are a representation of cobalt distribution on the sample. Thus, they make it clear that the white particles that were found on the powder grains are composed by cobalt. The particles and agglomerates sizes were in the nanometer to a few micrometers scale. On the other hand, titanium was largely spread along with nitrogen and silicon, since the reaction of its precursor with PHPS produced titanium nitride.

Figure 33 – SEM (a) with respective EDS mapping (b) of the powder PHTiCo5 obtained at 1000 ℃ under NH_3

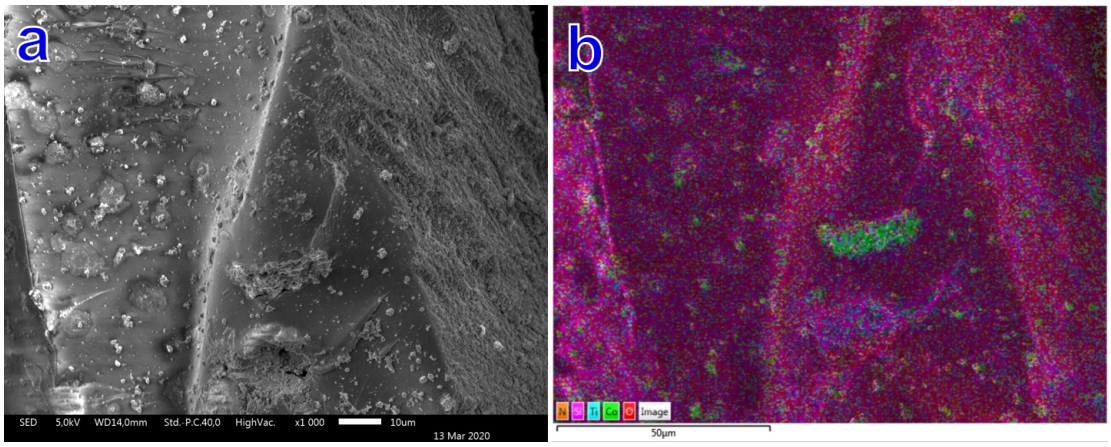

Several works illustrate the different possibilities with transition metals such as Ti and Co for the manufacturing of highly active catalysts, mainly in oxide systems (BAGHERI; MUHD JULKAPLI; BEE ABD HAMID, 2014; FENG, J.-X. et al., 2017; MEJIA; DEELEN; JONG, 2018). Xuanyu Feng et al. (2019) developed porous titanium metal-organic frameworks (Ti-MOFs) with cobalt secondary bridges to be employed in catalysis applications. The authors demonstrated that Co^{II}-hydride species are highly active for selective cascade reduction of N-heterocyclic rings of pyridines and quinolines. Another strategy involving the combination of cobalt and titanium was reported by L.C. Seitz et al. (2015), that synthesized $CoTiO_x$ catalysts for oxygen evolution reaction (OER) in electrochemical water splitting. The scientists explored the microstructure and chemical state of the materials produced via sol-gel technique, and could state that varying the concentrations of Ti and Co had an impact on their local geometric structure, activity, and electronic structure (SEITZ, Linsey et al., 2016). Based on published studies, the novel powders and monoliths generated in the present work could be further explored and tailored for a wide range of applications. This possibility is not only because of the metals catalytic activity, but also related to the outstanding performance proportionated by the silicon nitride system.

4.1.3 Design of micro-/mesoporous monoliths

The polytitanosilazane **PHTiPS2.5** was chosen among the produced polymetallosilazanes for the preparation of micro-/mesoporous monoliths according to the nanocasting procedure described in the methodology. The choice was done based on the excellent previous results and its lower cost compared to molybdenum and vanadium precursors. As illustrated, the polymer solutions were used to impregnate the activated carbon monoliths. The pyrolysis was performed until 400 ºC under N_2 for crosslinking and then the gas was switched to NH_3 for the carbon template removal during treatment until 1000 ℃. This strategy generated the monoliths **mPHTiPS2.5_10_NH_3**. The obtained monoliths were subjected to annealing under N_2 until 1400 ℃, and the resulting samples were called **mPHTiPS2.5_14_N_2**. Aiming the evaluation of **PHTiPS2.5** enhanced properties, monoliths were impregnated with pure PHPS and treated until 400 ºC under N_2 and until 1000 ℃ under NH_3 to generate PHPS-derived Si_3N_4 monoliths, here called **mSi_3N_4_10_NH_3**, to be considered as the blank. In Figure 34 it is possible to observe the monoliths after heat treatment.

Figure 34 – Monoliths after pyrolysis

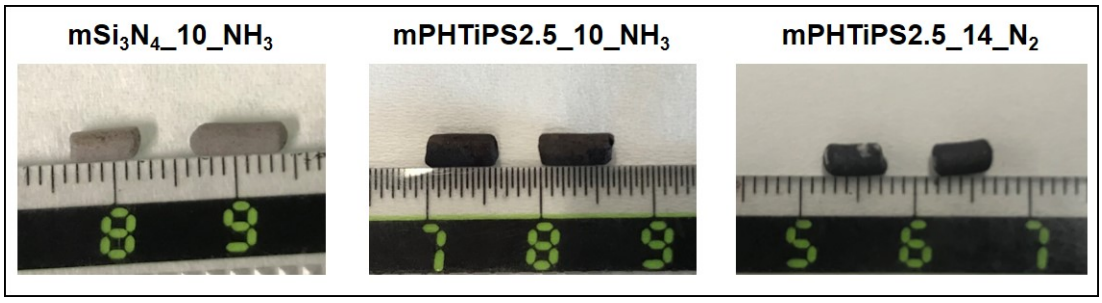

Few but important conclusions could be obtained after nanocasting. PHPS-derived monoliths were gray, the same colour as Si_3N_4 powder. That is indicative the carbon template was successfully removed due to ammonia treatment. Furthermore, the monoliths did not shatter, keeping the apparent shape. Gray spots could be detected on samples **mPHTiPS2.5_14_N_2**, that were certainly Si_3N_4. XRD, BET and SEM/EDS were the applied characterisation analyses to fully identify the pore arquitecture and the crystal structure.

Figure 35 displays the obtained BET isotherms and the respective pore size distribution (PSD) after analysis using the pyrolysed monoliths **mSi_3N_4_10_NH_3**. The sample **mSi_3N_4_10_NH_3** could be identified as mesoporous because of its isotherm type IV, which is linked to capillary condensation occurring in the mesopores. The adsorption and desorption isotherms are asymmetrical and were classified as type H2(a) according to the IUPAC

normative (THOMMES et al., 2015). In relation to its specific surface area (SSA), a value of 421.2 $m^2.g^{-1}$ was obtained, and pore size of 4.5 nm.

Figure 35 – BET isotherms and PSD for PHPS-derived Si_3N_4 monoliths pyrolysed at 1000 ℃ under NH_3

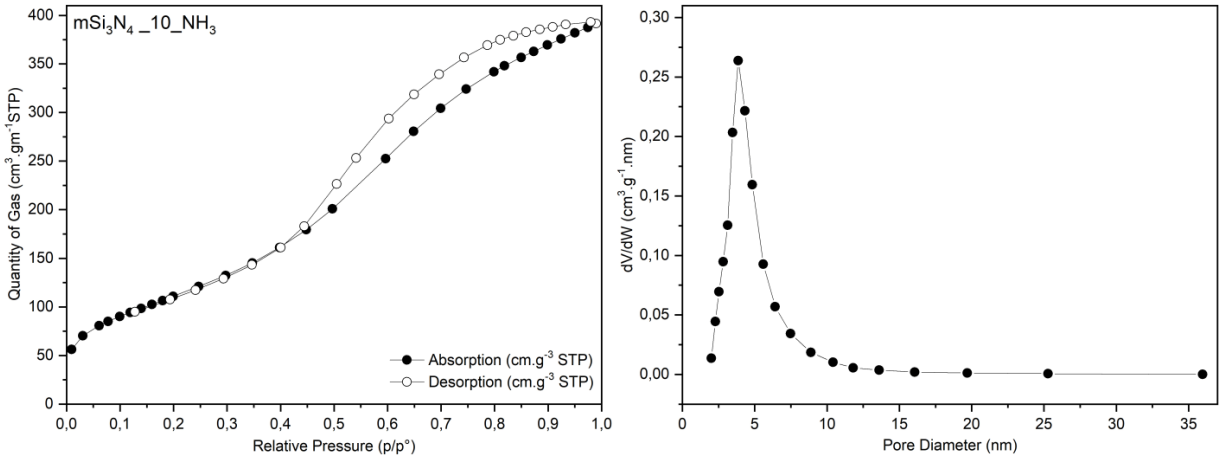

In previous studies from our research group, it has already been demonstrated that polysilazane-derived ceramics can form Si_3N_4 nanowires by means of heat treatment at temperatures above 1000 ℃ (MAJOULET et al., 2013). As a consequence, Si_3N_4 monoliths are not able to keep high surface areas at elevated temperatures, being 1000 ℃ the most suitable temperature for these specimens.

The BET isotherms of **mPHTiPS2.5_10_NH_3** suffered a modification in comparison to **mSi_3N_4_10_NH_3**. As it can be observed in Figure 36, the isotherms changed from type IV to a mixture of it with type II, suggesting the formation of microporosity at pressures P/P_0 below 0.45. Above this pressure, the occurrence of hysteresis loops type H2(a) between adsorption and desorption indicate mesoporosity. Such affirmations are of great importance for this work because it is possible to call the produced materials as micro-/mesoporous monoliths with interconnectivity, which is an excellent achievement for catalyst supports.

Regarding the SSA, a great increase for the nanocomposite monolith in comparison to pure PHPS-derived monolith was found: 1165.7 $m^2.g^{-1}$, which is among the best results already published for mesoporous PDCs. The pore size was around 2 nm. With further heating, the monoliths **mPHTiPS2.5_14_N_2** presented similar isotherm behavior (Figure 37), however the SSA dropped as the temperature increased. The SSA reached values of 857.6 $m^2.g^{-1}$ and pore size as small as 3 nm. It was necessary to examine the monoliths obtained at 1400 ℃ by SEM to assess the reasons for the drop in the SSA values.

According to the SEM images in Figure 38, at 1400 ℃ there was the formation of what were considered as Si_3N_4 nanowires and then confirmed by EDS mapping technique.

Figure 36 – BET isotherms and PSD for PHTiPS2.5 monoliths pyrolysed at 1000 ℃ under NH_3

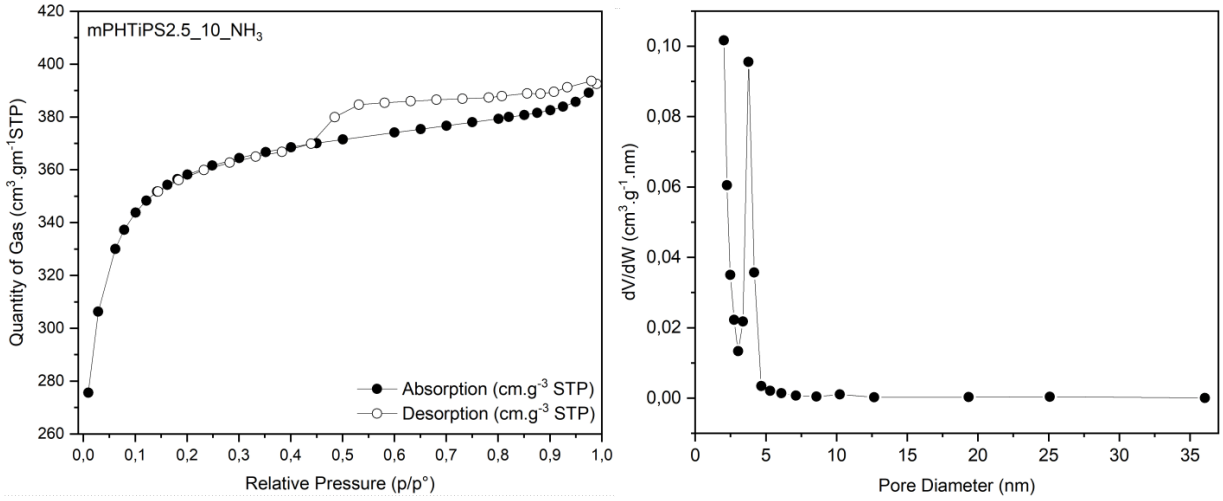

Figure 37 – BET isotherms and PSD for PHTiPS2.5 monoliths pyrolysed at 1000 ℃ under NH_3 and at 1400 ℃ under N_2

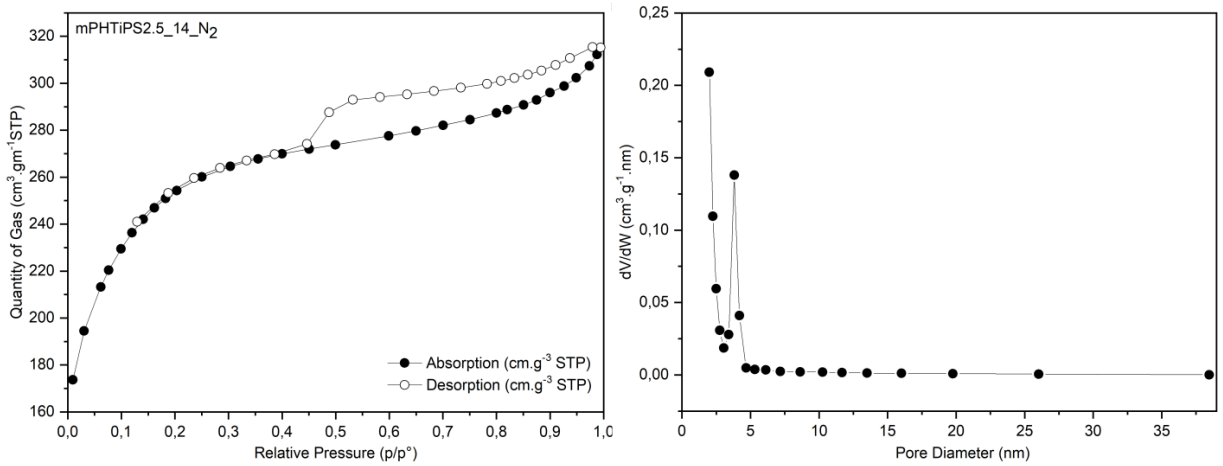

Such phenomenum can explain why the SSA values fell from 1165.7 to 857.6 $m^2.g^{-1}$. Furthermore, this could mean that a fraction of Si_3N_4 could be starting to crystallize, corroborating with the spotting of gray marks on the monoliths in Figure 34.

However, these facts were not enough to fully understand the great SSA for the nanocomposite monoliths, since pure PHPS generated much smaller values. As recently reported (Lale, Mallmann, et al. (2020)), the enormous SSA obtained in this work can be attributed to retention of the carbon template, as highlighted in Figure 39. Titanium nitride is widely used as diffusion barrier that separate adjacent materials from the metal interconnect, mainly in dielectrics and semiconductors materials. TiN work as an obstacle that does not allow the migration of atoms from the metallization to the surrounding parts or the silicon substrate, in a way that prohibits chemical reactions that could happen in the

devices stopping them from their functionality (SHIN et al., 2012; KIM et al., 2009; WU, W.-F. et al., 2005; KOHLHASE; MANDL; PAMLER, 1989). Based on these properties, TiN could also act as a diffusion barrier for NH_3 during pyrolysis, preventing the activated carbon to be completely removed. The initial treatment under N_2 until 400 ℃ for crosslinking, possibly promoted the formation of a coating over the surface of ACM that consequently protected the template when the gas was switched to NH_3.

Figure 38 – SEM analysis at 140 and 400x magnification on the surface of mPHTiPS 2.5_14_N_2

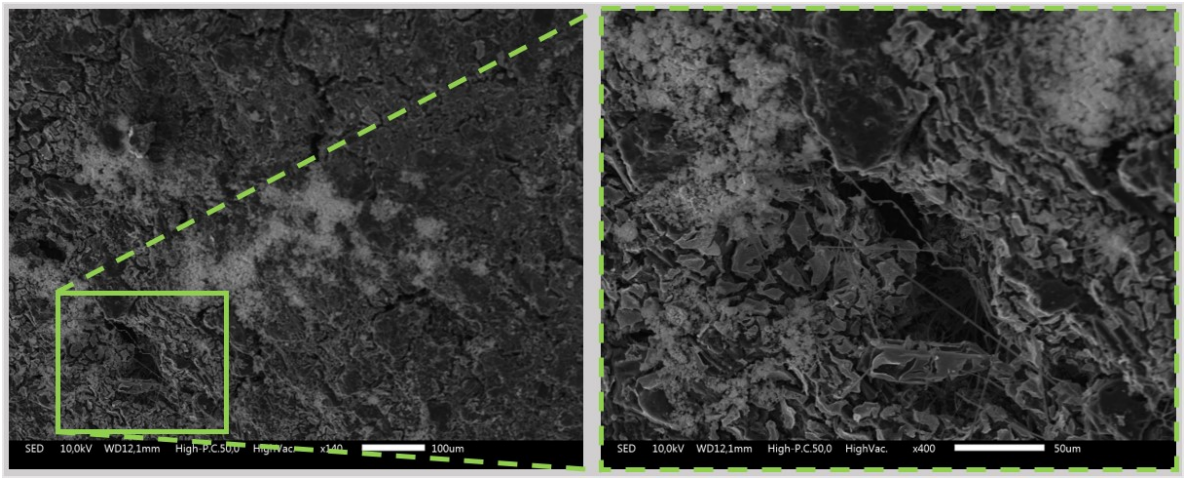

Figure 39 – SEM analysis on the surface of mPHTiPS 2.5_14_N_2 highlighting the Si_3N_4 nanowires and the activated carbon template

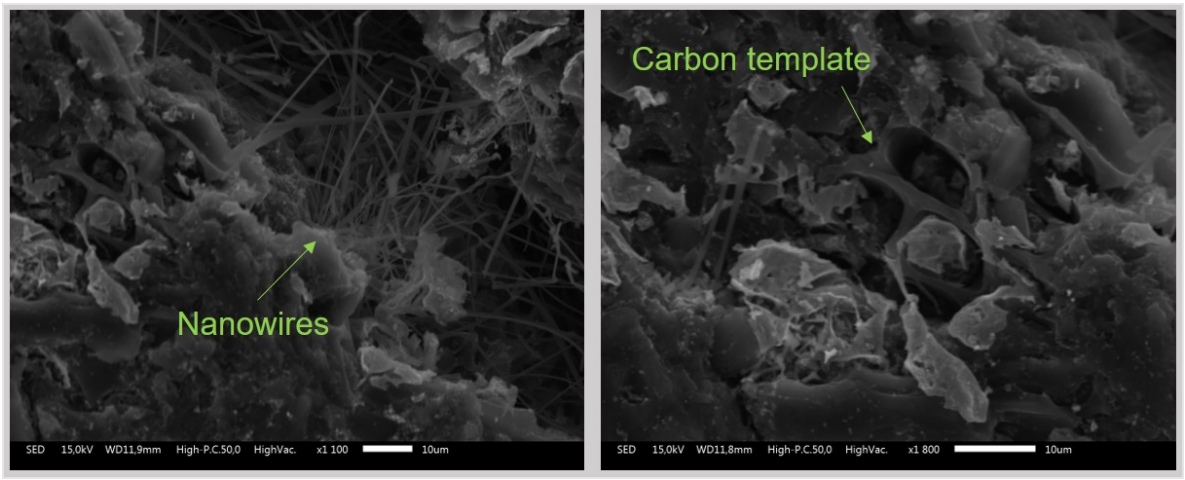

EDS mapping was used to observe the surface composition and elements distribution. The generated coloured images displayed in Figure 40 reinforced the idea that TiN acts as a diffusion barrier and protects the template, since it is noticeable that titanium was mostly present in the same location as carbon.

Figure 40 – EDS mapping for elements identification on the surface of mPHTiPS2.5_14_N_2

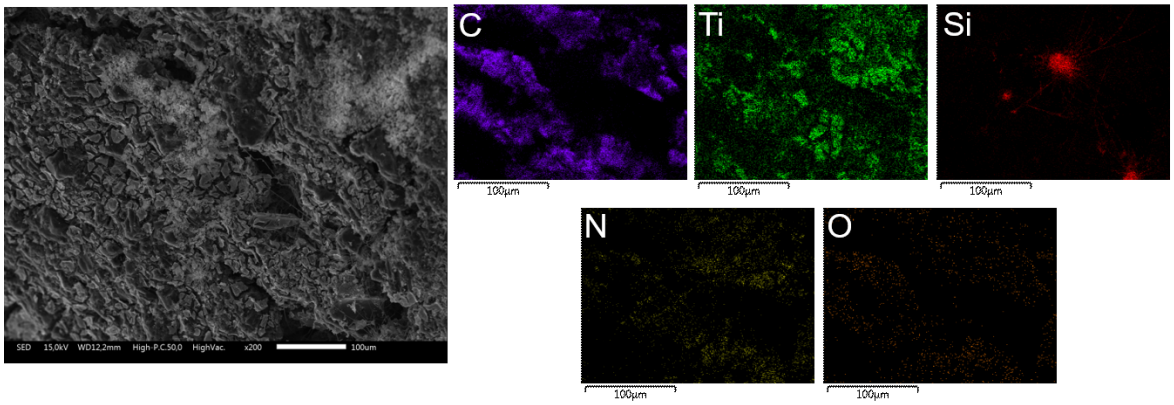

The produced monoliths were crushed into fine powders and analysed by XRD. Activated carbon monoliths (ACM) were also investigated after passivation at 600 ℃. The resulted patterns of the nanocomposite monoliths are shown in Figure 41 along with the blanks: **mSi$_3$N$_4$_10_NH$_3$** and **ACM**. At 1000 ℃ the material **PHTiPS2.5_10_NH$_3$** was amorphous. Annealing at 1400 ℃ promoted the crystallization of TiN and α-Si_3N_4 (marked with "α" in the graph), in agreement with SEM that evidenced the formation of Si_3N_4 nanowires.

Figure 41 – XRD of the monoliths: blanks and nanocomposites

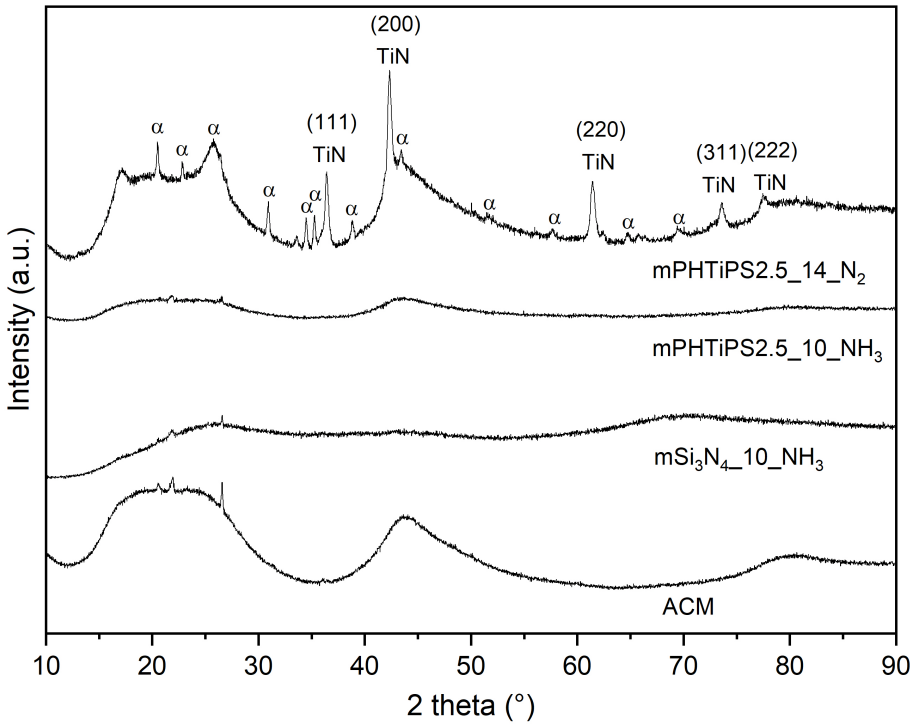

Interestingly, the crystallization was different comparing the monoliths to the pow-

ders discussed in the previous section. El-Sharkawy et al. (2008) worked with highly porous activated carbon and observed the template can act as a heat sink, i.e., it is able to drain a larger heat amount from the nanocomposite, causing a delay in the crystallization. Thus, TiN was not crystallizing at 1000 °C in the porous structure.

4.1.3.1 Deposition of metal nanoparticles on the micro-/mesoporous monoliths

Titanium nitride has been studied by several authors as active support for catalysts, mainly Pt nanoparticles. Our group has recently published a study (Lale, Mallmann, et al. (2020)) involving the synthesis of Pt nanoparticles by hydrogen gas, on micro-/mesoporous Si-Ti-N monoliths with outstanding catalysis properties in the hydrolysis of $NaBH_4$. TiN acted as co-catalyst, allowing the use of reduced quantities of Pt (1 wt%). In this work, a different strategy to produce Pt nanoparticles was applied. The method consisted in their reduction directly on the monoliths **mPHTiPS2.5_14_N_2** and posterior heat treatment at 450 °C under argon. Cobalt and nickel nanoparticles were also synthesized by this method, to compare the catalytic performance of the final materials.

Firstly, the nanoparticles were produced separately to observe their formation. The process was confirmed by colour conversions. Nickel and cobalt solutions were green and pink and became black and dark brown, respectively. For platinum, the initial solution was yellow and converted to black, revealing the reduction of Pt(IV) ions into Pt(0) nanoparticles. Figure 42 displays the UV-visible spectra for all the nanoparticles dispersed in water. The spectra are in accordance with the literature (KANWAL et al., 2019; KUMAR; GOVINDH; ANNAPURNA, 2017; AZUM et al., 2016; HAMMAD; SALEM; HARRISON, 2013; WU, H.-X. et al., 2010; CHEN et al., 2007; PATEL; KAPOOR, et al., 2005).

Accordingly, the nanoparticles were reduced directly on the monoliths applying a wet impregnation procedure. Pt, Co and Ni quantity were fixed to 1 wt% in relation to the monoliths. Interestingly, the solutions did not have the same colours as in the process without the monoliths, which demonstrates the reduction happened inside the pores. This also indicates a good compatibility between the particles and the support.

After the nanoparticles deposition on the nanocomposite monoliths obtained through the heat treatment until 1400 °C (**mPHTiPS2.5_14_N_2**), they were evaluated by SEM/EDS and XRD. The first technique allowed to see the elements distribution over the ceramic structure and also confirm the nature of such elements. The metals deposition was confirmed as it is possible to see in Figure 43. Besides Si, Ti, C, N and O, Na was also detected, which is a residue from the reduction of sodium borohydride applied for the nanoparticles reduction. Additionally, the metals massic quantity could be estimated between 1 and 3 wt%.

Figure 42 – UV-visible spectra of Pt, Co and Ni nanoparticles

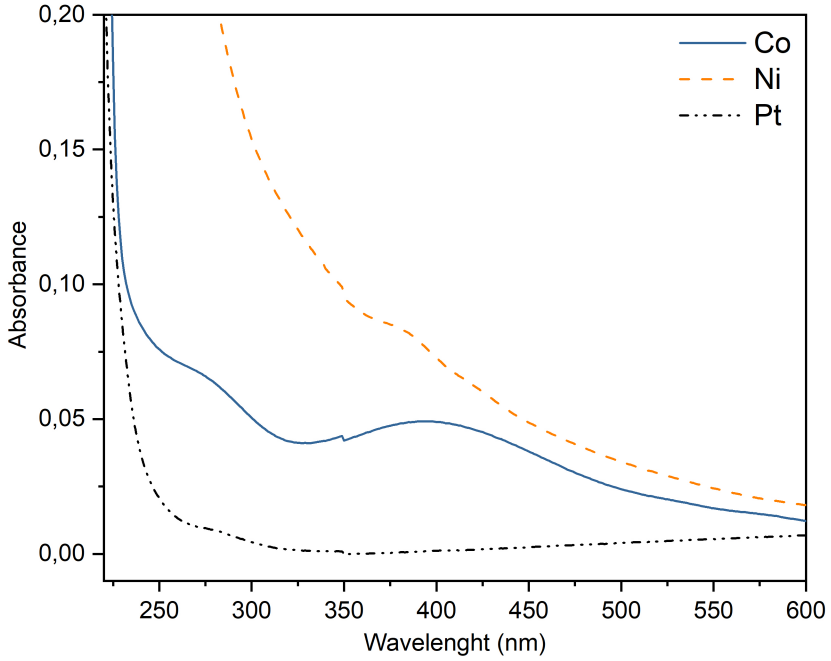

Figure 43 – EDS of mPHTiPS2.5_14_N_2 after Pt, Co and Ni nanoparticles deposition

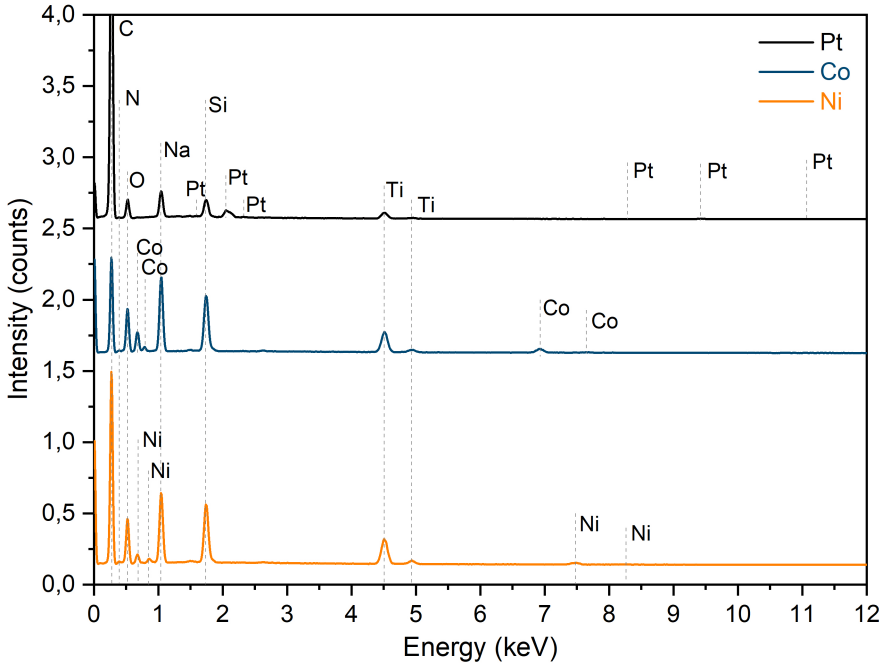

The samples were evaluated by XRD to verify if any pattern related to the metals could be found. As it can be seen in Figure 44, TiN and α-Si_3N_4 were identified, as expected. The monoliths impregnated with Pt displayed peaks at 2θ= 46.24°, 67.45° and 81.28°, that have correlation with the ICDD file No. 00-004-0802 for the planes (200), (220) and (311) of face-centered cubic structure of Pt. It was not possible to detect Co and Ni

patterns for the other two samples, and the explanation relies on the relation between the detection limit and the metal mass fraction.

Figure 44 – XRD patterns of mPHTiPS2.5_14_N_2 after Pt, Co and Ni nanoparticles deposition

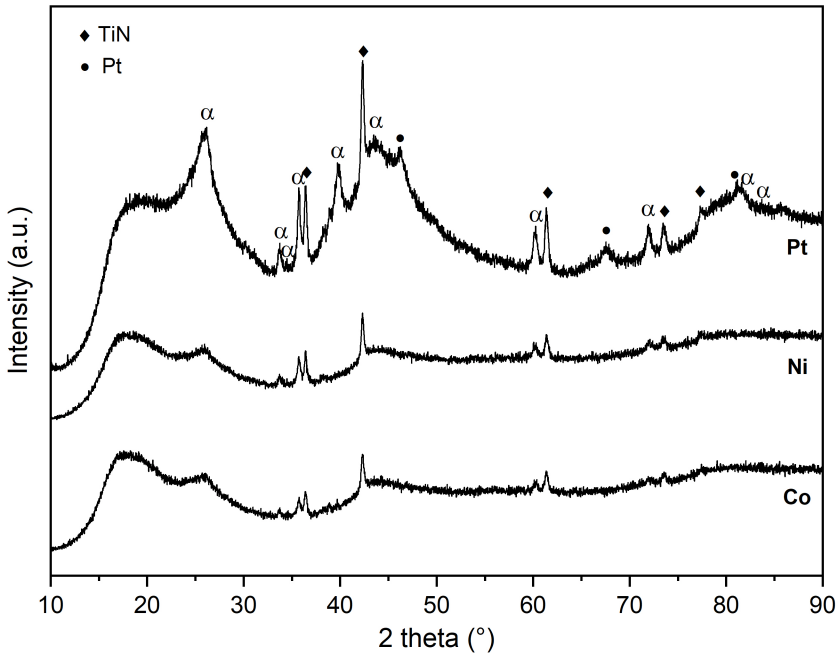

The monoliths specific surface area was measured by BET, with the objective of verifying if the nanoparticles deposition had affected the material porosity. The monoliths had a SSA of 857.6 $m^2.g^{-1}$ before nanoparticles deposition. After that, this value was reduce to 815 $m^2.g^{-1}$ for nickel, 770 $m^2.g^{-1}$ for cobalt and 601 $m^2.g^{-1}$ for platinum. The presence of nanoparticles reduced the SSA most probably because of their positioning within the pores. This can be verified analysing the samples t-plot, that is a method technique which allows the determination of micro- and/or mesoporous volumes (GALARNEAU et al., 2014). In comparison to **mPHTiPS2.5_14_N_2**, the same monoliths but after platinum deposition, presented a reduction in the t-plot micropore volume from 0.19 to 0.13 $cm^2.g^{-1}$. Thus, it is possible that micropores were blocked after *in-situ* formation of Pt nanoparticles. For Ni- and Co-functionalized monoliths, the t-plot values were 0.17 and 0.15 $cm^2.g^{-1}$. As it can be noticed, the micropore volumes had a direct relation with the samples SSA.

4.1.3.2 Micro-/mesoporous monoliths based on titanium and cobalt

Activated carbon monoliths were also applied as templates for the impregnation of **PHTiCo5**. The objective was to evaluate if the polymer was suitable for the impregnation process, yielding monoliths with high specific area and well distributted active sites. Thus, impregnated monoliths were pyrolysed under nitrogen until 400 °C, following the same

conditions specified for all monoliths produced in this work, and then the gas was switched to ammonia, with two different final temperatures: 800 and 1000 °C. This process generated the here named **mPHTiCo5_8_NH$_3$** and **mPHTiCo5_10_NH$_3$**.

Figure 45 shows both isotherms. The specific surface area values were 1073 and 1283 $m^2.g^{-1}$ for the monoliths obtained at 800 and 1000 °C, respectively. The monoliths were not pyrolysed at higher temperatures because of the poor stability of cobalt above 1000 °C, that was observed through TGA analyses. The BET results however, showed a great increase in the monoliths SSA along with the pyrolysis temperature.

Figure 45 – BET isotherms for PHTiCo5 monoliths pyrolysed at 800 and 1000 °C under NH_3

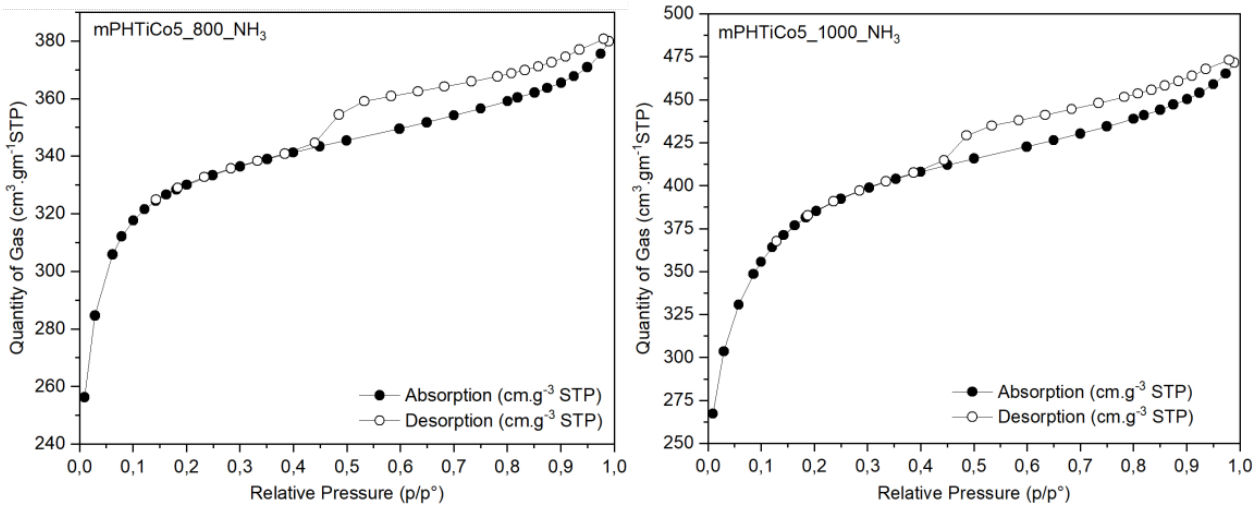

As already mentioned in this work, the elevated SSA is related to the retention of the activated carbon template caused by the action of TiN as diffusion barrier, preventing NH_3 reaction with carbon. Based on this hypothesis, the obtained monoliths were analysed by XRD, as exhibitted in Figure 46. **mPHTiCo5_8_NH$_3$** and **mPHTiCo5_10_NH$_3$** were compared to pure ACM, passivated at 600 °C as described in the methodology chapter. The main possible conclusion that could be made as the XRD results were studied was that the final monoliths structure was still amorphous and the activated carbon template was not fully removed, since the only detected signs were similar with pure ACM.

Moreover, the XRD is comparable to **mPHTiPS2.5_10_NH$_3$**, that was also amorphous (Figure 41). Thus, SEM coupled with EDS was used as an additional technique to observe the carbon template preservation at 1000 °C. EDS mapping of the monolith **mPHTiCo5_10_NH$_3$** can be observed in Figure 47. The detected elements were carbon, silicon, oxygen, titanium, nitrogen and cobalt.

Carbon was identified in expressive amounts in the sample, which corroborates

Figure 46 – XRD patterns of mPHTiCo5_8_NH_3 and mPHTiCo5_10_NH_3 compared to ACM

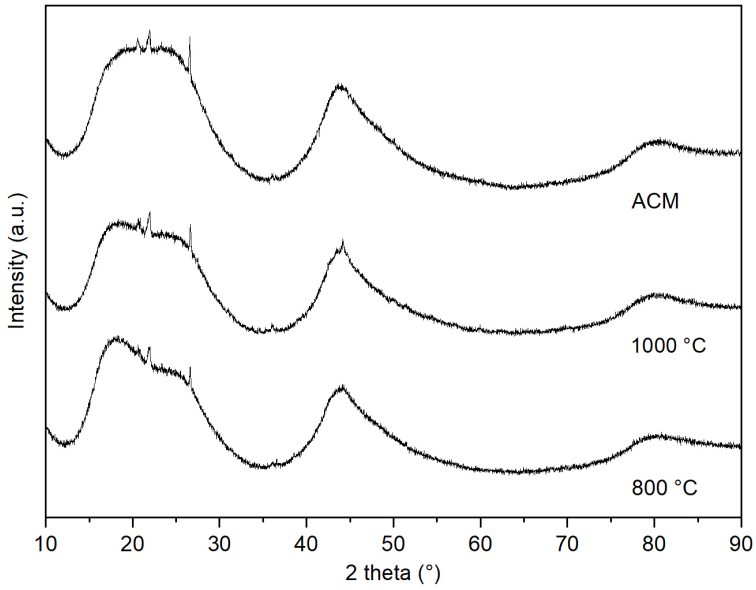

Figure 47 – EDS mapping for elements identification on the surface of mPHTiCo5_10_NH_3

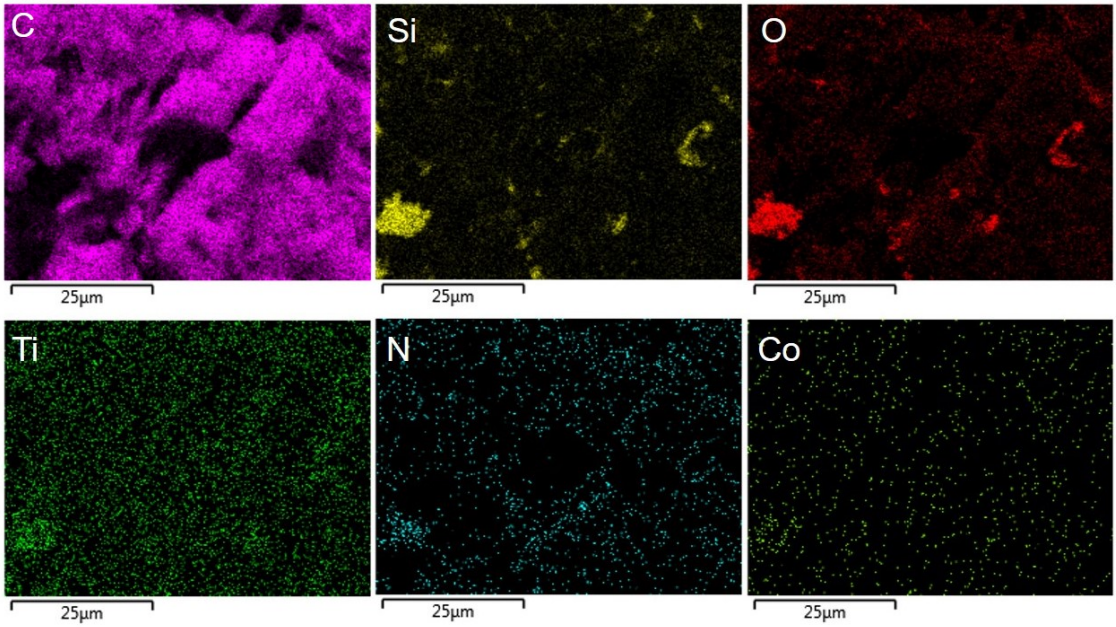

the affirmation the template is retained. Titanium was largely distributted and could be positioned as a coating over carbon, preventing its removal during heat treatment under ammonia.

4.1.4 Hydrolysis reactions

This section is dedicated for the presentation and discussion of the performance of the produced micro-/mesoporous monoliths as supported catalysts for the hydrolysis of sodium borohydride. As described in the methodology chapter, the materials catalytic performance was evaluated in alkaline solution (pH > 10) at 80 ℃ using 16 mg of the sample for the dehydrogenation of $NaBH_4$ during 180 minutes of reaction.

The graph presented in Figure 48 exposes the hydrogen volume (in mL) that was generated during hydrolysis of $NaBH_4$. The studied monoliths were **mPHTiPS2.5_14_N_2** (yellow curve) and the same monoliths but impregnated with cobalt (blue line), platinum (black line) and nickel (orange line) nanoparticles.

Pt-containing monoliths exhibitted the highest hydrogen generation among the samples, which was already expected by its enormous catalytic activity and the synergy between Pt nanoparticles and TiN nanoclusters. Such structures are known to have a smaller size than 2 nm and thus provide a bridge between metal atoms and nanoparticles (BAKIRHAN; OZKAN, 2018). The precipitation of TiN nanoclusters in the amorphous Si_3N_4 matrix promoted the great performance **mPHTiPS2.5_14_N_2** and justify the nanoparticles deposition on the nanocomposite monolith.

Figure 48 – Hydrogen volume generated by mPHTiPS2.5_14_N_2 before and after Nps deposition

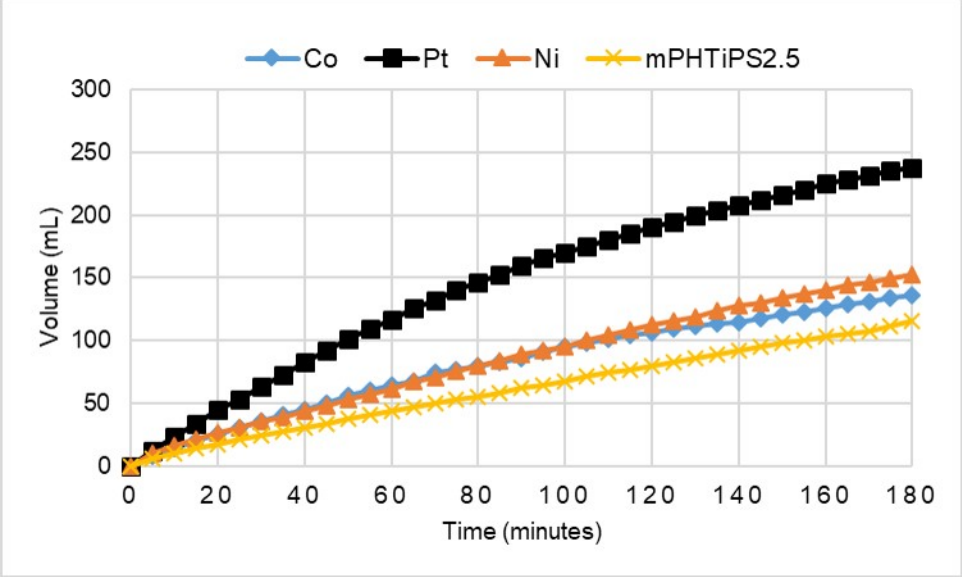

The hydrogen generation rate was calculated based on the slope of the curves at < 50 % conversion and considering 1 wt% of catalyst. The following values were obtained: 12 $L.min^{-1}.g_{Pt}^{-1}$ (**Pt**) , 6.4 $L.min^{-1}.g_{Co}^{-1}$ (**Co**) and 5.9 $L.min^{-1}.g_{Ni}^{-1}$ (**Ni**).

Cobalt and nickel nanoparticles presented lower hydrogen generation levels than platinum, that is explained by the strong catalytic activity of nobel metals. An increase in the Co/Ni nanoparticles wt% could be interesting to achieve enhanced hydrogen production.

In comparison to works found in the literature that reported the use of platinum catalyst-supported carbon materials, the results obtained in this thesis were expressively superior. Considering a proportional amount of catalyst in the system, Bai et al. (2006) could obtain a hydrogen generation of 1.8 $L.min^{-1}.g_{Pt}^{-1}$. Although applying activated carbon with elevated SSA as support, Xu, Zhang, and Ye (2007) produced 1.5 $L.min^{-1}.g_{Pt}^{-1}$ of hydrogen. This shows that not only the high SSA is important to achieve good levels of catalysis activity, but also the interaction between the metallic nanoparticles and the support.

More than that, the monolith **mSi_3N_4_10_NH_3** was also tested for $NaBH_4$ hydrolysis and presented high catalytic activity, demonstrating the amorphous Si_3N_4 is essential for promoting the great performance of the TiN/Si_3N_4 nanocomposite-based catalyst (LALE; MALLMANN, et al., 2020).

For a deeper understanding of the chemistry involved in the hydrolysis reaction, the surface acido-basic centers of **m_Si_3N_4_10_NH_3** sample were investigated by pyridine adsorption spectroscopy. Pyridine is the most applied basic probe molecule for surface acidity characterization (BUSCA, 1998). FTIR analyses enable the observation of vibrational perturbation caused by pyridine adsorption on the surface sites (KNOUZINGER, 1976; ZAWADZKI, 1988; ZAKI et al., 2001) Based on this investigation, it was possible to notice that during $NaBH_4$ hydrolysis, the Pt-TiN electron conductive nanoclusters produced hydridic hydrogen ($H^{\delta-}$). Silicon cations acted as acid sites, following Lewis definition, and reacted with species from the reaction medium (water) lowering the free energy of the atoms exposed on the surface of the material. By its turn, water saturated the coordinative unsaturations, which made Lewis acidity to completely disappear at the same time hydroxy-groups were formed, that could be responsible for BrØnsted acidity. Hydrogen generated from water molecule was possibly catalyzed by the acid site formed on the amorphous Si_3N_4 matrix, yielding a protonic hydrogen ($H^{\delta+}$) (LALE; MALLMANN, et al., 2020).

It is important to mention the nanocomposite structure of TiN/Si_3N_4 consists in electron conductive nanoclusters (TiN) embedded within electron insulating mesoporous amorphous matrix (Si_3N_4), and this structure plays a key role to efficiently provide $H^{\delta-}$ species, since TiN acted as an electron acceptor. In other words, a structure based on Pt-loaded TiN nanocrystallites would not generate the same levels of hydrogen volume as it does when embedded in the amorphous Si_3N_4 network. In Figure 49 is presented a scheme that comprises the possible synergistic effect that has just been explained.

The performance of the monoliths **mPHTiCo5_8_NH_3** and **mPHTiCo5_10_NH_3**

Figure 49 – Possible synergistic effect during $NaBH_4$ hydrolysis catalyzed for the hydridic and protonic hydrogen formations by Pt-TiN nanoclusters and acid sites on mSi_3N_4

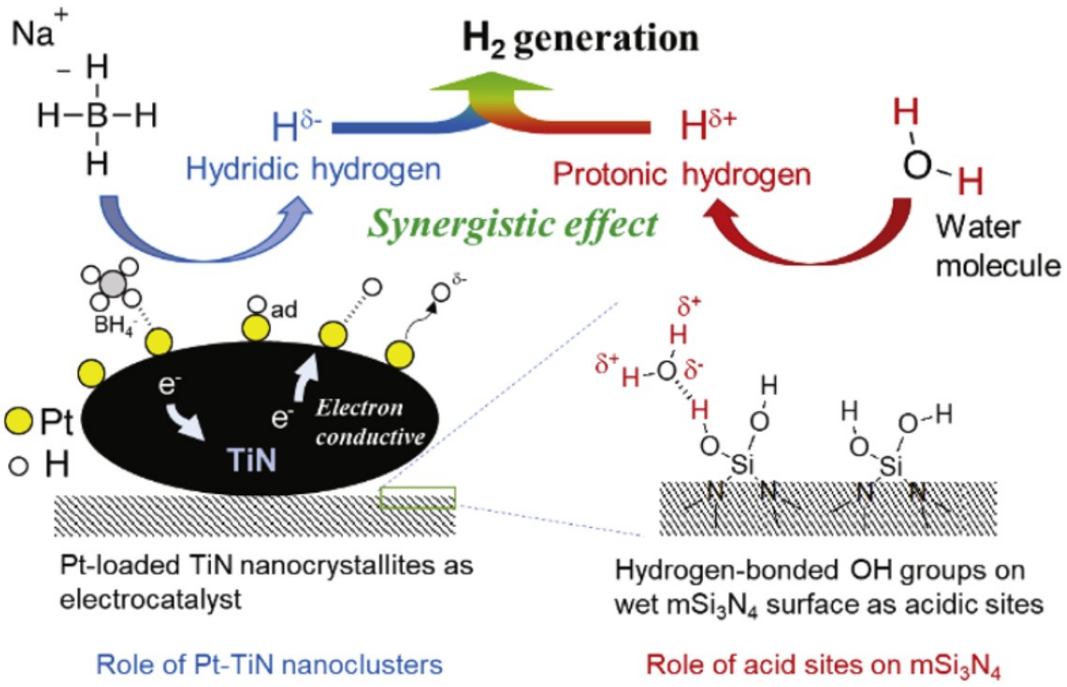

Source: Lale, Mallmann, et al. (2020)

were evaluated in hydrolysis reactions as well, under the same conditions used for the already presented monoliths. As it can be verified in the graph represented in Figure 50, the generated volume of hydrogen was similar for the monoliths treated at different temperatures (800 and 1000 ℃).

These materials were not able to generate expressive amounts of hydrogen during 180 minutes of reaction. One reason the can explain the behavior is related to Si_3N_4. The monolith **m_Si_3N_4_10_NH_3** presented high catalytic activity in similar reaction, demonstrating the amorphous Si_3N_4 is essential for promoting the great performance of the TiN/Si_3N_4 nanocomposite-based catalyst (LALE; MALLMANN, et al., 2020). In contrast, the monoliths based on the polymer PHTiCo5 had an earlier crystallization of α- and β-Si_3N_4, reducing the production of protonic hydrogen, that would take place on the surface of mesoporous amorphous Si_3N_4.

Figure 50 – Hydrogen volume generated by mPHTiCo5 obtained at 800 and 1000 ℃

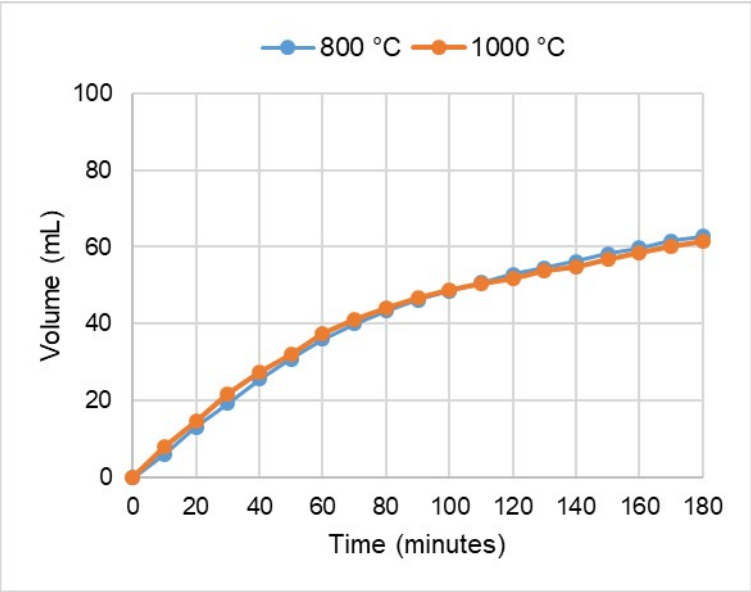

4.2 SYNTHESIS OF METAL-DOPED SILICON NITRIDE

The high reactivity of metal chlorides for the hydrolysis of sodium borohydride, along with their attractive cost compared to noble metal catalysts, sparked a growing interest in the varied possibilities for the use of such materials. Within this context, Co and Ni chlorides and complexes were studied in the present work and this section reports the synthesis of metal-doped silicon nitride (M@Si_3N_4, M= Co, Ni). The obtained polymers are characterized, as well as their polymer-to-ceramic conversion and the crystal structure of the obtained ceramics. Moreover, the mesoporous M@Si_3N_4 monoliths and their performance as catalytic supports for the hydrolysis of $NaBH_4$ are documented and discussed.

4.2.1 Synthesis of the polymers and ceramic conversion

4.2.1.1 PHPS and HTT1800 and MCl_2 for Co/Ni-doped polysilazanes

The organosilicon polymers applied in this approach were PHPS and HTT 1800. Firstly, they were reacted with $CoCl_2$ and $NiCl_2$ at a fixed molecular Si:M (M= Ni, Co) ratio of 5, for the period of three days. After solvent extraction, **PHCoPS5**, **PHNiPS5** and **HTTNi5** were solid polymers and **HTTCo5** was a viscous liquid. The polymers physical aspect can be observed in Figure 51.

Figure 51 – Obtained polymers of PHPS and HTT1800 on the reaction with MCl_2 (M= Co, Ni) after three days

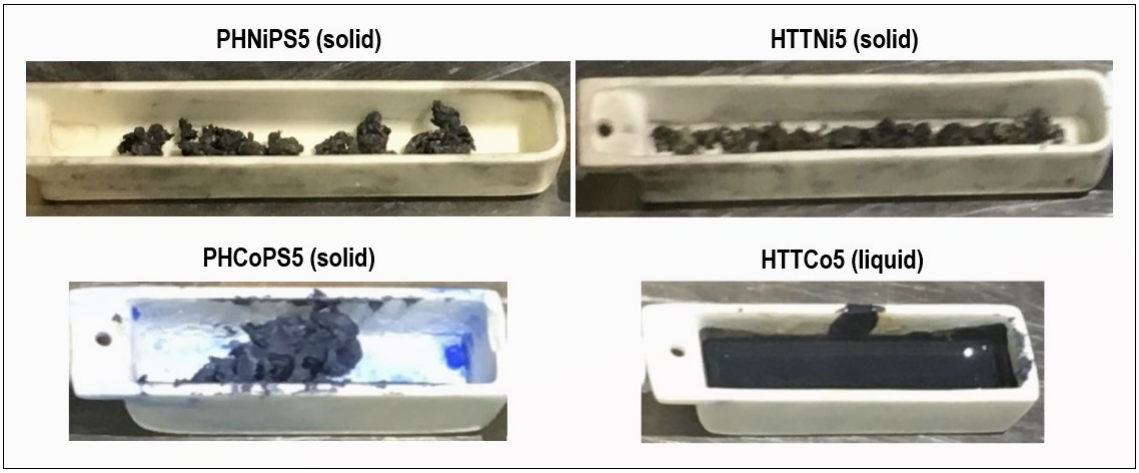

As-obtained materials were analyzed by FTIR to identify the chemical groups in the samples. The metal-doped polymers produced with HTT1800 are represented in Figure 52. The FTIR of pure polysilazane presents the expected absorption bands as reported in the literature: 3380 cm^{-1} (νN-H), 3049 cm^{-1} (νC=C), 2960 cm^{-1} (νC-H), 2120 cm^{-1} (νSi-H), 1590 cm^{-1} (δC=C), 1400 cm^{-1} (νC-H), 1250 cm^{-1} (δSi-CH_3) and 1160 cm^{-1}

(δN-H). The bands in the 1000-500 cm^{-1} range can be associated to stretching and deformation vibrations of Si-C, Si-N, C-H and C-C bonds, which overlap and are difficult to be individually identified (FLORES et al., 2013; SEIFOLLAHI BAZARJANI et al., 2011).

Figure 52 – Polysilazane HTT1800 spectrum compared to metal chlorides-doped HTT

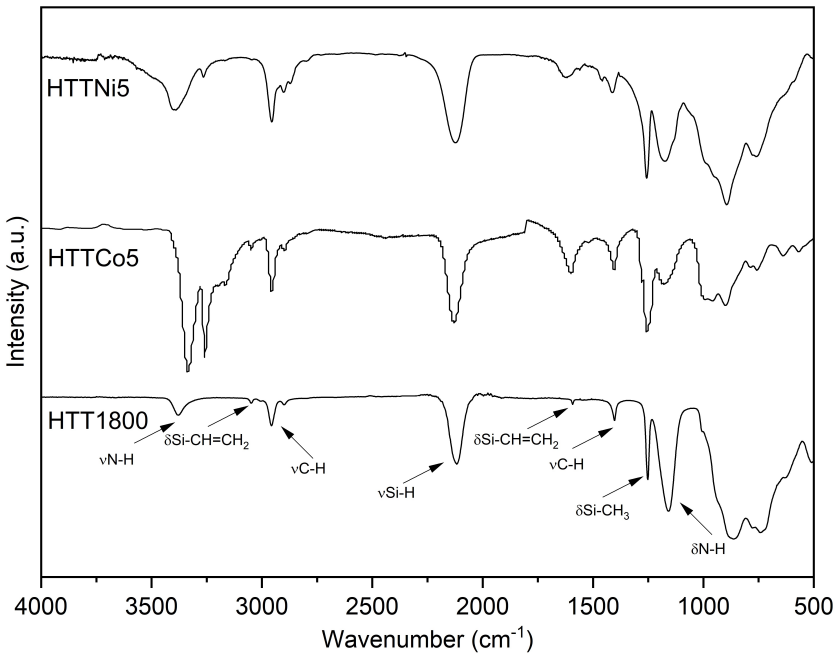

For **HTTCo5**, it is possible to notice that bands in the region below 1000 cm^{-1} suffer some modification in comparison to the pure polysilazane. Moreover, it presents two bands at 3330 and 3260 cm^{-1}, instead of one, which are characteristic of asymmetrical and symmetrical N–H stretching, respectively. In addition to that, a reduction of δN-H at 1160 cm^{-1} can be an indication of reduction of Si-NH-Si linkages and NH_3 release (SEIFOLLAHI BAZARJANI et al., 2011).

Figure 53 shows the FTIR evolution of **HTTCo5** when treated until 200 and 450 °C under NH_3. At 200 °C, Si-H bonds are reduced, which could be related to dehydrocoupling reactions of Si-H/Si-H and Si-H/N-H groups. At the same time, δN-H bonds at 1160 cm^{-1}, corresponding to Si-NH_2, disappear. According to Wan, Gasch, and Mukherjee (2002), the absence of Si-NH_2 signals indicates the reaction in Equation 11 can be occuring.

$$\equiv Si-NH_2 + CH_3-Si \equiv \longrightarrow \equiv Si-NH-Si \equiv + CH_4 \tag{11}$$

When the temperature is increased until 450 °C, other observations can be pointed out. Firstly, the appearance of bonds in the region from ~880 to ~1180 cm^{-1}, possibly related to Si-NH-Si bonds, and the appearance of broad N-H bonds at ~3400 cm^{-1}. Considering that the heat treatments were performed under NH_3, ammoniation reactions could be mentioned herein.

Figure 53 – FTIR spectra of HTTCo5 polymer and after treatment at 200 and 450 °C in NH_3 atmosphere

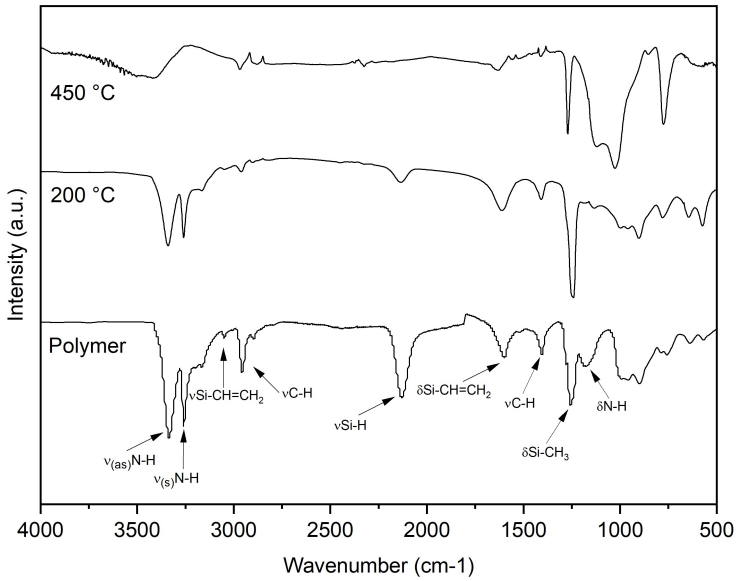

Wan, Gasch, and Mukherjee (2002) observed that when NH_3 is introduced in heat treatments, carbon-containing functional groups are replaced by NH_2 bonds through the reaction represented in Equation 12, which leads to the elimination of Si-CH_3 bonds at lower temperatures such as 600 °C. It is possible to observe a reduction tendency at 450 °C in Figure 53.

$$\equiv Si-CH_3 + NH_3 \longrightarrow \equiv Si-NH_2 + CH_4 \tag{12}$$

As reported by the authors, reactions 11 and 12 are responsible for inserting nitrogen into the polymer backbone and possibly increasing its content in the final ceramic material.

Figure 54 brings the spectra of the polymer **HTTNi5** and at 200 and 450 °C under NH_3. It is clear by the graphs that the type of MCl_2 interferes in the crosslinking reactions. For $NiCl_2$, Si-CH_3 and C-H bonds have almost disappeared at 450 °C. However, Si-NH-Si bonds are comparably reduced. Such occurences imply that Equation 12 is not the preferrable reaction for this polymer at this temperature. Taking that into account, it is possible to notice a great intensity increase in N-H bonds at 3380 cm^{-1}. The presence of NH_3 can lead to the reaction described in Equation 13.

$$\equiv Si-H + NH_3 \longrightarrow \equiv Si-NH_2 + H_2 \tag{13}$$

Kubota et al. (2014) studied absorption and desorption characteristics of NH_3 and several metal chlorides for ammonia storage. $NiCl_2$ exhibited a fast reaction rate along with

promising results for ammonia absorption. Hence, the $NiCl_2$ trend to absorb NH_3 might contribute for the increase of nitrogen content in the polymer network.

Figure 54 – FTIR spectra of HTTNi5 polymer and after treatment at 200 and 450 ℃ in NH_3 atmosphere

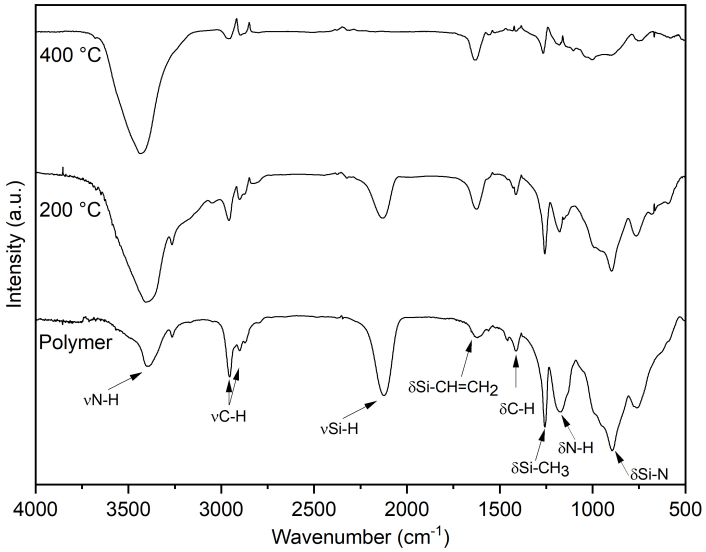

The PHPS FTIR spectrum was also compared to the metal-doped synthesized polymers. The graphs are exposed in Figure 55. It is possible to observe that N-H bonds reacted during the synthesis process. For **PHCoPS5**, there are two bands at 1623 and 1402 cm^{-1}, attributed to δN-H and δC-H, being C-H a possible evidence of remaining solvent and/or protective groups from PHPS, since the organosilicon does not present carbon in the structure (FUNAYAMA et al., 1995).

Figure 55 – PHPS spectrum compared to metal chlorides-doped PHPS

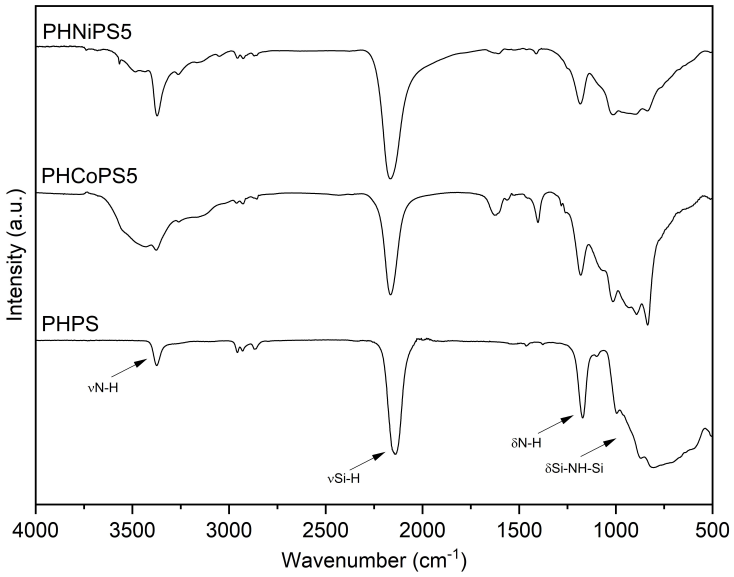

Figures 56 and 57 present the FTIR spectra of **PHCoPS5** and **PHNiPS5** and after treatment in NH_3 atmosphere. **PHCoPS5** sample at 200 ℃ already presents a considerable reduction of Si-H signs at ~2160 cm^{-1}, an indication of the occurence of Equation 13. The dehydrogenation reaction is reinforced as the temperature is increased in the NH_3 atmosphere, leading Si-H/N-H bonds and Si-H/Si-H bonds to form Si-N and Si-Si bonds.

Figure 56 – FTIR spectra of PHCoPS5 polymer and after treatment at 200 and 450 ℃ in NH_3 atmosphere

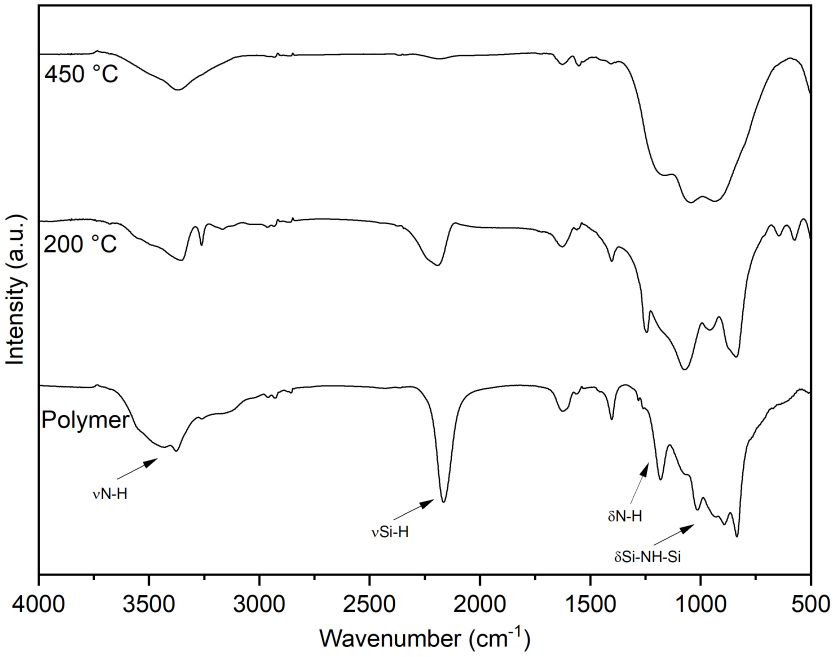

Interestingly, similar processes happened for **PHNiPS5** and **HTTNi5**, with noticeable nitrogen intake in the polymer structure. Hence, the nature of the metal chloride influences the reaction between the chloride and the organosilicon precursor under ammonia heat treatment, leading to more or less nitrogen intake in the material.

Metal-doped HTT1800 and PHPS were subjected to TGA analysis to observe the polymer-to-ceramic conversion, through their weight loss and consequent ceramic yield. The graph in Figure 58 exhibits the degradation behavior of the synthesized polymers **PHCoPS5**, **PHNiPS5**, **HTTNi5** and **HTTCo5**. The weight losses were 8.8, 10.5, 23.02 and 28.8 %, respectively.

A weight loss was detected below 200 ℃ for **PHCoPS5**, which is associated to the volatilization of low molecular weight compounds, and then suffered two weight losses, at 250 and 300 ℃, due to crosslinking reactions. The material presented the highest ceramic yield among the analysed polymers (91.2 wt%).

The thermal degradation of **PHNiPS5** was characterized by a weight loss of ~ 8 % between 200 and 300 ℃ and ~ 2.5 % between 320 and 600 ℃. The final ceramic

Figure 57 – FTIR spectra of PHNiPS5 polymer and after treatment at 200 and 450 °C in NH_3 atmosphere

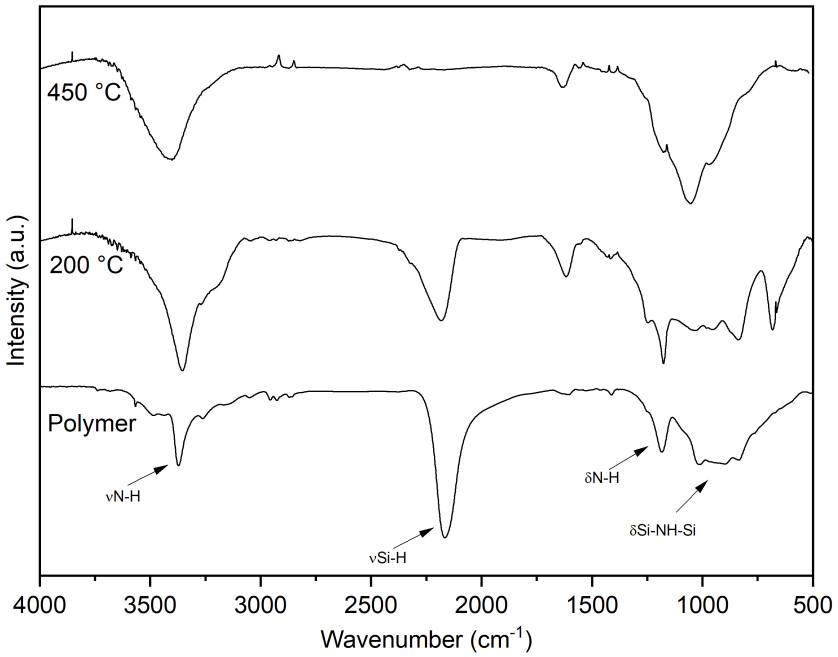

yield was close to **PHCoPS5**, 89.5 wt%. Both degradation behavior results demonstrate that the polymers were well crosslinked and this fact could be associated to an efficient synthesis process between PHPS and $CoCl_2$. As a comparison, the pure organosilicon precursor presented a weight loss of 32 % at 800 °C, which is in agreement with other authors findings. In consequence, the synthesized materials presented a ceramic yield ~22 % higher than the non-crosslinked silazane. According to Ma et al. (2014), when PHPS is heat treated in nitrogen atmosphere, the weight loss is directed by dehydrocoupling reactions, according to Equations 14, 15 and 16.

$$\equiv Si-NH_2 + HN= \longrightarrow \equiv Si-N= + NH_3 \tag{14}$$

$$\equiv SiH + HN= \longrightarrow \equiv Si-N= + H_2 \tag{15}$$

$$= N-SiH_3 + HSi\equiv \longrightarrow = N-Si\equiv + SiH_4 \tag{16}$$

The TGA curves of **PHNiPS5** and **PHCoPS5** were stable at 800 °C, when PHPS has converted into an amorphous ceramic. Lower ceramic yields were detected for **HTTNi5** and **HTTCo5**. The thermal degradation of HTT1800 under N_2 is marked by a first weight loss that occurs up to ~270 °C and corresponds to the evolution of low molecular weight oligomers and also dehydrocoupling crosslinking reactions. Transamination reactions take

Figure 58 – TGA of Co/Ni-doped PHPS and HTT1800 under nitrogen

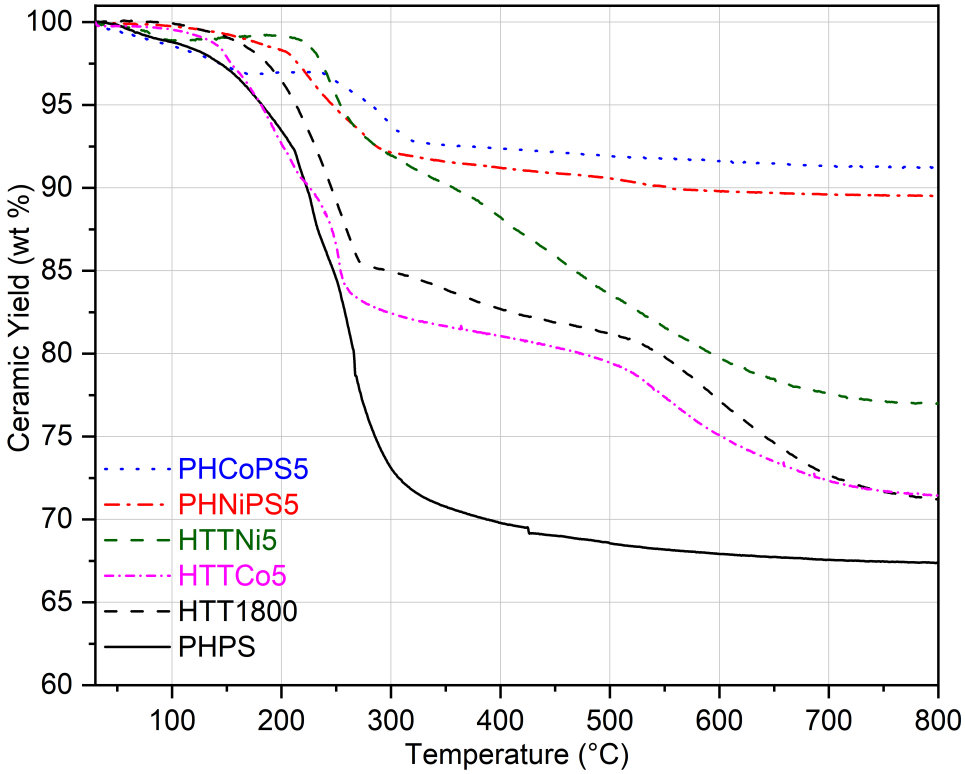

place above 300 ℃ with ammonia evolution and are followed by cleavage of C-C bonds and decomposition of Si-CH_3 groups, with CH_4 release (SEIFOLLAHI BAZARJANI et al., 2011).

According to differential thermogravimetric curves, **HTTNi5** suffered a 1.5 wt% loss at 90 ℃, a second weight loss between 220 ℃ to 300 ℃ (8.5 %) and a third loss between 380 ℃ and 700 ℃ (18.8 %). **PHCoPS5** had a degradation profile similar to HTT1800, but with a higher weight loss before 250 ℃. This behavior demonstrates the pre-pyrolysis crosslinking was not enough to increase the ceramic yield and the polymer is probably a simple mixture.

Reactions with shorter durations (~15 h) were tested and the obtained polymers characterizations presented below. The graph in Figure 59 comprises the FTIR spectra of the polymers synthesized with PHPS and $CoCl_2$ at different Si/Co ratios: 2.5, 5, 10 and 25.

Despite the chemical composition of all polymers is the same, the quantity of available Si-H and N-H reactive groups are different in each reaction. Ratio 25 spectrum demonstrates that when the amount of $CoCl_2$ is decreased, PHPS crosslinking is lower. Since PHPS reactive groups availability is high in Ratio 25, the result indicates this synthesis needs a longer time to promote higher crosslinking levels. In contrast, the absence of N-H groups in **PHCoPS5-15h** (Ratio 5) IR reveals the material suffered crosslinking.

Figure 59 – FTIR of PHPS and $CoCl_2$ polymers (15 h reaction) at Si/Co ratios: 2.5, 5, 10 and 25

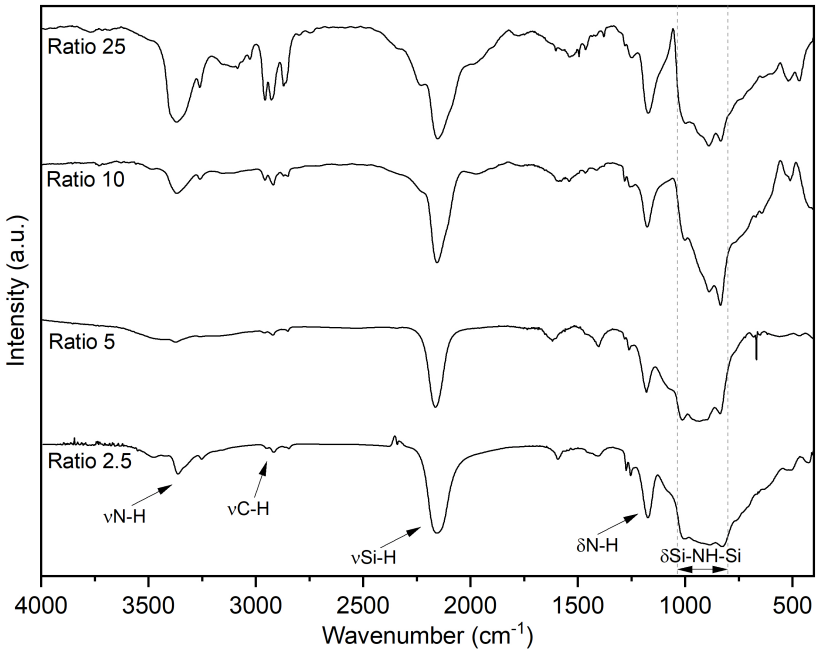

Figure 60 shows the FTIR spectra of **PHCoPS5-15h** just after the reaction and after treatment until 200 and 450 °C under ammonia with the intensities normalized to compare the samples. It is possible to observe that νN-H bonds were reduced in relation to pure PHPS and also to **PHCoPS5** (Figure 56). At 200 °C, νSi-H, δN-H and δSi-NH-Si suffered reductions and at 450 °C, νSi-H was not detected. These observations indicate that dehydrocoupling involving Si-H/Si/H and Si-H/N-H were the main reactions during synthesis and pyrolysis.

PHNiPS5-15h was a brownish viscous liquid after solvent extraction, and its IR is represented in Figure 61. The region that comprises δSi-NH-Si signs can be compared to the PHPS + $NiCl_2$ at the same ratio produced within three days (Figure 55), showing that dehydrocoupling reactions keep occuring after 15 h of reaction.

The thermogravimetrical curves of **PHCoPS5-15h** and **PHNiPS5-15h** under N_2 until 800 °C are displayed in Figure 62 along with the already discussed TGAs of the polymers produced with the same composition but in longer reactions (3 days ~ 72 h).

PHNiPS5-15h presented three main weight losses with the main exothermic peaks at 195, 273 and 306 °C. The final ceramic yield was 89.2 %, similar to the 72 h reaction, despite the higher weight loss that **PHNiPS5-15h** suffered between 200 and 340 °C. **PHCoPS5-15h** still had 86.3 % of the initial mass at the end of the analysis, a difference of ~ 5 % in comparison to **PHCoPS5-72h** (Figure 58), that can be attributed to a higher initial weight loss. Hence, when PHPS and $CoCl_2$ react for three days, the final polymer

Figure 60 – FTIR of PHPS and $CoCl_2$ ratio 5 (15 h reaction) polymer and after treatment at 200 and 450 °C under NH_3 (PHCoPS5-15h)

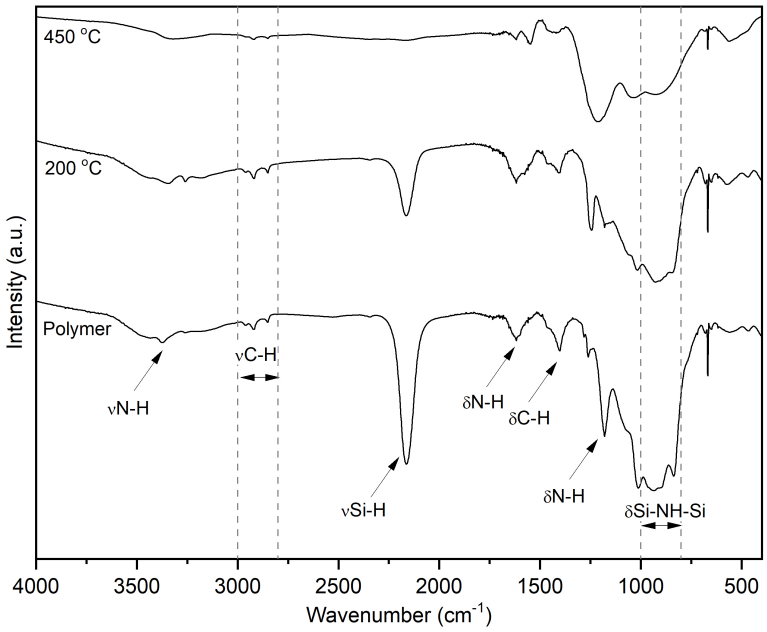

Figure 61 – FTIR of PHNiPS5-15h

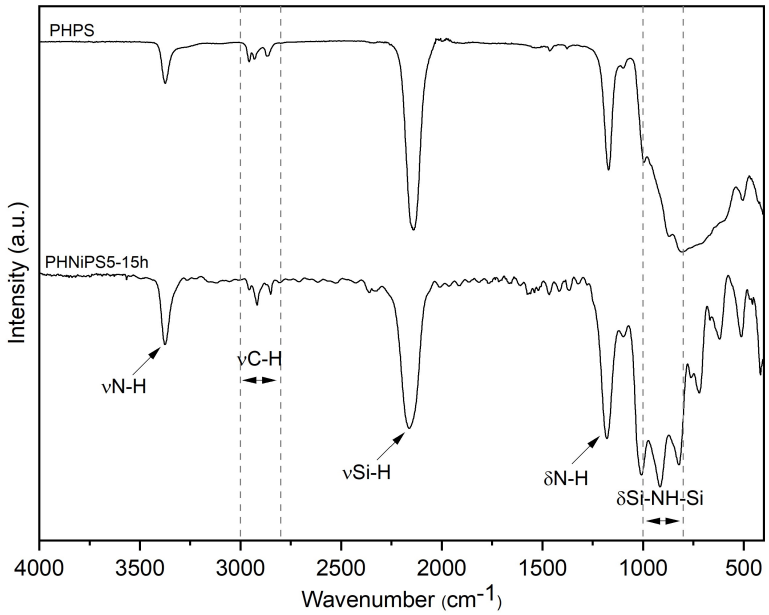

presents more extensive crosslinking. **PHCoPS5-15h** degradation curve derivative shows two main exothermic peaks at 117 °C, due to the loss of low molecular weight compounds, and at 250 °C, linked to dehydrogenation, corroborating with the FTIR spectra.

Figure 63 compares the degradation behavior of **PHCoPS5-15h** with the other ratios, and the weight losses were: 13.4 % (ratio 10), 16.7 % (ratio 2.5) and 17 % (ratio 25). The different Si and Co quantities in each medium were not determinant for the ceramic

Figure 62 – TGA of PHCoPS5 and PHNiPS5: comparison between 15 and 72 h of reaction

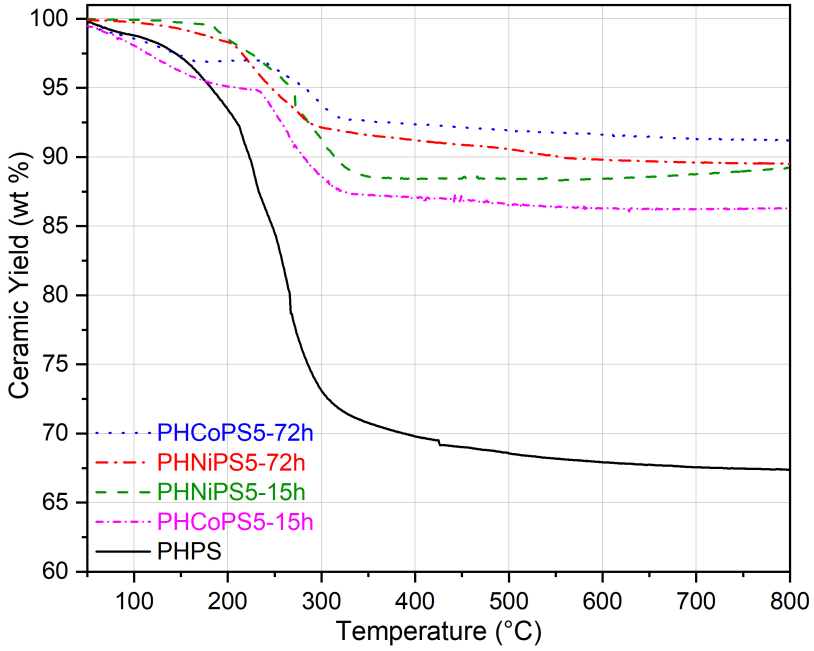

yield, since the values variated in a small as ~ 4 % range. The ratios, however, seemed to influence the degradation behaviors. Ratio 2.5 presented its main weight loss between 230 and 350 ℃, similar to what was detected for ratio 5. For ratios 10 and 25 there was a noticeable difference in the TG curve, that were more similar to pure PHPS, which was expected due to the elevated amount of PHPS in the reaction.

Figure 63 – TGA of PHCoPS-15h at different Si/Co ratios under nitrogen

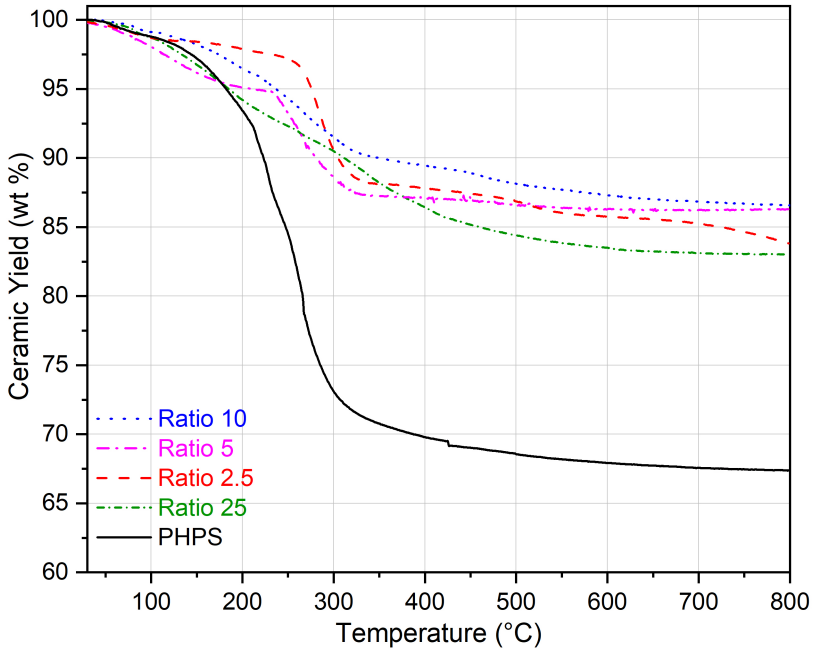

It is important to observe that even these ratios offered a great increase in the PHPS ceramic yield. The degradation of all polymers was stable above 700 ℃, except for the sample with ratio 2.5.

The results given above summarize the characterization of the metal-doped polysilazanes synthesized with Co/$NiCl_2$ and the organosilicon precursors PHPS and HTT1800.

It was possible to observe the metal chlorides were important to crosslink the organosilicon precursors and to increase their final ceramic yield. This is in agreement with a patent registered by Rochow (1963) in which the inventors claim that certain organosilicon polymers can be crosslinked through their nitrogen atoms through the activity of some metal salts, e.g., copper chloride, nickel chloride, thorium chloride and cobalt chloride. The inventors attributed to the metal salts the ability to split out the diamine from silylamine chains.

The polymers obtained herein were subjected to heat treatments under ammonia to produce Co/Ni-doped Si_3N_4. The powders characterization is discussed in subsection 4.2.2, and the micro-/mesoporous samples in subsection 4.2.3.

4.2.1.2 PHPS and metal-complexes for Co/Ni-doped polysilazanes

This section is dedicated to explore the features of synthesized Co/Ni-doped polysilazanes using four metal-complexes: tris(ethylenediamine) cobalt(III) chloride dihydrate ($[Co(en)_3]Cl_3{\cdot}2H_2O$); tris(ethylenediamine) nickel(II) chloride dihydrate ($[Ni(en)_3]Cl_2{\cdot}2H_2O$); hexaammine cobalt (III) chloride ($[Co(NH_3)_6]Cl_3$) and hexaammine nickel (III) chloride ($[Ni(NH_3)_6]Cl_2$).

The polymers were synthesized in reactions that lasted overnight (~ 15 h). After solvent extraction, **PHNiTris5** and **PHCoTris5** were solid, **PHNiHex5** was highly viscous and **PHCoHex5** was viscous liquid, as displayed in Figure 64.

Figure 64 – Obtained polymers of PHPS and Co/Ni-complexes

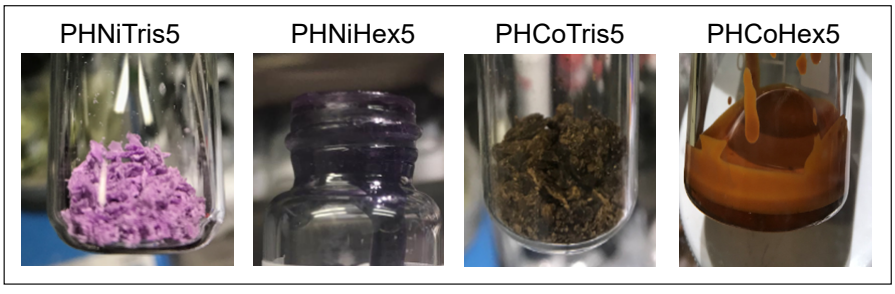

As shown in Figure 65, nickel complex $[Ni(en)_3]Cl_2{\cdot}2H_2O$ presented the following infrared signals: 3482 cm^{-1} (νN-H), 3332 - 3128 cm^{-1} (νN-H), 2941 and 2880 cm^{-1} (νC-H), 1586 cm^{-1} (δN-H), 1463 cm^{-1} (δC-H), 1332 cm^{-1} (δN-H), 1152 cm^{-1} (δN-H), 1026

cm^{-1} (δC-N), 655 cm^{-1} (δN-H). Compatible results have been reported by Srinivasan et al. (2009). **PHNiTris5** FTIR is illustrated in the same Figure. It was possible to indentify chemical groups derivative from PHPS and the nickel complex in the final polymer. A sign of δSi-N is visible at $\sim$ 845 cm^{-1}, in the δSi-NH-Si region, linked to the cleavage of δSi-N and overall δSi-NH-Si reduction. In addition, the reduction of ν and δN-H corroborates with the reactions attributed to dehydrocoupling reactions of Si-H and N-H units.

Figure 65 – FTIR of PHPS and tris (ethylenediamine) nickel(II) chloride dihydrate (PHNi-Tris5)

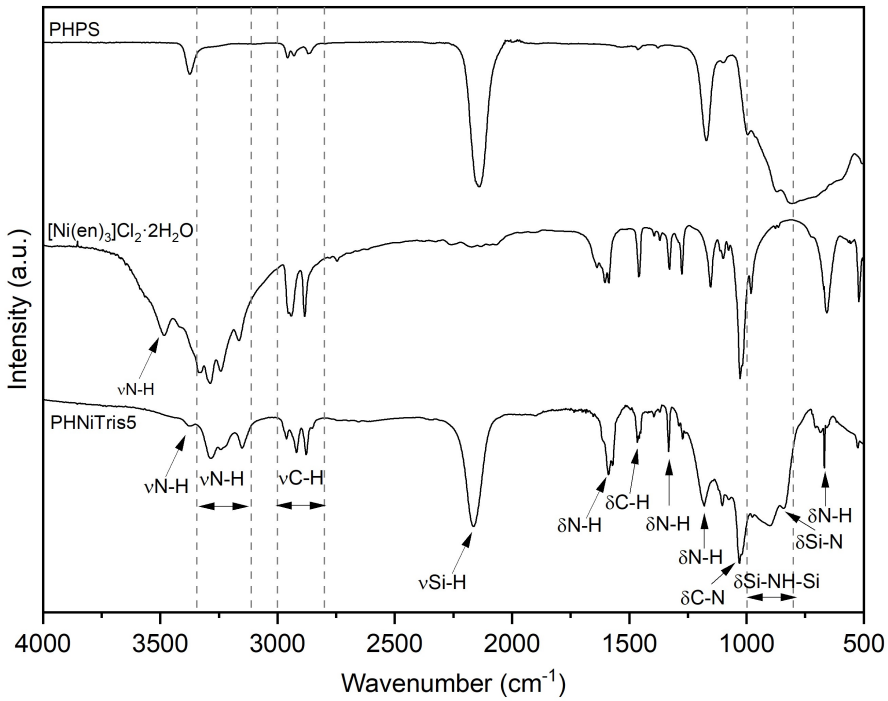

The graph corresponding to infrared spectra of **PHCoTris5** is represented in Figure 66, and the absorbances of $[Co(en)_3]Cl_3{\cdot}2H_2O$ are similar to $[Ni(en)_3]Cl_2{\cdot}2H_2O$. According to the study of Iwamoto, Kikuta, and Hirano (2000b), polysilazanes can be chemically modified throughout reactions with transition metal (e.g. Ti, Zr, Hf) alkoxides. The authors detected that for PHPS, the reactions with alkoxides occurred only at N-H groups, differently from the carbon-containing polysilazane HT1800, where it occurred at both N-H and Si-H groups. Qian Zhang et al. (2016) reported the synthesis of a polycobaltsilazane through the reaction of $Co(en)_3]Cl_3$ and a poly[(methylvinylsilazane) -co- (methylhydrosilazane)], whereas attributed the resultant polymer to three main effects: (1) the ethylenediamine N-H groups reacted with the silicon centers of the polysilizane, with the coordenation of cobalt (III) complex; (2) the hydrosylilation reaction between Si-H and Si-vinyl groups; (3) the incorporation of cobalt (III) complex into the crosslinked polysilazane by hydrosylilation without the presence of a catalyst (Co(III) ions). νC-H ($[Co(en)_3]Cl_3{\cdot}2H_2O$) and δN-H (PHPS

and $Co(en)_3]Cl_3{\cdot}2H_2O$) were the main reduced bonds in the **PHCoTris5** polymer reaction, revealing that dehydrogenation of such groups is the most probable occurrence.

Figure 66 – FTIR of PHPS and tris(ethylenediamine) cobalt(III) chloride dihydrate (PHCoTris5)

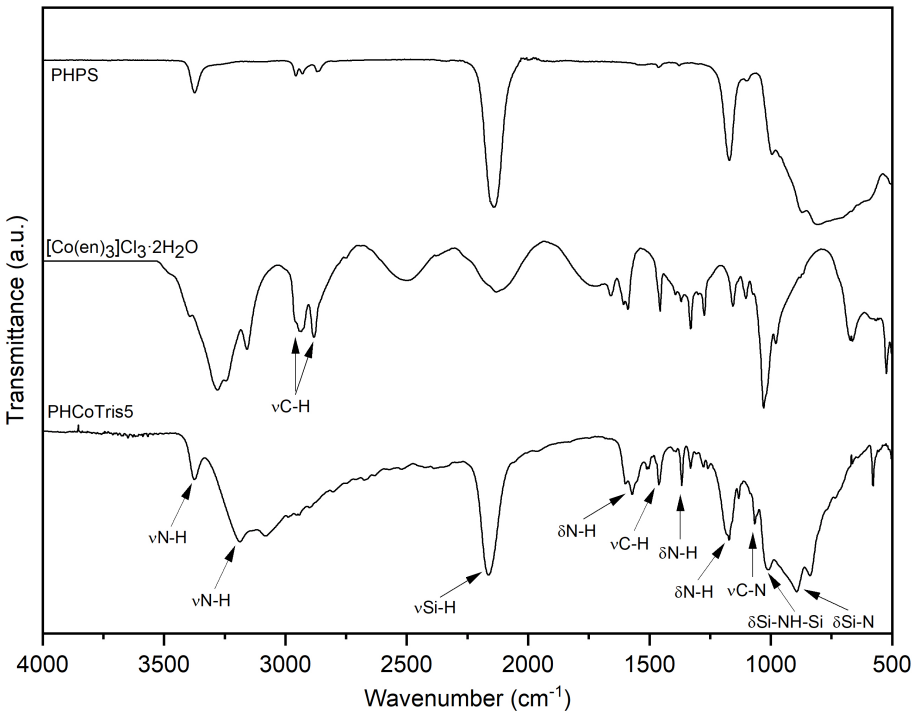

Infrared of the polymers obtained after reaction with $Co(NH_3)_6Cl_3$ and $Ni(NH_3)_6Cl_2$ are shown in Figures 67 and 68. The main peaks related to cobalt(III) complex were observed in the region from 3400 to 2850 cm^{-1}, 1618 cm^{-1} and 1327 cm^{-1}, assigned to N-H stretching vibrations and at 830 cm^{-1}, to NH_3 rocking vibration (NAQASH; MAJID, 2015). For Ni (II) complex, signs were detected at the wavenumbers 3350, 1600, 1172 and 684 cm^{-1}, which correspond to different vibrational modes of N-H (ADAMS; HAINES, 1991).

PHCoTris5 and **PHNiTris5** were also evaluated by TGA analysis (Figure 69). The first polymer exhibited four main weight losses between 70 and 116 ℃, 150 and 200 ℃, 230 and 280 ℃, 400 and 500 ℃, totaling a loss of 32.5 %. The second displayed three main losses, in the ranges 250 - 306, 312 - 400 and 500 - 550 ℃. At temperatures from 250 and 500 ℃, transamination and dehydrocoupling reactions can happen concomitantly (KROKE et al., 2000). Since there are no vinyl groups in PHPS, hydrosilylation reactions were not expected, hence the weight losses at temperatures as low as 100 ℃ are more probably attributed to the evolution of volatile compounds of low molecular weight. Qian Zhang et al. (2016) reported a weight loss of 80 wt% for the pure Co(III) complex and

Figure 67 – FTIR of PHPS and hexaammine nickel(II) chloride (PHNiHex5)

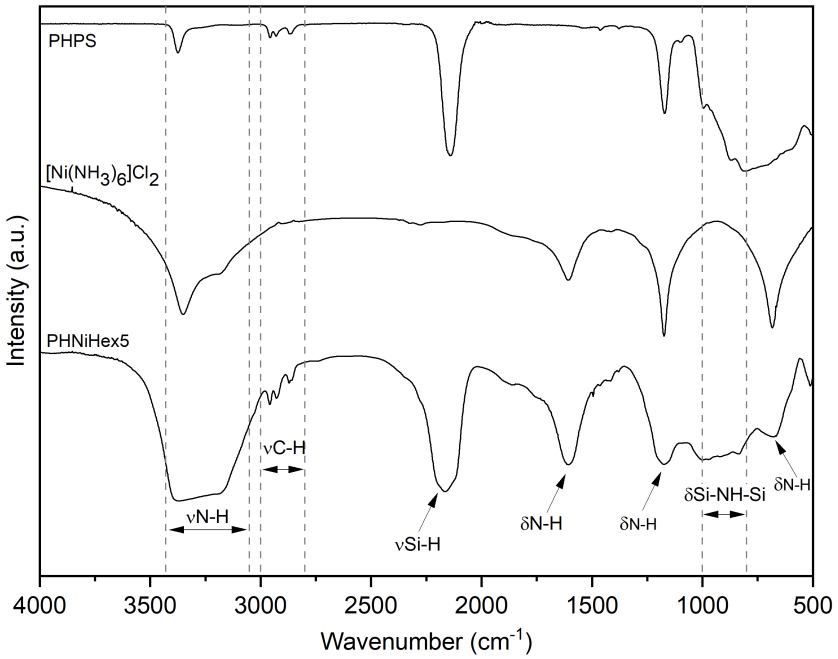

Figure 68 – FTIR of PHPS and hexaamminecobalt(III) chloride (PHCoHex5)

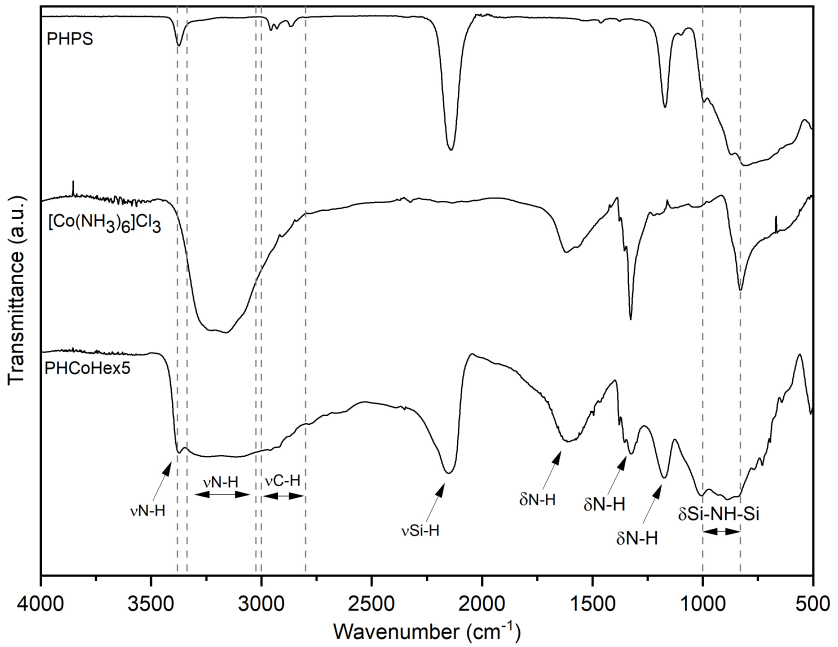

affirm that a lower weight loss of the polycobaltsilazane can be resulted from a crosslinking enhancement provided by the complex.

As displayed in the TGA (Figure 69), **PHCoHex5** presented three main weight losses when evaluated until 1000 ℃. By the curve first derivative, the exothermic peaks were detected at 150, 293 and 823 ℃. At 700 ℃, this complex still had 68 % of its initial

Figure 69 – TGA of PHPS with Nickel (II) and Cobalt (III) complexes under nitrogen

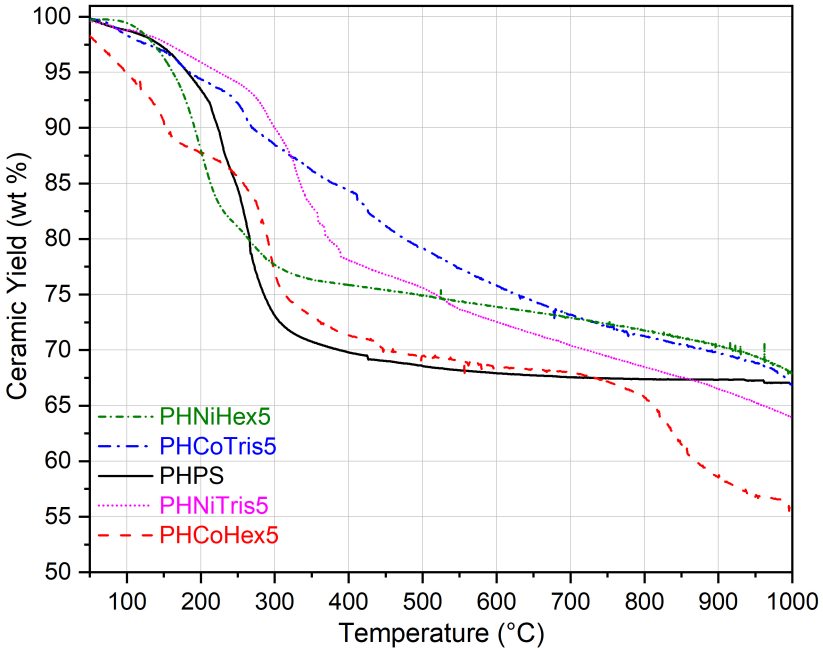

mass, however the final loss above 800 ℃ let the polymer with a final ceramic yield of 56.4 wt%. **PHNiHex5** had a first weight loss from 100 to 230 ℃, a second from 250 to 300 ℃ and a continuous loss until 100 ℃, the final ceramic yield was 68 wt%.

Rejitha, Ichikawa, and Mathew (2011) studied the thermal decomposition of hexaammine nickel(II) halides (Cl, Br) under helium gas flow. The authors analyzed the mass spectra along with TGA, which provided information on the reactions according to the temperature increase. First, between 79 and 140 ℃, hexaammine nickel(II) chloride released four NH_3 molecules, assigned to deamination reaction (Equation 17). The second step was characterized by the release of two NH_3 molecules between 140 and 280 ℃, resulting in the formation of $NiCl_2$ (Equation 18). Above 600 ℃, $NiCl_2$ started to decompose, identified by the release of chlorine, and, at 740 ℃ the authors assigned to an endotherm peak the dechlorination reaction and formation of metallic nickel. The total weight loss at 1000 ℃ was 74.6 %.

$$Ni(NH_3)_6Cl_2 \longrightarrow Ni(NH_3)_2Cl_2 + 4NH_3 \tag{17}$$

$$Ni(NH_3)_2Cl_2 \longrightarrow NiCl_2 + 2NH_3 \tag{18}$$

$$NiCl_2 \longrightarrow Ni + Cl_2 \tag{19}$$

Based on the thermogravimetrical curves, ceramic yield and on the equations mentioned above, the best temperature for pyrolysis of Co(III) and Ni(II)-doped PHPS was between 700 and 800 °C. Hence, the ceramics were characterized and the results are reported in the next subsection, along with the ceramics obtained from the polymers described in previous subsection (4.2.1.1).

4.2.2 Ceramics characterization from 700 to 1000 °C as powders

Co/Ni-doped polysilazanes produced with M-chlorides and M-complexes (M=Co, Ni) were subjected to pyrolysis under NH_3 and the obtained powders were characterized by XRD to observe their crystallization patterns. The first graph that is discussed refers to the powders generated by pyrolysis of **HTTCo5** at 700, 800, 900 and 1000 °C and is represented in Figure 70.

Figure 70 – XRD patterns of HTTCo5 treated under NH_3

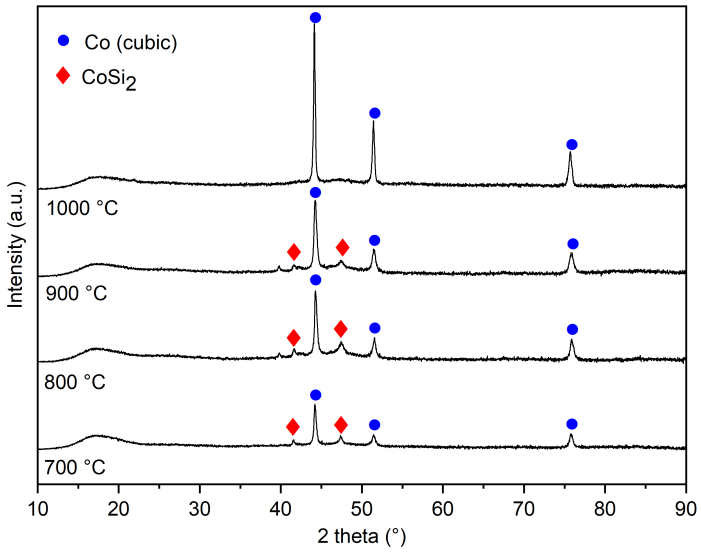

Three main peaks were observed in the XRD, and correspond to cobalt in cubic crystal system, identified by the signals at 2θ = 44.2158° (111), 51.5225° (200) and 75.7378° (220). From 700 to 900 °C, peaks at 41.5603 and° 47.3798° were also detected, assigned to (100) and (101) reflections of cobalt disilicide ($CoSi_2$). Si_3N_4 was still amorphous at 1000 °C. CoSi and $CoSi_2$ are known by their excellent properties in electronic, optoelectronic, and electromechanical devices, and their formation can happen at 700 and 800 °C, respectively (CHOU et al., 2008). According to Seo et al. (2007), $CoCl_2$ vapor reacts with a silicon substrate at high temperatures to form CoSi nanowires by the reactions described

in Equations 20 and 21.

$$2CoCl_{2(g)} + 3Si_{(s)} \longleftrightarrow 2CoSi_{(s)} + SiCl_4 \tag{20}$$

$$CoCl_{2(g)} + SiCl_{4(g)} \longleftrightarrow CoSi_{(s)} + 3Cl_{2(g)} \tag{21}$$

It is important to observe that these reactions demonstrate CoSi can be generated by direct reaction of $CoCl_2$ with a silicon substrate (in this case is the polysilazane) or by means of a gas-phase reaction of $CoCl_2$ and $SiCl_4$. However, according to Vakifahmetoglu et al. (2010) and Seo et al. (2007), the reduction of $CoCl_2$ to micrometersized metallic cobalt particles upon pyrolysis in inert atmosphere and their interaction with the silicon-containing matrix are responsible for the formation of CoSi in ceramics. Esconjauregui, Whelan, and Maex (2006) verified cobalt silicide formation at 825 °C and reported that the chemical reaction between cobalt and silicon promoted the adhesion between the metal catalyst and the substrate.

Nevertheless, to achieve enhanced performances in hydrolysis reactions, it is essential to provide highly accessible active sites, i.e., the compound with great catalytic activity should be evenly distributted for an easy access for reaction. Hence, the presence of pure cobalt is desirable to achieve increased hydrolysis rates, whilst $CoSi_2$ has not been researched for this application yet.

Regarding **HTTNi5** XRD analyses (Figure 71), characteristic peaks at 44.6434°, 52.0398° and 76.6998° correspond to (111), (200) and (220) planes of face centered cubic (fcc) phase of Ni, in agreement with reported data from ICDD (The International Centre for Diffraction Data), file No. 04-0850. The presence of only Ni peaks indicates the material consists on a pure phase. Above 900 °C, crystallization of α- and β-Si_3N_4 could be observed.

Depending on the pyrolysis atmosphere, the polymer-to-ceramic conversion of HTT1800 results in SiCN or Si_3N_4 ceramics. Lale (2017) obtained amorphous materials until 1400 °C after heat treatment of HTT1800 under ammonia. Crystals of α- and β-Si_3N_4 were identified only after annealing at 1500 °C. Nevertheless, Baney and Bujalski (1988) discovered that mixing silazanes with nickel, cobalt or iron compounds could lead to highly crosslinked SiC or Si_3N_4 ceramics after pyrolysis to at least 750 °C.

According to previous studies published by Mitomo (1977) and Pan and Baptista (1996), transition metals such as iron, cobalt and nickel form eutectic liquid i.e. homogeneous mixtures with Si, that promotes free carbon precipitation and formation of metal silicides.

Figure 71 – XRD patterns of HTTNi5 treated under NH_3

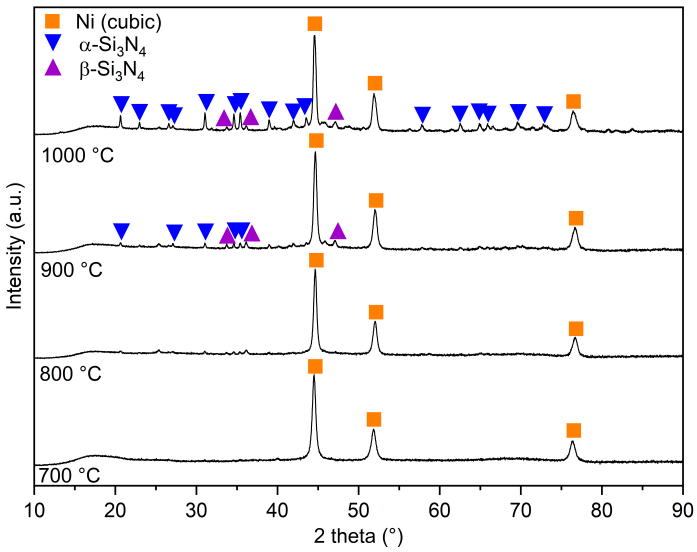

Xiaofei Zhang et al. (2014) produced Ni-containing polysilazanes to study their behaviour as pyrolysis precursors for Ni-containing PDCs. The authors observed that nickel atoms from $NiCp_2$ (nickelocene) reacted with Si–C–N amorphous phase, crystallizing Ni_2Si and favoring the formation of α-Si_3N_4 and SiC crystals. The polymer that consisted of 8 wt% of $NiCp_2$ and 92 wt% of polysilazane, after heat treatment under argon resulted in a ceramic composed by a mixture of four phases: α-Si_3N_4, Ni_2Si, SiC and graphitic carbon, yielded between 1100 and 1300 ℃.

Segatelli, Pires, and Yoshida (2008) investigated the elaboration of SiC_xO_y ceramics obtained by pyrolysis of a hybrid polymer produced with poly(methylsiloxane) and divinylbenzene. The reactions were performed in the presence or absence of anhydrous nickel acetate. Ni-containing polymers promoted a more effective crystallization of β-SiC. The reactive pyrolysis atmosphere was the main distinction from **HTTNi5** to the materials produced in such studies, because the pyrolysis under NH_3 led to carbon removal, consequently, SiC was not detected. In agreement with the authors, crystallization of α- and β-Si_3N_4 was favored by Ni presence, that in this work occurred even at temperatures lower than 1000 ℃.

Figure 72 (a) represents the XRD patterns of **PHCoPS5** treated under NH_3 from 700 to 1000 ℃ and (b) is related to **PHCoPS5-15h**.

The reaction between $CoCl_2$ and PHPS during 72 h led to formation of $CoSi_2$ and Co (cubic) at 700 ºC. In comparison to **HTTCo5**, it is noticeable that PHPS tends to crystallize more easily than HTT1800, probably due to the higher availability of Si-H groups. This can also be linked to the formation of $CoSi_2$ and Co_2Si, once this depends on the reaction between Si-H and $CoCl_2$. The crystallization of α- and β-Si_3N_4 was detected

Figure 72 – XRD patterns of PHCoPS5 (a) and PHCoPS5-15h (b) treated under NH_3

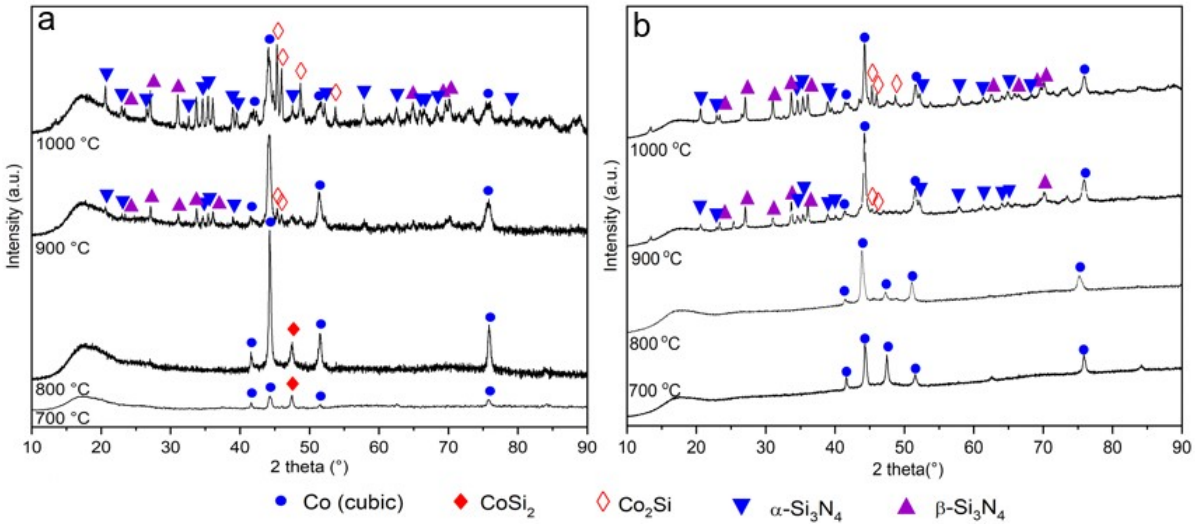

at temperatures above 900 °C. **PHCoPS5-15h** exhibited only peaks of Co (cubic) at 800 °C: 41.55869°, 44.49970°, 47.42228° and 75.82813° are in accordance with ICDD file No. 04-001-3273, and 51.59432° with file No. 00-001-1254. **PHCoPS5** XRD evidenced the formation of $CoSi_2$ at the same temperature. This fact shows that reducing the reaction time was crucial to avoid $CoSi_2$ formation below 800 °C.

The polymers synthesized with PHPS and $CoCl_2$ (**PHCoPS**) at ratios 2.5, 5, 10 and 25 were investigated and compared at 700 (Figure 73) and 800 °C (Figure 74).

Figure 73 – XRD patterns of PHCoPS-15h at ratios 2.5, 5, 10 and 25 treated under NH_3 at 700 °C

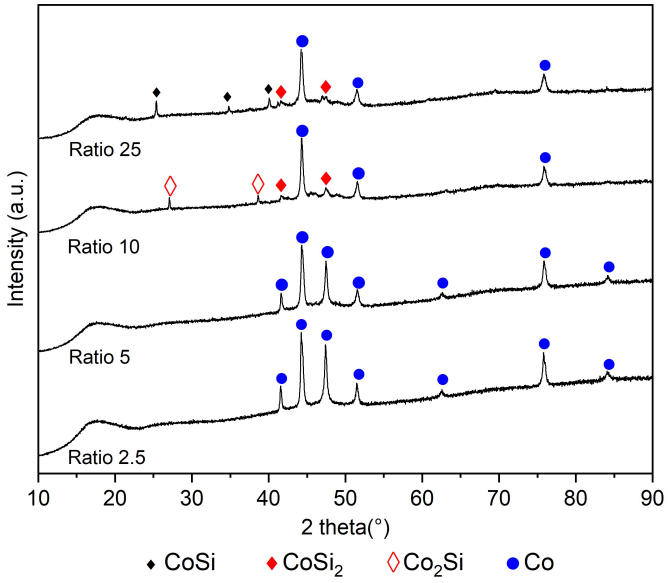

Figure 74 – XRD patterns of PHCoPS-15h at ratios 2.5, 5, 10 and 25 treated under NH_3 at 800 °C

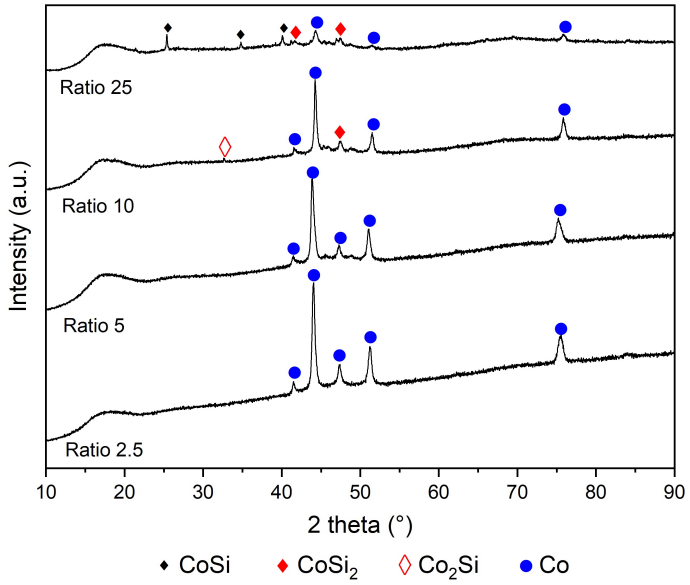

Formation of cobalt silicides was observed for higher ratios (10 and 25). Accordingly, decreasing the molecular Si/Co ratio promoted the decrease of silicide phase content. Such silicides were observed as CoSi, $CoSi_2$ and Co_2Si. Besides $CoCl_2$ reaction with Si, CoSi phase can be constituted at approximately 550 °C, by a reaction between metallic Co and underlying Si. CoSi phase is then transformed into $CoSi_2$ and Co_2Si with further heating (LEE; RHEE; AHN, 2002). The XRD results corroborate with what was detected by FTIR (Figure 59) i.e., lower molecular ratios led to more crosslinked polymers, supporting pure cobalt crystallization in the amorphous Si_3N_4 matrix.

PHCoPS-15h Si/Co ratio 5 was observed through Scanning Electron Microscopy (SEM) coupled with Energy Dispersive X-Ray Spectroscopy (EDS) at various temperatures: 700, 800, 900 and 1000 °C. Figure 75 presents a general outlook of the powders.

The powders were constituted of agglomerated grains of different sizes that became more homogeneous as the pyrolysis temperature incresed. At 1000 °C, rounded grains of nanometers to a few micrometers could be observed. EDS spectra were collected in several spots of the grains, which generated the graph that is shown in Figure 76.

Cobat, silicon, nitrogen and negligible amounts of oxygen and carbon were detected at all temperatures. It is important to mention that a carbon tape was used on the stub for sample preparation. At 700 °C there was also a small quantity of chlorine, that was not observed above this temperature. Elemental mapping was carried out as a qualitative observation of the elements distribution over the material surface. In Figure 76 there is an acquired image showing that cobalt was found all over the powders.

Figure 75 – SEM images of PHCoPS5-15h treated under NH_3 at different temperatures: (a) 700 ℃, (b) 800 ℃, (c) 900 ℃ and (d) 1000 ℃

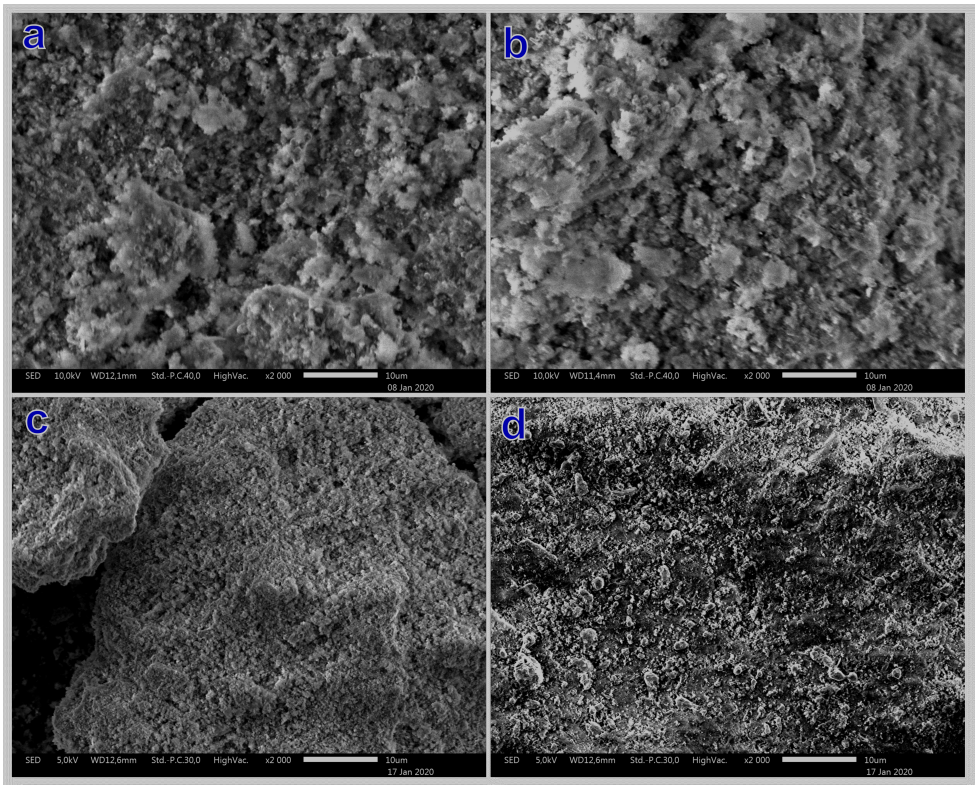

Figure 76 – EDS of PHCoPS5-15h (700 to 1000 ℃) and cobalt-mapping on the powder obtained at 1000 ℃

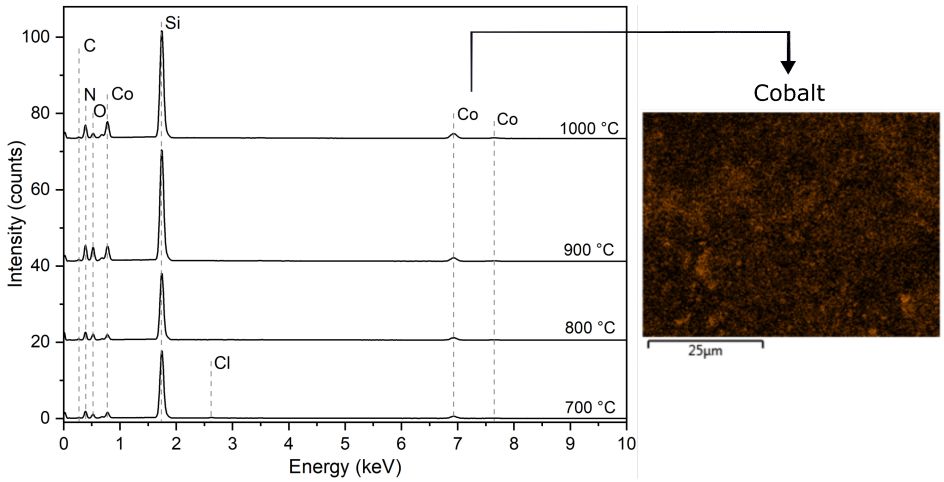

XRD results that were obtained for **PHNiPS5** and **PHNiPS5-15h** are exposed in Figure 77. Crystallization of α- and β-Si_3N_4 was not observed for either reaction durations. Nickel (cubic) characteristic peaks were identified and assigned in the graphs. Thus, it is possible to state that the heat treatment of **PHNiPS5** until 1000 ℃ under NH_3 resulted in an amorphous Si_3N_4 ceramic matrix doped with cubic nickel crystals at 1000 ℃. Moreover,

these results reinforce the idea that $CoSi_2$ can promote Si_3N_4 crystallization.

Figure 77 – XRD patterns of PHNiPS5 (a) and PHNiPS5-15h (b) treated under NH_3

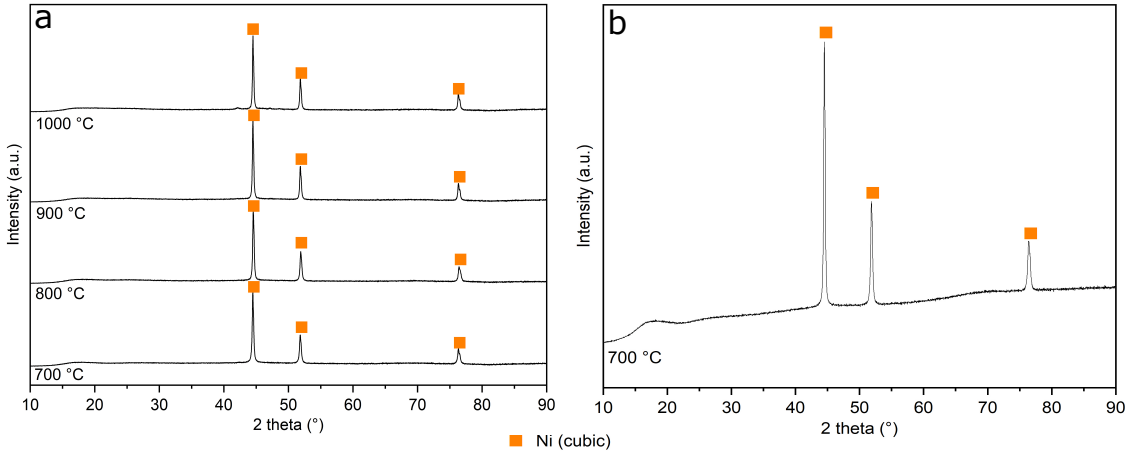

The powder **PHNiPS5-15h** was analysed by EDS, and the technique allowed the confirmation on the presence of Si, Ni, N and O. Nickel sites were found spread over the powder sample, as it can be observed in Figure 78.

Figure 78 – EDS and nickel-mapping on PHNiPS5-15h treated under NH_3 at 700 ℃

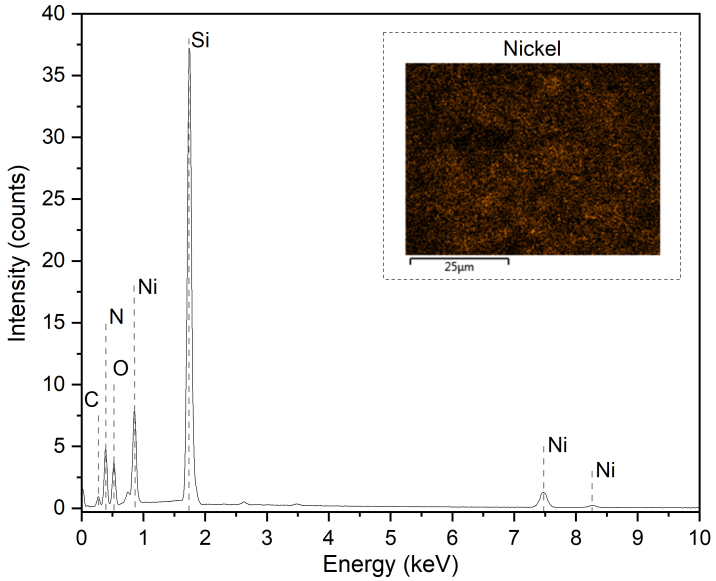

XRD analyses of $Co/NiCl_2$ and PHPS/HTT1800- derived ceramics indicated the synthesized polymers generated Co- and Ni-containing amorphous Si_3N_4 ceramics at 700 ℃. Based on these results, the polymers produced with PHPS and Co/Ni-complexes were treated under NH_3 at 700 and 800 ℃ to observe the materials behavior. The graph corresponding to **PHCoHex5** XRD is shown in Figure 79.

Figure 79 – XRD patterns of PHCoHex5 treated under NH_3 at 700 and 800 °C

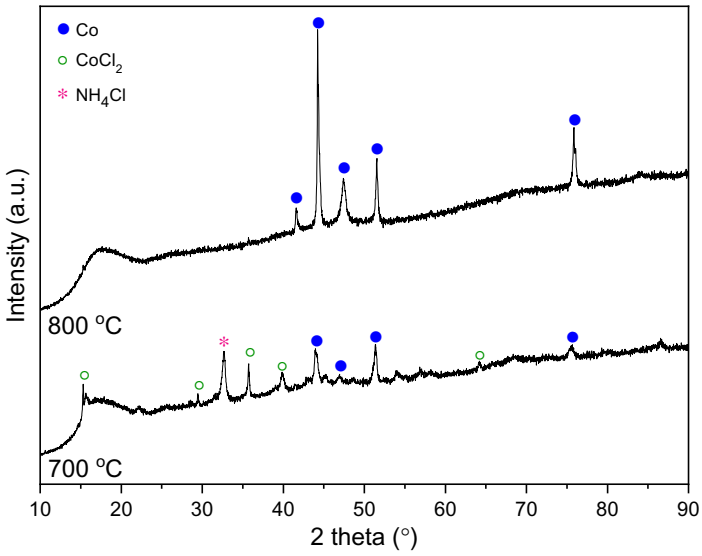

PHCoHex5 at 700 °C exhibited peaks assigned to $CoCl_2$ at 15.21141°, 29.48374°, 35.69816°, 39.00725° and 64.19769°, corresponding to (003), (101), (104), (015) and (024) planes of its crystal system, respectively, in agreement with ICDD file No. 01-085-0446. In addition, a peak observed at approximately 32° seems to coincide with the diffraction lines of NH_4Cl phase (110), standard spectrum ICDD file No. 00-002-0887. NH_4Cl could be formed in this medium by a reaction between ammonia$_{(g)}$ and hydrochloric acid$_{(g)}$ (THOMPSON et al., 2019). The remaining appearance of such chlorides at 700 °C indicate that at least a part of the reagents did not react. All the signs related to $CoCl_2$ and NH_4Cl disappear over this temperature, consequently only pure cobalt was found at 800 °C.

In contrast, **PHCoTris5** presented only Co patterns at 700 and 800 °C (Figure 80), with no traces of chlorides. This difference could be related to the greater amount of NH_3 molecules in the hexaammine cobalt (III) chloride complex in comparison to tris(ethylenediamine) cobalt(III) chloride dihydrate structure. **PHNiHex5** and **PHNiTris5** were also subjected to a heat treatment under ammonia, until 700 °C, and the XRD patterns are exposed in Figure 81.

Both compounds presented structures with characteristic peaks of (111), (200) and (220) planes of face centered cubic (fcc) phase of Ni (ICDD file No. 04-0850). Si_3N_4 was not crystallized at this temperature and, in addition, there were no signs of Ni_2Si. This demonstrates that silicon did not react with nickel to form silicides (SHANG et al., 2008).

Co/Ni-complexes and PHPS-derived powders at 700 °C were investigated by EDS, as shown in Figure 82. Element chlorine was detected for both Co and Ni hexaamine-complex-derived samples. Regarding **PHNiHex5**, since the presence of chlorine detected by EDS was not related to $NiCl_2$ or NH_4Cl formation in the powder (patterns were not

Figure 80 – XRD patterns of PHCoTris5 treated under NH_3 at 700 and 800 °C

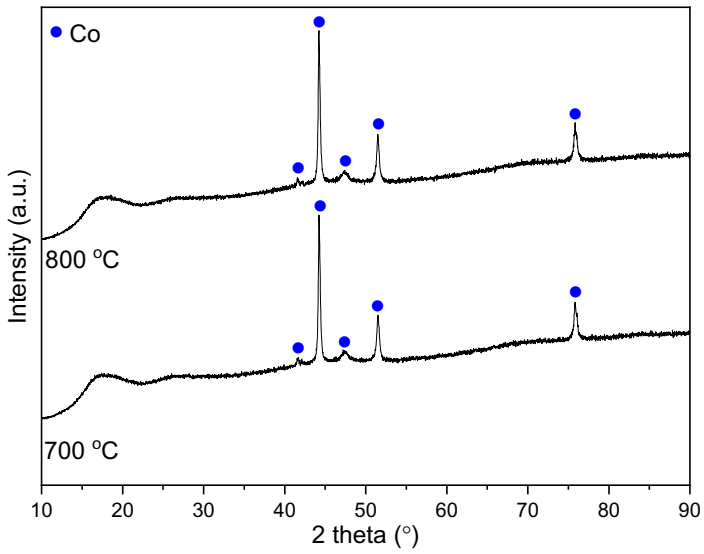

Figure 81 – XRD patterns of PHNiHex5 and PHNiTris5 treated under NH_3 at 700 °C

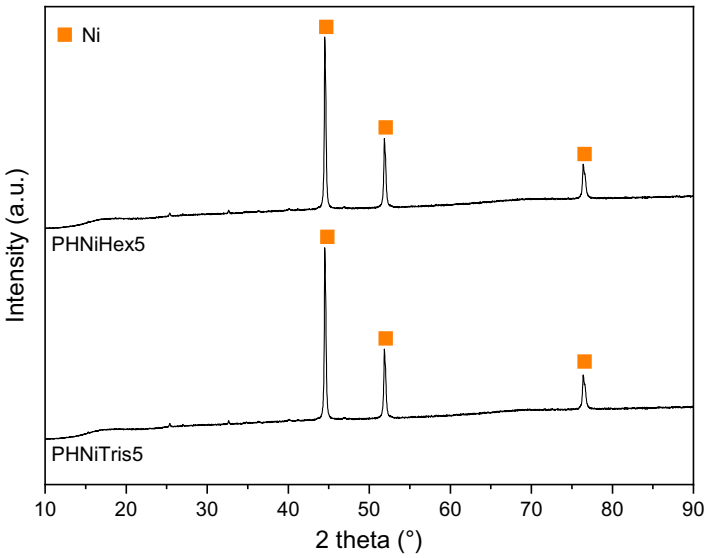

observed by XRD), this is a supporting evidence the complex could lead to formation of pure Ni particles.

SEM images of **PHCoTris5** and **PHNiTris5** powders generated at 700 °C revealed interesting wire-like structures along with the grains, as indicated by the arrows in Figure 83. EDS confirmed the main composition of such formations as silicon. The powder morphology was unexpected and presented a distinct behavior in comparison to other materials.

Vakifahmetoglu et al. (2010) studied the growth of one-dimensional (1D) nanostructures in porous PDCs by a process called CAP (Catalyst-Assisted Pyrolysis), apply-

Figure 82 – EDS of Co/Ni-complex@PHPS powders treated under NH_3 at 700 °C

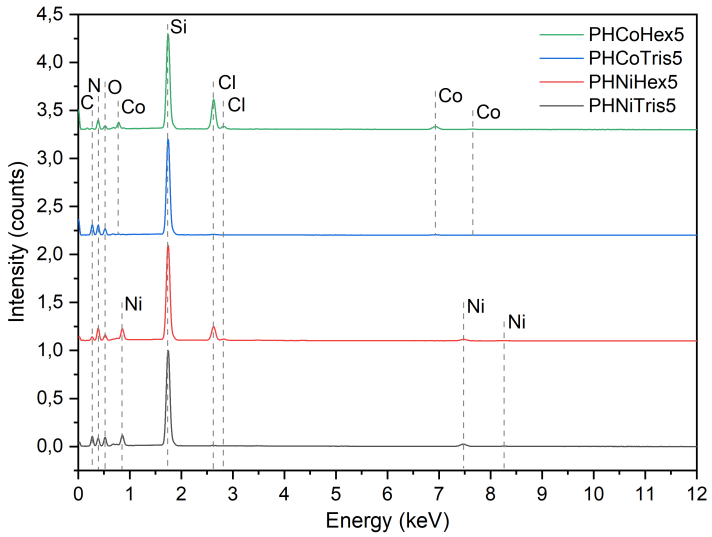

ing $CoCl_2$ as the catalyst. In this method, the authors achieved the formation of Si_3N_4 nanowires upon pyrolysis under N_2. The authors mentioned that the release of decomposition gases, during the heat treament of preceramic polymers at high temperature in inert atmosphere, can favor the development of such 1D nanostructures in the pores of the formed ceramics. Considering the samples **PHCoTris5** and **PHNiTris5**, one explanation for the distinct morphology might rely on the gases evolution during pyrolysis, that caused the formation of pores in the grains structure and subsequently wire-like aspect.

Figure 83 – SEM of PHCoTris5 (a-b) and PHNiTris5 (c-d) powders obtained at 700 °C

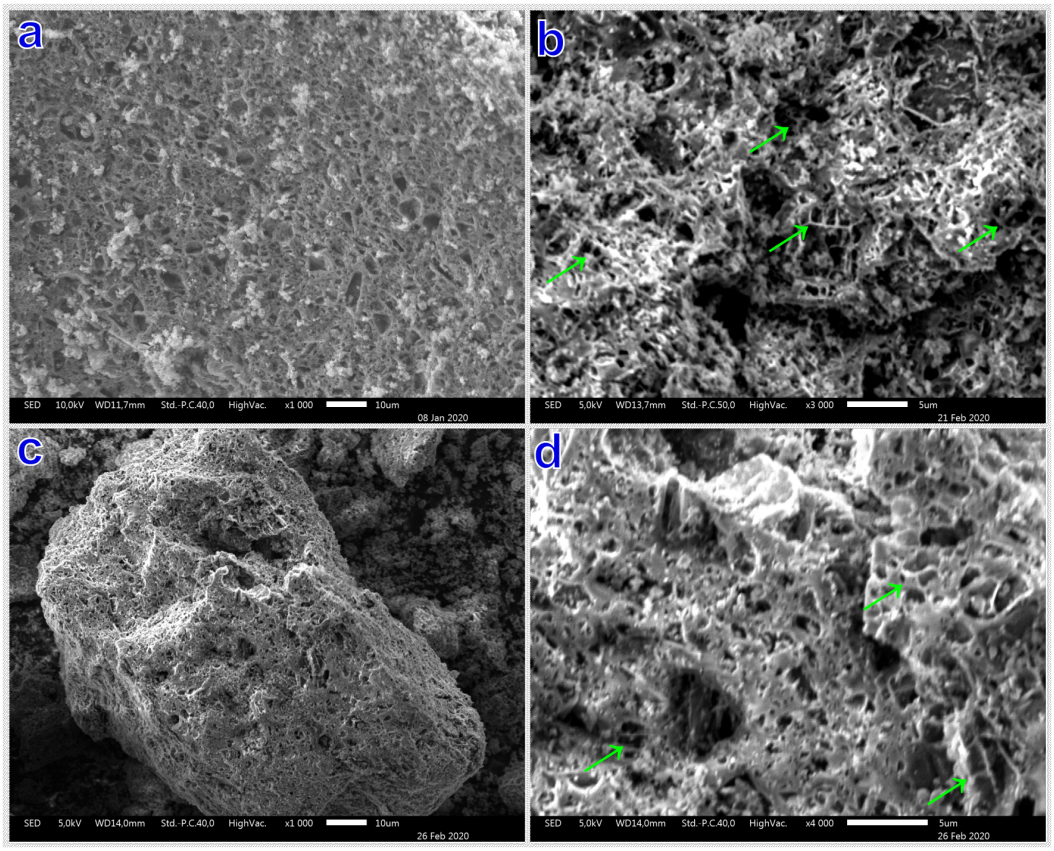

4.2.3 Design of micro-/mesoporous samples

Activated Carbon Monoliths (ACM) were impregnated with the generated polymers throughout the nanocasting process detailed in the methodology chapter. After the full heat treatment, which comprised the polymer crosslinking under N_2, polymer-to-ceramic conversion and carbon template removal under NH_3, the produced ceramic monoliths were characterized using BET technique by nitrogen gas adsorption-desorption measurements at 77 K, to assess the samples specific surface area and type of porosity that was created in the system. Additionally, the monoliths were crushed into fine powders and analysed by XRD to confirm the formation of desired ceramic phase.

ACM impregnated with **HTTCo5**, **HTTNi5**, **PHCoPS5** and **PHNiPS5** were treated until 1000 ℃ under NH_3 and the products were labelled as follows: **mHTTCo5_10_NH_3**, **mHTTNi5_10_NH_3**, **mPHCoPS5_10_NH_3** and **mPHNiPS5_10_NH_3**. Figure 84 displays the monoliths BET isotherms of these samples.

All samples were identified as mixtures of isotherms types II and IV. This observation was based on the curve modification as the pressure increased. At pressures p/p^0 lower than 0.45, all the samples presented a type II isotherm behavior, attributed to monolayer-multilayer adsorption, suggesting the presence of microporosity at such relative pressures. With the pressure p/p^0 above 0.45, type IV isotherms were clear, associated to capillary condensation taking place in the mesopores. This fact is noticeable by the distinct hysteresis loops which take place between the adsorption and desorption curves, i.e., the saturation pressures are not equal for condensation and evaporation inside the pores, so that adsorption and desorption isotherms do not coincide. Considering the IUPAC classification for hysteresis loops, the monoliths that were analysed in this work can be classified as type H2(a) (THOMMES et al., 2015). This hysteresis is commonly found in disordered porous materials or in ordered mesoporous materials with 3D cage-like and interconnected pores (MASON, 1982; SING et al., 1985). Considering the activated carbon template structure, the latter would most probably be the case of the present materials.

Measured data on BET specific surface areas, pore volume and pore size distribution (PSD) are exposed in Table 4. Among these monoliths, the maximum SSA value was assessed on sample mPHNiPS5_10_NH_3, 870.7 $m^2.g^{-1}$, and its PSD, 3.53 nm, calculated using the desorption branch of Barrett-Joyner-Halenda Method (BJH) curve, was the smallest value in comparison to the average pore size of the other samples. Also, it was possible to observe that HTT1800-based monoliths generated smaller SSA than PHPS-based. The high SSA values are in agreement with previous studies from our research group applying metal-modified polysilazanes and ACM.

Figure 85 displays the XRD patterns of **mPHCoPS5_10_NH_3** crushed monoliths

Figure 84 – BET isotherms for Co/Ni-doped mesoporous Si_3N_4 monoliths

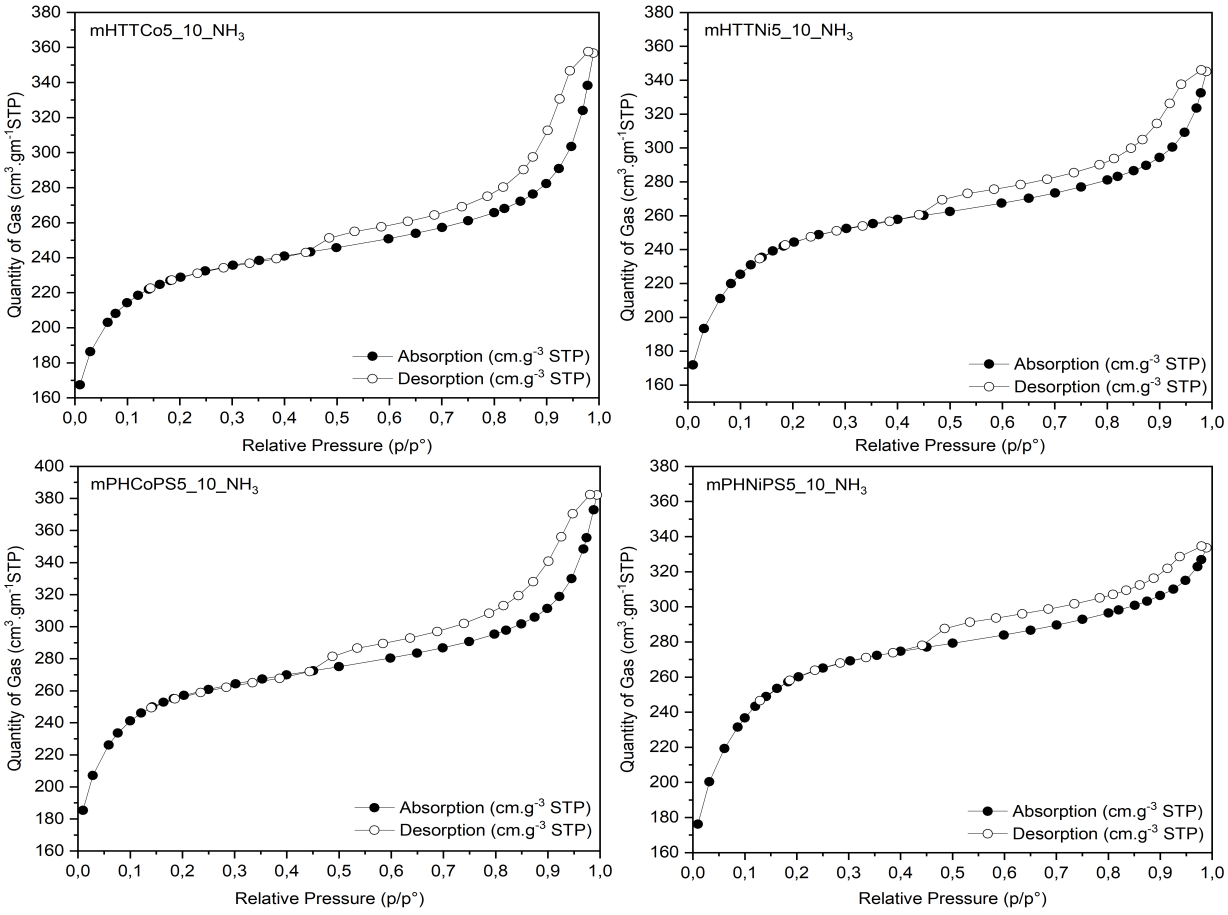

Table 4 – Specific Surface Area (SSA), Pore Volume and Pore Size Distribution (PSD) of HTT1800/PHPS and Co/$NiCl_2$-derived mesoporous Si_3N_4 monoliths generated at 1000 ℃

Sample Name	SSA ($m^2.g^{-1}$)	Pore Volume ($cm^3.g^{-1}$)	PSD (nm)
mHTTCo5_10_NH_3	756.07	0.47	6.28
mHTTNi5_10_NH_3	779.42	0.48	6.02
mPHCoPS5_10_NH_3	849.62	0.52	5.76
mPHNiPS5_10_NH_3	870.70	0.49	3.53

compared to ACM template and to a monolith impregnated only with PHPS (**mPHPS**). For ACM, two major broad peaks centered at 24 ° and 44 °, attributed to the reflection from (002) and (100) planes, respectively, were detected, evidencing the amorphous structure of activated carbon (WANG, S. et al., 2020). Sharp peaks at around 20, 22 and 26 ° are related to graphitic carbon, formed during ACM synthesis, and these signs were also observed for **mPHPS** and **mPHCoPS5** (GULER, 2014; OSMAN et al., 2020).

Figure 85 – XRD patterns of mPHCoPS5 and mPHPS at 1000 ℃ compared to ACM

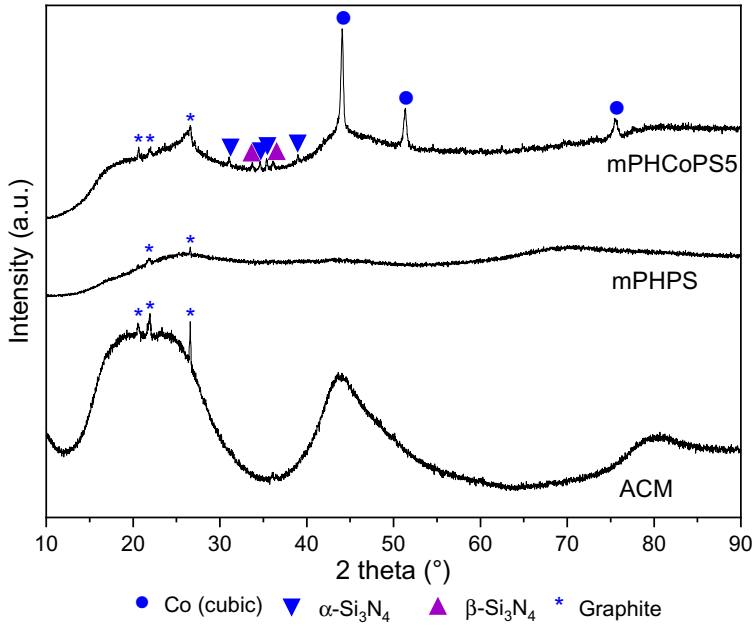

Patterns attributed to (111), (200) and (220) planes of cubic cobalt (ICDD File No. 00-015-0806) were evident for **mPHCoPS5**. More than that, α- and β-Si_3N_4 peaks could be identified, in contrast to **mPHPS**, which exhibitted a totally amorphous structure. Therefore, cobalt might have acted as a catalyst for silicon nitride crystallization. As opposed to the powder **PHCoPS5**, it is important to mention that no silicides were formed in the monolith produced with the same polymer. The treatment under nitrogen until 400 ℃ for crosslinking probably assisted the prevention of cobalt silicides formation.

Figure 86 comprises the SEM images of both mHTTCo5 and mPHCoPS5 samples treated at 1000 ℃. It was possible to detect white particles contrasting over the monolith structure. The particles are mainly evident on Figure 86(d). Energy-dispersive spectroscopy (EDS) was applied to acquire the elements information, providing the certainty that such particles consist on cobalt (Figure 87). In addition, EDS identified the presence of carbon on the monoliths, confirming the XRD observation that part of the ACM template structure was not removed during pyrolysis.

PHCoPS-15h polymers at Si/Co ratios 2.5, 5, 10 and 25 were also tested in the impregnation of ACM. Seeing that reducing the reaction duration and the pyrolysis temperature led to more suitable results for the powders, heat treatments were perfomed using the same conditions, however the final temperature was set to 800 ℃. This process generated the following products: **mPHCoPS2.5-15h_800_NH_3**, **mPHCoPS5-15h_800_NH_3**, **mPHCoPS10-15h_800_NH_3** and **mPHCoPS25-15h_800_NH_3**. The generated isotherms

Figure 86 – SEM images of mHTTCo5_10_NH_3 (a-b) and mPHCoPS5_10_NH_3 (c-d)

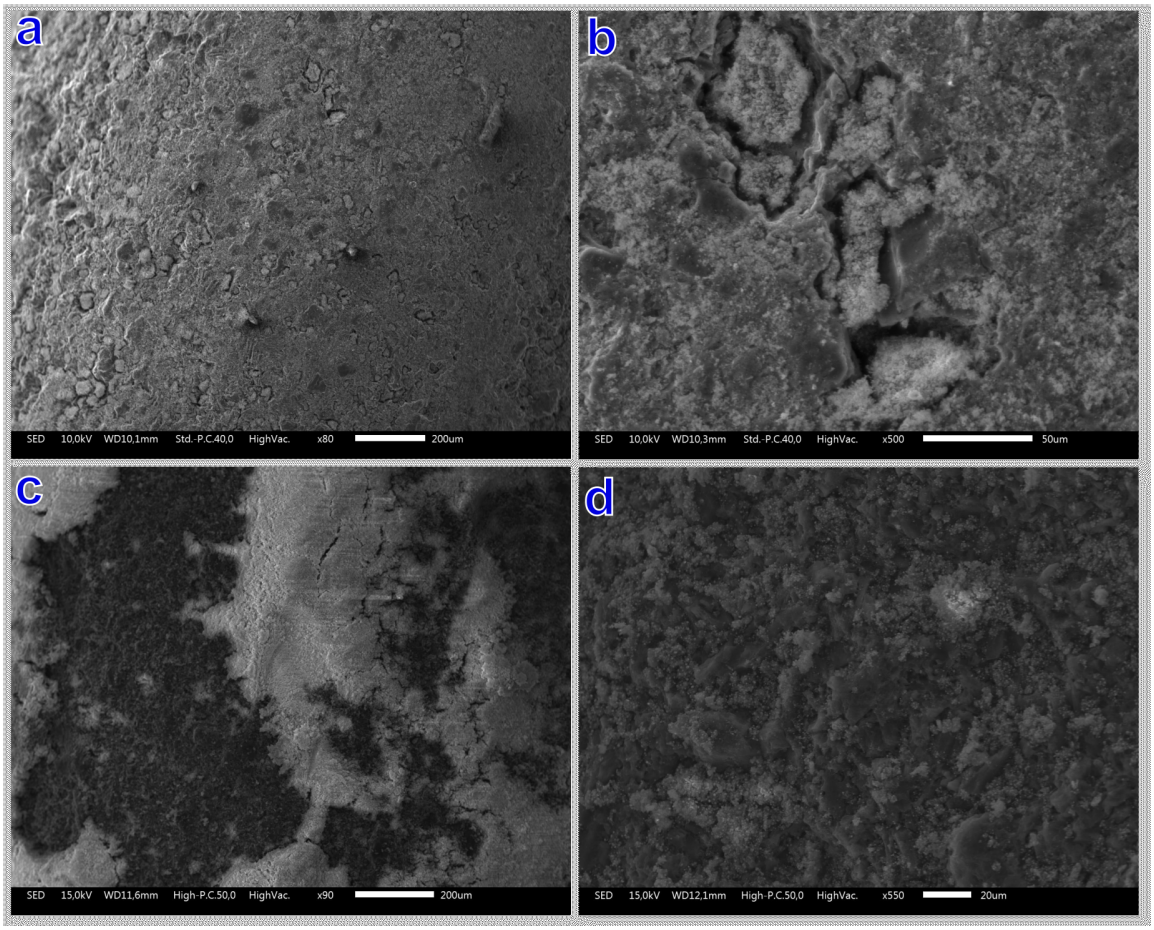

are displayed in Figure 89.

The monoliths presented similar behavior, isotherms types II and IV and hysteresis loop of H2(a) type. Such results are in accordance with previous studies published by our research group that reported the application of activated carbon monoliths as mesoporous templates.

Data concerning SSA, pore volume and PSD is presented in Table 5. One of the samples, ratio 25, was treated also at 700 ℃ to verify the SSA evolution with the temperature. The SSA increased from 765 $m^2.g^{-1}$ at 700 ℃ to 859 $m^2.g^{-1}$ at 800 ℃, which is related to the NH_3 treatment.

In comparison to different pore-formation strategies, the activated carbon monoliths applied herein seem to be an advantageous approach. Fotoohi, Kazemzad, and Mercier (2018) applied a surfactant as structure directing agent to develop mesoporous silica for catalytic purposes, obtaining a maximum SSA of 731 $m^2.g^{-1}$ and pore size between 8 and 12 nm. Hao Wang et al. (2005) prepared porous SiCN ceramics by a sacrificial method using a polysilazane as SiCN precursor and silica spheres as the sacrificial template.

Figure 87 – Elements identified by EDS on the monoliths obtained at 1000 ℃

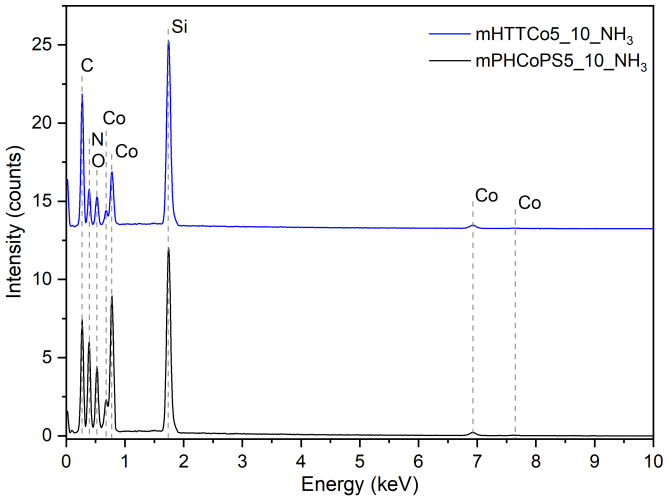

Figure 88 – SEM image of mPHNiPS5_10_NH_3 and EDS on the monoliths obtained at 1000 ℃

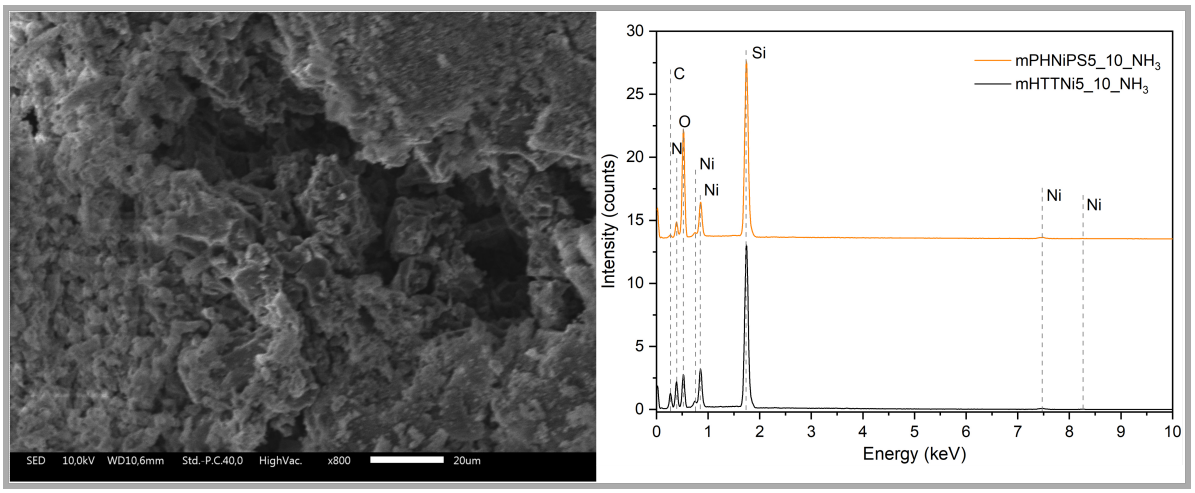

Posterior to a heat treatment until 1250 ℃ under N_2 followed by etching process for the template removal, surface areas in the range between 250 and 455 $m^2.g^{-1}$ were generated, with macropores interconnected by 20-80 nm windows and 3-5 nm mesopores embedded in the SiCN frameworks.

In this work, the monoliths generated by nanocasting of the produced polymers using ACM as template support, displayed relatively high specific surface areas. As shown in Table 5, the maximum SSA value was generated for sample **mPHCoPS5-15h_800_NH_3**, 921.45 $m^2.g^{-1}$. Considering the similar pore volume, PSD and SSA range among the samples, it was possible to observe that Si/Co ratio was not a strongly influent factor for the porosity. Zhong Li et al. (2017), in contrast, reported a decrease on the SSA from 246 to 173 $m^2.g^{-1}$ as the amount of cobalt increased in the produced sample.

Figure 89 – BET isotherms for PHPS and $CoCl_2$-derived mesoporous Si_3N_4 monoliths (15 h reaction)

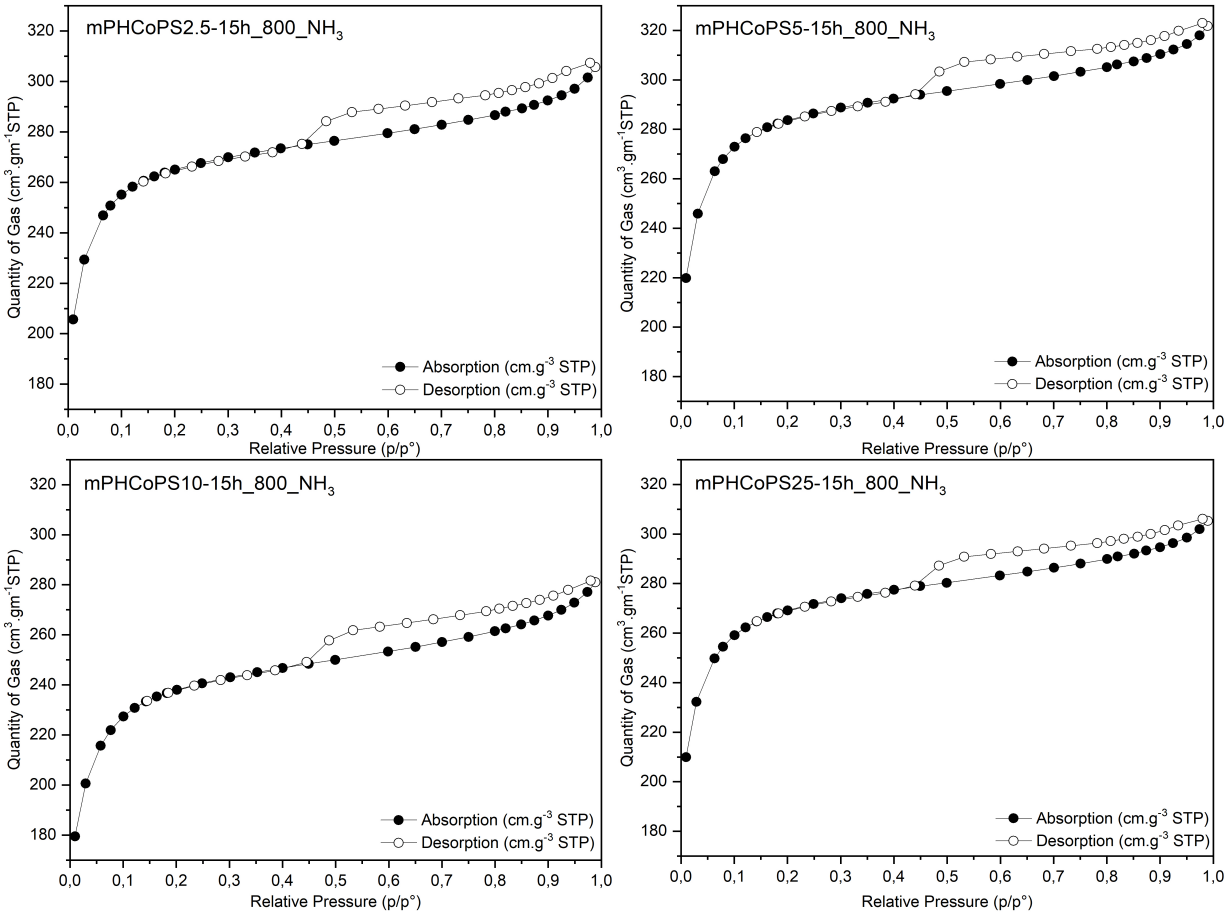

An interesting fact about these results is related to samples **mPHCoPS5_10_NH_3** and **mPHCoPS5-15h_800_NH_3**, differentiated by reaction duration and pyrolysis final temperature. The SSA value increased from 849.62 $m^2.g^{-1}$ to 921.45 $m^2.g^{-1}$ reducing the reaction from 72 to 15 h and the pyrolysis temperature from 1000 to 800 °C. This finding is specially important to demonstrate the microstructure influence on the material morphology features.

Additionally, **PHCoPS-15h** monoliths were crushed into fine powders and evaluated by XRD. The patterns can be observed in Figure 90. The broad signs correspond to amorphous carbon, indicating that carbon monolith was not completely removed during pyrolysis, which contributted for the high SSA value (LALE; MALLMANN, et al., 2020). Cubic cobalt patterns for Si/Co ratios 5 and 2.5 are in accordance with the database (ICDD File No. 00-015-0806). For Si/Co ratios 10 and 25, cobalt was poorly crystallized.

The monoliths were analysed by SEM. Samples **mPHCoPS2.5-15h_800_NH_3** and **mPHCoPS5-15h_800_NH_3** are exhibited in Figure 91. It was possible to observe the monoliths porous structure with the presence of nanoparticles and agglomerates (as high-

Table 5 – Specific Surface Area (SSA), Pore Volume and Pore Size Distribution (PSD) of Co-doped mesoporous Si_3N_4 monoliths obtained after impregnation of PHPS and $CoCl_2$ resulting polymers

Sample Name	Pyrolysis Temperature (°C)	SSA ($m^2.g^{-1}$)	Pore Volume ($cm^3.g^{-1}$)	PSD (nm)
mPHCoPS2.5-15h	700	765.00	0.42	4.13
mPHCoPS2.5-15h	800	859.28	0.46	3.95
mPHCoPS5-15h	800	921.48	0.49	3.72
mPHCoPS10-15h	800	779.62	0.43	3.94
mPHCoPS25-15h	800	873.93	0.46	3.72

Figure 90 – XRD of mPHCoPS-15h (ratios 2.5, 5, 10 and 25) treated at 800 °C

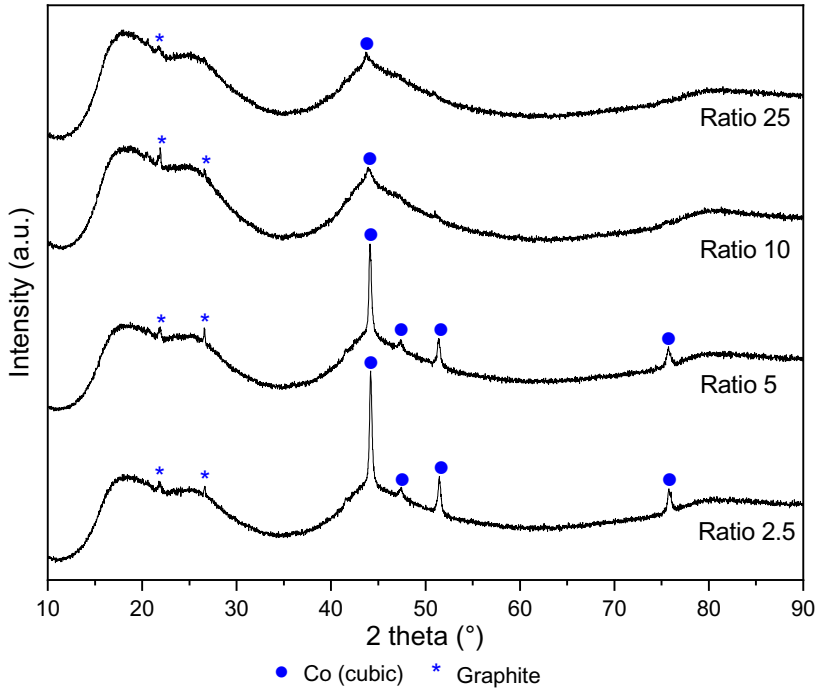

lighted by the green arrows) over the surface and inside the pores. The particles composition was confirmed by EDS.

Formation and distribution of nanoparticles (< 100 nm) and agglomerates (> 100 nm < 500 nm) confirmed the impregnation process efficiency. Moreover, the heat treatment under NH_3 was able to promote the growth of cobalt particles in the amorphous Si_3N_4 structure. Taking into account the literature approach on catalysis processes, this is a satisfactory result. The catalytic activity of supported metallic particles strongly depends on their size and shape, thus nanostructured catalysts are highly active, since most of the particle surface can be available for the reaction (SOMORJAI; BORODKO, 2001;

Figure 91 – SEM of mPHCoPS-15h (ratios 2.5 (a-b) and 5 (c-d)) treated at 800 ℃

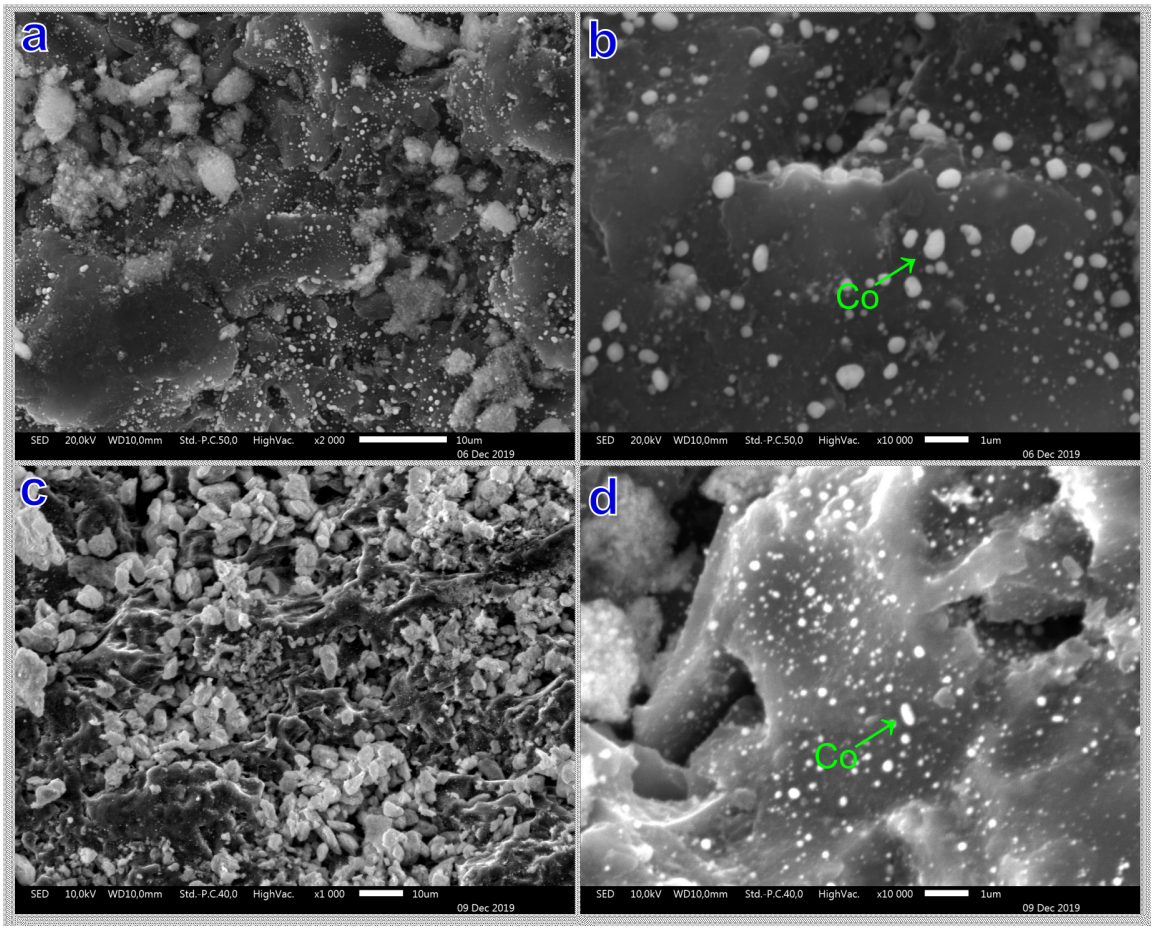

FERREIRA; RANGEL, 2009).

Monoliths named **mPHCoPS10-15h_800_NH_3** and **mPHCoPS25-15h_800_NH_3**, corresponding to the impregnations of PHPS and $CoCl_2$ with Si/Co ratios 10 and 25, respectively, were also analysed by SEM, as shown in Figure 92. The monoliths general aspect could be ascertained as similar to ratios 2.5 and 5. Cobalt particles were also detected (white spots in the SEM images), but in smaller amount than the other ratios, attesting that the quantity of cobalt in the reaction did not dictate the occurrence of particle formation. In other words, cobalt particles were successfully produced applying all ratios, however, it is clear that lower molecular amounts of cobalt in the reaction generated less particles, as expected, which means that less active sites are available in these monoliths.

1D formations were observed on the monoliths **mPHCoPS10-15h_800_NH_3**. It was imprecise to determine specifically the nanowires composition using SEM/EDS because of the high magnification required. Various point verifications and mapping detected Si and Co on the regions with nanowires, but the signals could be overlapped, since the Co particles were in the same area. Their nanochemical composition could also be cobalt

silicide, since it was verified on the powder XRD that Co_2Si and Co_2Si had been formed.

Figure 92 – SEM of mPHCoPS-15h (ratios 10 (a-c) and 25 (d-f) treated at 800 ℃

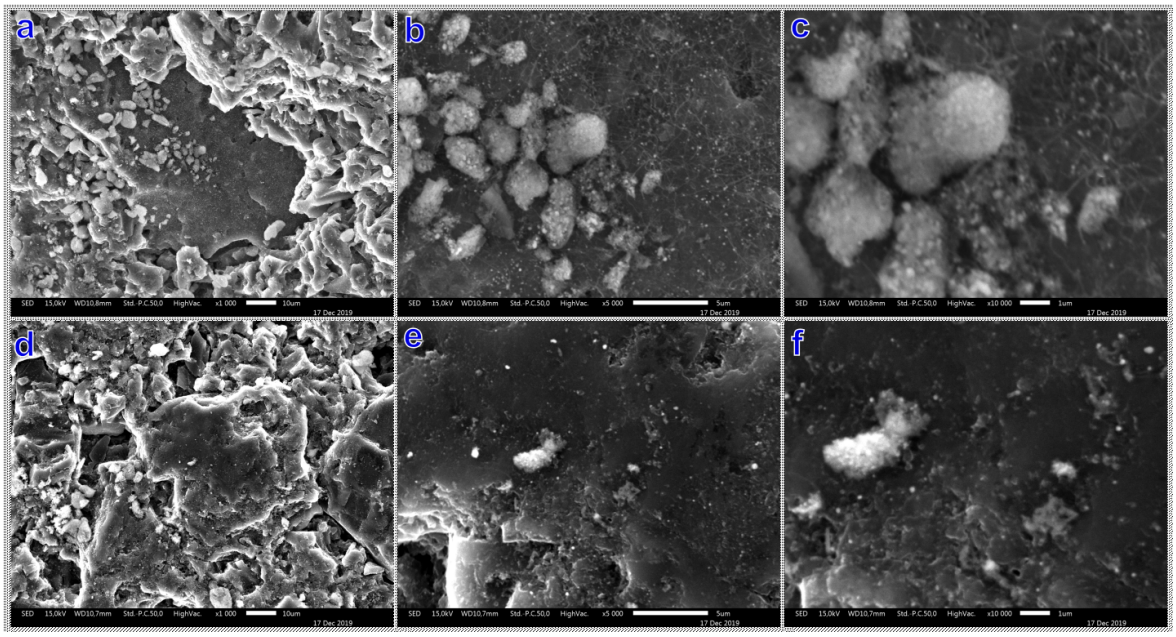

In conclusion to this section, it is important to state the PDC route associated with nanocasting technique efficiently provided conditions to produce new advanced materials with various applications possibilities. More than that, the properties of the final materials can be tailored with chemical modifications in the early steps of the route.

4.2.4 Hydrolysis reactions

The produced monoliths performance as catalytic supports for the hydrolysis of $NaBH_4$ was evaluated and is reported in this section. The methodology for the hydrolysis tests was the same as the one applied for the monoliths which performance was described in the previous chapter.

Before the performance of such materials is shown and compared, it is necessary to bring attention to some parameters. The hydrogen generation rate is given as $L.min^{-1}.g^{-1}_{catalyst}$. Thus, it means the amount of catalyst present in the sample is inversely proportional to the hydrogen rate. In this chapter, molecular ratios between the organosilicon precursor and the metal precursor were fixed. However, it was not possible to precisely determine the amount of Co/Ni that reduced into nanoparticles, formed silicides or were present in metallic state.Thus, the used estimation is theoretical and implies the whole amount of Co/Ni that was added in the beginning of the reaction is present in the monoliths as active sites, capable to catalyse the reaction. The calculated values, the volume of hy-

drogen produced after one cycle (180 minutes) and the hydrogen generation rate (calculus based on the theoretical amount of Co/Ni) are exposed in Table 6.

Samples **mPHCoPS5_10_NH$_3$**, **mHTTCo5_10_NH$_3$** and **mPHNiPS5_10_NH$_3$** (Si:M ratio 5), had a theoretical Co/Ni amount of 16.52 %. The highest volume (mL) was generated by the sample **mPHCoPS5_10_NH$_3$**. The monolith based on PHPS and $NiCl_2$, with an expressive SSA of 870.7 $m^2.g^{-1}$, was less active than the Co-containing materials. A graph showing the hydrogen evolution within the 180 minutes of reaction is presented in Figure 93.

Liu, Li, and Suda (2006) had already observed that Co powders showed higher catalytic activity than Ni powders. The authors tested pure nickel and cobalt powders with 0.5-1 and 1-2 μm size and 1.15 and 1.98 $m^2.g^{-1}$ of specific surface area, respectively, for the hydrolysis of $NaBH_4$. The hydrogen generation rate was 0.02 $L.min^{-1}.g_{Ni}^{-1}$ and 0.13 $L.min^{-1}.g_{Co}^{-1}$. More than that, the authors tested Ni and Co chlorides, borides and Raney (Al alloys) and the maximum rate was 0.65 $L.min^{-1}.g_{catalyst}^{-1}$. These results demonstrate the effectiveness of using a mesoporous support, capable to enormously increase the surface area and at the same time, drastically reduce the amount of catalyst needed for the reaction, still yielding better results.

Table 6 – Hydrogen generation rate and total volume produced after 180 minutes of reaction

Sample name	Si:M	Theoretical Amount Co/Ni (%)	Volume of H_2 (mL) after 180 minutes	H_2 Generation Rate ($L.min^{-1}.g_{catalyst}^{-1}$)
mPHCoPS2.5-15h_800_NH3	2.5	24.25	107.80	0.29
mPHCoPS5-15h_800_NH3	5	16.52	85.30	0.35
mPHCoPS10-15h_800_NH3	10	10.08	165.30	0.71
mPHCoPS25-15h_800_NH3	25	4.68	81.60	1.11
mPHCoPS5_10_NH3	5	16.52	221.65	0.70
mHTTCo5_10_NH3	5	16.52	197.20	0.54
mPHNiPS5_10_NH3	5	16.52	135.20	0.34

Besides that, **mPHCoPS5_10_NH$_3$** was more effective than **mHTTCo5_10_NH$_3$**, demonstrating that carbon-containing composites show less activity in the hydrolysis of $NaBH_4$ (LALE, 2017), corroborating with the preference for nitrides.

When it comes to the hydrogen generation rate, although the percentage of active sites is certainly lower than 16.52 %, the difference among the materials can be discussed. Taking into consideration the same amount of metal for the three samples, not only the volume yielded during the reaction but the rate at which hydrogen was produced was higher for **mPHCoPS5_10_NH$_3$** than for HTT/Co and PHPS/Ni systems.

Based on these results, the monoliths prepared by impregnation of PHPS and $CoCl_2$ polymers at different Si:Co ratios in reactions of 15 h were also tested in hydrolysis

Figure 93 – Hydrogen volume generated by the monoliths mPHCoPS5, mPHNiPS5 and mHTTCo5 pyrolysed at 1000 ℃

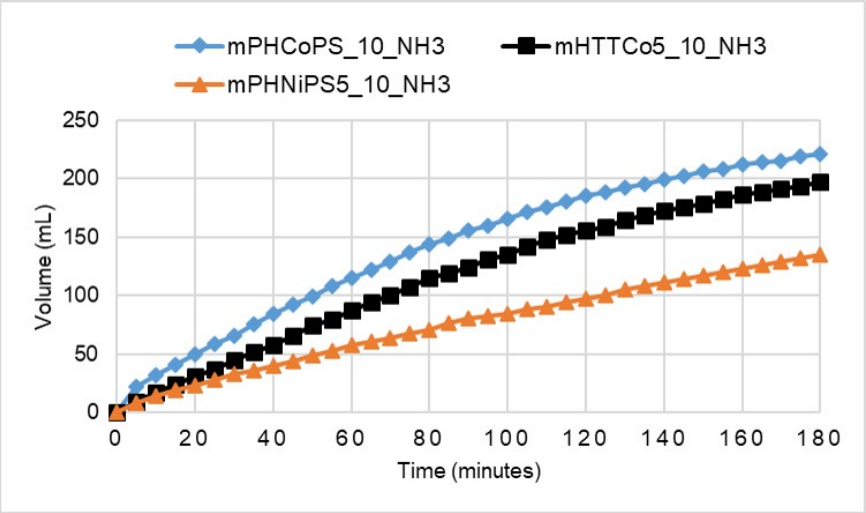

reactions. It is important to notice that these monoliths were heat treated until 800 ℃ whilst the just mentioned until 1000 ℃. The graph exhibitted in Figure 94 correspond to the collected data during hydrolysis of $NaBH_4$ using the monoliths **mPHCoPSX-15h_800_NH_3** (X = Ratio 2.5, 5, 10, 25).

Figure 94 – Hydrogen volume generated by mPHCoPSX-15h_800_NH_3 (X = Ratio 2.5, 5, 10, 25)

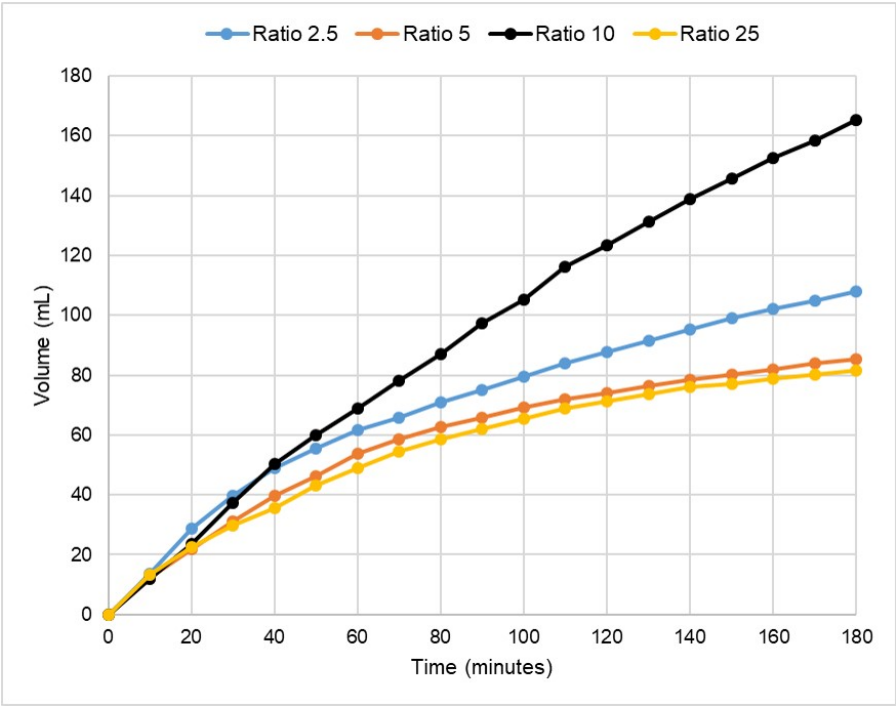

Observing the graph, ratio 10 was the monolith with the highest catalytic activity.

Ratios 5 and 25 had almost similar behavior, which is interesting given the low amount of $CoCl_2$ in the second sample. Then, Table 6 should be checked again. Ratio 10 produced 165.3 mL of hydrogen in 180 minutes with a rate of 0.71 $L.min^{-1}.g_{Co}^{-1}$, whilst ratio 25 could yield only 81.6 mL, but with a ratio of 1.11 $L.min^{-1}.g_{Co}^{-1}$, because of the low amount of cobalt in the monolith.

It is interesting to notice that the highest level of hydrogen evolution was achieved by the monoliths that presented cobalt nanoparticles and 1D wire-like formations (Figure 92). Further investigations using Transmission Electron Microscopy could be helpful for the determination of their constitution and formation process.

Comparing **mPHCoPS5_10_NH_3** with **mPHCoPS5-15h_800_NH_3**, hydrogen evolution decreased from 221.65 to 85.30 mL. A possible explanation for this activity drop is that at 800 °C cobalt particles are surrounded by the Si_3N_4 matrix and for this reason are not accessible for hydrolysis reaction. Although the matrix is micro-/mesoporous, the increase in the pyrolysis temperature could allow for the migration of the metals to the surface, enhancing the disponibility for reaction. A proof is that the perfomance of **mPHCoPS5_10_NH_3** is quite similar to pure **mSi_3N_4**, as shown in our paper (LALE; MALLMANN, et al., 2020).

4.2.4.1 Brief comparison between Co@Si_3N_4 and Co@Si-O-N

This section is dedicated to the study of the performance of cobalt-doped silicon nitride and cobalt-doped silicon oxynitride on the hydrolysis of sodium borohydride. For that, the polymers **PHCoPS10-15h** and **PHCoPS25-15h**, that exhibitted the highest generation rates among the monoliths produced with polymers under reactions of 15 h, were used to impregnate passivated monoliths, that were subjected to the same heat treatment program, but with one difference: after the crosslinking step under nitrogen until 400 °C, the monoliths were treated under air instead of ammonia. The procedure successively generated Co@Si-O-N micro-/mesoporous monoliths, called **mPHCoPS10-15h_800_air** and **mPHCoPS25-15h_800_air**. BET analyses have shown the same behavior for the samples obtained under NH_3 and under air, and the SSA of the latter was 1230 and 983 $m^2.g^{-1}$ for ratios 10 and 25, respectively.

Hydrolysis tests were conducted applying the same methodology used for all the samples already described in this thesis. The performance of the catalyst systems for hydrogen generation is exposed in Figure 95. The oxide monoliths presented poor results in the hydrolysis of $NaBH_4$, producing 70.4 mL (Ratio 10) and 72 mL (Ratio 25).

Using the same theoretical values for cobalt amount in the final samples, the hydrogen generation rate was calculated in similar manner for all the samples. Sample

Figure 95 – Hydrogen volume generated by mPHCoPSX-15h_800 (X = Ratio 10, 25) after heat treatment under NH_3 or air

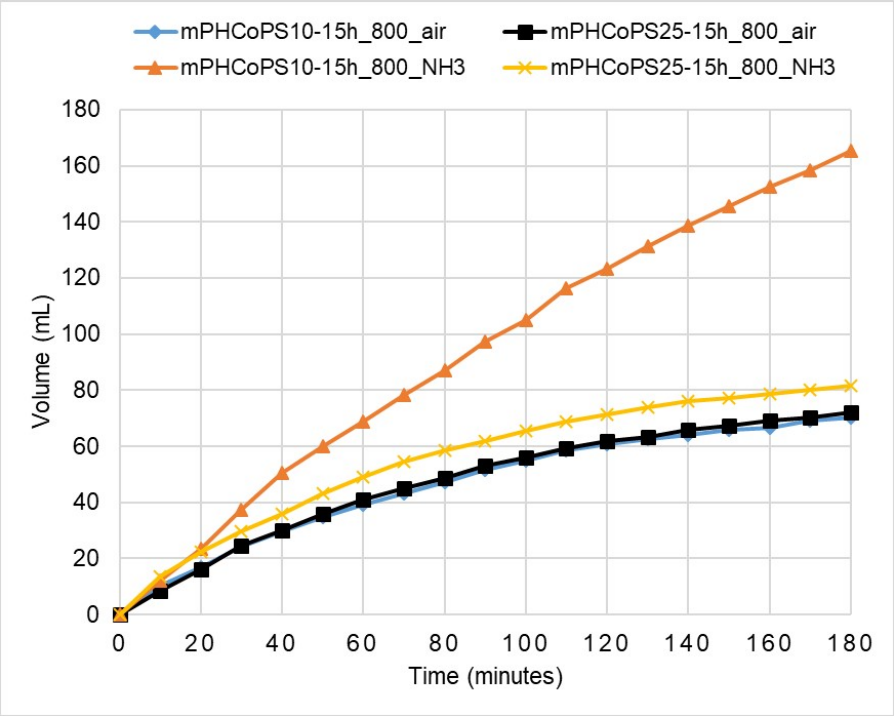

mPHCoPS10-15h_800_air had a rate of 0.26 $L.min^{-1}.g_{Co}^{-1}$ and **mPHCoPS25-15h_800_air** 0.28 $L.min^{-1}.g_{Co}^{-1}$. The samples prepared under ammonia displayed higher activity, which attests a greater interest on nitrides over oxides for the hydrolysis of $NaBH_4$.

5 CONCLUSION

This thesis focused on the synthesis of metal-modified/doped silazanes for the production of nanocomposites. For that, the polymeric precursor PHPS was applied in synthesis reactions with metal precursors, chlorides and complexes in controlled molar ratios to generate Co and Ni nanoparticles distribution and/or the formation of metal nitrides, during the arrangement of a silicon nitride matrix during pyrolysis. The impregnation of activated carbon monoliths with the as-synthesized modified-silazanes and further heat treatment under ammonia lead to micro-/mesoporous monoliths with high specific surface area.

In the first chapter, the reaction between PHPS and the titanium precursor TDMAT was deeply investigated and was proven to have great reproducibility and can be extended to other transition metal precursors, forming MN/Si_3N_4 (M=Ti, Mo, V) ceramics. Expressive SSA values (up to 1165.7 $m^2.g^{-1}$) were obtained for TiN/Si_3N_4 monoliths, that revealed the impossibility to completely remove the activated carbon template due to TiN activity as an diffusion barrier that prevented ammonia from reacting with carbon.

Platinum, nickel and cobalt nanoparticles were successfully reduced on TiN/Si_3N_4 monoliths, and presented robustness to withstand the hydrolysis conditions and good catalytic activity on hydrogen generation. The hydrogen generation rates, based on the slope of the curves at < 50 % conversion and considering 1 wt% of catalyst, reached the values: 12 $L.min^{-1}.g^{-1}_{Pt}$ (Pt) , 6.4 $L.min^{-1}.g^{-1}_{Co}$ (Co) and 5.9 $L.min^{-1}.g^{-1}_{Ni}$ (Ni). A synergistic effect between Pt-TiN nanoclusters and Si_3N_4 was confirmed to be essential for the high hydrogen generation rate.

Moreover, a novel nanocomposite based on titanium and cobalt was produced and demonstrated to have high potential for catalytic applications, due to the interesting distribution of cobalt nanoparticles within the nanocomposite. Further studies are necessary to enhance the access to the active sites, since the monoliths that were obtained by the impregnation of the titanium-cobalt-modified silazane did not present efficient results in the hydrolysis of $NaBH_4$.

In the second chapter, polymers and ceramics obtained after reactions between PHPS/HTT1800 with nickel and cobalt chloride were investigated. The obtained polymers based on PHPS and Co or Ni presented high crosslinking levels and therefore excellent ceramic yields (91.2 and 89.5 wt%). PHPS with $NiCl_2$ generated amorphous Si_3N_4 ceramics until 1000 ℃, with nickel nanocrystals in the structure, differently from $CoCl_2$, that presented the formation of, along with Co, $CoSi_2$, that proved to accelerate α- and β-Si_3N_4 crystallization. The reactions could be extended to the also synthesized Co and Ni-complexes. Modifications in the pyrolysis and reaction time changed the crystallization

processes and once more proved the excellent features provided by the PDC route in the tailoring of ceramic materials. Thus, it was possible to promote the growth of cobalt and nickel particles in an amorphous silicon nitride matrix applying an one-step process.

Hydrolysis tests showed the sample **mPHCoPS5_10_NH_3** was able to produce the highest volume of hydrogen after 180 minutes of reaction (221.65 mL). The samples obtained at 800 °C presented lower hydrogen production because cobalt nanoparticles were probably surrounded by the Si_3N_4 matrix, reducing the sodium borohydride access to the active sites during hydrolysis. However, reducing the reaction time from 72 to 15 h and the pyrolysis temperature from 1000 to 800 °C, yielded monoliths capable of generating 165.3 mL of hydrogen in a Si/Co molar ratio of 10. This demonstrates that such monoliths can still be tailored and might be able to promote greater catalysis activity. Nitride and oxynitride systems were compared, evidencing the better performance of nitride in such reaction.

In conclusion to this work, it can hopefully contribute to the efforts in research & development that have been growing to achieve breakthroughs in energy-related fields. The demand for energy that can be dense, ready-to-use and cost-effective increases everyday. The scientific community can surely provide enormous opportunities to advance in these areas in the following years.

REFERÊNCIAS

ABE, JO; AJENIFUJA, E; POPOOLA, OM. Hydrogen energy, economy and storage: review and recommendation. **International Journal of Hydrogen Energy**, Elsevier, 2019.

ACAR, Canan; DINCER, Ibrahim. The potential role of hydrogen as a sustainable transportation fuel to combat global warming. **International Journal of Hydrogen Energy**, Elsevier, 2018.

ADAMS, David M; HAINES, Julian. Vibrational spectroscopy at high pressures. 58. An IR study of phase transitions in the hexaamminenickel (II) halides. **The Journal of Physical Chemistry**, ACS Publications, v. 95, n. 18, p. 7068–7071, 1991.

AMENDOLA, Steven C; BINDER, Michael, et al. **System for hydrogen generation**. [S.l.]: Google Patents, 2003.

AMENDOLA, Steven C; SHARP-GOLDMAN, Stefanie L, et al. A safe, portable, hydrogen gas generator using aqueous borohydride solution and Ru catalyst. **International Journal of Hydrogen Energy**, Elsevier, v. 25, n. 10, p. 969–975, 2000.

AZUM, Naved et al. Kinetic Behavior of Cobalt Nanoparticles Facilitated by Cationic Surfactant. **Chemical Engineering Communications**, Taylor & Francis, v. 203, n. 4, p. 446–451, 2016.

BAGHERI, Samira; MUHD JULKAPLI, Nurhidayatullaili; BEE ABD HAMID, Sharifah. Titanium dioxide as a catalyst support in heterogeneous catalysis. **The Scientific World Journal**, Hindawi, v. 2014, 2014.

BAHLOUL, Djamila et al. Preparation of Silicon Carbonitrides from an Organosilicon Polymer: I, Thermal Decomposition of the Cross-linked Polysilazane. **Journal of the American Ceramic Society**, Wiley Online Library, v. 76, n. 5, p. 1156–1162, 1993.

BAI, Ying et al. Carbon-supported platinum catalysts for on-site hydrogen generation from NaBH4 solution. **Materials Letters**, Elsevier, v. 60, n. 17-18, p. 2236–2239, 2006.

BAKIRHAN, Nurgul K; OZKAN, Sibel A. Quantum Dots as a New Generation Nanomaterials and Their Electrochemical Applications in Pharmaceutical Industry. In: HANDBOOK of Nanomaterials for Industrial Applications. [S.l.]: Elsevier, 2018. P. 520–529.

BANEY, Ronald H; BUJALSKI, Duane R. **Ceramic materials with increased crystallinity from silazane polymers**. [S.l.]: Google Patents, 1988. US Patent 4,757,035.

BECHELANY, Mirna; PROUST, Vanessa; GERVAIS, Christel, et al. In situ controlled growth of titanium nitride in amorphous silicon nitride: A general route toward bulk nitride nanocomposites with very high hardness. **Advanced Materials**, Wiley Online Library, v. 26, n. 38, p. 6548–6553, 2014.

BECHELANY, Mirna; PROUST, Vanessa; LALE, Abhijeet, et al. Nanocomposites through the chemistry of single-source precursors: understanding the role of chemistry behind the design of monolith-type nanostructured titanium nitride/silicon nitride. **Chemistry–A European Journal**, Wiley Online Library, v. 23, n. 4, p. 832–845, 2017.

BERNARD, Samuel. **Design, Processing, and Properties of Ceramic Materials from Preceramic Precursors**. [S.l.]: Nova Science Publishers, 2012.

BERNARD, Samuel; FIATY, Koffi, et al. Kinetic modeling of the polymer-derived ceramics route: investigation of the thermal decomposition kinetics of poly [B-(methylamino) borazine] precursors into boron nitride. **The Journal of Physical Chemistry B**, ACS Publications, v. 110, n. 18, p. 9048–9060, 2006.

BERNARD, Samuel; MAJOULET, Olivier, et al. Direct Synthesis of Periodic Mesoporous SilicoBoron CarboNitride Frameworks via the Nanocasting from Ordered Mesoporous Silica with Boron-Modified Polycarbosilazane. **Advanced Engineering Materials**, Wiley Online Library, v. 15, n. 3, p. 134–140, 2013.

BERNARD, Samuel; MIELE, Philippe. Polymer-derived boron nitride: a review on the chemistry, shaping and ceramic conversion of borazine derivatives. **Materials**, Multidisciplinary Digital Publishing Institute, v. 7, n. 11, p. 7436–7459, 2014.

BERNARDO, Enrico et al. Advanced ceramics from preceramic polymers modified at the nano-scale: a review. **Materials**, Multidisciplinary Digital Publishing Institute, v. 7, n. 3, p. 1927–1956, 2014.

BIROT, Marc; PILLOT, Jean-Paul; DUNOGUES, Jacques. Comprehensive chemistry of polycarbosilanes, polysilazanes, and polycarbosilazanes as precursors of ceramics. **Chemical reviews**, ACS Publications, v. 95, n. 5, p. 1443–1477, 1995.

BMW. **Hydrogen fuel cell cars: everything you need to know**. 2000. Available from: `https://www.bmw.com/en/innovation/how-hydrogen-fuel-cell-cars-work.html`. Visited on: 22 Feb. 2020.

BORCHARDT, Lars et al. Preparation and application of cellular and nanoporous carbides. **Chemical Society Reviews**, Royal Society of Chemistry, v. 41, n. 15, p. 5053–5067, 2012.

BRACK, Paul; DANN, Sandie E; WIJAYANTHA, KG Upul. Heterogeneous and homogenous catalysts for hydrogen generation by hydrolysis of aqueous sodium borohydride (NaBH4) solutions. **Energy Science & Engineering**, Wiley Online Library, v. 3, n. 3, p. 174–188, 2015.

BUSCA, Guido. Spectroscopic characterization of the acid properties of metal oxide catalysts. **Catalysis today**, Elsevier, v. 41, n. 1-3, p. 191–206, 1998.

CAKANYILDIRIM, Cetin; GURU, Metin. Production of NaBH4 and hydrogen release with catalyst. **Renewable energy**, Elsevier, v. 34, n. 11, p. 2362–2365, 2009.

_____. Supported CoCl2 catalyst for NaBH4 dehydrogenation. **Renewable Energy**, Elsevier, v. 35, n. 4, p. 839–844, 2010.

CHAVEZ, Ricardo et al. Effect of ambient atmosphere on crosslinking of polysilazanes. **Journal of Applied Polymer Science**, Wiley Online Library, v. 119, n. 2, p. 794–802, 2011.

CHEN, Langxing et al. Characterization of Ag/Pt core-shell nanoparticles by UV–vis absorption, resonance light-scattering techniques. **Spectrochimica Acta Part A: Molecular and Biomolecular Spectroscopy**, Elsevier, v. 68, n. 3, p. 484–490, 2007.

CHOONG KWET YIVE, N. S. et al. Thermogravimetric analysis/mass spectrometry investigation of the thermal conversion of organosilicon precursors into ceramics under argon and ammonia. 2. Poly(silazanes). **Chemistry of Materials**, v. 4, n. 6, p. 1263–1271, 1992.

CHOU, Yi-Chia et al. In-situ TEM observation of repeating events of nucleation in epitaxial growth of nano CoSi2 in nanowires of Si. **Nano letters**, ACS Publications, v. 8, n. 8, p. 2194–2199, 2008.

CHRISTODOULOU, Leo; VENABLES, John D. Multifunctional material systems: The first generation. **JOM**, Springer, v. 55, n. 12, p. 39–45, 2003.

COLOMBO, P; BERNARDO, E; PARCIANELLO, G. Multifunctional advanced ceramics from preceramic polymers and nano-sized active fillers. **Journal of the European Ceramic Society**, Elsevier, v. 33, n. 3, p. 453–469, 2013.

COLOMBO, Paolo; MERA, Gabriela, et al. Polymer-derived ceramics: 40 years of research and innovation in advanced ceramics. **Journal of the American Ceramic Society**, Wiley Online Library, v. 93, n. 7, p. 1805–1837, 2010.

CROUSE, Heather F et al. Quenching of tryptophan fluorescence in various proteins by a series of small nickel complexes. **Dalton Transactions**, Royal Society of Chemistry, v. 41, n. 9, p. 2720–2731, 2012.

DALEBROOK, Andrew F et al. Hydrogen storage: beyond conventional methods. **Chemical Communications**, Royal Society of Chemistry, v. 49, n. 78, p. 8735–8751, 2013.

DAWOOD, Furat; ANDA, Martin; SHAFIULLAH, GM. Hydrogen production for energy: An overview. **International Journal of Hydrogen Energy**, Elsevier, 2020.

DEBE, Mark K. Electrocatalyst approaches and challenges for automotive fuel cells. **Nature**, Nature Publishing Group, v. 486, n. 7401, p. 43–51, 2012.

DEMIRCI, U; MIELE, P. Cobalt in NaBH 4 hydrolysis. **Physical Chemistry Chemical Physics**, Royal Society of Chemistry, v. 12, n. 44, p. 14651–14665, 2010.

DEMIRCI, Umit B; MIELE, Philippe. Sodium tetrahydroborate as energy/hydrogen carrier, its history. **Comptes Rendus Chimie**, Elsevier, v. 12, n. 9, p. 943–950, 2009.

DINCER, Ibrahim; ACAR, Canan. Review and evaluation of hydrogen production methods for better sustainability. **International journal of hydrogen energy**, Elsevier, v. 40, n. 34, p. 11094–11111, 2015.

DOE. **Clean Energy**. 2020. Available from: `https://www.energy.gov/science-innovation/clean-energy`.

EDWARDS, Peter P et al. Hydrogen and fuel cells: towards a sustainable energy future. **Energy policy**, Elsevier, v. 36, n. 12, p. 4356–4362, 2008.

ERTL, G. et al. **Handbook of Heterogeneous Catalysis, 8 Volume Set**. [S.l.]: Wiley, 2008. ISBN 9783527312412.

ESCONJAUREGUI, Santiago; WHELAN, Caroline M; MAEX, Karen. Carbon nanotube catalysis by metal silicide: resolving inhibition versus growth. **Nanotechnology**, IOP Publishing, v. 18, n. 1, p. 015602, 2006.

FARCAS, Alin C; DOBRA, Petru. Adaptive control of membrane conductivity of PEM fuel cell. **Procedia Technology**, Elsevier, v. 12, p. 42–49, 2014.

FENG, Guangwen et al. Platinum decorated mesoporous titanium cobalt nitride nanorods catalyst with promising activity and CO-tolerance for methanol oxidation reaction.

International Journal of Hydrogen Energy, Elsevier, v. 43, n. 36, p. 17064–17068, 2018.

FENG, Jin-Xian et al. Efficient hydrogen evolution electrocatalysis using cobalt nanotubes decorated with titanium dioxide nanodots. **Angewandte Chemie International Edition**, Wiley Online Library, v. 56, n. 11, p. 2960–2964, 2017.

FENG, Xuanyu et al. Cobalt-bridged secondary building units in a titanium metal-organic framework catalyze cascade reduction of N-heteroarenes. **Chemical science**, Royal Society of Chemistry, v. 10, n. 7, p. 2193–2198, 2019.

FERREIRA, Hadma Sousa; RANGEL, Maria do Carmo. Nanotecnologia: aspectos gerais e potencial de aplicacao em catalise. **Quimica nova**, SciELO Brasil, v. 32, n. 7, p. 1860–1870, 2009.

FLORES, Octavio et al. Selective cross-linking of oligosilazanes to tailored meltable polysilazanes for the processing of ceramic SiCN fibres. **Journal of Materials Chemistry A**, Royal Society of Chemistry, v. 1, n. 48, p. 15406–15415, 2013.

FOTOOHI, Babak; KAZEMZAD, Mahmood; MERCIER, Louis. Additive-free synthesis of robust monolithic mesoporous silica support used in catalysis. **Ceramics International**, Elsevier, v. 44, n. 16, p. 20199–20210, 2018.

FUNAYAMA, Osamu et al. Synthesis and pyrolysis of thermosetting copolymer of polysilastyrene and perhydropolysilazane. **Journal of the Ceramic Society of Japan**, The Ceramic Society of Japan, v. 103, n. 1197, p. 424–429, 1995.

GALARNEAU, Anne et al. Validity of the t-plot method to assess microporosity in hierarchical micro/mesoporous materials. **Langmuir**, ACS Publications, v. 30, n. 44, p. 13266–13274, 2014.

GARDELLE, B et al. Thermal degradation and fire performance of polysilazane-based coatings. **Thermochimica acta**, Elsevier, v. 519, n. 1-2, p. 28–37, 2011.

GLATZ, Germund et al. Copper-Containing SiCN Precursor Ceramics (Cu@ SiCN) as Selective Hydrocarbon Oxidation Catalysts Using Air as an Oxidant. **Chemistry–A European Journal**, Wiley Online Library, v. 16, n. 14, p. 4231–4238, 2010.

GREIL, Peter. Polymer derived engineering ceramics. **Advanced engineering materials**, Wiley Online Library, v. 2, n. 6, p. 339–348, 2000.

GROEN, Johan C et al. Direct demonstration of enhanced diffusion in mesoporous ZSM-5 zeolite obtained via controlled desilication. **Journal of the American Chemical Society**, ACS Publications, v. 129, n. 2, p. 355–360, 2007.

GULER, Omer. Mechanical and thermal properties of a Cu-CNT composite with carbon nanotubes synthesized by CVD process. **Materials Testing**, Carl Hanser Verlag, v. 56, n. 9, p. 662–666, 2014.

GUNTHNER, Martin et al. High performance environmental barrier coatings, Part I: Passive filler loaded SiCN system for steel. **Journal of the European Ceramic Society**, Elsevier, v. 31, n. 15, p. 3003–3010, 2011.

HAMILTON, Charles W et al. B–N compounds for chemical hydrogen storage. **Chemical Society Reviews**, Royal Society of Chemistry, v. 38, n. 1, p. 279–293, 2009.

HAMMAD, Talaat M; SALEM, Jamil K; HARRISON, Roger G. Structure, optical properties and synthesis of Co-doped ZnO superstructures. **Applied Nanoscience**, Springer, v. 3, n. 2, p. 133–139, 2013.

HECTOR, Andrew L. Synthesis and processing of silicon nitride and related materials using preceramic polymer and non-oxide sol-gel approaches. **Coordination Chemistry Reviews**, Elsevier, v. 323, p. 120–137, 2016.

HUANG, K et al. Novel VN/C nanocomposites as methanol-tolerant oxygen reduction electrocatalyst in alkaline electrolyte. **Scientific reports**, Nature Publishing Group, v. 5, p. 11351, 2015.

IEA. **The Future of Hydrogen, IEA, Paris**. 2019. Available from: https://www.iea.org/reports/the-future-of-hydrogen.

INGOLE, Sudeep Prabhakar et al. **Tribology for Scientists and Engineers: From Basics to Advanced Concepts**. [S.l.]: Springer, 2013.

IONESCU, Emanuel. Polymer-derived ceramics. **Ceramics science and technology**, Wiley Online Library, p. 457–500, 2013.

IONESCU, Emanuel; KLEEBE, Hans-Joachim; RIEDEL, Ralf. Silicon-containing polymer-derived ceramic nanocomposites (PDC-NCs): Preparative approaches and properties. **Chemical Society Reviews**, Royal Society of Chemistry, v. 41, n. 15, p. 5032–5052, 2012.

IWAMOTO, Yuji; KIKUTA, Koichi; HIRANO, Shin-ichi. Crystallization and microstructure development of Si3N4-Ti (C, N)-Y2O3 ceramics derived from chemically modified

perhydropolysilazane. **Journal of the Ceramic Society of Japan**, The Ceramic Society of Japan, v. 108, n. 1264, p. 1072–1078, 2000.

_____. Synthesis of poly-titanosilazanes and conversion into Si3N4-TiN ceramics. **Journal of the Ceramic Society of JAPAN**, The Ceramic Society of Japan, v. 108, n. 1256, p. 350–356, 2000.

JAIN, IP; JAIN, Pragya; JAIN, Ankur. Novel hydrogen storage materials: A review of lightweight complex hydrides. **Journal of Alloys and Compounds**, Elsevier, v. 503, n. 2, p. 303–339, 2010.

JEHN, Hermann. Molybdenum and Nitrogen. In: MO Molybdenum. [S.l.]: Springer, 1989. P. 1–66.

KANEKO, Katsumi. Determination of pore size and pore size distribution: 1. Adsorbents and catalysts. **Journal of membrane science**, Elsevier, v. 96, n. 1-2, p. 59–89, 1994.

KANWAL, Zakia et al. A comparative assessment of nanotoxicity induced by metal (silver, nickel) and metal oxide (cobalt, chromium) nanoparticles in Labeo rohita. **Nanomaterials**, Multidisciplinary Digital Publishing Institute, v. 9, n. 2, p. 309, 2019.

KAUR, Arshdeep; GANGACHARYULU, Dasaroju; BAJPAI, Pramod K. KINETIC STUDIES OF HYDROLYSIS REACTION OF NaBH4 WITH γAl2O3 NANOPARTICLES AS CATALYST PROMOTER AND CoCl2 AS CATALYST. **Brazilian Journal of Chemical Engineering**, SciELO Brasil, v. 36, n. 2, p. 929–939, 2019.

KIM, Seongjun et al. Improving the reliability of Si die attachment with Zn-Sn-based high-temperature Pb-free solder using a TiN diffusion barrier. **Journal of electronic materials**, Springer, v. 38, n. 12, p. 2668, 2009.

KNOUZINGER, Helmut. Specific poisoning and characterization of catalytically active oxide surfaces. In: ADVANCES in catalysis. [S.l.]: Elsevier, 1976. v. 25. P. 184–271.

KOHLHASE, A; MANDL, M; PAMLER, W. Performance and failure mechanisms of TiN diffusion barrier layers in submicron devices. **Journal of applied physics**, American Institute of Physics, v. 65, n. 6, p. 2464–2469, 1989.

KONEGGER, Thomas et al. Asymmetric polysilazane-derived ceramic structures with multiscalar porosity for membrane applications. **Microporous and Mesoporous Materials**, Elsevier, v. 232, p. 196–204, 2016.

KRISHNAN, Palanichamy; HSUEH, Kan-Lin; YIM, Sung-Dae. Catalysts for the hydrolysis of aqueous borohydride solutions to produce hydrogen for PEM fuel cells. **Applied Catalysis B: Environmental**, Elsevier, v. 77, n. 1-2, p. 206–214, 2007.

KROKE, Edwin et al. Silazane derived ceramics and related materials. **Materials Science and Engineering: R: Reports**, Elsevier, v. 26, n. 4-6, p. 97–199, 2000.

KRUGER, Carl R; ROCHOW, Eugene G. Polyorganosilazanes. **Journal of Polymer Science Part A: General Papers**, Wiley Online Library, v. 2, n. 7, p. 3179–3189, 1964.

KUBOTA, Mitsuhiro et al. Absorption and desorption characteristics of NH3 with metal chlorides for ammonia storage. **Journal of Chemical Engineering of Japan**, The Society of Chemical Engineers, Japan, 13we294, 2014.

KUMAR, M NARESH; GOVINDH, BODDETI; ANNAPURNA, NOWDURI. Green synthesis and characterization of platinum nanoparticles using sapindus mukorossi Gaertn. Fruit Pericarp. **Asian J. Chem**, v. 29, p. 2541–4, 2017.

KUZNETSOVA, Tatyana et al. Surface microstructure of Mo(C)N coatings investigated by AFM. **Journal of Materials Engineering and Performance**, Springer, v. 25, n. 12, p. 5450–5459, 2016.

LALE, Abhijeet. **Synthesis and characterization of silicon and boron -based nitride nanocomposites as catalytic mesoporous supports for energy applications**. 2017. PhD thesis – Chimie et Physico-Chimie des Matériaux, Université de Montpellier.

LALE, Abhijeet; MALLMANN, Maira Debarba, et al. Highly Active, Robust and Reusable Micro-/Mesoporous TiN/Si3N4 Nanocomposite-based Catalysts for Clean Energy: Understanding the Key Role of TiN Nanoclusters and Amorphous Si3N4 Matrix in the Performance of the Catalyst System. **Applied Catalysis B: Environmental**, Elsevier, p. 118975, 2020.

LALE, Abhijeet; PROUST, Vanessa, et al. A comprehensive study on the influence of the polyorganosilazane chemistry and material shape on the high temperature behavior of titanium nitride/silicon nitride nanocomposites. **Journal of the European Ceramic Society**, Elsevier, v. 37, n. 16, p. 5167–5175, 2017.

LALE, Abhijeet; SCHMIDT, Marion, et al. Polymer-Derived Ceramics with engineered mesoporosity: From design to application in catalysis. **Surface and Coatings Technology**, Elsevier, v. 350, p. 569–586, 2018.

LALE, Abhijeet; WASAN, Awin, et al. Organosilicon polymer-derived mesoporous 3D silicon carbide, carbonitride and nitride structures as platinum supports for hydrogen

generation by hydrolysis of sodium borohydride. **international journal of hydrogen energy**, Elsevier, v. 41, n. 34, p. 15477–15488, 2016.

LAVEDRINE, A et al. Pyrolysis of polyvinylsilazane precursors to silicon carbonitride. **Journal of the European Ceramic Society**, Elsevier, v. 8, n. 4, p. 221–227, 1991.

LEE, Heui Seung; RHEE, Hwa Sung; AHN, Byung Tae. Improved morphological stability of CoSi2 layer by in situ growth on polycrystalline silicon using reactive chemical vapor deposition. **Journal of The Electrochemical Society**, The Electrochemical Society, v. 149, n. 1, p. 16–20, 2002.

LI, Ya-Li et al. Thermal cross-linking and pyrolytic conversion of poly (ureamethylvinyl) silazanes to silicon-based ceramics. **Applied organometallic chemistry**, Wiley Online Library, v. 15, n. 10, p. 820–832, 2001.

LI, Zhong et al. The effect of Co-doping on the humidity sensing properties of ordered mesoporous TiO2. **Applied Surface Science**, Elsevier, v. 412, p. 638–647, 2017.

LINARES, Noemi et al. Mesoporous materials for clean energy technologies. **Chemical Society Reviews**, Royal Society of Chemistry, v. 43, n. 22, p. 7681–7717, 2014.

LIU, Bin Hong; LI, Zhou Peng; SUDA, S. Nickel-and cobalt-based catalysts for hydrogen generation by hydrolysis of borohydride. **Journal of Alloys and Compounds**, Elsevier, v. 415, n. 1-2, p. 288–293, 2006.

LU, A-H; SCHUTH, Ferdi. Nanocasting: a versatile strategy for creating nanostructured porous materials. **Advanced Materials**, Wiley Online Library, v. 18, n. 14, p. 1793–1805, 2006.

MA, Feng Ling et al. Thermal Cure and Ceramization Kinetics of Perhydropolysilazane. In: TRANS TECH PUBL. KEY Engineering Materials. [S.l.: s.n.], 2014. P. 81–86.

MAJOULET, O et al. Preparation, characterization, and surface modification of periodic mesoporous silicon–aluminum–carbon–nitrogen frameworks. **Chemistry of Materials**, ACS Publications, v. 25, n. 20, p. 3957–3970, 2013.

MARRERO-ALFONSO, Eyma Y et al. Hydrogen generation from chemical hydrides. **Industrial & engineering chemistry research**, ACS Publications, v. 48, n. 8, p. 3703–3712, 2009.

MASON, Geoffrey. The effect of pore space connectivity on the hysteresis of capillary condensation in adsorption—desorption isotherms. **Journal of Colloid and Interface Science**, Elsevier, v. 88, n. 1, p. 36–46, 1982.

MAZLOOMI, Kaveh; GOMES, Chandima. Hydrogen as an energy carrier: Prospects and challenges. **Renewable and Sustainable Energy Reviews**, Elsevier, v. 16, n. 5, p. 3024–3033, 2012.

MCWHORTER, Scott et al. Materials-based hydrogen storage: attributes for near-term, early market PEM fuel cells. **Current Opinion in Solid State and Materials Science**, Elsevier, v. 15, n. 2, p. 29–38, 2011.

MEJIA, Carlos Hernandez; DEELEN, Tom W van; JONG, Krijn P de. Activity enhancement of cobalt catalysts by tuning metal-support interactions. **Nature communications**, Nature Publishing Group, v. 9, n. 1, p. 1–8, 2018.

MERA, Gabriela et al. Ceramic nanocomposites from tailor-made preceramic polymers. **Nanomaterials**, Multidisciplinary Digital Publishing Institute, v. 5, n. 2, p. 468–540, 2015.

MITOMO, M. Effect of Fe and Al additions on nitridation of silicon. **Journal of Materials Science**, Springer, v. 12, n. 2, p. 273–276, 1977.

MOLLER, Kasper T et al. Hydrogen-A sustainable energy carrier. **Progress in Natural Science: Materials International**, Elsevier, v. 27, n. 1, p. 34–40, 2017.

NAQASH, Waseem; MAJID, Kowsar. Synthesis, characterization and study of effect of irradiation on electronic properties of polyaniline composite with metal complex of Co (III). **Materials Research**, SciELO Brasil, v. 18, n. 5, p. 1121–1127, 2015.

NAVLANI-GARCIA, Miriam et al. Recent strategies targeting efficient hydrogen production from chemical hydrogen storage materials over carbon-supported catalysts. **NPG Asia Materials**, Nature Publishing Group, v. 10, n. 4, p. 277–292, 2018.

NIAZ, Saba; MANZOOR, Taniya; PANDITH, Altaf Hussain. Hydrogen storage: Materials, methods and perspectives. **Renewable and Sustainable Energy Reviews**, Elsevier, v. 50, p. 457–469, 2015.

ORTEL, Erik et al. Supported mesoporous and hierarchical porous Pd/TiO2 catalytic coatings with controlled particle size and pore structure. **Chemistry of Materials**, ACS Publications, v. 24, n. 20, p. 3828–3838, 2012.

OSMAN, Ahmed I et al. the production and application of carbon nanomaterials from high alkali silicate herbaceous biomass. **Scientific reports**, Nature Publishing Group, v. 10, n. 1, p. 1–13, 2020.

PAN, Yi; BAPTISTA, Joao L. Chemical instability of silicon carbide in the presence of transition metals. **Journal of the American Ceramic Society**, Wiley Online Library, v. 79, n. 8, p. 2017–2026, 1996.

PATEL, Kirti; KAPOOR, Sudhir, et al. Synthesis of Pt, Pd, Pt/Ag and Pd/Ag nanoparticles by microwave-polyol method. **Journal of Chemical Sciences**, Springer, v. 117, n. 4, p. 311–316, 2005.

PATEL, Nainesh; MIOTELLO, Antonio. Progress in Co–B related catalyst for hydrogen production by hydrolysis of boron-hydrides: a review and the perspectives to substitute noble metals. **International Journal of Hydrogen Energy**, Elsevier, v. 40, n. 3, p. 1429–1464, 2015.

PAVIA, Donald L et al. Introdução a Espectroscopia.Tradução da 4a. edição norte-americana. **São Paulo: Cengage Learning**, 2010.

PETZOW, G; HERRMANN, M. Silicon nitride ceramics. In: HIGH performance non-oxide ceramics II. [S.l.]: Springer, 2002. P. 47–167.

REJITHA, KS; ICHIKAWA, T; MATHEW, S. Thermal decomposition studies of [Ni (NH 3) 6] X 2 (X= Cl, Br) in the solid state using TG-MS and TR-XRD. **Journal of thermal analysis and calorimetry**, Springer, v. 103, n. 2, p. 515–523, 2011.

REN, Jianwei et al. Current research trends and perspectives on materials-based hydrogen storage solutions: a critical review. **International Journal of Hydrogen Energy**, Elsevier, v. 42, n. 1, p. 289–311, 2017.

RIEDEL, Ralf; CHEN, I-Wei. **Ceramics Science and Technology, Volume 1: Structures**. [S.l.]: John Wiley & Sons, 2015.

RIEDEL, Ralf; MERA, Gabriela, et al. Silicon-based polymer-derived ceramics: synthesis properties and applications-a review dedicated to Prof. Dr. Fritz Aldinger on the occasion of his 65th birthday. **Journal of the Ceramic Society of Japan**, The Ceramic Society of Japan, v. 114, n. 1330, p. 425–444, 2006.

ROCHOW, Eugene G. **Polymeric silazanes**. [S.l.]: Google Patents, 1963. US Patent 3,098,830.

RODRIGUEZ-ABREU, Carlos et al. A combination of hard and soft templating for the fabrication of silica hollow microcoils with nanostructured walls. **Nanoscale research letters**, Springer, v. 6, n. 1, p. 330, 2011.

ROGELJ, J. et al. **Chapter 2: Mitigation pathways compatible with 1.5C in the context of sustainable development**. [S.l.]: Intergovernmental Panel on Climate Change, 2018.

ROUQUEROL, J et al. Recommendations for the characterization of porous solids (Technical Report). **Pure and Applied Chemistry**, De Gruyter, v. 66, n. 8, p. 1739–1758, 1994.

SACHAU, Sabrina M et al. Micro-/Mesoporous Platinum–SiCN Nanocomposite Catalysts (Pt@ SiCN): From Design to Catalytic Applications. **Chemistry–A European Journal**, Wiley Online Library, v. 22, n. 43, p. 15508–15512, 2016.

SAHA, Shubhanwita et al. Graphene supported bimetallic G–Co–Pt nanohybrid catalyst for enhanced and cost effective hydrogen generation. **international journal of hydrogen energy**, Elsevier, v. 39, n. 22, p. 11566–11577, 2014.

SALAMEH, Chrystelle et al. Monodisperse platinum nanoparticles supported on highly ordered mesoporous silicon nitride nanoblocks: superior catalytic activity for hydrogen generation from sodium borohydride. **RSC Advances**, Royal Society of Chemistry, v. 5, n. 72, p. 58943–58951, 2015.

SANKIR, Mehmet; SANKIR, Nurdan Demirci. **Hydrogen Storage Technologies**. [S.l.]: John Wiley & Sons, 2018.

SANTOS, DMF; SEQUEIRA, CAC. Sodium borohydride as a fuel for the future. **Renewable and Sustainable Energy Reviews**, Elsevier, v. 15, n. 8, p. 3980–4001, 2011.

SATO, Shintaro et al. Carbon nanotube growth from titanium–cobalt bimetallic particles as a catalyst. **Chemical Physics Letters**, Elsevier, v. 402, n. 1-3, p. 149–154, 2005.

SCHLESINGER, HI et al. Sodium borohydride, its hydrolysis and its use as a reducing agent and in the generation of hydrogen1. **Journal of the American Chemical Society**, ACS Publications, v. 75, n. 1, p. 215–219, 1953.

SCHUTH, F; BOGDANOVIC, B; FELDERHOFF, M. Light metal hydrides and complex hydrides for hydrogen storage. **Chemical communications**, Royal Society of Chemistry, n. 20, p. 2249–2258, 2004.

SCHUTH, Ferdi. Endo-and exotemplating to create high-surface-area inorganic materials. **Angewandte Chemie International Edition**, Wiley Online Library, v. 42, n. 31, p. 3604–3622, 2003.

SCHWAB, Stuart T; PAGE, Richard A. Nanostructure of polymer-derived silicon nitride. **Materials Science and Engineering: A**, Elsevier, v. 204, n. 1-2, p. 201–204, 1995.

SEGATELLI, Mariana Gava; PIRES, Alfredo Tiburcio Nunes;
YOSHIDA, Inez Valeria Pagotto. Synthesis and structural characterization of carbon-rich SiCxOy derived from a Ni-containing hybrid polymer. **Journal of the European Ceramic Society**, Elsevier, v. 28, n. 11, p. 2247–2257, 2008.

SEIFOLLAHI BAZARJANI, Mahdi et al. Nanoporous silicon oxycarbonitride ceramics derived from polysilazanes in situ modified with nickel nanoparticles. **Chemistry of Materials**, ACS Publications, v. 23, n. 18, p. 4112–4123, 2011.

SEITZ, L.C. et al. CoTiOx catalysts for the oxygen evolution reaction. **Journal of The Electrochemical Society**, IOP Publishing, v. 162, n. 12, h841, 2015.

SEITZ, Linsey et al. Tuning composition and activity of cobalt titanium oxide catalysts for the oxygen evolution reaction. **Electrochimica Acta**, Elsevier, v. 193, p. 240–245, 2016.

SEO, Kwanyong et al. Magnetic properties of single-crystalline CoSi nanowires. **Nano letters**, ACS Publications, v. 7, n. 5, p. 1240–1245, 2007.

SHANG, Rujing et al. Silicon nitride supported nickel catalyst for partial oxidation of methane to syngas. **Catalysis Communications**, Elsevier, v. 9, n. 11-12, p. 2103–2106, 2008.

EL-SHARKAWY, II et al. Experimental investigation on activated carbon–ethanol pair for solar powered adsorption cooling applications. **International journal of refrigeration**, Elsevier, v. 31, n. 8, p. 1407–1413, 2008.

SHI, Limin et al. Graphene modified Co-B catalysts for rapid hydrogen production from NaBH4 hydrolysis. **International Journal of Hydrogen Energy**, Elsevier, v. 44, n. 33, p. 17954–17962, 2019.

SHIN, Byungha et al. Control of an interfacial MoSe2 layer in Cu2ZnSnSe4 thin film solar cells: 8.9% power conversion efficiency with a TiN diffusion barrier. **Applied Physics Letters**, American Institute of Physics, v. 101, n. 5, p. 053903, 2012.

SIMAGINA, VI et al. Cobalt oxide catalyst for hydrolysis of sodium borohydride and ammonia borane. **Applied Catalysis A: General**, Elsevier, v. 394, n. 1-2, p. 86–92, 2011.

SING, Kenneth SW et al. International union of pure commission on colloid and surface chemistry including catalysis reporting physisorption data for gas/solid systems with

special reference to the determination of surface area and porosity. **Pure Appl. Chem**, v. 57, n. 4, p. 603–619, 1985.

SOMORJAI, GA; BORODKO, YG. Research in nanosciences-great opportunity for catalysis science. **Catalysis letters**, Springer, v. 76, n. 1-2, p. 1–5, 2001.

SRINIVASAN, Bikshandarkoil R et al. Synthesis and structural characterization of tris (ethylenediamine) nickel (II) dichromate. **Journal of Coordination Chemistry**, Taylor & Francis, v. 62, n. 22, p. 3583–3591, 2009.

TAGLIAZUCCA, Valeria; LEONI, Matteo; WEIDENTHALER, Claudia. Crystal structure and microstructural changes of molybdenum nitrides traced during catalytic reaction by in situ X-ray diffraction studies. **Physical Chemistry Chemical Physics**, The Royal Society of Chemistry, v. 16, n. 13, p. 6182–6188, 2014.

THOMMES, Matthias et al. Physisorption of gases, with special reference to the evaluation of surface area and pore size distribution (IUPAC Technical Report). **Pure and Applied Chemistry**, De Gruyter, v. 87, n. 9-10, p. 1051–1069, 2015.

THOMPSON, Stephen et al. The counterdiffusion of HCl and NH3: An experimental and modeling analysis of topochemistry, diffusion, reaction, and phase transitions. **The Journal of chemical physics**, AIP Publishing LLC, v. 150, n. 15, p. 154306, 2019.

TOREKI, William et al. Synthesis and applications of a vinylsilazane preceramic polymer. In: WILEY ONLINE LIBRARY. 14TH Annual Conference on Composites and Advanced Ceramic Materials: Ceramic Engineering and Science Proceedings. [S.l.: s.n.], 1990. P. 1371–1386.

TOYOTA. **Fuel cell electric technology explained**. 2019. Available from: `https://www.toyota-europe.com/world-of-toyota/feel/environment/better-air/fuel-cell-vehicle`. Visited on: 22 Feb. 2020.

VAKIFAHMETOGLU, Cekdar et al. Growth of one-dimensional nanostructures in porous polymer-derived ceramics by catalyst-assisted pyrolysis. Part II: cobalt catalyst. **Journal of the American Ceramic Society**, Wiley Online Library, v. 93, n. 11, p. 3709–3719, 2010.

VEPREK, S et al. Composition, nanostructure and origin of the ultrahardness in nc-TiN/a-Si3N4/a-and nc-TiSi2 nanocomposites with Hv=80 to 105 GPa. **Surface and Coatings Technology**, Elsevier, v. 133, p. 152–159, 2000.

WALTER, Joshua C et al. Sodium borohydride hydrolysis kinetics comparison for nickel, cobalt, and ruthenium boride catalysts. **Journal of Power Sources**, Elsevier, v. 179, n. 1, p. 335–339, 2008.

WAN, Julin; GASCH, Matthew J; MUKHERJEE, Amiya K. Effect of Ammonia Treatment on the Crystallization of Amorphous Silicon-Carbon-Nitrogen Ceramics Derived from Polymer Precursor Pyrolysis. **Journal of the American Ceramic Society**, Wiley Online Library, v. 85, n. 3, p. 554–564, 2002.

WANG, Hao et al. Preparation of three-dimensional ordered macroporous SiCN ceramic using sacrificing template method. **Microporous and mesoporous materials**, Elsevier, v. 80, n. 1-3, p. 357–362, 2005.

WANG, Shuang et al. Adsorption of acetic acid and hydrogen sulfide using NaOH impregnated activated carbon for indoor air purification. **Engineering Reports**, Wiley Online Library, v. 2, n. 1, e12083, 2020.

WEE, Jung-Ho; LEE, Kwan-Young; KIM, Sung Hyun. Sodium borohydride as the hydrogen supplier for proton exchange membrane fuel cell systems. **Fuel processing technology**, Elsevier, v. 87, n. 9, p. 811–819, 2006.

WU, Hui-Xia et al. Preparation and magnetic properties of cobalt nanoparticles with dendrimers as templates. **Materials Chemistry and Physics**, Elsevier, v. 121, n. 1-2, p. 342–348, 2010.

WU, Wen-Fa et al. Novel multilayered Ti/TiN diffusion barrier for Al metallization. **Journal of electronic materials**, Springer, v. 34, n. 8, p. 1150–1156, 2005.

XIAO, Yonghao et al. Titanium cobalt nitride supported platinum catalyst with high activity and stability for oxygen reduction reaction. **Journal of Power Sources**, Elsevier, v. 284, p. 296–304, 2015.

XIE, Junfeng; XIE, Yi. Transition metal nitrides for electrocatalytic energy conversion: opportunities and challenges. **Chemistry–A European Journal**, Wiley Online Library, v. 22, n. 11, p. 3588–3598, 2016.

XIE, Yibing; TIAN, Fang. Capacitive performance of molybdenum nitride/titanium nitride nanotube array for supercapacitor. **Materials Science and Engineering: B**, Elsevier, v. 215, p. 64–70, 2017.

XU, Dongyan; DAI, Ping, et al. Carbon-supported cobalt catalyst for hydrogen generation from alkaline sodium borohydride solution. **Journal of Power Sources**, Elsevier, v. 182, n. 2, p. 616–620, 2008.

XU, Dongyan; ZHANG, Huamin; YE, Wei. Hydrogen generation from hydrolysis of alkaline sodium borohydride solution using Pt/C catalyst. **Catalysis Communications**, Elsevier, v. 8, n. 11, p. 1767–1771, 2007.

YIVE, NS et al. Thermogravimetric analysis/mass spectrometry investigation of the thermal conversion of organosilicon precursors into ceramics under argon and ammonia. 2. Poly(silazanes). **Chemistry of materials**, ACS Publications, v. 4, n. 6, p. 1263–1271, 1992.

YUAN, Jia et al. Single-source-precursor synthesis of hafnium-containing ultrahigh-temperature ceramic nanocomposites (UHTC-NCs). **Inorganic chemistry**, ACS Publications, v. 53, n. 19, p. 10443–10455, 2014.

ZAKI, Mohamed I et al. In situ FTIR spectra of pyridine adsorbed on SiO2–Al2O3, TiO2, ZrO2 and CeO2: general considerations for the identification of acid sites on surfaces of finely divided metal oxides. **Colloids and Surfaces A: Physicochemical and Engineering Aspects**, Elsevier, v. 190, n. 3, p. 261–274, 2001.

ZAWADZKI, Jerzy. An infrared study of acid sites on carbons by pyridine adsorption. **Carbon**, Elsevier, v. 26, n. 5, p. 627–633, 1988.

ZHANG, Q; SMITH, GM; WU, Y. Catalytic hydrolysis of sodium borohydride in an integrated reactor for hydrogen generation. **International journal of hydrogen energy**, Elsevier, v. 32, n. 18, p. 4731–4735, 2007.

ZHANG, Qian et al. Synthesis of Novel Cobalt-Containing Polysilazane Nanofibers with Fluorescence by Electrospinning. **Polymers**, Multidisciplinary Digital Publishing Institute, v. 8, n. 10, p. 350, 2016.

ZHANG, Xiaofei et al. Nickel silicide nanocrystal-containing magnetoceramics from the bulk pyrolysis of polysilazane and nickelocene. **Ceramics International**, Elsevier, v. 40, n. 5, p. 6937–6947, 2014.

ZHU, Qi-Long et al. Controlled synthesis of ultrafine surfactant-free NiPt nanocatalysts toward efficient and complete hydrogen generation from hydrazine borane at room temperature. **ACS Catalysis**, ACS Publications, v. 4, n. 12, p. 4261–4268, 2014.

ZHU, Qing et al. Cobalt/titanium nitride@ N-doped carbon hybrids for enhanced electrocatalytic hydrogen evolution and supercapacitance. **New Journal of Chemistry**, Royal Society of Chemistry, v. 43, n. 36, p. 14518–14526, 2019.